David Barton • Stephen Earle

Professional
Engineering
Publishing

BRAKES 2000

INTERNATIONAL CONFERENCE ON

Automotive Braking – Technologies for the 21st Century

Brakes 2000

Collected papers from the International Conference on *Brakes 2000*
Automotive Braking – Technologies for the 21st Century
held at Royal Armouries Museum and Conference Centre, Leeds, UK, 11–12 July 2000.

The Conference was organized by
The Yorkshire Centre, Automobile Division of
The Institution of Mechanical Engineers (IMechE)

In Association with
The University of Leeds
The Society of Automotive Engineers

Conference Organizing Committee

Professor David Barton (Joint Chairman)
University of Leeds

Mr Steve Earle (Joint Chairman)
JRI (Manufacturing) Limited

Dr Martin Haigh
WABCO Automotive UK Limited

Mr John Hahn
BBA Friction Limited

Mr Bert Smales
Consultant

Mr Stuart Cowling
Vickers Defence Systems

Mr Jim Douglas
IMechE Yorks Admin Officer

Cover design/illustration by Terry Bambrook, Leeds, UK.
Tel: + 44 (0)113 236 2855

The International Conference on

Brakes 2000

Automotive Braking – Technologies for the 21st Century

Edited by

David Barton

and

Stephen Earle

Professional Engineering Publishing Limited
Bury St Edmunds and London, UK.

First Published 2000

ISBN 1 86058 261 3

A CIP catalogue record for this book is available from the British Library.

Printed and bound in Great Britain by Antony Rowe Limited, Chippenham, Wiltshire, UK.

Readers may also be interested in; 'Professional Automobile Engineering in Yorkshire: The Millennium' by A W Crossland. Copies are available from IMechE Yorkshire Region Administration Officer, 19 Greenbanks Drive, Horsforth, Leeds, LS18 5BH

Contents

Materials and Modelling

Braking Systems and Vehicle Performance

Foreword

Once again the Yorkshire Centre of IMechE's Automotive Division have taken on the organisation of a major international braking technology meeting. This year's event, the third in the series, has been elevated to the status of a full IMechE Conference. Importantly, this has entailed the referring of all submitted papers, a lengthy and sometimes tortuous process, but one which we hope has improved the standard of the papers as they appear in this volume. Thanks are due to all referees and authors for their hard work and co-operation and, in particular, to Bert Smales and Martin Haigh of the Conference Planning Committee for their individual efforts in this process.

The first half of this volume, and the first day of the Conference, is devoted to problems of brake refinement i.e. NVH issues. This emphasis is not surprising given that, in a recent survey of UK braking experts, noise and judder were identified as the two most important issues facing the industry, far ahead of other issues such as friction stability or alternative lightweight materials. The first three papers in the first Brake Refinement session describe largely experimental studies of brake squeal and suggest practical solutions whilst the next two take a more theoretical approach to the same topic. The following paper also adopts a modelling approach but this time directed to problems of judder. Papers in the second Brake Refinement session concentrate on experimental techniques of squeal measurement including a summary of the recent deliberations of the US working group on brake noise.

The third session, entitled Materials and Modelling, commences with papers on the prediction of the thermal performance of brake rotors and the effect of non-uniform temperature gradients on deformations and inelastic strain accumulation. This theme is continued with the third paper in the session which considers rotor cracking test procedures. The next two papers are concerned with thermally sprayed coatings for brake discs which may become an important means of protecting lightweight rotors from extreme temperature conditions. The other half of the friction pair, i.e. the pad or shoe material, is then considered in the next three papers, concluding with a critical review of the UK composite friction material industry.

The final session, entitled Braking Systems and Vehicle Performance, considers the foundation brake within the context of the whole vehicle and its systems. Papers cover compressed air systems for CV brakes, testing of ABS operation and the effect on vehicle performance of brake variations. This whole area is one where braking engineers must work closely with colleagues in related disciplines such as electronic/pneumatic control and vehicle dynamics.

This year's event was held for the first time at the Royal Armouries Museum, Leeds. As co-chairmen of the Conference Planning Committee, we would like to thank the staff of the Armouries for their kind assistance in staging the event. Many thanks are also due to the Leeds University Conference Office, clerical staff in the School of Mechanical Engineering and to the other members of the Planning Committee for all their hard work in organising the Conference. Finally, thanks to the staff at PEP for publishing this volume of proceedings to their usual high standard and to Terry Bambrook for the front cover art work which has become an important feature of the Conference promotion. We hope that all readers find the papers interesting and useful and that many of them will be able to attend our next event planned for Summer 2002.

David Barton and Stephen Earle
Joint Chairmen of the Brakes 2000 Planning Committee

Brake Refinement – I

This page intentionally left blank

A study of the interface pressure distribution between pad and rotor, the co-efficient of friction and calliper mounting geometry with regard to brake noise

J D FIELDHOUSE
School of Engineering, The University of Huddersfield, UK

ABSTRACT

It is generally accepted that the coefficient of friction between the friction pair, the pad and rotor, plays a significant role in the propensity of a brake to generate noise. Because of the ease with which changes may be made to the pad compound material it is this which is more often the subject of change when there is a problematic noisy brake with both the rotor and the calliper tending to remain "isolated" from examination. This paper investigates the propensity of a brake to generate noise over a range of temperatures and pressures under conditions which allow a mechanically induced offset centre of pressure between the pad and rotor to be varied. It is shown that for a high volume production car brake there is an increased tendency for it to generate noise when a very specific leading offset centre of pressure is engineered. With this condition it is shown that a situation is promoted whereby the brake becomes mechanically unstable with system changes such as brake pressure and temperature variations having little influence on the brake to alter its tendency to generate noise. Furthermore it is shown that the critical offset centre of pressure may be related to the coefficient of friction between the friction pair and the mounting geometry of the calliper. Confirmation of the findings are supported by a repeat investigation of the vehicle's alternative brake calliper. It is suggested that the source of a noisy brake may lie as much in basic mechanical design as inappropriate material choice.

1 INTRODUCTION

Disc brake noise is accepted to be a complex subject but it is known from the vast range of literature already published on the subject that the principal vibration characteristic of the disc is a diametral mode, the fundamental mode being a two diameter resulting in a frequency of around 2000Hz. It may be shown (1) that in all cases of disc brake noise, whether the system is a sliding fist or rigid type calliper, the dynamic noise frequency may be related directly to the free mode vibration characteristic of the disc. In an attempt to explain the mechanisms involved a variety of mathematical models have been proposed, each of which go some way to explain the phenomenon over a specific frequency range. No single mathematical model is currently available or capable of expressing the differing mechanisms involved nor the vast range of interacting individual modes of vibrations which are inextricably linked by the brake system as a whole - the range is too broad 300Hz to 20,000Hz for a dynamically unstable system. Regardless of how the mathematical models are limited they do allow the designer to introduce basic parameters and criteria at the design stage in an attempt to reduce the propensity of a brake to generate noise. By experience it is generally accepted that the higher the coefficient of friction at the pad/disc interface the greater the tendency will be for the brake to promote noise. This increase in friction coefficient increases the pad/disc interface force for a given pressure which in turn results in a greater braking torque. What it does not indicate is why there is a greater tendency for the disc to be excited in a lateral mode, that is, the movement of a disc vibrating in a diametral mode order. It is some time ago that work by Spurr (2) had shown that a spragging affect could cause instability resulting in a variable lateral force if the sprag angle equated to the interface friction coefficient. Indeed the mechanism was represented by a semi-rigid strut which was inclined to a rubbing surface and pushed horizontal to the surface. When the inclination angle was set at the "sprag angle" of $\tan^{-1}\mu$ or greater the strut would "dig-in" and the normal force to the rubbing surface would increase until flexure of the system allowed a secondary strut arrangement to be established whereby the sprag angle was reduced, the normal force would reduce and the strut would then continue to slide. Clearly because of the construction of the test rig, and the in-built flexibility of the members, the system was able to establish more than one sprag angle for it to work. The calliper is a similar system with a multiple of "sprag angles" and it is this mechanism in relation to the coefficient of friction at the pad/disc interface which this paper examines.

2. EXPERIMENTAL DETAILS

2.1 Test Rig and Instrumentation:

A diagrammatic representation of the test rig is shown in Figure 1 and is designed to allow the fist type calliper under investigation to be mounted in a manner resembling that in a car. Full details of the design are outlined in previous work (3) where the principal concerns outlined were the need to ensure the transmission system imposed no extraneous vibrations in the brake and that the design had mechanical integrity in the sense that it held the knuckle assembly safely against the braking load yet allowed it to vibrate without restriction. Drive to the brake was from a 15kW DC motor through a double reduction pulley arrangement and twin universal joint to give a final speed of 10 r/min.

A torsion bar fitted with strain gauges was included in the final drive of the rig design to allow input torque to be measured and in affect the friction coefficient of the disc/pad interface. This

torsion bar was calibrated using a torque arm and dead weight. The friction coefficient of the disc/pad interface was determined over the test temperature range and for 3 disc speeds, 5, 10 and 20 r/min using this torsion bar as shown in Figure 2. Although Figure 2 represents only one typical friction characteristic the complete calibration was carried out for pressures ranging from 0.068 MPa to 0.952 MPa. Full details of the friction measurements are outline in earlier work (5). It is significant to note that non-linearity of results were observed for pressure readings up to 0.2 MPa. It is suspected that this non-linearity was as a result of calliper threshold pressure which required a correction of 100 μstrain to be applied to the calibration curves.

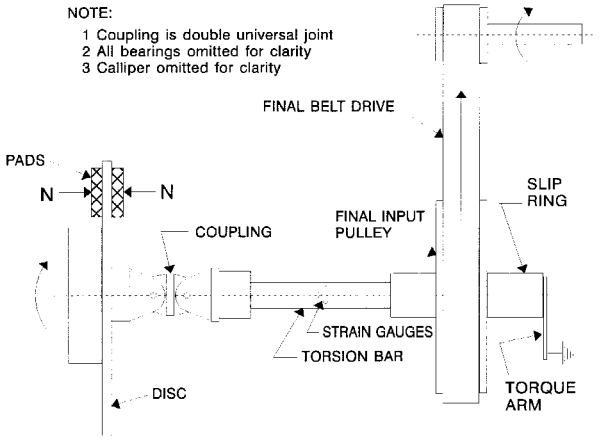

Figure 1 - Sketch showing position of final drive torsion bar.

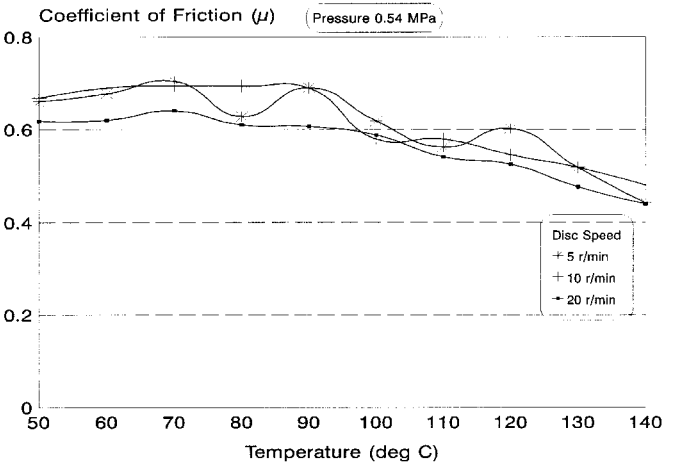

Figure 2 - Variation in pad coefficient of friction, μ, with disc surface temperature - fixed system pressure and disc speed.

Two sliding fist type callipers were tested, the Teves (FN54) combined abutment and Lucas (Collette) trailing abutment. Disc speed, surface temperature, brake pressure, noise frequency and noise level were the principal data recorded for each test. Pressure was applied using a screwed actuator acting on the master cylinder and recorded on a glycerine filled pressure gauge whereas temperature was measured using a rubbing thermocouple on the disc surface. Noise characteristics were detected using a 1" condenser microphone with the frequency and noise level being recorded on a frequency spectrum analyser. The microphone was positioned 500 mm from the disc face and normal to the face. An artificially high friction coefficient was used throughout.

2.2 Test Procedure:

For a calliper to be capable of spragging it is a requirement that the centre of pressure providing the force normal to the disc surface as generated by the calliper pistons would need to be offset from the centreline of the calliper mounting arrangement. To examine the noise propensity of the brake to generate noise with a varying centre of pressure offset on the full sized pads, the contact position between the piston and piston pad was varied by using a 0.75mm diameter silver steel wire inserted between the piston face and pad backplate as shown in Figure 3. The offset of the wire was varied 18mm either side of the piston centre, generally in increments of 6mm but in increments of 3mm at critical points. The wire was supported by a backing plate to prevent local indentation of the wire as a result of the piston wall.

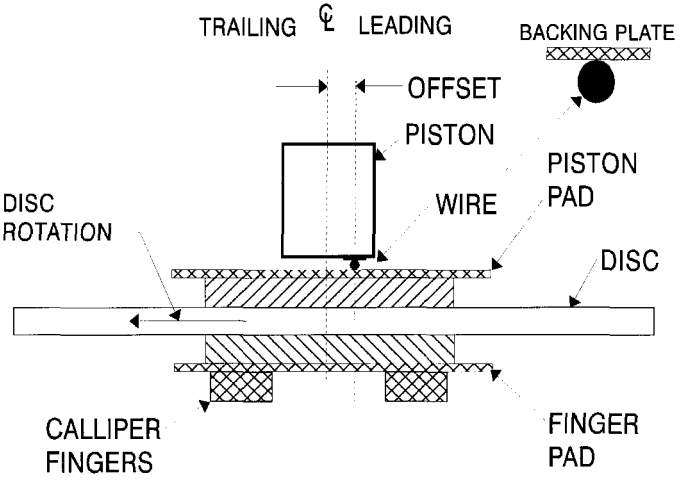

Figure 3 - Diagram showing position of wire to offset contact between piston and pad

The process of testing was, at each wire setting, to increase the disc surface temperature to over 150°C and then to vary the system pressure from 1MPa, in increments of 0.136MPa (20psi) down to zero and then back up to 1MPa. The temperature was then allowed to fall 10°C and the process repeated. During this cycle of events the noise frequency, duration and

amplitude was noted over several revolutions of the disc to ensure a steady situation was being recorded. Between each new wire setting the pad was re-bedded to ensure each test began under similar conditions. The wire was repositioned and the whole test procedure repeated for the next setting. The test variable parameters were therefore the wire offset, the disc surface temperature and the system pressure with the measured results being the frequency of noise generated, the amplitude and the duration. The full test was carried out twice giving a total of 1764 individual results in total.

3.0 RESULTS

The noises generated were often complex with a combination of frequencies, amplitudes and duration over a single revolution of the disc. Because of this complex situation the events were reduced over a single revolution to an equivalent noise level $\left(L_{eq}\right)$ using the expression.

$$L_{eq} = 10\log_{10}\left[\left(1/T\right)\Sigma t_n 10^{0.1L_{pi}} \right] \qquad [1]$$

where T is the time for one revolution, t_n is the period of time over which the noise occurs during one revolution and L_{pi} is the unweighted sound pressure level of that noise.

The results showed that over the test pressure range the noise level was relatively independent of pressure (although frequency would often vary slightly) and therefore an equivalent noise level was calculated over the pressure range using the following expression.

$$L_{eq(tot)} = 10\log_{10}\left[\left(1/P\right)\Sigma p_n 10^{0.1L_{eq}} \right] \qquad [2]$$

where $L_{eq(tot)}$ is the equivalent noise pressure level over the full pressure range, over one revolution of the disc, P is the total pressure range, p_n is the pressure band incremental adjustment over which the noise was measured and L_{eq} is the equivalent noise level for one revolution as calculated in equation 1.

Noise Frequency - The calculations do not account for different frequencies. The initial concern was that the noise falls within the audible range of up to 16kHz. The brake is unstable and generating audible noise - and that is fundamentally unacceptable. The inclusion of frequency may be taken into account using curves of equal loudness – Phon curves.

3.1 Teves FN 54 Calliper

The equivalent noise level results are presented in Table 1 for falling pressure only, the full set of results being available in the complete workings (5).

Table 1 - Total Noise Level Equivalent ($L_{eq(tot)}$) - Teves Brake - Falling Pressure

	OFFSET								
	TRAILING			Zero	LEADING				
Temp(°C)	-18	-12	-6	0	6	9	12	15	18
120	0	0	0	75.2	77.9	0	94.6	0	0
110	62.5	46.7	63.6	70.3	55.7	47.8	95.1	72.8	46.7
100	60.8	72.6	72.1	58.2	79.8	59.4	98.4	94.3	52.2
90	59.4	78.6	82.7	53.4	89.9	64.4	100.3	95.3	61.6
80	63.5	75.8	87.7	55.4	83.8	87.7	100.7	95.7	0
70	77.7	80.3	90.5	78.6	89.0	82.6	102.4	100.8	66.5
60	83.8	80.0	88.2	86.5	85.5	90.0	100.5	101.7	77.1

The affects of the various influencing test parameters can be conveniently considered from the graphical presentations as shown in Figures 4 to 7 which are typical for a reducing pressure situation.

3.1.1 ***Offset/Magnitude for a Range of Temperatures - Figures 4***

The three dimensional plot, Figure 4, shows that as the temperature reduces the tendency for noise to occur increases over the full range of offset wire positions. With regard to this feature it is significant to note (Figure 2) that the coefficient of friction of the pad material rises from 0.45 at 140°C up to 0.65 at 50°C at low sliding speeds. With a leading offset of between 12mm and 15mm the system generally generated noise regardless of temperature, the more stable situations being obtained with a trailing offset arrangement. It is further observed that as the temperature reduces, with a resulting increase in coefficient of friction, the critical offset changes from 12mm at 120°C (μ=0.55) towards 15mm at 60°C (μ=0.7). This is due to a variation in the spragging angle as discussed in Section 4.

The same results are presented as a two dimensional plot in Figure 5 which again readily shows the tendency to generate noise with a 12mm to 15mm leading offset. If the 12mm position is studied in detail it is concluded that when a system is inherently unstable, due to geometric instability, the system becomes insensitive to temperature variations. This is highlighted by a region of converging, or cluster of, curves. The insensitivity is seen more clearly by consideration of the temperature affects for various offsets (Figure 6), the 12mm offset being the upper line.

3.1.2 *Magnitude/**Temperature for the Various Wire Offsets - Figure 6.***

This plot generally confirms the last statement and it is seen with a 12mm leading offset the graph is reasonably independent of temperature. The same is true with a 15mm leading offset up to 100°C when the system rapidly becomes more unstable. Again it must be emphasised that it is a feature of the friction material that at around 100°C there is a change in slope on the μ/temperature graph with the friction increasing at that point and then remaining almost constant over the temperature range of 100 down to 50°C. With the exception of the 12mm

leading offset all the curves tend to replicate the μ/temperature graph in that they become relatively stable below 100°C and generally fall away above that temperature.

It will be noted that the relatively stable position of zero offset (the lower line at 80°C) also tends to be unaffected by temperature although the noise level intensity is rather less. This infers that if the centre of pressure can be maintained at the centre of the pad the system would have a lesser tendency to generate noise and would be more predictable because it is apparently insensitive to temperature affects. In general the further the system is away from the situation of mechanical instability (12mm leading offset) the more it becomes sensitive to temperature variations and the more erratic and unpredictable the noise behaviour becomes.

3.1.3 *Magnitude/**Pressure for a Set Temperature of 70°C - Figure 7.***
These curves again demonstrate that at the unstable position of 12mm leading offset the system is relatively unaffected by pressure variations. They also show that the system is more sensitive to pressure variations as it tends away from the mechanically unstable situation. At the extreme positions of 18mm, probably the most mechanically stable (non spragging) positions (reference Figure 7), the situation is almost erratic.

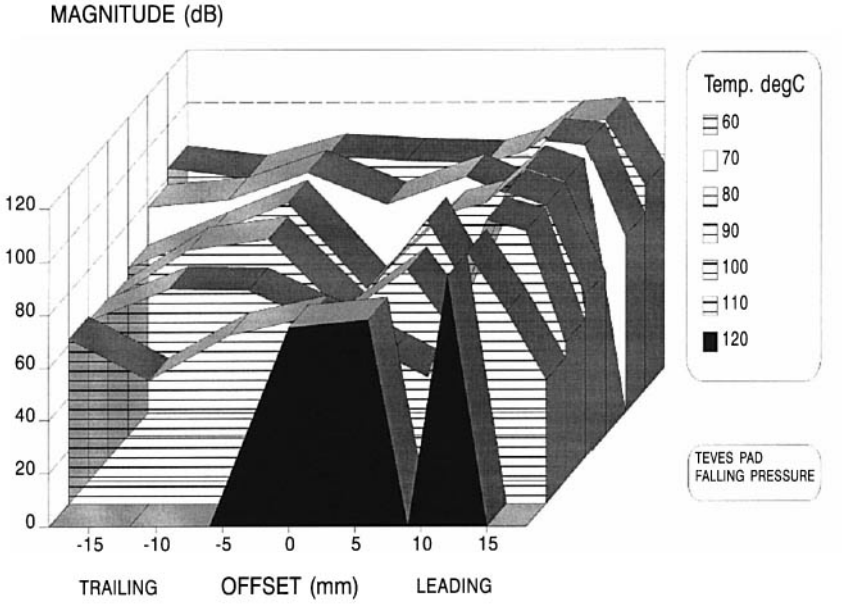

Figure 4 – Offset/Magnitude ($L_{eq(tot)}$) for a Range of Temperatures

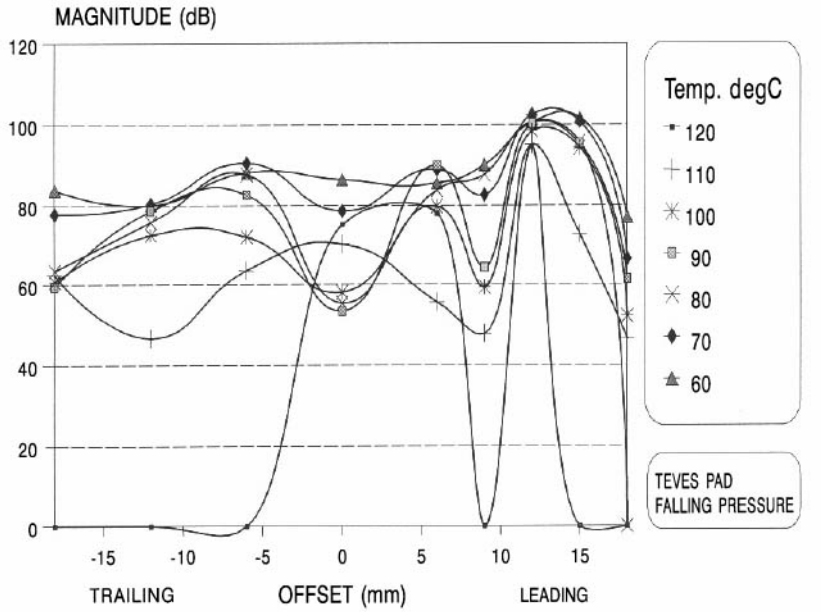

Figure 5 – Offset/Magnitude ($L_{eq(tot)}$) for a Range of Temperatures

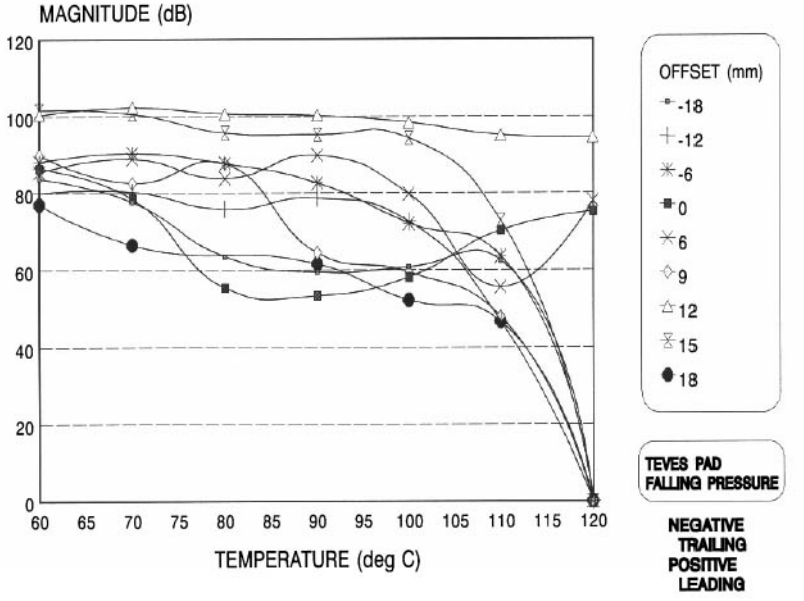

Figure 6 – Magnitude ($L_{eq(tot)}$)/Temperature for Various Wire Offsets

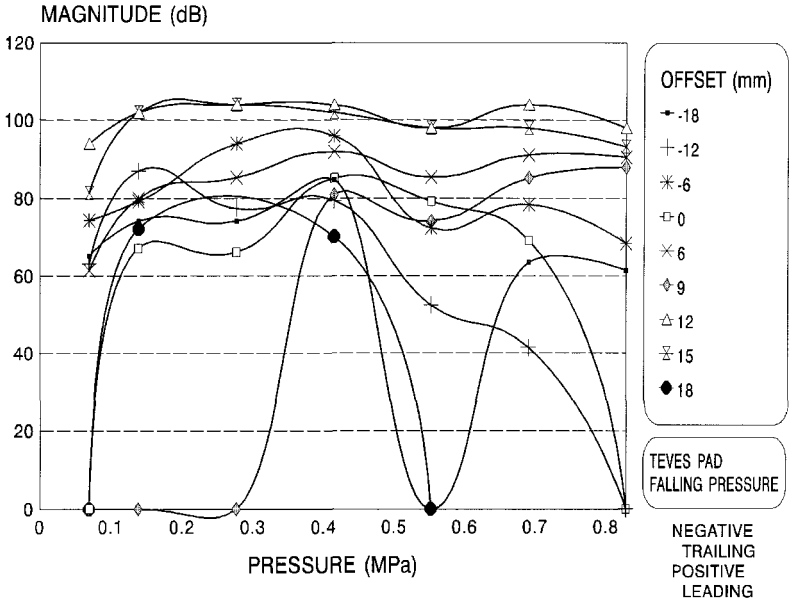

Figure 7 – Magnitude($L_{eq(tot)}$)/Pressure for Set Temperature 70°C

4. CONSIDERATION OF BRAKE GEOMETRY AND THE SPRAGGING ANGLE:

4.1 Alfred Teves Brake (FN Series):

The basic dimensions for the brake system are given in Figure 8 (a & b)and this information enables some calculations to be made relating the brake geometry and spragging affects.

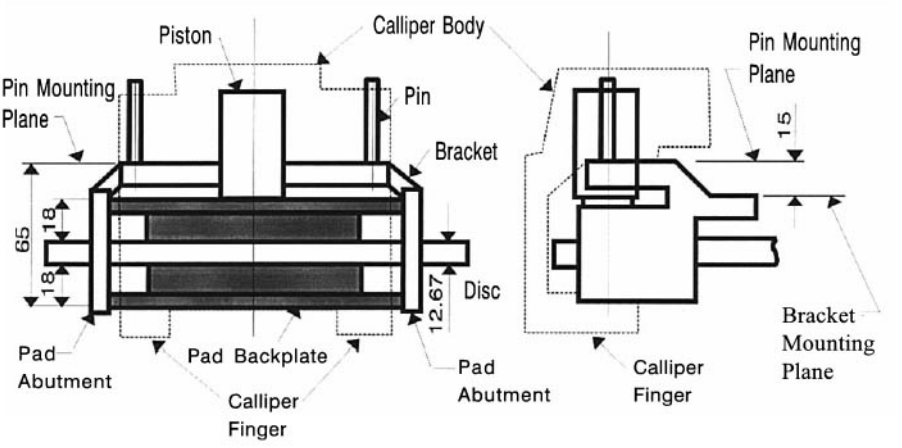

Figure 8a - Basic dimensional details of the Teves calliper

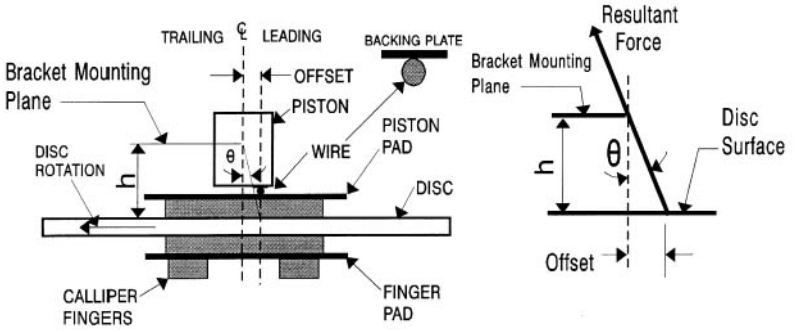

Figure 8 b - Diagram showing wire offset contact position relative to intersect with calliper piston centreline

Figure 8 - Details of Teves sliding fist type calliper

The coefficient of friction, μ, for the material is around 0.7 over the measured temperature range, reference Figure 2, which gives rise to a spragging angle

$$\theta = \text{Tan}^{-1}\mu = 35° \qquad [3]$$

As the critical offset is from 12 to 15mm then from Figure 8b the height "h" is

$$h = \text{offset}/\tan\theta \qquad [4]$$

thus when offset = 12mm $h = 12/0.7 = 17.1\text{mm}$ [5]

and when offset = 15mm $h = 15/0.7 = 21.4\text{mm}$ [6]

Reference to the dimensional details in Figure 8a gives the following distances:

Disc/Piston Pad Interface to Pin Mounting Plane = 65 - (18 + 12.67) = 34.33mm [7]

Disc/Piston Pad Interface to Bracket Mounting Plane = 34.33 - 15 = 19.33mm [8]

and

Piston Pad Backplate to Pin Mounting Plane = 34.33 - 18 = 16.33mm [9]

Piston Pad Backplate to Bracket Mounting Plane = 19.33 - 18 = 1.33mm [10]

Comparing these measured feature distances, [7] to [10], to the calculated value of "h", obtained from the critical offsets in [5] and [6], it is seen that the distance from the disc/piston pad interface to the bracket mounting plane [8] provides a compatible result, almost the exact average of [5] and [6].

Since the forces are generated at the disc/pad interface, with the resultant being the affect of the friction force and the piston normal force, then, allowing for the possible variation in the coefficient of friction, it would appear that noise would tend to be generated more readily when the resultant line of action passes through the intersect between the bracket mounting plane and the centre line of the piston (or normal force), as shown in Figure 8b.

With such an arrangement the calliper would not be subject to twisting, due to a couple being imposed on the calliper mounting bracket, or the pin arrangement, and the resulting displacement would be linear along the resultant force line of action. If this is the case then such a system would not be affected by pad wear since the resulting spragging angle and intersect position would be independent of the pad thickness.

4.2 Lucas Brake (Collette):

Similar results for the Lucas Collette brake are shown in Figures 9 & 10 and are included for completeness.

With this brake the pin mounting plane and the bracket mounting plane are in line and therefore the distance to both features, from the disc/pad interface, is the same at 19.33mm.

The critical offset for the Lucas Girling brake was found to be around 9mm (leading) at the higher temperatures between 70 and 90°C and then increases to 12mm at the lower temperatures as shown in Figure 9 and Figure 10. This trend and the resulting offsets compare reasonable well with the Alfred Teves brake which would infer that mechanical instability relates to the bracket mounting plane which is the same for both brakes. With the Lucas brake it is noticeable that there are two pronounced areas of stability, at ± 6mm, with the areas of instability being at 12mm trailing, zero offset and at the 12 to 15mm leading offset. This affect is almost the inverse of the Teves brake, where there was a tendency towards instability at ± 6mm. This may possibly relate to the pin mounting plane differences, the sliding arrangement, or possibly to the variation in the structural design of the calliper body where the Lucas calliper has a cross beam connecting the abutment fingers.

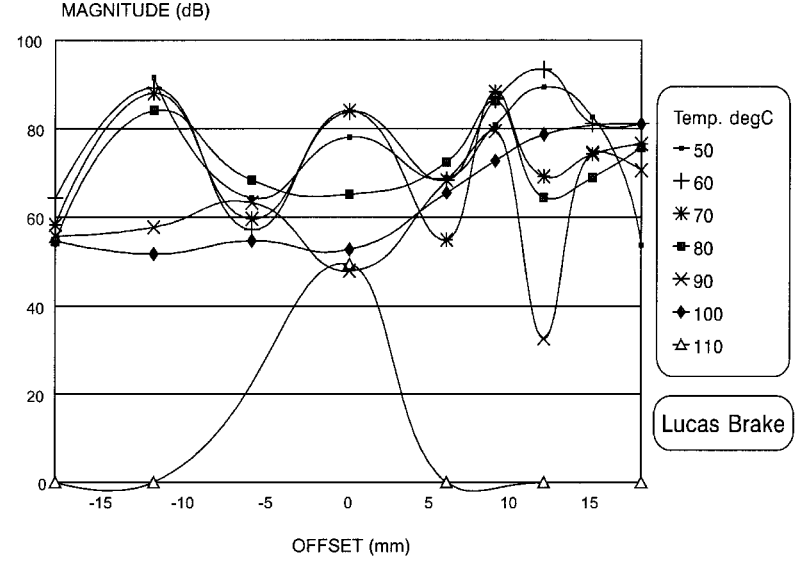

Figure 9 - Offset/Magnitude ($L_{eq(tot)}$) for a range of temperatures - Lucas Brake

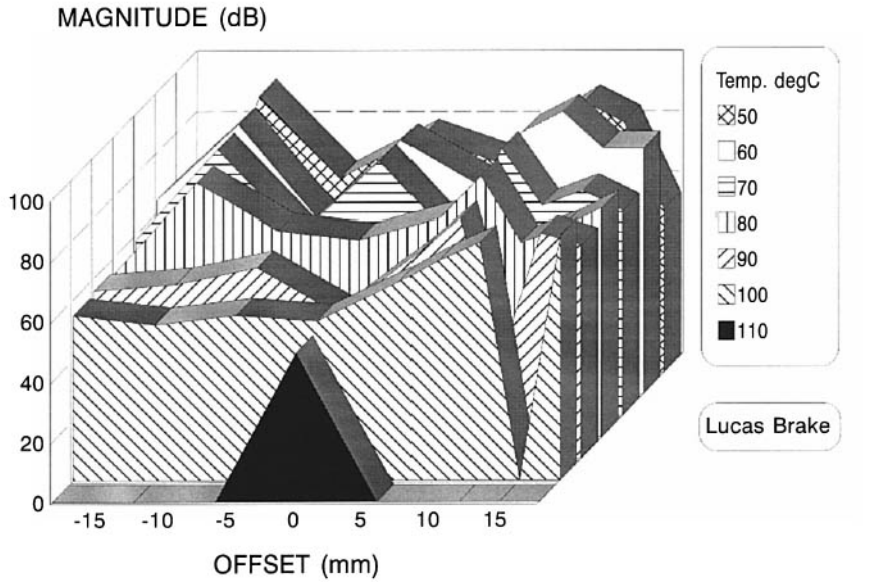

Figure 10 - Offset/Magnitude ($L_{eq(tot)}$) for a range of temperatures - Lucas Brake

5.0 ANALYSIS OF ABUTMENT AFFECTS:

In a practical situation there will be an interaction between frictional affects at the pad abutment, between pad backplate and calliper finger, with the various dimensions of the braking pad when it is in equilibrium. A measure of the relationships involved for the different types of abutment may be established and compared if it is assumed that the various forces acting on the pad are coplanar as indicated in Figure 11. The full analysis is shown in previous work (5) which basically requires taking moments of the forces involved. The summary of the analysis is shown in Table 2 following where δ is the offset of centre of pressure "R" to piston force "N".

These results indicate that a leading abutment requires the highest coefficient of friction between pad backplate ends and abutment finger to achieve equilibrium without offset centre of pressure compensation and was found to be the most unstable arrangement. The combined arrangement required the next lowest coefficient of friction with the trailing abutment needing the lowest. The latter was found to be the most stable arrangement in all the tests.

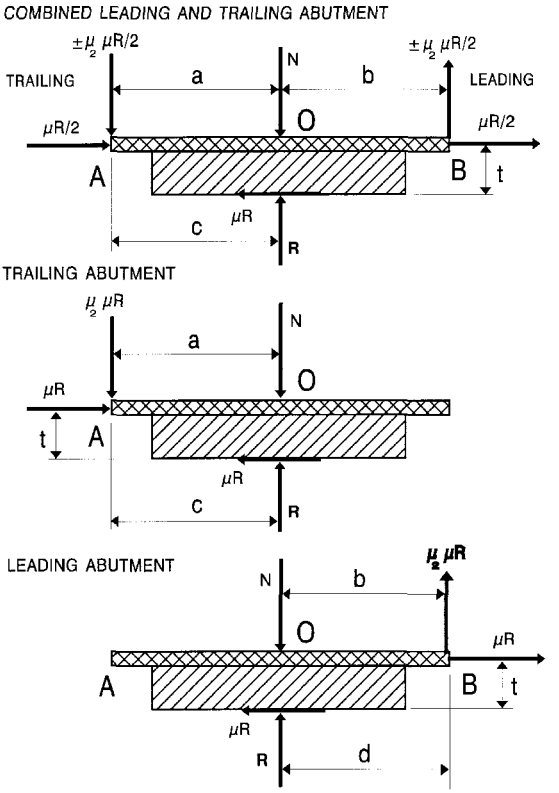

Figure 11 - Free body diagram of brake pad assuming coplanar frictional forces and differing abutment arrangements.

TABLE 2: Summary of analysis of abutment affects giving details of minimum value of μ_2 to avoid offset pressure compensation to achieve equilibrium, δ, and maximum offset as the pad/calliper finger interface coefficient of friction, μ_2, tends to zero.

Abutment	Minimum μ_2	Offset δ	Maximum Offset
Combined	0.214	$\delta = \mu[t-(a+b)\mu_2/2]$	μt leading
Trailing	0.200	$\delta = \mu(t-a\mu_2)$	μt leading
Leading	0.231	$\delta = \mu(b\mu_2 - t)$	μt leading

The above summary of analysis is plotted for varying pad/calliper coefficient of friction for a fixed pad material coefficient of friction and is shown in Figure 12. This shows the trailing abutment to marginally achieve "stability" before the other abutment arrangements as a result of the increase in pad/abutment friction μ_2.

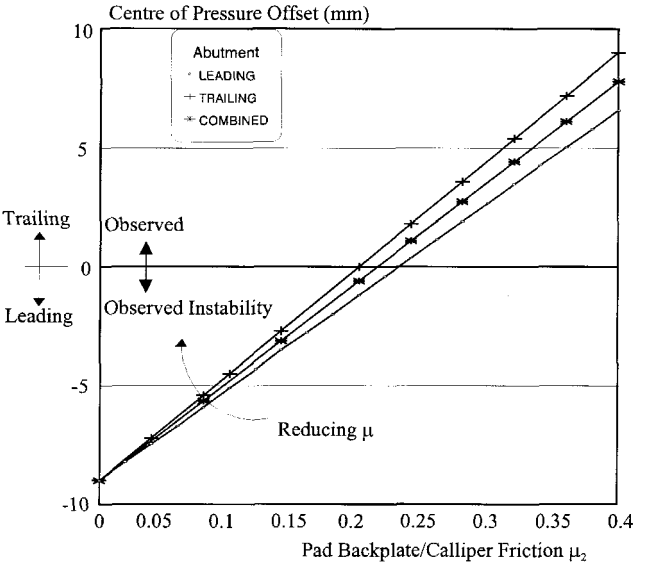

Figure 12 - Affect of centre of pressure offset necessary to maintain equilibrium with varying pad backplate/calliper finger interface coefficient of friction, μ_2.

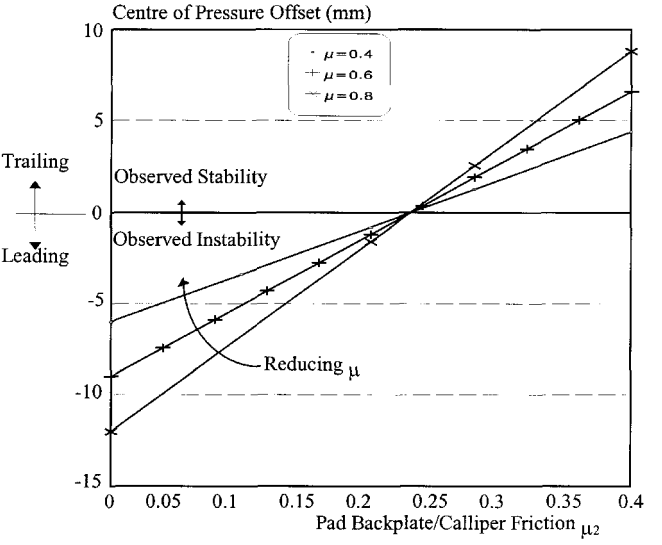

Figure 13 - The affect of reducing pad coefficient of friction, μ, results in tendency towards system stability.

Figure 13 shows the affect of varying the pad material coefficient of friction for a given abutment arrangement and friction level. Generally a low pad material coefficient of friction reduces the maximum leading offset possible although the position of transition from leading to trailing offset is still controlled by the pad/calliper abutment interface friction, μ_2.

In general the brake system need is for a high pad/calliper abutment interface friction yet a low pad material coefficient of friction. The trailing edge abutment was the most difficult system with which to stimulate noise. The conditions were at the extremes of the detected range and were obtained under light braking conditions. With moderately high pressures noise could not be generated.

Abutment affects suggest that mechanical changes may answer the question as to why a brake system may be noisy and "sharp" on a cold morning yet be quiet the rest of the time. When the system is cold the whole system will contract due to the lower temperatures and generally become dimensionally stabilised. In this instance, and dependent upon the initial clearances, there may be a preference for the Teves pad to have a leading abutment (normally a combined abutment pad). Additionally the material coefficient of friction is at a higher value at these reduced temperatures (Figure 2) and thus the tendency towards a leading centre of pressure offset. The system will therefore tend to be noisy but because of the low thermal inertia of the pad and its close proximity to the disc it will increase in temperature faster than the calliper mounting bracket and as a consequence will quickly tend towards a trailing abutment arrangement when the system would then become quiet. Under dynamic road conditions the system would rarely become thermally stable and other variables come into play, such as varying coefficient of friction with temperature, and the whole prediction of noise is less certain.

6. DISCUSSION OF RESULTS:

The test has demonstrated that with this system the creation of a mechanically unstable brake arrangement will readily generate noise irrespective of the changes in the value of the coefficient of friction resulting from the temperature/pressure variations; it becomes relatively independent of external influence. If such a mechanically unstable system were recreated in reality it would be readily described as a bad design and could not be easily improved by modifications in the operating conditions or by the introduction of a different, yet still effective, friction material since this may still not provide a favourable spragging situation to avoid instability.

Equally so an apparently mechanically stable design may perform well within known boundary conditions but would become unstable because of the variables introduced as a result of the friction/temperature/pressure interactions and influences together with geometric changes in the brake. Such a system is designed around the grey area of the mechanically unstable domain and can be readily enveloped within it due to parameter changes (4, 5). Most problematic noisy brake systems would fall in this category, the reason for them falling into the unstable domain being as a result of a combination of many variables, the problem being described as fugitive. A high coefficient of friction material could possibly exacerbate this

problem and this scenario may go some way to provide an additional answer as to why high friction materials generally promote noisy brakes.

7.0 CONCLUSIONS:

- A mechanical instability which is not influenced by temperature or pressure fluctuations is possible within a brake system.
- Pad abutment is important with a trailing abutment being found to be the most stable arrangement.
- The co-planar forces acting on the pad tend to promote a leading offset - at minimum friction for the pad/calliper abutment interface the offset tends towards the critical offset value.
- To promote stability a disc brake requires a high friction coefficient between pad abutment and calliper mounting bracket and a low friction material coefficient.
- The position of the mounting plane for the calliper carrier bracket is important because of its influence over the spragging angle. It needs to be as close to the plane of the disc rubbing surface as possible.
- A deliberate trailing centre of pressure was created on a noisy brake by machining a 10 mm chamfer on the leading end of the pad. When the chamfer reduced to 6 mm, due to natural wear, the noise returned. Re-establishing the 10 mm chamfer recreated a stable and quiet brake.

8.0 ACKNOWLEDGEMENTS:

The author and The University of Huddersfield would like to thank Alcon Components for the opportunity to test the theory on a noisy vehicle.

9.0 REFERENCES:

1. Fieldhouse J.D. and Newcomb T.P. "The Techniques of Double Pulsed Holographic Interferometry Applied to the Problems of Noisy Disc brakes" - Vibration and Noise '95 pp 453-457. An international conference on vibration and noise. April 1995, Venice, Italy.
2. Spurr R.T. "Brake Squeal" Paper No. C95/71, Symposium on Vibration and Noise in Motor Vehicles, IMechE 1971 pp 13-16.
3. Fieldhouse J.D. and Newcomb T.P. "The Application of Holographic Interferometry to the Study of Disc Brake Noise" SAE International Congress and Exposition, Detroit, USA. Paper Number 930805, March 1-5 1993.
4. Fieldhouse J.D. and Newcomb T.P. "An Experimental Investigation into Disc Brake Noise" Paper Number C444-036 "International Conference on the Braking of Road Vehicles" IMechE, London, March 1993 pp 145-159.
5. Fieldhouse J.D. "An Analysis of Disc Brake Noise Using Holographic Interferometry" PhD Thesis, The University of Huddersfield, 1993.

Brake squeal reduction by the design of the interface calliper – friction pads – brake shoe holder

P HEPPES
Gehrden, Germany

ABSTRACT

Usually brake manufacturers reduce brake squeal by the application of noise insulators to the brake pad's backplate. In some cases it is necessary to optimise not just the parameter "damping material" but also to use specially designed noise damping shims combined with other constructional countermeasures at the interface calliper - friction pads - brake shoe holder. First some examples of current designs are given, and after that a new way to achieve a pressure point shift by using special geometries of noise insulators is introduced. Finally the noise reduction which can be achieved by this new design is illustrated by the results of the brake noise analysis carried through during the development of an application.

NOMENCLATURE

A	area (general); effective pressurized part of the contact area of a spared out shim
M_{xx}	moment of delocation referring to the axis x - x
p	pressure
r_i	inner radius of the brake piston's contact area
r_o	outer radius of the brake piston's contact area
x, y	coordinates
y_{cg}	y-coordinate of the centre of gravity of the effective pressurized part of the contact area
y_d	distance in y-direction of the spare-out-line to the axis x - x

1 INTRODUCTION

At the 2nd International Seminar on "Automotive Braking - Recent Developments and Future Trends", it was shown that brake squeal can be reduced significantly by using noise insulators. Because usually the manufacturers of these noise damping shims are involved late into the development process, selecting the best suited damping material is the method mostly applied to optimise noise reduction (1).

However, sometimes a certain noise problem cannot be solved solely by using a plain noise insulator and the selection of the best damping material. In such cases there's need for further constructional countermeasures, which are applied to the sensitive interface calliper - friction pads - brake shoe holder. With an adequate design of a noise insulator being placed in the centre of this interface it is possible to supply these countermeasures efficiently.

First this contribution will give an overview of the "classical" constructions and their aims in influencing the noise occurrence. After that a method to minimize brake squeal by a suitable designed geometry of the noise insulators will be presented in detail.

2 CONSTRUCTIONAL COUNTERMEASURES TO INFLUENCE BRAKE NOISE

Constructional countermeasures to minimize brake squeal may be divided into three groups:

- additional isolation of the brake pads towards contacting brake components ("normal" isolation means the isolation of the backplate from the brake piston or the fist of the calliper by the noise damping shims)
- detuning of the vibration system "wheel brake"
- shift of the overall centre point of the brake force being applied to the brake pad (in short term: pressure point shift)

The first two groups will be shortly introduced in the following subchapters by some examples. Because of additional parts, which have to be mounted to the brake or complicated noise insulator geometries, such solutions normally are very expensive. For this, the third chapter shows methods to realize a pressure point shift, which can be applied in a cheaper way.

2.1 Isolation of the brake pad from brake components in the neighbourhood

An example for additional isolating countermeasures at the contacting areas of the brake pad to the brake shoe holder and the brake piston respectively the calliper's fist, which are very expensive, are shown in figure 1.

Depending on the direction of motion the backplate of the brake pad touches the left or right guide surface of the brake shoe holder. The clips of the damping shim being bent over the front sides of the backplate work as a decoupling mechanism between these tangential guide surfaces. Besides, the lower supporting area of the brake pad is isolated by another pair of clips.

As a further countermeasure to decouple the brake pad from the pressure applying parts of the calliper, the damping shim has bore holes built in placed around the contact areas. These bore holes are filled with a defined amount of grease, and an additional gliding sheet made of stainless steel is clipped to the brake pad. By this expensive solution it is also intended, that the brake pad moves to the guide surface as fast as possible to activate the decoupling-/damping-mechanism of the shim's clips (3).

As another example for getting better isolation by bent clips of a damping shim, the contact areas of springs fitting the brake pad into a defined position should be mentioned.

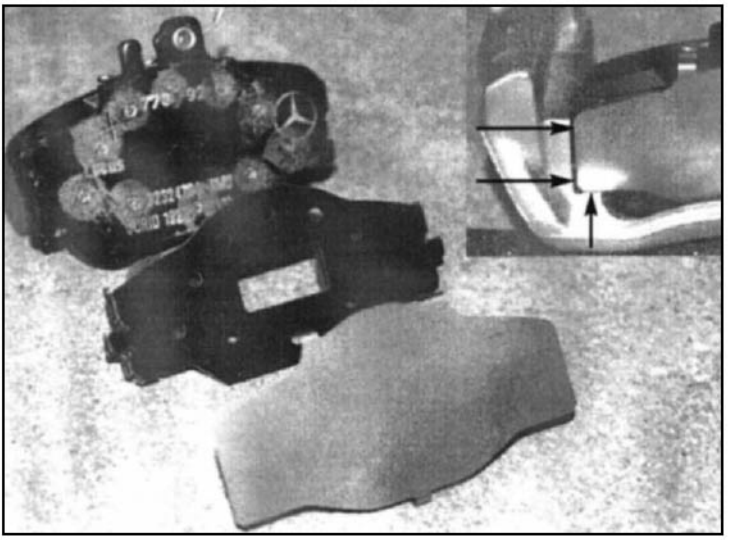

Figure 1: Additional isolating countermeasures

2.2 Detuning of the vibration system "wheel brake"

Under the generic term "detuning of the vibration system wheel brake" come countermeasures which cause that the coupling of the brake pads with the brake piston or the fist of the calliper becomes either as loose or as close as possible. The gliding sheet described in the previous chapter may be an example for a very loose coupling.

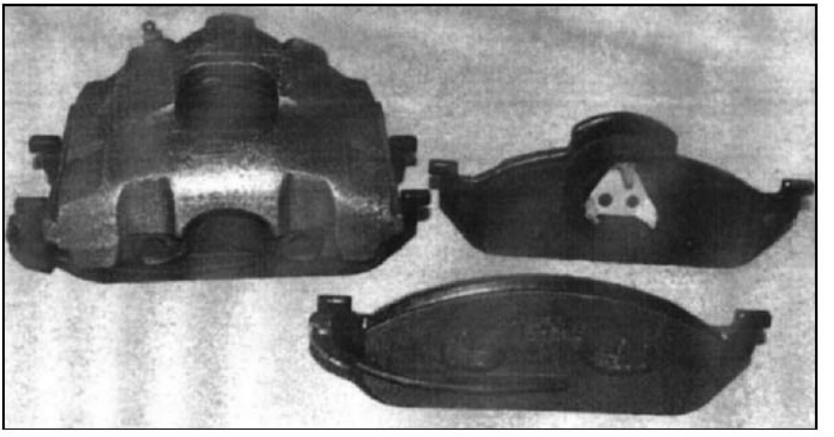

Figure 2: Coupling of the brake pads with calliper and brake piston

A very close coupling can be achieved by piston springs or springs which clamp the outer brake pad to the calliper. An example of such construction is shown in figure 2. An easier variant to realize such kind of close coupling is to use a damping shim coated with pressure sensitive adhesive on both surfaces. Even though the work of extension is not suited best for

the glued joint, the necessary strength is restored by every brake application if high cleanness of the contacting areas of the piston and the calliper was assured during the first assembly of the brake pads. Beside the detuning of the vibration system the close coupling assists the re-setting of the brake pads after brake application and thus helps to avoid brake squeal occurring in an unpressurized brake system.

3 PRESSURE POINT SHIFT BY NOISE INSULATORS AND GLIDING SHEETS

3.1 Series applications

During the brake application a friction force appears between the front side of the brake pad's backplate and the guide surface of the brake shoe holder. This friction force retroacts with a lever-arm equal to half of the distance of the brake pad guides towards the force of pressure which is passed into the brake pad. By the moment induced by this friction force an asymmetric distribution of the pressure is caused within the contact area between friction material and brake disc (given, that for economical reasons the brake piston shall be arranged symmetrically to the brake pad). This effects not only unfavourable wear characteristics but also leads to a higher amount of brake squeal. Therefore, it is usual to apply different constructional measures which aim to create a moment retroacting to the moment induced by the friction force (4). One possibility is to use noise insulators and gliding sheets which are spared out as shown in figure 3. Other countermeasures may be to built in a step in the contact area of the brake piston or to use two pistons with different diameters.

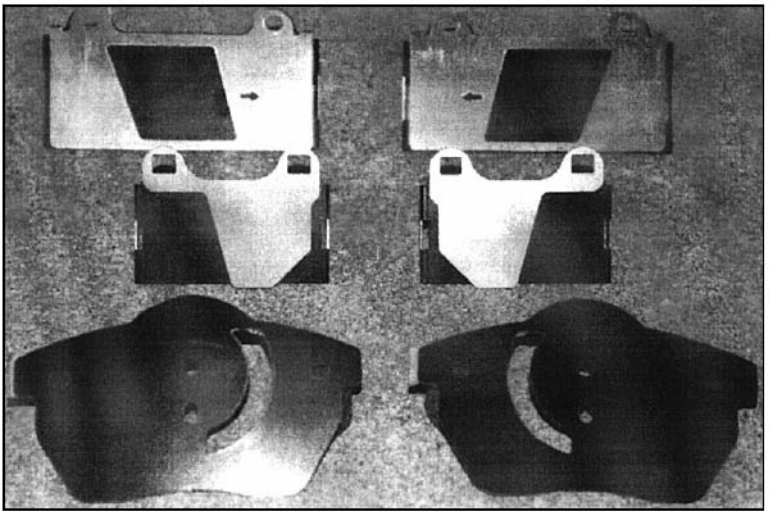

Figure 3: Noise insulators and gliding sheets for pressure point shifting

3.2 Estimation of the grade of efficiency and selection of the shift direction

The question how to select geometry and orientation of the areas missed out of the noise insulator or gliding sheet cannot simply be answered by computing. One reason is that the friction force within the guide surface depends on the tolerances of the parts as well as on the brake pressure applied and therefore the moment to compensate varies. In addition to this the

elasticity of the wheel brake during brake application cannot be calculated or measured easily (4).

Therefore in the following a method based upon simplified edge conditions is presented, which shall help to estimate the relative grade of efficiency of differing geometries. By this kind of estimation it should be possible to select such a low number of variants that their effect in brake squeal reduction can be proved by dynamometer or road tests.

For a first approach in determining the moment of dislocation which can be applied referring to the axis of symmetry of the projection of the piston's contact area, some terms used in the following equations are introduced in figure 4. To simplify the computation the pressure within the contact area should be assumed to be constant. This assumption is based upon the consideration that the stiffness of the guide of the brake piston within the calliper is much higher than the stiffness of the guide of the brake pads in the brake shoe holder. Therefore the moment which is forced by an asymmetrical contact area between brake piston and brake pad will be compensated mostly by the guide of the brake piston and for that the local differences in the pressure distribution of the contact area become small.

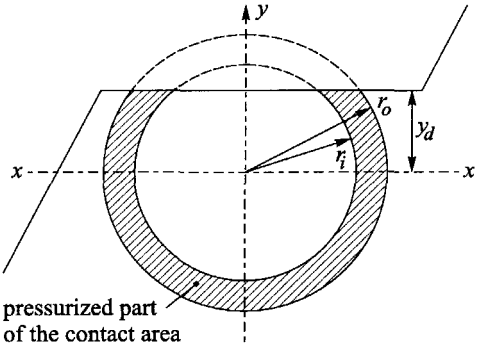

Figure 4: terms and geometry of a linear spared gliding sheet

The following derivation will be given by the example of the geometry of a linear spared gliding sheet as shown in figure 3 in the middle and in the background. It also may be transferred to any arbitrary geometry of the contact area of gliding sheets or damping shims.

The resulting moment which the brake piston applies referring to the axis x - x generally is given by

$$M_{xx}(y_d) = \int_{y=-r_o}^{y_d} p \cdot y \, dA(y) \qquad (1)$$

Using the mentioned assumption of the pressure being constant in the piston's contact area, p hasn't to be considered for integration and one can make use of the properties of symmetry: the parts of the pressurized contact areas placed symmetrically to the axis x - x have moment components which are equal but in an opposite direction. Therefore the resulting moment of dislocation is equal to that component of moment which results from the pressurized part of the contact area being placed opposite of the unpressurized part. This resulting moment of dislocation may be computed e. g. by setting

$$dA(y) = x(y)\, dy \tag{2}$$

$$\text{with} \quad x(y) = \begin{cases} 2 \cdot \sqrt{r_o^2 - y^2} & |y| \in [r_i, r_o] \\ 2 \cdot \left(\sqrt{r_o^2 - y^2} - \sqrt{r_i^2 - y^2} \right) & |y| \in [0, r_i] \end{cases} \tag{3}$$

and integration of equation 1. Another possibility is to substitute the integral of equation 1 by the term

$$y_{cg} = \frac{1}{A} \cdot \int_{(A)} y\, dA(y) \tag{4}$$

known from the way of calculation of the area's centre of gravity (5). With this the moment of dislocation formally equals to

$$M_{xx} = p \cdot y_{cg} \cdot A \tag{5}$$

In this term y_{cg} and A are functions of the dimensions r_i, r_o and y_d, which one can find in standard works like (6). For linear spared gliding sheets as shown in figures 3 and 4 after some computation the resulting moment of dislocation follows as

$$|M_{xx}(y_d)| = \begin{cases} \frac{2}{3} \cdot p \cdot \left[\sqrt{\left(r_o^2 - y_d^2\right)^3} - \sqrt{\left(r_i^2 - y_d^2\right)^3} \right] & |y_d| < r_i \\ \frac{2}{3} \cdot p \cdot \sqrt{\left(r_o^2 - y_d^2\right)^3} & r_i \le |y_d| \le r_o \end{cases} \tag{6}$$

The maximum moment of dislocation results for the shape of the contact area being the half of a circular ring (which means $y_d = 0$ in figure 4) as

$$|M_{xx,max}| = \frac{2}{3} \cdot p \cdot \left(r_o^3 - r_i^3 \right) \tag{7}$$

To show the grade of efficiency of a selected geometry independent of the applied brake pressure p, the moment of dislocation from equation 6 will be referred to the maximum moment from equation 7.

Figure 5 shows the dependence of the referred moment of dislocation on the variation of the geometry for some examples of brake piston dimensions. This referred moment of dislocation may also be called "grade of efficiency of a pressure point shift". Additionally figure 5 shows some proposals for varying the dimensions of the parts to miss out of the gliding sheet following the principle of increasing or lowering the grade of efficiency by equal sized steps.

The direction of the pressure point shift can be selected by the following way: before and directly after the first dynamometer test - which is usually run without noise insulators or with a standard plain noise insulator to indicate the initial amount of brake squeal - the thickness of the friction material is measured and the resulting thickness worn is drawn over the friction

area as a kind of contour lines. Now the axis x - x to which the moment of dislocation will be applied has to be oriented parallel to the averaged direction of these contour lines.

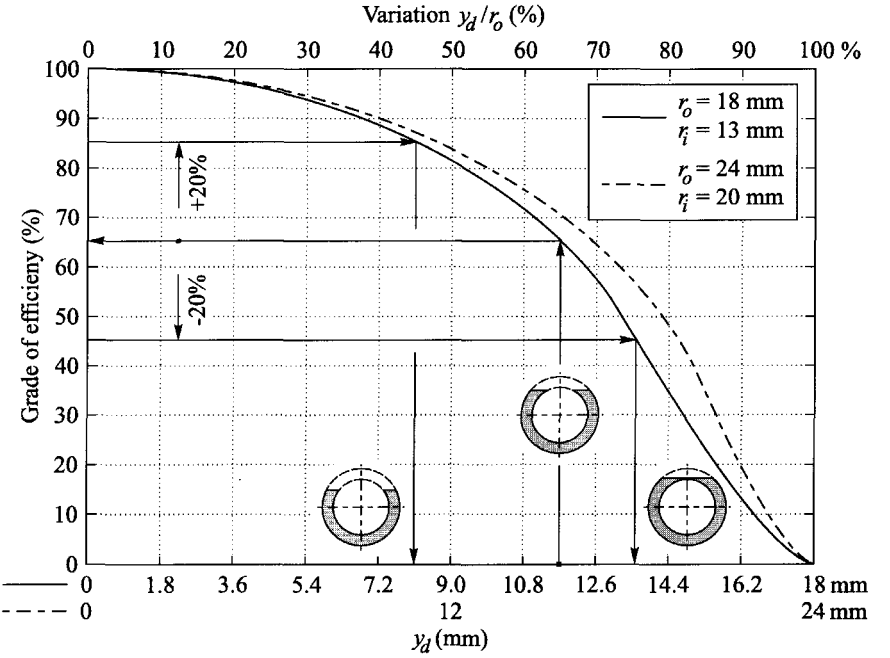

Figure 5: Dependence of the moment of dislocation on the geometric dimensions

3.3 New geometries and their grade of efficiency

With geometric shapes used in current series applications it sometimes happens that the brake pad tilts relative to the brake piston. This means that the contact area between brake piston and damping shim or gliding sheet reduces to an extended contact at three places. At these reduced contact areas the pressure becomes very high. Having an elastomer coating at such contact areas it will be abrased fast due to this high pressure, mostly combined with vibrational motions. Furthermore, if a damping shim such as in the foreground of figure 3 is used without an additional gliding sheet, direct contact of the brake piston and the brake pad's backplate becomes possible which ruins the isolating effect of the damping shim.

To solve this problem new geometric shapes of spared out damping shims have been developed. These shapes applied as patent (7) have the advantage that they prevent the brake piston contacting the brake pad's backplate directly. Figure 6 shows the grade of efficiency which can be reached by the new shapes compared to the ones currently used. To be able to compare the different geometric shapes directly the horizontal axis is made dimensionless by referring the parameter which is varied to the difference between the lower and upper limits of contact areas remaining ("lower limit" always means that the half of a circular ring is missed out of the damping shim, "upper limit" means the contact area is a full circular ring). The grade of efficiency is outlined the same as described for figure 5. Also figure 6 was computed for typical dimensions of the brake piston.

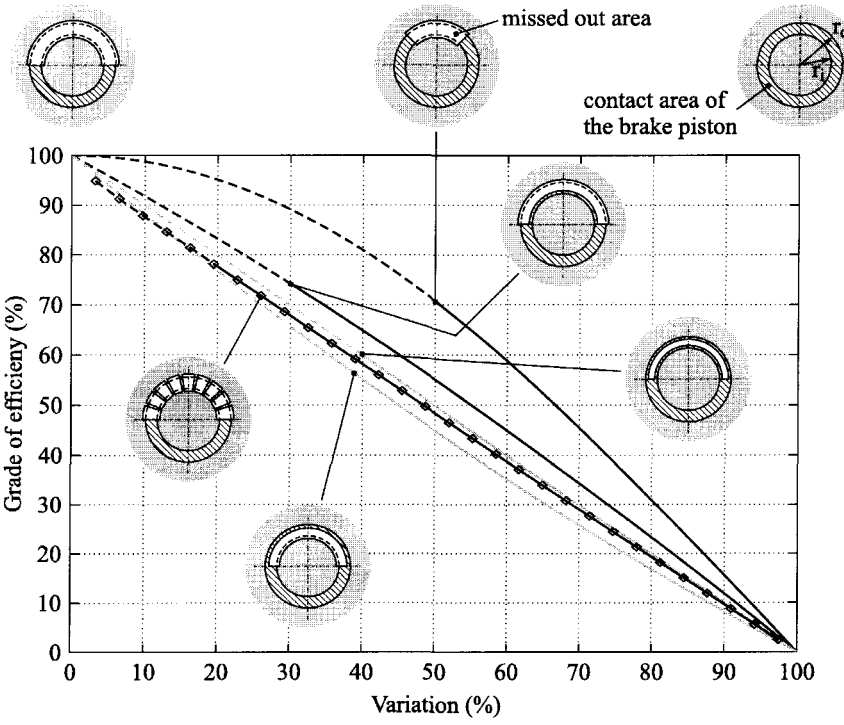

Figure 6: Efficiency of new geometries for a pressure point shift

The geometric parameters being varied are the inner or outer radius of the brake piston's contact area or both radii at the same time, but always making sure that the brake piston cannot contact the brake pad's backplate directly; another way to achieve this is to leave thin bridges in the missed out area.

In figure 6 the lines for the different shapes become dashed beyond certain levels of efficiency. For the given dimensions of the brake piston at the transition the limit is exceeded where the request of preventing contact can be certain to be fulfilled considering usual work tolerances. Because with the new geometric shapes a higher percentage of the contact area can be spared out until the limit is exceeded, nearly the same grades of efficiency will be reached as with the damping shims spared out in the "classical" way.

4 DEVELOPMENT EXAMPLE

Finally, the efficiency in brake squeal reduction of the measurements described in the previous chapters will be shown by an example. Figure 7 shows the results of the characteristic steps of this development.

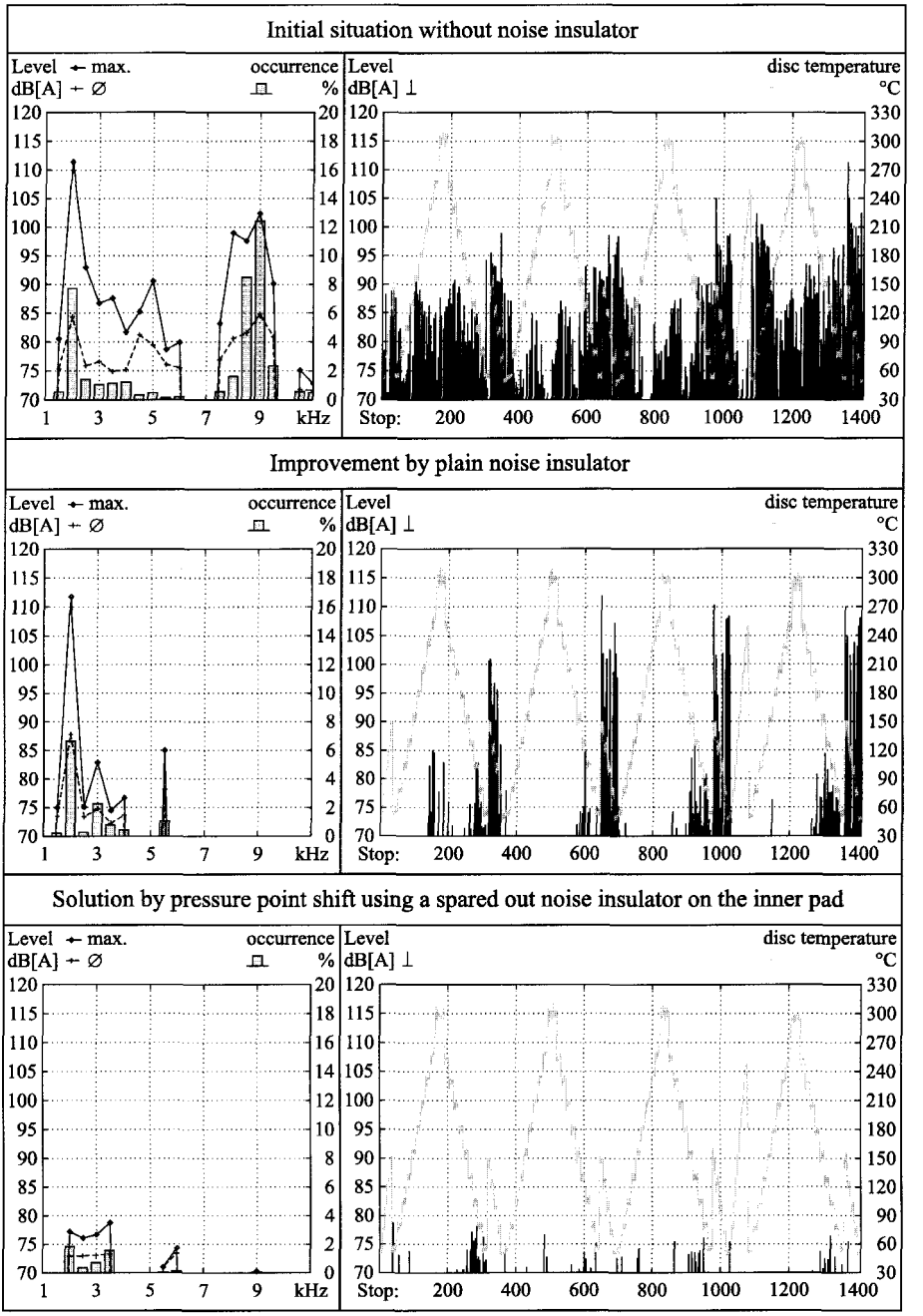

Figure 7: Test results

Initially - without noise insulator - the brake was very noisy, refer to the frequency of occurrence as well as the high level of the brake squeal. The dominant brake squeal occurred within frequency ranges around 2 kHz and 8.5 to 9 kHz and reached levels up to 110 dB[A]. All tests were run according to a standard noise search program, so from the temperature curve it becomes obvious that the high-level noise occurred especially when driving alternately forward and reverse with generally decreasing brake disc temperature.

Using plain noise insulators out of standard damping materials the brake squeal problem within the upper frequency range could be eliminated completely, but the 2 kHz squeal was still occurring at high noise levels. Even after an extensive variation of the damping material that problem couldn't be solved.

After having driven some brake pads several times, non-uniform wear of them became obvious. For the following test to the inner pad additionally a thin damping shim was applied which had been missed out as shown in figure 6 on the right hand within the graph's frame. The shift direction had been selected as explained at the end of section 3.2. Finally, with this variant the 2 kHz problem could be solved. The lower part of figure 7 shows the corresponding results of the noise analysis: with a low frequency of occurrence and an average level of about 75 dB[A], the remaining sound will not be audible within the car.

5 ACKNOWLEDGEMENTS

The author would like to thank the VDI-publishers for their kind permission to transfer essential excerpts of reference (2) into the English language.

6 REFERENCES

(1) Heppes, P.: Noise insulators for brake squeal reduction - influence and selection of the damping material. In: Barton, D./Haigh, M. (editors): The Second International Seminar on Automotive Braking; Professional Engineering Publishing Limited, Bury St. Edmunds and London, UK, 1998, p. 15-26.

(2) Heppes, P.: Gestaltung von Sekundärdämpfungsblechen zur Verringerung des Bremsenquietschens. In: VDI-Berichte 1491 - Maschinenakustik '99, ed. by Verein Deutscher Ingenieure. Düsseldorf: VDI-publishers, 1999, p. 273-284 (first-publication).

(3) Bremsbelag für eine Teilbelag-Scheibenbremse. German patent DE 41 42 196 C1 dated 08-April-1993.

(4) Burkhardt, M.: Fahrwerktechnik: Bremsdynamik und Pkw-Bremsanlagen. Vogel publishers, Würzburg, 1991.

(5) Hahn, H. G.: Technische Mechanik. Carl Hanser publishers, Munich, Vienna, 2nd ed. 1992, p. 77.

(6) Beitz, W./Grothe, K.-H. (editors): Dubbel – Taschenbuch für den Maschinenbau. Springer-publishers, Berlin, Heidelberg, New York, 19th ed. 1997, p. B14.

(7) Dämpfungsblech. Publication of German patent application (Offenlegungsschrift) DE 197 56 553 A1 dated 08-July-1999.

A study of initialization and inhibition of disc-brake squeal

M ERIKSSON, P BERGMAN, and **S JACOBSON**
Department of Materials Science, Uppsala University, Sweden

SYNOPSIS

Brake squeals arise from coupled vibrations of the brake components, excited by friction forces acting at the interface between the brake pads and the disc. In this investigation the onset and suppression of such vibrations have been controlled by the use of a brake disc with a grit-blasted sector, a surface treatment that earlier, when applied to a whole disc, has been shown to lower μ and to inhibit brake squeal (1).

When testing the disc with a grit-blasted sector, squeal was always fully inhibited, at the latest, when the whole pads were sliding against the sector. Squeal was then regenerated, at the earliest, when the whole pads were again sliding against untreated disc surface. Thus, brake squeal can be maintained with less than the whole pad sliding against disc surface with a high coefficient of friction but not initialised with less than the whole pad surface experiencing a high coefficient of friction.

When the surface conditions promoted squeal generation, the squeal was initialised in less than 0.05 seconds. Then, the squeal diminished almost as rapidly, when the excitation mechanism was prevented. These results show that the activation time often experienced in field tests is due to slow changes in the contact conditions between disc and pads rather than due to slow mechanical initialisation of the squeal.

Key words: Brake squeal, Disc brake, Surface topography

1 INTRODUCTION

Automotive brakes have to fulfil a complex set of requirements, with safety being the most important. The brakes have to work safely and predictably during all circumstances, which calls for a stable friction level regardless of temperature and environmental factors. However, as modern brake systems generally have sufficient braking performance, the comfort and absence of brake squeal have become increasingly important.

The brake squeal phenomenon has puzzled many engineers and scientists over the years and still there is very little understanding of the initiation of brake squeal, especially regarding the friction contact conditions on the microscale. Mainly, the problem has been studied on a macroscopic level (2-9)

The present authors have recently shown that small pits covering the disc surface can prevent the excitation of brake squeal (1). The pits were produced by grit blasting the whole disc surface, which was then run in to a smooth finish, but covered with pits.

The coefficient of friction was reduced some 25-30% by this treatment. During the initial period of the test, when the coefficient of friction was below 0.4, no squeal occurred. After some period of wear however, squeal was starting to be generated, and after a short while the system generated as much squeal as a system with a normal smooth disc. It was assumed that the friction reduction was the primary mechanism behind the squeal prevention.

In the present investigation, the squeal preventive action of grit blasting the disc is utilised to perform a unique study of the initialisation and inhibition of squeal. To achieve this, a sector of the disc was treated and the variation in squeal generation due to the repeated passage of this sector between the brake pads was closely monitored.

2 EXPERIMENTAL

2.1 Test rig

The tests were performed in a rig developed for squeal testing of disc brakes (10). It basically consists of a complete front wheel suspension including brake, wheel and drive shaft from a Volvo S/V 70, see figure 1. The brake assembly utilises the standard single piston sliding calliper and the standard brake disc. Brake-line pressure and rotational speed can be adjusted independently and a number of parameters including disc surface temperature, friction force, brake-line pressure and noise level can be measured during the tests.

2.2 Materials

A set of brake pads, well known to generate squeal over a wide range of temperatures and brake pressures, were tested against a standard ventilated grey cast iron disc. The pad friction material had a formulation close to that of the production pads.

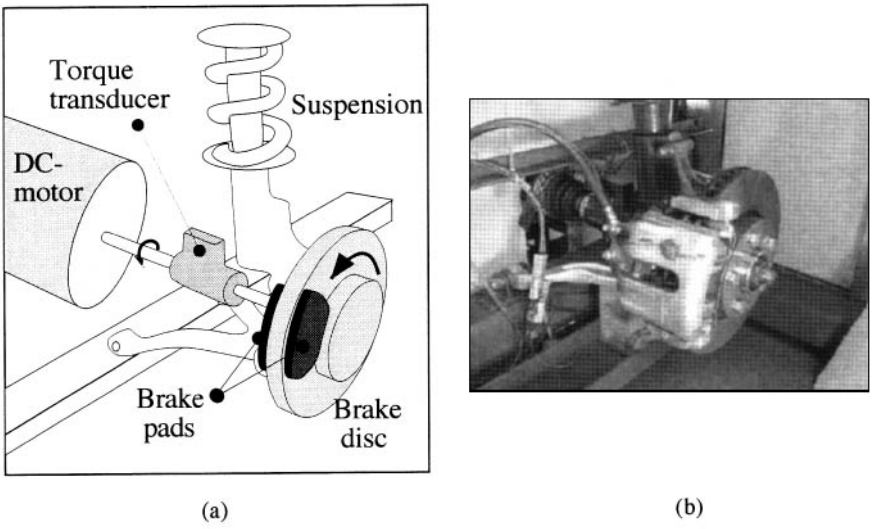

Fig. 1. (a) Schematic of the test rig. An electric motor drives the brake disc via the original drive shaft. (b) Photography of the rotor, calliper and drive shaft. During testing a wheel was fitted on the hub.

2.3 Pre-treatment of the brake components

The disc and the pads were first subjected to a run-in procedure of 210 brakings at brake line pressures between 3 and 24 bar. This procedure has previously been shown to generate well run-in disc and pad surfaces with a stable friction over time. After the run-in procedure, a 108° sector of the disc was grit-blasted with angular SiC-particles producing a rough surface, see figure 2. This surface treatment has been shown to prevent brake squeal when applied to the whole disc (1). The run-in procedure was then repeated to remove sharp edges on the grit-blasted portion of the disc, leaving a rather smooth surface with small pits. An example of the grit-blasted disc surface after the run-in and test is shown in figure 3. During the starting stage of running in, the surface roughness was estimated to Ra = 4 μm, measured over an area of 0.9 x 1.1 mm. The surface area in figure 3, measured after the test, had a roughness of Ra = 1.6 μm and the run-in surface prior to grit blasting had a roughness of Ra = 0.3 μm. The surface roughness values were measured from silicon rubber replicas using vertical scanning white light profilometry.

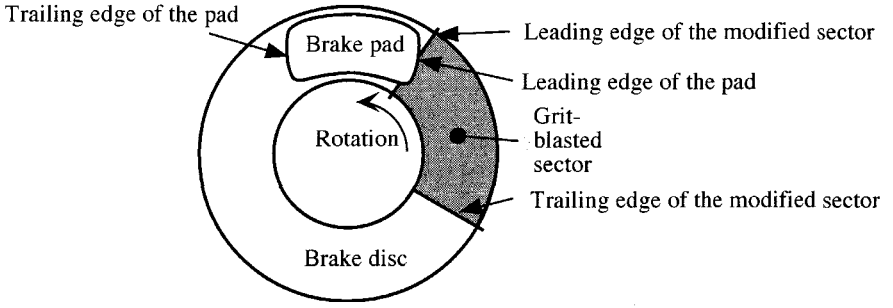

Fig. 2. Schematic view of the brake pad and the brake disc with the grit-blasted sector.

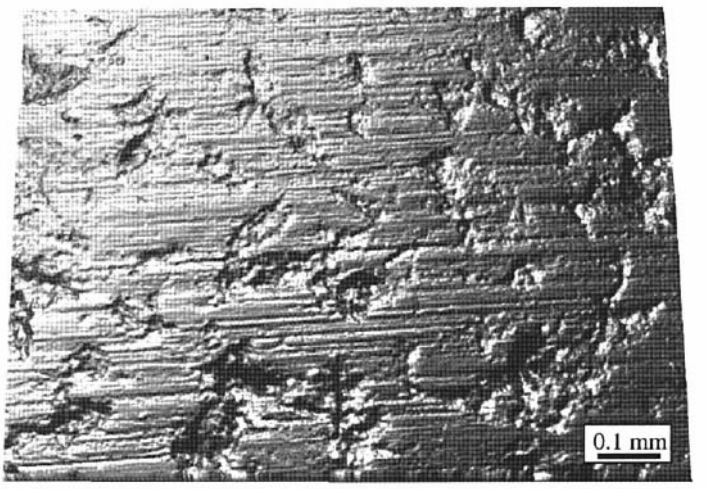

Fig. 3. Grit-blasted disc surface measured after the test (white-light profilometry). The larger pits are 15-20 μm deep while the smaller and shallower pits are 1-5 μm deep. Sliding direction from left to right.

2.4 Measurement set-up

In order to keep track of the disc position four magnets were placed along the rim of the wheel. A coil was mounted so that an electric current was induced each time a magnet passed. The magnets were placed so that four specific disc positions were indicated, see figure 4.

When a brake squeal occurs, both the brake disc and the pads vibrate with the frequency of the squeal. The pad vibration was found to be a more reliable source for identifying squeals than were the acoustic measurements, as the latter also picked up sounds from the electric motor and the transmission. For this reason the pad vibration (squeal) was measured with a small accelerometer mounted in the centre of the back-plate on the finger side pad (the pad on the side of the disc facing away from the drive shaft, cf. figure 1). Preliminary results showed that the vibration of the pad was well correlated to the emitted sound, concerning amplitude and frequency.

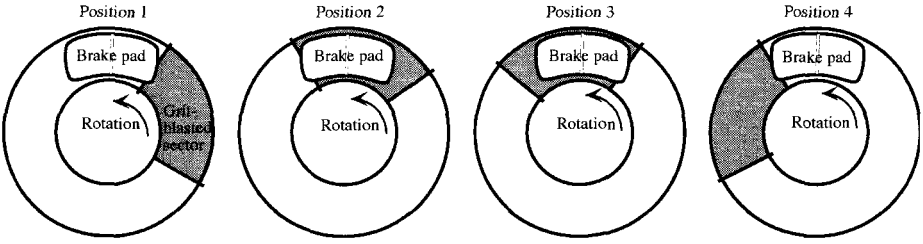

Fig. 4. The four electronically indicated positions of wheel rotation: 1. The leading edge of the pad passes the leading edge of the grit-blasted sector. 2. The trailing edge of the pad passes the leading edge of the sector. 3. The leading edge of the pad passes the trailing edge of the sector. 4. The trailing edge of the pad passes the trailing edge of the sector.

The accelerometer signal was analogically collected, band-pass filtered (1-20 kHz), amplified and finally rectified, giving a DC-signal equal to the rms.-value of the pad vibration amplitude. This DC-signal was sampled by the measurement computer at 100 Hz sampling rate, parallel to the rest of the measured parameters, see section 2.5. This signal will be referred to as the "vibration level". Note that, to represent a quantitative value of the brake squeal, the measured vibration level is the envelope of the vibrations between 1 and 20 kHz, only.

2.5 Test procedure

The test procedure was designed to give detailed information about how the brake-line pressure, friction coefficient and pad vibration varied as the grit-blasted sector repeatedly passed between the pads. The test consisted of 120 brakings, each 14 seconds long, with brake-line pressures between 3 and 8 bar. Each braking was preceded by a 242 seconds long cooling period. During each braking the rotational speed was reduced either from 3 to 2 rps or from 2 to 1 rps. The brake-line pressure, torque, vibration and position signals were sampled with a frequency of 100 Hz. To reduce the amount of collected data, the sampling periods were limited to 2 seconds followed by 5 seconds unrecorded periods during each braking.

In addition, manual tests were performed at lower, constant speeds. During these tests the brake-line pressure was manually adjusted to generate squeal.

3 RESULTS

The results from the brake squeal tests are exemplified in figure 5, showing the brake-line pressure, coefficient of friction, vibration level and the overlap between brake pad and grit-blasted sector variations over time.

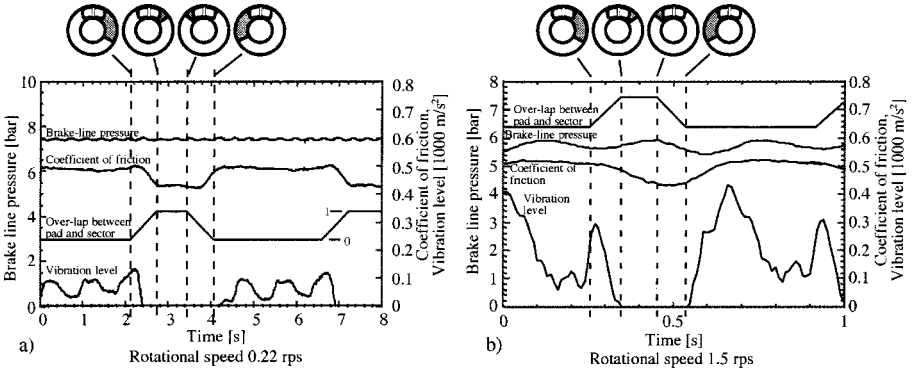

Fig. 5. Brake-line pressure, coefficient of friction, vibration level and overlap between pad and grit-blasted sector during a short time at a) 0.22 rps and b) 1.5 rps. Note that the vibration level is a band-pass filtered and rectified measure of the pad vibration between 1 and 20 kHz, a value indicating the squeal noise level within this frequency interval.

A number of effects were observed to be independent of brake-line pressure and rotational speed. These are discussed below.

The most obvious effects originating from the passage of the grit-blasted sector between the pads were the squeal inhibition and the decrease in friction coefficient during the end of and just after the passage.

It was observed that the vibration level (i.e. the squeal) was reduced to zero at the latest when the disc reached position 2 (i.e. the trailing edge of the pad had passed the leading edge of the sector). Further, the vibration level did not resume before position 4 was reached (i.e. when the whole pad had reached the untreated disc surface).

At the higher speed, the vibration of the pad increased very rapidly when resuming the squealing contact conditions. Generally, this increase was faster than the decrease when the sector entered between the pads. The vibration reached 50 % of its maximum value in approximately 0.05 seconds at 1.5 rps, corresponding to a sliding distance of half a pad length.

At the lower speed, the friction coefficient dropped significantly each time more than half of the pad had entered the grit-blasted sector. Note that at this position the vibration level has already decreased to zero, as in the case of the higher speed. The coefficient of friction reached its lowest level when the whole pad was sliding against the grit-blasted surface. The friction then started to increase when half the pad had left the sector at 0.22 rps and when the whole pad had left the sector at 1.5 rps. Further, at 0.22 rps the friction had stabilised at the higher level when the pad had been sliding against normal disc surface for half a pad-length. At 1.5 rps the stabilisation of the friction required more than one pad length extra sliding distance.

The inhibition of squeal occurred at positions when the friction coefficient was just below 0.5. This value is some 20% higher than the threshold level published by Bergman et al. (1) for the same type of pad run against discs where the whole surface had been prepared by grit blasting.

During the manually operated tests, the intermittent vibration was confirmed through hearing as being well correlated to brake squeal. The audiable noise was inhibited once each revolution when the treated sector passed between the pads.

4 DISCUSSION

The very rapid increase of the vibration level found after each passage of the grit-blasted sector indicates that squeal is generated almost instantaneously when the surface conditions are right. Further, the internal damping of the system seemed to decrease the vibration almost as rapidly, when the excitation mechanism was prevented. This means that the excitation mechanism has to be constantly active to keep a brake squealing and powerful enough to overcome the internal damping of the system. It also indicates that the short delay, typically a few seconds, from applying the brake pressure until a squeal has become fully developed is just the time needed for the surfaces to adapt to each other and for "squealing surface conditions" to evolve. This delay is often experienced in field tests when trying to provoke brake squeals.

A previous investigation by Bergman et al. (1) has shown that the coefficient of friction is of major importance for the generation of brake squeal. For the same type of pad as used in the present test, a threshold value for squeal generation was found at μ=0.4. Squeal did not occur below this friction level. Hence, the low friction against the grit-blasted sector may be the major factor explaining why squeal is not generated. However, in the present investigation the vibration level (squeal) decreased to zero when the friction coefficient was reduced to just below 0.5. This higher level as compared with the results for continuous low friction sliding (1) may be indicating that an uneven and changing friction distribution along the pad is enough to inhibit brake squeal.

The whole grit-blasted sector needs to be outside the pad for squeal to be initialised. Further, the squeal can maintain its intensity almost until the sector has entered under the whole pad. This indicates that “squealing conditions”, including a high coefficient of friction, have to be fulfilled over the entire pad surface, for squeal to be initialised. However, once initialised the squeal can maintain its intensity with only a small part of the pad fulfilling these squealing conditions.

5 CONCLUSIONS

- Squeal is generated almost instantaneously when the contact conditions are right and is maintained only if the contact conditions are continuously promoting it. When the excitation mechanism ceases the squeal diminishes very rapidly due to the effective damping. The excitation mechanism thus needs to be quite powerful to be able to overcome the internal damping of the system.

- The braking time often needed to activate squeal in field tests is due to relatively slow changes of the contact conditions, rather than any other mechanism for vibration initialisation. The surfaces need to run in against each other in order for the coefficient of friction to increase to a level where squeal is generated.

- A brake disc prepared by grit blasting a sector with coarse SiC grits has proven a powerful tool for studies of initialisation and inhibition of brake squeal. The contact against the prepared sector was always silent. Thus, during otherwise squealing conditions the sector in effect worked as an off switch for brake squeals.

- When using the brake disc with the "silenced" sector, the squeal ends when the whole pad has entered the sector. The squeal starts when the whole pad has left the sector, i.e. when the whole pad once again slides against the unmodified disc surface. Thus, a high and evenly distributed coefficient of friction is needed to initialise a brake squeal. However, when a squeal is established it can be maintained with only a small part of the pad experiencing a coefficient of friction high enough for the squeal to be initialised.

6 ACKNOWLEDGEMENTS

The authors gratefully acknowledge the financial support from the Swedish board for Technical Development (NUTEK), Volvo Technological Development for providing test materials and Claes Kuylenstierna for valuable discussions.

7 REFERENCES

1. Bergman, F., Eriksson, M., and Jacobson, S., *Influence of Disc Topography on Generation of Brake Squeal.* Wear, 1999, 225-229, p. 629-639.
2. Fosberry, R.A.C. and Holubecki, Z., *Interim Report on Disc Brake Squeal.* M. I. R. A, 1959, 1959/4.
3. Rhee, S.K., Tsang, P.H.S., and Wang, Y.S., *Friction-induced noise and vibration of disc brakes.* Wear, 1989, 133, p. 39-45.
4. Matsuzaki, M. and Izumihara, T., *Brake noise caused by longitudinal vibration of the disc rotor.* SAE Technical Papers Series, 1993, 930804.
5. Lang, A.M. and Smales, H., *Approach to the Solution Of Disc Brake Vibration Problems.* I Mech E Conference Publications, 1983, 2, p. 223-231.
6. Felske, A., Hoppe, G., and Matthaei, H., *Oscillations in squealing disc brakes - analysis of vibration modes by holographic interferometry.* SAE Trans, 1978, 87.

7. Earles, S.W.E. and Chambers, P.W., *Predicting Some Effects Of Damping On the Occurrence Of Disc - Brake Squeal Noise*. American Society of Mechanical Engineers, Dynamic Systems and Control Division, 1985, 1, p. 317-323.
8. Nishiwaki, M., *Generalized theory of brake noise*. Proceedings of the Institution of Mechanical Engineers, Part D: Journal of Automobile Engineering, 1993, 207(3), p. 195-202.
9. Sherif, H.A., *On the design of anti- squeal friction pads for disc brakes*. SAE Trans, 1991, 100(Sect), p. 678-686.
10. Bergman, F., Eriksson, M., and Jacobson, S., *A software based measurement system for test and analysis of automotive brake squeal*. TriboTest journal, Leaf Coppin Publ. Ltd., 1999, 5(3).

This page intentionally left blank

Modelling of high-frequency disc-brake squeal

J FLINT
Institute of Applied Physics, University of Southern Denmark, Odense, Denmark

ABSTRACT

Discomfort from disc brake squeal is a major concern in the developing of brake systems and friction materials.This paper will cover the progress made in applying a specialized mathematical modelling technique for high frequency disc brake squeal analysis. This technique is suited for representing the complex vibrational behaviour of continuous elements in a model with a low number of degrees of freedom. The paper presents a model of a disc brake system that illustrates a mechanism that can cause squeal. The purpose is to gain an insight into the fundamental causes of squeal and thereby facilitate the process of finding new ways to eliminate it. The model presented here combines the continuous elements representing brake rotor and linings with discrete elements representing the pistons and the caliper. The aim of this work is to preserve a simplified modelling approach which allows for conceptual understanding of the squeal generation mechanism and still to incorporate a wider range of effects inf luencing the system response. New features in the presented modelling approach is the inclusion of pistons and caliper and of damping.

NOMENCLATURE

A_1	Cross section area of disc	b	Width of disc	r_p	Gyration radius
$C[\,]$	Differential damping operator	c_{ij}	Damping matrix elements	t	Thickness of lining
E_1	Youngs modulus of disc	f	Eigenfrequency	u	Thickness of backplate
E_pI_p	Stiffness of pad p = 2,3	h	Thickness of disc	w	Lateral displacement
E_l	Youngs modulus of lining	k'	Cross section formfactor	δ	Dirac delta function
G_1	Shear modulus of disc	k_{ij}	Stiffness matrix elements	λ^2	Eigenvalue of matrix
I_1	Moment of inertia of disc	k_l	Lining stiffness	μ	Coefficient of friction
K_{pp}	Stiffness of spring	k_m	Stiffness of mounting	ρ_b	Density of backplate
L	Disc equiv. length	l	Length of pad	ρ_d	Density of disc
$L[\,]$	Differential stiffness operator	m_{ij}	Mass matrix elements	ρ_l	Density of lining material
$M[\,]$	Differential mass operator	m_p	Mass per unit length	ϕ	Test function
N_0	Normal force	n	Mode number	ω	Angular eigenfrequency
a_{ppn}	Location of spring	p	Index for part number		

1. INTRODUCTION

Brake squeal is an annoying disturbance and especially in the comfortable cars of today it will stand out as a very distracting noise unless it is eliminated. Extensive work has been made in this field of research and the problem has been attacked both from an experimental 'trial-and-error' approach and from a theoretical approach. The theoretical work ranges from a highly abstract and simplified analytical treatment to very detailed numerical analysis using the finite element method.

This article will describe the behaviour of the brake system using mathematical tools and extend the work by Spurr [1] and Jarvis and Mills [2] on sprag-slip models and the work of Earles [3] and North [4] on kinematic constraint instability. In the context of drum brake noise this type of analysis has been done among others by Lang [5] under the heading of binary flutter instability and by Hultén [6] who described the instability as being induced by lining deformation.

Analytical methods have been used in various ways to generate system models. As opposed to most of the previous work on disc brake squeal that is based on rigid body mechanical structures some of the parts in the analysis presented here are represented by flexible, continuous elements. The disc and pad component are modelled using the modal properties of the real, continuous parts as a reference. The appropriate properties of the components in this analysis are chosen to achieve a good agreement between the eigenfrequencies of the free-free components in the analysis and the resonance frequencies of the actual parts. The eigenfunctions are then used as test functions in a Galerkin discretization procedure to calculate the stiffness, damping and mass matrices for the complete system. Some work using this method has been published in reference [7], but in the present paper the effect of damping is considered and additional parts of the brake system are modelled (caliper and pistons).

2. BRAKE SYSTEM MODELLED WITH CONTINUOUS AND DISCRETE ELEMENTS

Figure 1 below shows the idealized brake system to be analyzed. The disc (1), as well as the two pads (2) and (3) are continuous, flexible elements. They are inter-connected by the friction material which is modelled as a continuous spring. At the abutment the pads are in contact with the carrier, a part of the brake not included in this model and only represented by a flexible contact to ground.

The pistons (4) and (5) are in contact with the backplate of the inboard pad and they are modelled as rigid bodies with one degree of freedom in the lateral direction. The pistons are connected to the caliper by springs and dampers. The caliper consists of two parts (6) and (7) each with two degrees of freedom: One translation in the lateral direction and one rotation about the centre of gravity. The caliper is connected to ground via two springs and dampers located at the point of contact between caliper pins and the brake carrier.

In order to be able to describe the system components that will be modelled as continuous flexible bodies, the differential equations for these parts have to be established.

2.1 Modelling the brake disc

At a certain level of abstraction the brake disc is a two dimensional annular plate, but in this modelling approach the disc is 'cut' and unfolded to a one-dimensional beam. The boundary conditions at the ends are chosen to represent the cyclo-symmetric nature of the disc and this makes it possible to arrive at a good agreement between the model and the physical disc of the system.

This simplification makes it considerably more easy to generate an analytical model. The simplification can be justified based on the fact that the eigenfunctions for transverse vibrations along the length of a beam with cyclo-symmetric boundary conditions are identical to the eigenfunctions for the transverse vibrations of a disc along its circumference.

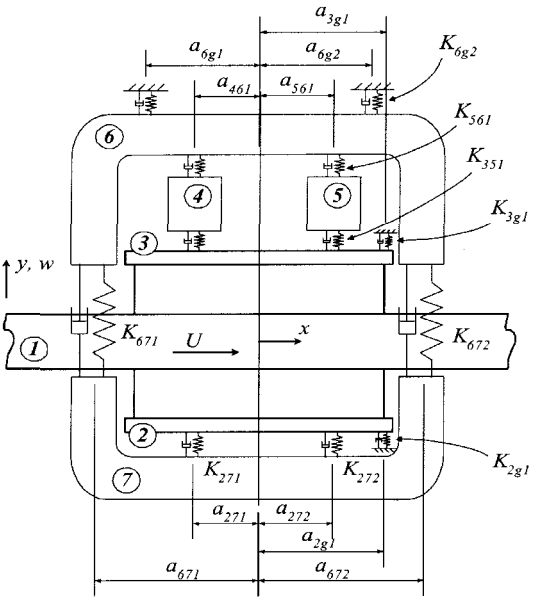

Figure 1 Disc brake model with two rigid caliper parts (6) and (7), two lumped mass pistons (4) and (5), two flexible pads (2) and (3) and a continuous disc (1).

However this model will not account for disc modes with nodal circumferential lines or for in-plane modes.

2.1.1 A simple beam model

The method presented here uses an Euler-Bernoulli beam theory that includes the disc mounting stiffness k_m. The governing differential equation for the beam in this context is

$$EI\frac{\partial^4 w}{\partial x^4} + k_m w + c\frac{\partial w}{\partial t} + m\frac{\partial^2 w}{\partial t^2} = 0, \tag{1}$$

where the subscript 1 for the disc has been omitted. Figure 2 shows the frequencies of the actual disc and the prediction using the Euler-Bernoulli theory without and with mounting stiffness. The mounting stiffness is basically an elastic foundation over the complete length, and the undamped angular eigenfrequencies can (according to [8]) be calculated as

$$\omega_n = \frac{4\pi^2 n^2}{L^2}\sqrt{\frac{EI}{m}}\sqrt{1+\frac{k_m}{EI\left(\frac{4\pi^2 n^2}{L^2}\right)^2}} \tag{2}$$

By matching the calculated and measured values the equivalent length L of the beam was found to be about 1.2 times the nominal middle circumference of the disc and the moment of inertia I about 0.8 times the inertia of a prismatic beam with the same dimensions as a section of the disc. This gave the predicted curves shown in figure 2. The average error for a Euler-Bernoulli beam without foundation is 14% while the average error with the disc mounting modelled as a foundation is 11%.

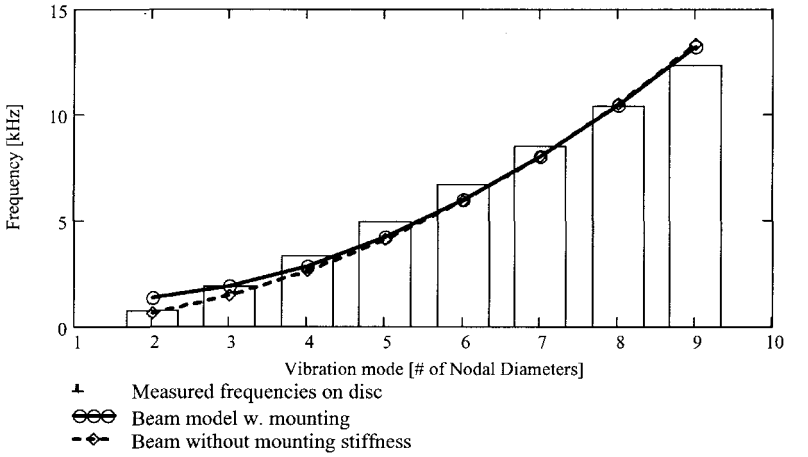

Figure 2 Results from an Euler-Bernoulli beam model compared with frequencies of a real disc.

2.2 Modelling the pads and caliper

The pads are also modelled by Euler-Bernoulli beams but with free-free boundary conditions. The stiffness E_pI_p, $p = 2, 3$ is chosen to represent the modal properties obtained from measurements on the pads alone in the best possible manner.

The caliper is a complicated structure and difficult to model analytically, but it consists basically of two long cast-iron bars connected in the ends. For this analysis only four degrees of freedom have been included. These degrees of freedom represents rigid body translation and rotation and the frequencies of these vibration modes have been compared with frequencies obtained from finite element and modal analysis. By suitable choice of stiffness in the springs connecting the two parts of the caliper the modes and frequencies agrees well for a translation mode at 1054 Hz and a rotation mode at 2046 Hz. This choice is based on the understanding that the disc and pads are the primary source of higher frequency vibration, but further studies may reveal a need to include more modes on the caliper.

The in-plane motion of the disc or other components are not modelled in this analysis, but the direction of rotation of the disc defines the direction of the friction forces.

3. CREATING A DISCREET MODEL

The equations of motion for the continuous elements in this system are converted to a general form. This will make it more straightforward to implement the model in a systematic way.

The general formulation in terms of operators of an equation of motion for a continuous, linear second order system without external excitation is given as follows:

$$M[\ddot{w}] + C[\dot{w}] + L[w] = 0. \tag{3}$$

where L, C and M are linear differential operators of the form

$$L[w] = A_1 w \square A_2 \frac{d}{dx} w + 4A_3 \frac{d^2}{dx^2} w \square A_4 \frac{d^3}{dx^3} w + \ldots \tag{4}$$

The differential equation can be converted to a system of ordinary algebraic equations using a Galerkin discretization technique. To achieve a matrix representation the stiffness and mass matrices will be generated by calculating the inner product related to the differential operators

$$m_{ij} = \int_D \phi_i M\left[\phi_j\right] dD \text{ and } k_{ij} = \int_D \phi_i L\left[\phi_j\right] dD, \tag{5}$$

where the $\phi's$ are test functions, $i, j = 1, 2, ..., n$ are indices for the different modes involved and D is the domain of the system for which the integral extends. [9]

3.1 Test functions

The assumed modes or test functions needed for calculating the matrix elements according to (5) are a subset of the eigenvectors of the individual components of the system. The test functions corresponding to the cyclo-symmetric boundary conditions on the disc are the sine and cosine functions defined by

$$\phi_1(n,x) = \begin{cases} \cos\left(\frac{2\pi x}{L}\frac{n+1}{2}\right) & for \quad n\ odd \\ \sin\left(\frac{2\pi x}{L}\frac{n}{2}\right) & for \quad n\ even. \end{cases} \tag{6}$$

The pads are assumed to have two rigid body modes (translation and rotation) and a set of flexible modes

$$\phi_p(n,x) = \begin{cases} 1 & if \quad n = 1 \\ \frac{2x}{l} & if \quad n = 2 \\ y(n,x) & if \quad n > 2 \end{cases} \text{ for } p = 2, 3, \tag{7}$$

where $y(n,x)$ is the free-free beam mode shape as derived from the Euler-Bernoulli theory

$$y(n,x) = a_n \sin\beta_n x + b_n \cos\beta_n x + c_n \sinh\beta_n x + d_n \cosh\beta_n x. \tag{8}$$

The pistons have only a rigid body lateral displacement degree of freedom

$$\phi_p(n,x) = 1 \text{ for } p = 4, 5, \tag{9}$$

while the two caliper parts have two rigid body modes for translation and rotation:

$$\phi_p(n,x) = \begin{cases} 1 & if \quad n = 1 \\ \frac{2x}{L_p} & if \quad n = 2 \end{cases} \text{ for } p = 6, 7 \tag{10}$$

3.2 Differential operators

For the pads a Euler-Bernoulli beam theory with the addition of the effect of rotary inertia has been used. See [7] for the derivation of expressions for this case. The stiffness differential operator for the disc is as follows

$$L_1 = L_{L1} + L_{l1}, \tag{11}$$

$$L_{L1}\left[w_1\right] = E_1 I_1 \frac{\partial^4 w_1}{\partial x^4} + k_m w_1, \tag{12}$$

$$L_{l1}\left[w_1, w_2, w_3\right] = \frac{\mu k_l h}{2}\left(2\frac{\partial w_1}{\partial x} \sqcup \frac{\partial w_2}{\partial x} \sqcap \frac{\partial w_3}{\partial x}\right) + k_l\left(2w_1 \shortparallel w_2 \shortparallel w_3\right) + 2\mu N_0 \frac{\partial w_1}{\partial x} \tag{13}$$

where L_{L1} is for the complete disc length while L_{l1} is for the part covered by the pads. For the pads the stiffness operator is

$$L_p\left[w_1, w_2, w_3\right] = E_p I_p \frac{\partial^4 w_p}{\partial x^4} + \mu k_l t\left(\frac{\partial w_1}{\partial x} \sqcap \frac{\partial w_p}{\partial x}\right) \sqcup k_l\left(w_1 \sqcup w_p\right) \sqcup \mu N_0 \frac{\partial w_1}{\partial x}, p = 2, 3. \tag{14}$$

The mass differential operators are

$$M_1[\ddot{w}_1] = \rho_1 A_1 \ddot{w}_1 \text{ and} \tag{15}$$

$$M_p[\ddot{w}_p] = \rho_p A_p \ddot{w}_p - k_p^2 m_p \frac{\partial^2 w_p}{\partial x^2}, p = 2, 3, \tag{16}$$

where the last term in the expression for the pads are the rotational inertia term.

3.3 Applying damping

The damping properties for the components are taken from modal analysis results, while the stiffness and the damping properties for the springs and dampers representing the contact between the components are taken from measured and estimated data.

In this analysis a proportional viscous damping has been applied. The general form of stiffness and mass proportional damping is

$$[C] = \alpha[M] + \beta[K] \tag{17}$$

but for internal damping in the disc and friction material only the stiffness proportional damping is relevant. The fraction of critical damping is $\xi = c/2\sqrt{km}$ for a single degree of freedom system defined by

$$m\ddot{q} + c\dot{q} + kq = 0. \tag{18}$$

This means that the damping factor $c = \beta k$ defines the stiffness proportional part $\beta = 2\xi/\sqrt{\frac{K}{M}} = 2\xi/\omega_n$, where ω_n is the natural frequency of interest. As a wide range of frequencies is covered in the analysis a characteristic ω_n has been employed in calculating the damping matrix as

$$[C] = \beta[K] = \frac{2\xi}{\omega_n}[K]. \tag{19}$$

The calculation of the mass and stiffness matrix elements together with this procedure allow for a representation of the complete system with continuous and discrete components in one matrix formulation.

3.4 Stability of the system

In the formulation derived here the brake system is treated as a mechanical system with N degrees of freedom. It can be modelled by a set of N second order differential equations of motion in the form

$$\left[\bar{M}\right]\{\ddot{q}\} + \left[\bar{C}\right]\{\dot{q}\} + \left[\bar{K}\right]\{q\} = \{0\}, \tag{20}$$

where $\{q\}$ is the generalized coordinates, $\left[\bar{M}\right]$ is the mass matrix, $\left[\bar{C}\right]$ the damping matrix, and $\left[\bar{K}\right]$ the stiffness matrix. In order to solve this system of second order equations it is convenient first to restate it in standard form and then to bring it into a state space formulation.
The standard form is obtained by premultiplying the equation by the inverse of the mass matrix and by defining $[C] = \left[\bar{M}\right]^{-1}\left[\bar{C}\right]$ and $[K] = \left[\bar{M}\right]^{-1}\left[\bar{K}\right]$. Now (20) can be rewritten as

$$\{\ddot{q}\} + [C]\{\dot{q}\} + [K]\{q\} = \{0\}. \tag{21}$$

Adding an extra set of equations of the form $\{\dot{q}\} - \{\dot{q}\} = \{0\}$ then allow for rewriting the system of N equations into a system of $2N$ equations

$$\begin{Bmatrix} \{\ddot{q}\} \\ \{\dot{q}\} \end{Bmatrix} = \begin{bmatrix} -[C] & -[K] \\ [I] & [0] \end{bmatrix} \begin{Bmatrix} \{\dot{q}\} \\ \{q\} \end{Bmatrix} = \{0\}. \tag{22}$$

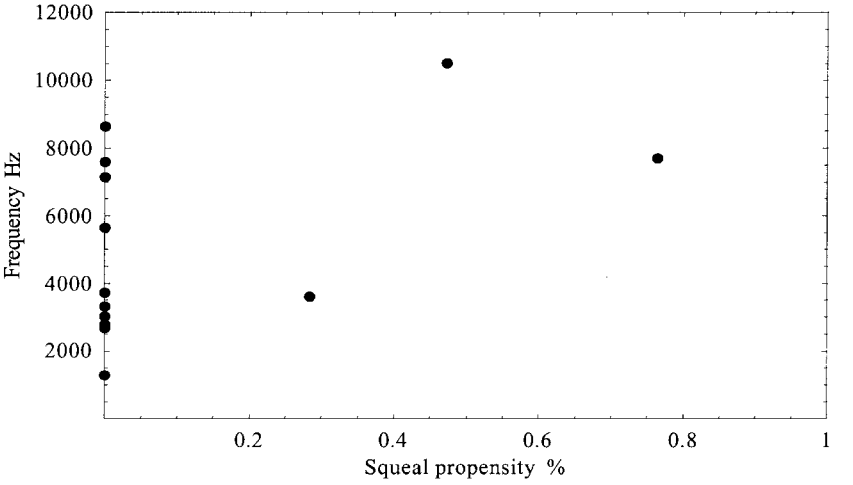

Figure 3 Eigenvalues with positive imaginary part (positive frequency) and positive real part (squeal propensity) for baseline parameter values ($\mu = 0.35$), but without damping.

This system of second order differential equations can then be written as a set of first order equations by introducing the state space notation $\{\eta\} = \begin{Bmatrix} \{\dot{q}\} \\ \{q\} \end{Bmatrix}$ and (22) now become

$$\{\dot{\eta}\} \sqcap [H]\{\eta\} = \{0\}, \tag{23}$$

where the characteristic system matrix is

$$[H] = \begin{bmatrix} \sqcap [C] & \sqcap [K] \\ [I] & [0] \end{bmatrix}. \tag{24}$$

The solution to equation (23) is assumed to be of the form $\{\eta\}_i = \{\psi(x)\}_i e^{\lambda_i t}$, where $i = 1..2N$, λ_i is the eigenvalue and $\{\psi(x)\}_i$ is the eigenvector. Inserting the solution in (23) yields

$$[\lambda_i [I] \sqcap [H]]\{\psi\}_i = \{0\} \tag{25}$$

and non-trivial solutions requires the determinant to be equal to zero, i.e. $|\lambda [I] \sqcap [H]| = 0$. This constitutes the characteristic equation for the system and it can be solved for λ_i, $i = 1..2N$. When an eigenvalue λ_i is found the accompanying eigenvector $\{\psi\}_i$ can be found from (25). The eigenfrequencies in Hz are calculated as $f_i = \frac{1}{2\pi} \operatorname{Im} \lambda_i$. The stability of the solution is determined by the real part of the normalized eigenvalue

$$\alpha_i = \operatorname{Re} \frac{\lambda_i}{|\lambda_i|}. \tag{26}$$

α is here termed 'squeal propensity' as it results in an increase in vibration amplitude.

4. RESULTS

The formulation of the system matrices are done according to the description in section 3 while the solutions to the matrix equation are obtained as described in section 3.4. The complex eigenvalues are used as an indication of the stability of the system.

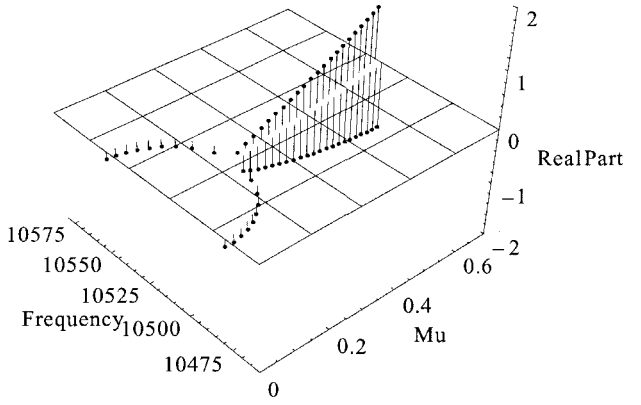

Figure 4 A trace of eigenvalues near 10.500 Hz for a variation of μ from 0 to 0.7. Two modes couple at the same frequency and the real parts splits into a positive and a negative value.

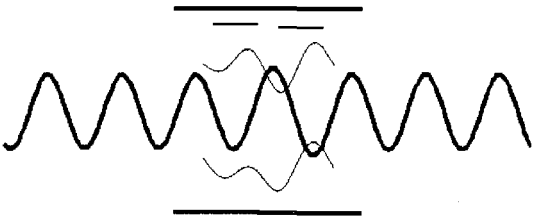

Figure 5 An instantaneous deflection shape of the system as described by the eigenvector associated with the eigenfrequency at 10.515 Hz. The thick solid line in the middle is the disc, the thin lines are the pads, the heavy solid lines the caliper parts and the two short lines the pistons.

Calculations with this model have been made using 22 assumed modes on the disc and 6 on each of the pads. This choice leaves a total of 40 degrees of freedom in the model and it is based on the convergence of the solutions.

4.1 Solutions with positive real part

Figure 3 shows the result of a calculation with baseline parameter values, but without damping. Three roots with a positive real part or a positive squeal propensity are displayed.

For a zero coefficient of friction the system is stable. Applying the friction forces drives some of the modes into a state of oscillation with increasing amplitude as indicated by a positive real

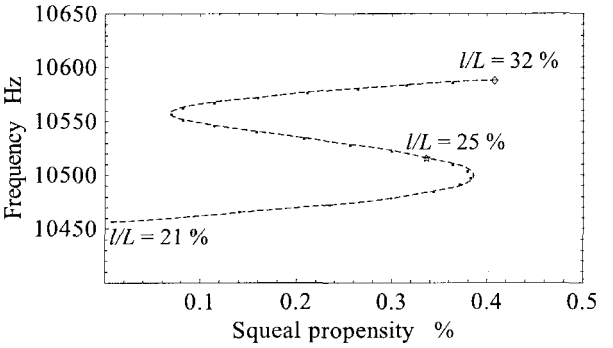

Figure 6 Change of squeal propensity and frequency of the instability near 10.500 Hz for a variation of the relative length of the pad.

part of the eigenvalue. As indicated in figure 4 the increase in friction can forces two modes to couple. The imaginary parts coalesce while the real parts diverge into one positive and one negative. Only particular modes and modes sufficiently close may couple while other modes don't couple no matter how close they are.

Field testing and noise measurements on this brake system have reported a variety of noises mainly in the high frequency domain, but as this model is mainly conceptual no attempt has been made to adjust the parameters of the model to simulate a specific set of noises and test conditions.

4.2 Mode shapes of the unstable solutions

The eigenvector for each unstable mode is calculated according to (25). A complex eigenvector is associated with each unstable mode and an animation of the system based on the eigenvector of the solution show that a traveling wave on the disc is generated. Figure 5 shows the mode shape at 10.515 Hz at a certain time. The wave travels in the direction of rotation of the disc. The influence of some system parameters on this mode have been investigated.

4.3 Length of pad

A variation in the length of the pads has a significant influence on the instability. Figure 6 shows the variation of the response for a variation of length of the pads. The trace indicate that for some geometrical proportions between length and wave pattern the instability is more pronounced but the calculations show that in general a shorter pad is preferrable.

4.4 The effect of damping

The effect of adding damping to the pads is shown in figure 7. The pad damping is seen to decrease the level of instability.

Adding a small amount of damping to the disc also has the effect of decreasing the instability level for the high frequencies as shown in figure 8. At some of the low frequencies a closer examination shows that damping can in fact have the opposite effect.

5. DISCUSSION

The unstable response calculated by this model are complex modes of vibration as opposed to normal modes. A travelling wave is the most general form of a complex mode. A wave travelling in the direction of rotation of the disc has been measured in a squealing disc brakes by Fieldhouse and Newcomb [10]. In a squealing drum brake, Hultén, Flint and Nellemose

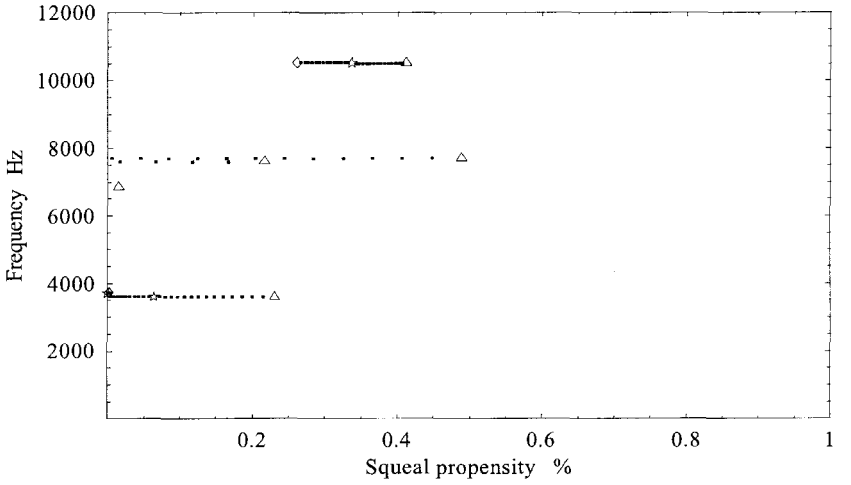

Figure 7 The effect of increasing damping in the friction material. The triangular markers indicate zero pad damping, the star the nominal value and a diamond the maximum value (twice the nominal value).

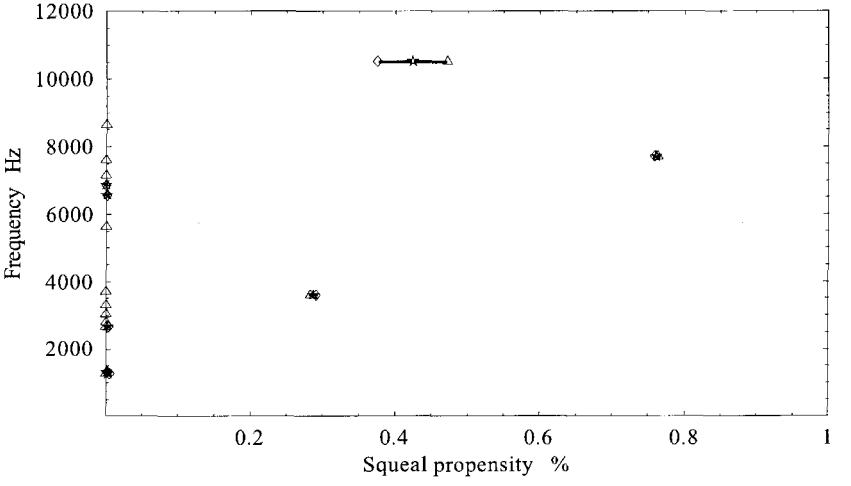

Figure 8 The effect of variation of disc damping from 0 (triangle) to 0.002 (diamond).

[11] have measured a traveling wave in the direction of rotation of the drum. Hultén [12] has presented a hypothesis on the wave generation in a drum brake. In [7] Hultén and Flint propose a hypothesis on the mechanism generating travelling waves in disc brakes. The basic mechanism in this hypothesis is as follows:

- A relative displacement of disc and pads gives rise to a lining deformation that increases the normal force magnitude on one side of the disc and decrease it on the other side.
- The magnitude of the friction forces are then no longer equal on the two sides.
- A moment is generated by the uneven friction forces on the upper and lower faces of the disc.
- The moment rotates the disc and pushes a wave forward in the direction of rotation of the disc.
- The wave increases the relative displacement between the disc and pads and thereby closes the loop in an increasing oscillatory motion.

6. CONCLUSION

This model is able to simulate some important aspects of a noise generation mechanism that can be active in automotive disc brakes. The disc and pads are modelled as continuous elements, which allows for the presence of higher order vibration modes. This formulation allow for the evaluation of the effect of the distributed parameters.

The effect of a variation in pad length is an instructive example of the possible design implications that can be derived from a simple model with continuous elements.

The pistons and the caliper are rigid bodies with a limited number of degrees of freedom, and therefore only a crude estimate of their influence on the system behaviour can be expected. A subsequent model including the flexible behaviour of the caliper is believed to enhance the ability of this kind of model to predict the vibrational stability of a disc brake system.

As a rule and in agreement with general expectations the addition of damping has a positive effect in reducing instability of the modes, but different unstable modes are influenced differently by the addition of damping. For some modes damping may have a slight destabilizing effect. The location of the damping is important for determining it's effect.

A future closer investigation of the calculated response compared to frequencies and mode shapes measured on a operating brake system will be an important test for the validity of the predictions based on this model.
The ongoing numerical calculations based on this model are expected to allow for more general conclusions on the effects of variations in system parameters. Preliminary investigations show a clear effect of increasing instability with an increase in the friction coefficient. This is a general tendency in all models of brake squeal which also apply to the presence of squeal in the specific brake system modelled in this paper.

A further analysis of the effects of variation of parameters over the length of the pads is a possible and interesting utilization of this modelling approach.

7. REFERENCES

[1] Spurr, R.T. A Theory of Brake Squeal. *Proc. Instrn. Mech. Engrs., No. 1*, 1961-62.

[2] Jarvis, R.P., Mills, B. Vibrations Induced by Dry Friction. *Proc. Instn. Mech. Engrs. Vol. 178 Pt 1, pp 847-866*, 1963-64.

[3] Earles, S.W.E., Badi, M.N.M. On the Interaction of a Two-Pin-Disc System with Reference to the Generation of Disc-Brake Squeal. *SAE 780331*, 1978.

[4] North, M.R.. Disc Brake Squeal. *IMechE C38*, 1976.

[5] Lang, A.M., Newcomb, T.P., Brooks, P.C. Brake squeal - the influence of rotor geometry. *IMechE 1993*, 1993.

[6] Hultén, J.. Drum Brake Squeal - A self-Exciting Mechanism with Constant Friction. *SAE 932965*, 1993.

[7] Hultén, J., Flint J. An assumed modes method approach to disc brake squeal analysis. *SAE 1999-01-1335*, 1999.

[8] Young D.H., Weaver W.Jr., Timoshenko, S. *Vibration Problems in Engineering*. John Wiley and Sons, New York, 1974.

[9] Meirovitch, L. *Analytical Methods in Vibrations*. The MacMillan Company, New York, 1967.

[10] Fieldhouse J.D., Newcomb P. The application of holographic interferometry to the study of disc brake noise. *SAE930805*, 1993.

[11] Hultén, J., Flint, J., Nellemose, T. Mode Shape of a Squealing Drum Brake. In *Proceedings of the 1997 Noise and Vibration Conference*, volume 3, pages 1231–1245, Traverse City, Michigan, May 1997. SAE paper 972028.

[12] Hultén, J. Some Drum Brake Squeal Mechanisms. In *Proceedings of the 1995 Noise and Vibration Conference*, volume 1, pages 377–388, Traverse City, Michigan, May 1995. SAE paper 95 12 80.

Evaluation of friction materials' tribological properties and their effect on the dynamic response of disc-brake systems

A M A EL-BUTCH
Engineering Department, The American University in Cairo, Egypt

ABSTRACT

It was thought that dry friction between pad and disc is the main cause of vibration in disc brakes. The comprehensive research work in the field showed that variation of the coefficient of friction with relative velocity was insufficient to cause vibration. Other factors like geometry, flexibility of the brake elements, contact parameters and surface roughness were found to affect the vibration levels in disc brake system.

In the present work, the influence of the tribological properties of the friction material on the vibration levels in a disc brake is studied. Two friction models to take account of the variation of the friction coefficient with applied load, temperature, velocity and design are suggested [1]. The effect of pressure, temperature and sliding velocity on the system response is studied.

The present investigation has shown that the variation of the coefficient of friction with pressure and temperature should be considered and by the careful choice of friction material it could be possible to avoid some unwanted vibration.

NOTATION

a_1	Disc brake design factor.
a, b	The position of the two pistons from the pad center, 0.02305 and 0.02305 m.
c_1 & c_2 ..& c_5	Contact damping between brake components, 6.6, 3.139, 6.6, 22.04, 22.04 Ns/m respectively
c_{t1} & c_{t2} & c_{t3}	Rotary damping, 11.2×10^{-3}, 0.036×10^{-6}, 11.2×10^{-3} Nms/rad. respectively

d_1, d_3	Pad Thickness, 0.009, 0.009 m.
d_2	Disc Thickness, 0.006 m.
e_1	Thermal diffusivity
F_1, F_2	Frictional forces, N.
F_p	Applied piston force, N.
I_1, I_3	Pad's mass moment of inertia, kgm^2.
I_2	Disc mass moment of inertia, kgm^2.
K	Thermal conductivity of the friction material, Nm/hKm.
k_1 & k_2... & k_5	Contact stiffness between brake components, 1.2×10^9, 229×10^6, 1.2×10^9, 93×10^6 and 93×10^6 N/m respectively.
k_{t1} & k_{t2} & k_{t3}	Rotary stiffness, 264×10^3, 378.53×10^6 and 264×10^3 Nm/rad respectively
m_1, m_3	Pad mass, 0.4492 kg.
m_2	Disc mass, 1.52 kg.
P, P_{max}	Applied and maximum piston pressure, N/m^2.
T_i, T	The initial temperature and temperature of the pad surface, °K.
t, t_s	Time and stopping time, sec.
α	Pressure exponent.
β	Velocity exponent.
γ	Temperature exponent.
v, v_{max}	Sliding velocity and maximum velocity, m/sec.
μ, μ_0	Dynamic coefficient of friction and static coefficient of friction between disc and pad, ($\mu_0 = 0.4$).
$q''_{(0)}$	Heat flux.

Other symbols are defined when first mentioned in the manuscript.

1. INTRODUCTION

The principal function of the friction material that is used in brake linings is to reduce the relative movement between the friction material and the rotor through the conversion of kinetic energy to heat. The stability of a vehicle during braking is highly influenced by many factors. One of these is the change of the friction material tribological properties with the operating conditions. This could lead to a change in the coefficient of friction especially in asbestos-free brake materials that are now commonplace.

Friction and wear of the friction materials are found to be highly dependent on a number of factors like pressure, temperature and sliding velocity [1]. Generally, the friction materials may be classified into four categories, metallic, metal ceramic, asbestos filled resin composites and asbestos-free composites [2]. Any of these friction materials should meet two major requirements, the first is high resistance to wear at elevated temperature and the second is to provide a suitable level of friction. Since there is a conflict between the two requirements, there is still a need for further research to develop new friction materials with superior properties and to study the effect of their tribological behaviour on the vehicle stability during braking.

The main cause of brake instability, as was studied by many authors [3-7], is the negative slope of the coefficient of friction with relative speed. Based on the present investigation, the negative slope may be due to a combined effect of increasing speed, temperature and applied piston pressure. Grunt, groan, grind, and moan are some categories of low frequency disc brake noise that occur in the frequency range of 100 to 1000 HZ. Low and high frequency squeal are occur in the frequency range over 1000 HZ [8]. One means used to reduce the above types of brake noise and squeal is to improve the friction characteristics of the friction material, this involves reducing the pressure, temperature and speed dependence of the friction coefficient of the friction material as much as possible.

In this study a nine degree of freedom model of a disc brake system is suggested to study the dynamic behaviour of the system with friction and wear properties of the friction material.

2. FRICTION MODEL

Two friction models to correlate the coefficient of friction with temperature, pressure and sliding speed are assumed [1], however, many other models depending on the behaviour of the friction material with the three variables can be considered. Experimental results can also be used to generate the mathematical friction model by calculating the polynomial representing experimental relationship using least square method.

The general form of the two models under study is:

$$\mu = \mu_0 \ (a_1 \ P^{\alpha} \ v^{\beta} \ T^{\gamma}) \qquad (1)$$

where;
a_1, α, β and γ are taken to be equal to 1.85, -0.112, -0.053, and -0.031 respectively in **the first model**. and equal to 1.025, -0.047, 0.012 and -0.046 respectively in the **second model**. The type of the friction material and/or filler would control the variation of the coefficient of friction and hence, appropriate coefficients or new model would be used.

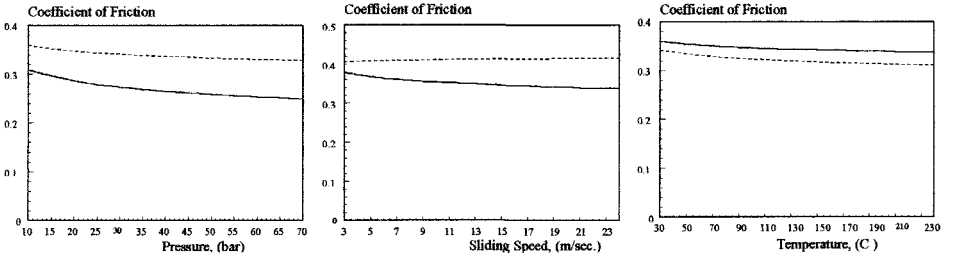

Fig 1. Variation of the coefficient of friction with pressure, velocity and temperature.
——— (First model) ------ (Second model)

The variation of coefficient of friction with pressure, velocity and temperature separately for the two models is given in Fig.1.

3. DISC BRAKE MODEL

A nine degrees of freedom disc brake model is suggested, Fig. 2, in which two pads are acting on the rotor, one on each side. Each part is given three degrees of freedom namely, vertical, horizontal and rotational, (y_i, x_i and θ_i) where i=1,2 and 3. The mass of the pistons is assumed to be very small relative to other masses. Contact damping and stiffness are assumed between individual contacted components. The linear stiffness and damping are k_1 to k_5 and c_1 to c_5 respectively, and the rotary stiffness and damping are k_{t1} to k_{t3} and c_{t1} to c_{t3} respectively.

The excitation forces acting on the brake components are the piston forces F_p and the frictional forces F_1 and F_2. The excitation moments are the product of the friction forces F_1 and F_2 by the half rotor and pad thicknesses.

The friction forces can be written as following;

$$F_1 = \mu_0 \ a_1 P^{\alpha} (v - \dot{x}_1 - \dot{x}_2)^{\beta} \ T^{\gamma} \ [k_4(y_1 - y_2) + c_4(\dot{y}_1 - \dot{y}_2)] \tag{2}$$

$$F_2 = \mu_0 \ a_1 P^{\alpha} (v - \dot{x}_2 - \dot{x}_3)^{\beta} \ T^{\gamma} \ [k_5(y_2 - y_3) + c_5(\dot{y}_2 - \dot{y}_3)] \tag{3}$$

The applied piston force is assumed to increase linearly with time and is given as;

$$P(t) = P_{\max}(\frac{t}{t_s}) \tag{4}$$

Where t_s is the stopping time. Assuming deceleration rate of 8m/sec^2 and initial velocity of 56km/hr, the stopping time is calculated as $t_s = 2$ sec.
The variation of disc velocity with time is assumed to decrease linearly with time and is given as;

$$v(t) = v_{\max}(\frac{t_s - t}{t_s}) \tag{5}$$

The disc surface temperature as a function of time for single stop is given by the following formula [9];

$$T - T_i = \left(\frac{5}{4}\right)^{0.5} \left(\frac{q''_{(0)}}{K}\right) (e_1 t)^{0.5} \left(1 - \frac{2t}{3t_s}\right) \tag{6}$$

Where e_1 is the thermal diffusivity, K is the thermal conductivity, T_i is the disc initial temperature and $q''_{(0)}$ is the heat flux.

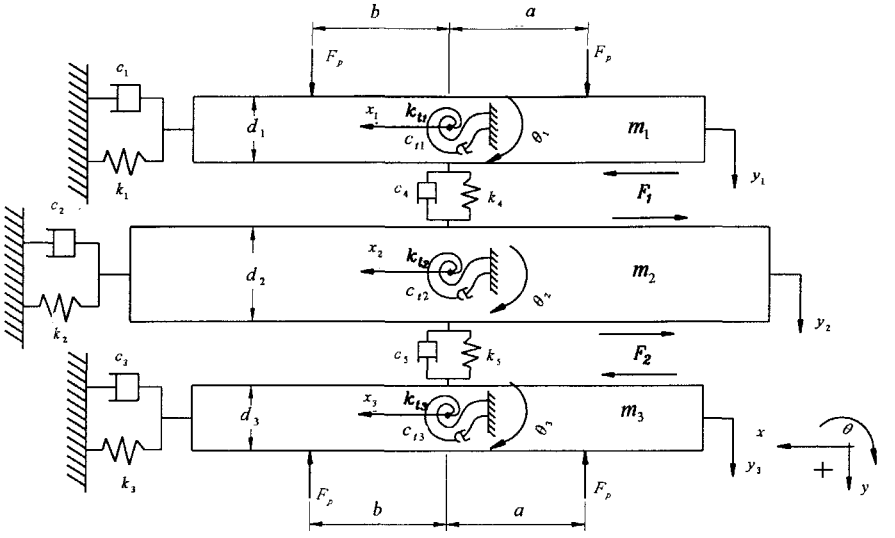

Fig. 2 Disc brake model

System Equations of Motion

Applying the Lagrangian's energy approach to generate the system equations of motion, the kinetic, potential and dissipative energies will be as following;

The kinetic Energy

$$T = \frac{1}{2}m_1\ddot{x}_1 + \frac{1}{2}m_1\ddot{y}_1 + \frac{1}{2}I_1\ddot{\theta}_1 + \frac{1}{2}m_2\ddot{x}_2 + \frac{1}{2}m_2\ddot{y}_2 + \frac{1}{2}I_2\ddot{\theta}_2 + \frac{1}{2}m_3\ddot{x}_3 + \frac{1}{2}m_3\ddot{y}_3 + \frac{1}{2}I_3\ddot{\theta}_3 \qquad (7)$$

The potential energy

$$V = \frac{1}{2}k_1x_1^2 + \frac{1}{2}k_2x_2^2 + \frac{1}{2}k_3x_3^2 + \frac{1}{2}k_4(y_1 - y_2)^2 + \frac{1}{2}k_5(y_2 - y_3)^2 + \frac{1}{2}k_{t1}(\theta_1 - \theta_2)^2 + \frac{1}{2}k_{t2}(\theta_2)^2 + \frac{1}{2}k_{t3}(\theta_2 - \theta_3)^2 \qquad (8)$$

The dissipative energy

$$D=\frac{1}{2}c_1\dot{x}_1^2+\frac{1}{2}c_2\dot{x}_2^2+\frac{1}{2}c_3\dot{x}_3^2+\frac{1}{2}c_4(\dot{y}_1-\dot{y}_2)^2+\frac{1}{2}c_5(\dot{y}_2-\dot{y}_3)^2+\frac{1}{2}c_{t1}(\dot{\theta}_1-\dot{\theta}_2)^2+\frac{1}{2}c_{t2}(\dot{\theta}_2)^2+\frac{1}{2}c_{t3}(\dot{\theta}_2-\dot{\theta}_3)^2 \tag{9}$$

The equations of motion can be obtained by applying the following lagrangian expression;

$$\frac{d}{dt}\left(\frac{\partial T}{\partial \dot{\vartheta}_i}\right)+\frac{\partial D}{\partial \dot{\vartheta}_i}+\frac{\partial V}{\partial \vartheta_i}=Q_{\vartheta_i} \tag{10}$$

Where;

$\vartheta_i = x_1,\ y_1,\ \theta_1, x_2,\ y_2,\ \theta_2\ x_3,\ y_3$, and θ_3 respectively, and;

$Q_{\vartheta_i}=Q_{x1},\ Q_{y1},\ Q_{\theta 1},\ Q_{x2}, Q_{y2}, Q_{\theta 2}, Q_{x3}, Q_{y3}$ and $Q_{\theta 3}$ are the generalized forces and moments.

The elements of the Q_{ϑ_i} vector are as follows;

$Q_{x1}=0$

$Q_{y1}=2F_p$

$Q_{\theta 1}=F_p(a-b)+F_1\ d_1/2$

$Q_{x2}=0$

$Q_{y2}=0$

$Q_{\theta 2}=(F_1-F_2)d_2/2$

$Q_{x3}=0$

$Q_{y3}=F_p(b-a)-F_2\ d_2/2$

The second order differential equations of motion can be generated by substituting equations (7-9) in the Lagrangian expression (10). The equations of motion in matrix form will be as follows;

$$M\ddot{x}+C\dot{x}+Kx=Hx_\circ \tag{11}$$

where

$x=(x_1\ y_1\ \theta_1\ x_2\ y_2\ \theta_2\ x_3\ y_3\ \theta_3)^T$, H is the force distribution matrix and $x_\circ$ is the force vector.

The equations of motion are rewritten in a state space representation and solved in time domain using PC MATLAB to calculate the system response. The state space first order equations reads;

$$\dot{Z}=AZ+Bx_\circ \tag{12}$$

Where $Z=(x_1\ y_1\ \theta_1\ x_2\ y_2\ \theta_2\ x_3\ y_3\ \theta_3\ \dot{x}_1\ \dot{y}_1\ \dot{\theta}_1\ \dot{x}_2\ \dot{y}_2\ \dot{\theta}_2\ \dot{x}_3\ \dot{y}_3\ \dot{\theta}_3)^T$,

$$A=\begin{bmatrix}[0] & [I]\\ -M^{-1}K & -M^{-1}C\end{bmatrix}_{18x18} \quad \text{and} \quad B=\begin{bmatrix}[0]\\ M^{-1}H\end{bmatrix}$$

4. RESULTS AND DISCUSSIONS

Disc brake noise and squeal is caused by the friction force generated between the rotating disc and the stationary friction material. The friction forces depending upon many factors like the variation of the coefficient of friction between the disc and pad with the tribological behaviour of the friction material. Many studies have been carried out considering the variation of the coefficient of friction and hence the friction force with sliding speed. Fading of the friction material means that the coefficient of friction deteriorates greatly at elevated temperature. This means that the negative gradient of the coefficient of friction with temperature should be also considered.

The coefficient of friction of some friction materials is sensitive to the applied load as well as temperature and sliding speed. The combined effect of these three variables on the coefficient of friction and hence the friction force responsible on generating brake noise should be considered. These results, based mainly on the variation of the coefficient of friction with the three variables for the two friction models under study as given in Fig. 1. In the first model the gradient of the coefficient of friction with the three variables is negative while, in the second model, it is assumed that the gradient is negative with pressure and temperature while it is positive with speed.

In order to study the influence of the friction material's wear on the brake dynamic performance, different values of pads thickness d_1 and d_3 are used while keeping all other system variables unchanged. It is found that, decreasing the pad's thickness does not affect significantly the responce of all system degrees of freedom because the pad thickness only affects the value of the excitation moments. On the other hand, if wear along the pad is not uniform, the distances a and b could be affected. This change in geometry may affect the generated friction forces and hence the responce.

In the current brake model, it is found that the most affected degree of freedom is the disc rotary velocity $(\dot{\theta}_2)$, therefore, the time domain response of such degree of freedom is used to show how the tribological parameters of the frictional material would affect the system dynamic response.

Fig 3 shows the response under the combined effect of speed, pressure and temperature for the two friction models. It is found that the first model, in which the negative gradient of the coefficient of friction is higher, displays higher response oscillation.

For the first model, three values of α, namely 50%, 100% and 150% of its nominal value, are used to show the effect of piston pressure variation on the response, Fig. 4. The values of a_1, β, γ, and other variables were kept constant in this case. The same is done to study the effect of speed and temperature, Fig. 5 and 6 respectively which show the effect of the last two variables on the disc rotary oscillation. The three figures (4,5 and 6) show that there is a considerable effect of taking the alternation of the coefficient of friction with such variables into account.

5. CONCLUSIONS

1- There must be a friction model for each friction material to test the combined effect of the tribological parameters on the system stick slip vibrations.
2- The negative gradient of the coefficient of friction as being influenced by the interface temperature and applied force of some friction materials should be taken into consideration as well as the negative gradient of the μ / v curve.
3- The uniform wear of the two pads does not significantly affect the stick slip vibrations.
4- By careful choice of friction material it is possible to avoid some unwanted vibration and further intensive research work is to be done to invent new stable friction materials in which the coefficient of friction is independent of the operating conditions.

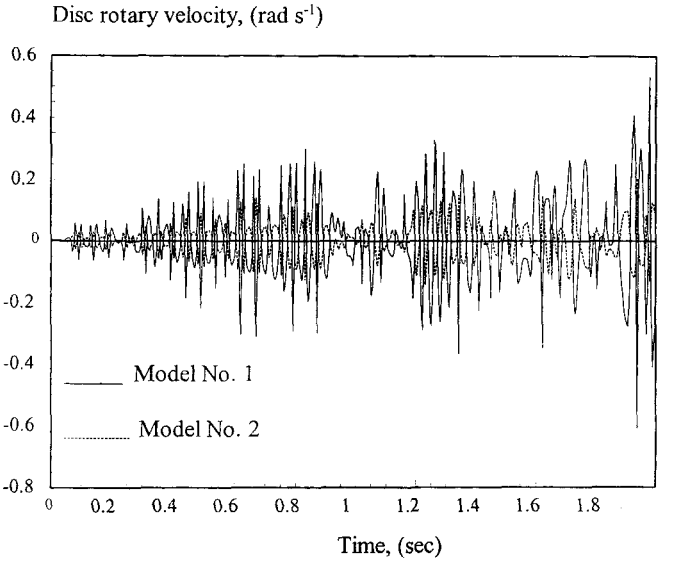

Fig. 3 Comparison between the two models

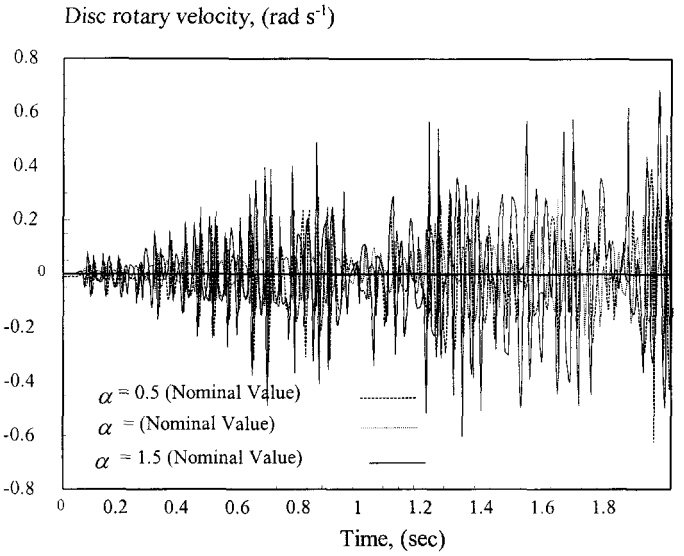

Fig.4 Effect of applied pressure on the response, (Model 1).

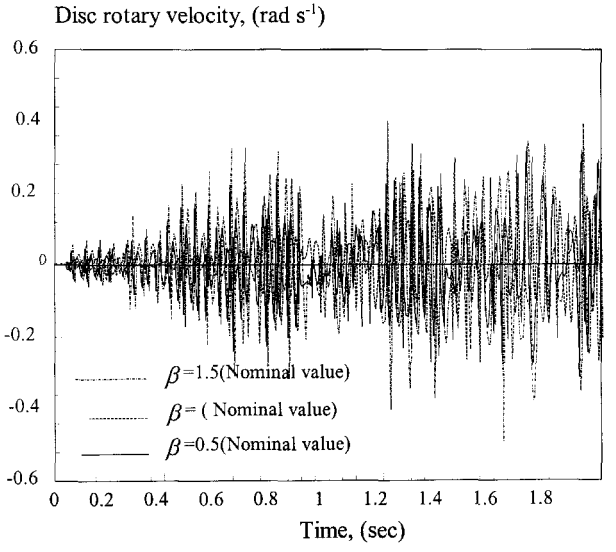

Fig.5 Effect of sliding velocity on the response, (Model 1).

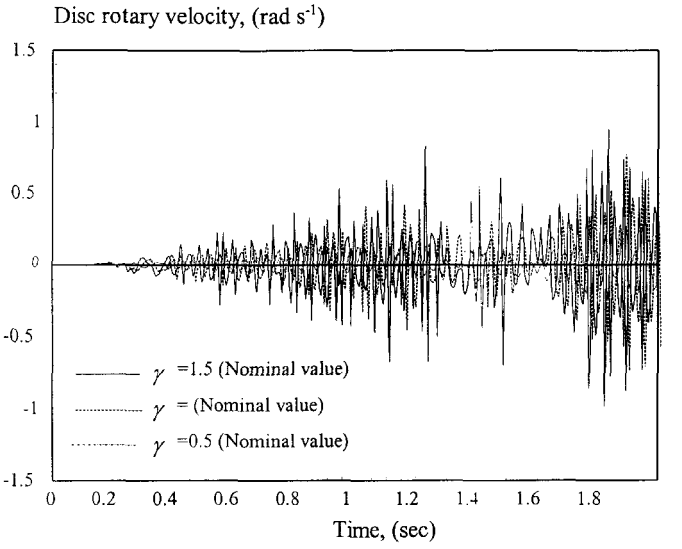

Fig.6 Effect of the friction material temperature on the response, (Model 1).

REFERENCES

(1) J. Todorovic, C. Duboka and Z. Arsenic, " Modelling of friction materials tribological properties for the assessment of braking force distribution", IMechE paper No. C382/057, 1989.

(2) L. B. Newman, "Friction Materials , recent advances", Noyes Data Corporation, 1978.

(3) A. M. El-Butch, I. M. Ibrahim, "Modeling and analysis of geometrically induced vibration in disc brakes considering contact parameters", SAE paper No. 99PC-231, 1999.

(4) P. C. Brooks, D. A. Crolla, A. M. Lang, and D. R. Schafer, "Eigenvalue sensitivity analysis applied to disc brake squeal. C444/004/93, Proceeding of the institution of mechanical engineers, 1993.

(5) I. M. Ibrahim, A. M. El-Butch and T El-Mahdy, "FE-Lumped parameter analysis of friction induced vibration in disc brake system considering pad longitudinal elasticity", Engng. Res. Jour., Vol. 58, Helwan University, Faculty of Engineering, Mataria, 1998.

(6) T. Hamabe, I. Yamazaki, K. Yamada, H. Matsui, S. Nakagawa and M. Kawamura, " Study for reducing drum brake squeal", SAE paper No. 1999-01-0144

(7) S.W.E. Earles, A Mechanism of Disc-Brake Squeal. SAE Transactions, (84), SAE 770181.

(8) K. Brent Dunlap, Michael A., and Richard E., "An investigative overview of automotive disc brake noise", SAE paper No. 1999-01-0142, 1999.

(9) R. Limpert, "Brake design and safety", Published by: Society of Automotive Engineering, Inc., 1992.

Modelling of disc-brake judder in passenger cars

H JACOBSSON
Chalmers University of Technology, Göteborg, Sweden

ABSTRACT

Brake judder can be explained as a dynamical amplification of brake torque and pressure variations when passing through, or coming close to, a critical speed of a vehicle. A previous model by the author predicts how the amplitude of the vibration changes with time, and also the absolute value, provided the brake pressure is high enough. However, in measurements a deflection from the predicted value is seen for low decelerations/brake pressures. A hypothesis is that the deviation is due to the fact that the theory had neglected the effect of ground contact, rolling resistance, aerodynamic drag and engine brake. In the present paper these effects is included in the model and the vibration level is reduced. Some of the shortcomings of the previous model was thereby removed. However, the non-linearity of the measured vibration-deceleration characteristics could not be explained by adding these effects.

1 INTRODUCTION

Brake judder is a forced vibration occurring in different types of vehicles during braking. The frequency of the vibration can be as high as 500 Hz, but usually remains below 100 Hz and often even as low as 10-20 Hz. The vibrations are transmitted to the car body, and are perceived by driver and passengers either through the steering wheel or brake pedal, seat track, floor, or the whole vehicle.

Judder is traditionally classified into cold and hot or thermal judder. Normally, judder consists of a combination of cold and hot judder, why the terms "hot" and "cold" are somewhat misleading. The vibration frequency of brake judder is directly proportional to the wheel speed and therefore also to the velocity of the vehicle. Therefore it is usual to relate the judder frequencies to the wheel speed order; for example frequencies at twice the number of wheel rotations per second are called second order.

Experimental investigations (1) (5) (13) has showed that the instantaneous DTV is the primary contributor to disc brake judder of passenger cars. DTV causes a normal force variation of the brake pad, leading to Brake Pressure Variation BPV. The normal force variation will also generate a proportional friction force variation on the disc surface and hence to Brake Torque Variation, BTV. As BTV and BPV are coupled and normally proportional to each other (and to

DTV (1)), they can usually be looked upon as one entity. DTV is a very complex phenomena consisting of

1. initial DTV from manufacturing and mounting.
2. a result of "off-brake" wear, when the pads lightly touch the disc without braking. The main factor for this is the relative amount of motorway driving (7).
3. more or less permanent areas, with locally different specific volume, friction and wear properties caused by phase transformations when locally overheating the disc.
4. uneven "friction film" generation
5. temporary thermal growth of DTV during each brake application due to uneven heating and localized contact area and pressure (8)(11).

It is known (5) that DTV grows asymptotically from its initial value to a maximum, due to wear within a timescale of thousands of brakings. However, DTV also can also increase much faster, from one second to the next, because of the instantaneous changes of the brake pressure and temperature fields of the brake during braking. Hence, the brake application time (1),(11) and how often the braking is repeated (10) are also important factors for bake judder generation.

The main part of the published work on brake judder concentrates on the various physical effects generating deviation from ideal disc/drum geometry, temperature and pressure field and so on. However, Engel et al. (6) have focuses upon the effect of brake vibrations in the vehicle. The strategy was to monitor the dynamic brake-disc geometry during judder in order to achieve a better understanding. Numerical simulation of the vehicle response to BPV/BTV has been made by Augsburg et al. (1), Bosworth (3), Kim et al. (12). The simulations were all made under quasi-static conditions, i.e. constant speed and temperature etc.

The aim of the development of the brake judder model by the author was to generate a model that can simulate the brake judder levels in a street-going vehicle during braking (9). The response of this model to a BTV with constant amplitude and linearly decreasing disc speed i.e. constant deceleration, is in fig. 1. The vibrations of the stator (i.e. caliper) grows drastically when the rotor speed passed through the critical speed. This is the typical "judder behaviour" qualitatively described in litterature(4) (7). The conclusion was drawn that brake judder is a forced vibration and that no specific friction characteristics are needed for judder to occur.

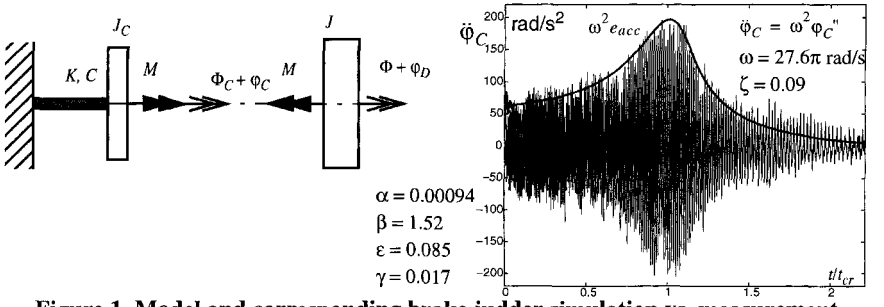

Figure 1. Model and corresponding brake judder simulation vs. measurement.

To verify the brake judder model a passenger car with strong DTV on one of its front brake discs was instrumentated to measure the vibrations of the caliper. Brake applications, with constant brake pressure (and hence constant deceleration), from 140 km/h to 30 km/h, were repeated, see Jacobsson (9) and (10). As seen in fig. 1, the shapes of the theoretically generated

amplitude functions e_{acc} were found to be very close to the measured vibration $\dot{\phi}_C$. Hence the amplitude functions can be used in experimental brake judder analysis as an alternative to FFT techniques, which demands nearly constant speed (i.e. low brake pressure and deceleration). The eigenfrequency and total equivalent viscous damping factor derived from the analysis where found to be the same (13.8 Hz and 0.09) for all measurements in this specific vehicle.

Introduction of the scaled amplitude function $\Psi = \gamma e_{acc}/\varepsilon$ which is independent of the parameters ε and γ, solves the problem caused by the fact that the BTP/BPV level cannot be controlled during a brake application (9). By measuring BTV and/or BPV and then scaling the measured vibration with the corresponding parameter ε, there is no need for constant conditions such as speed, temperature, pressure etc., see Jacobsson (10). Therefore this function is ideal when analysing road tests.

The calculated Ψ_{max} (i.e. the maximal value of Ψ during a braking) from measurements using a constant γ is shown as a function of α in fig. 2 and compared with the theoretically generated function $\Psi_{max}(\alpha)$ with $\zeta = 0.09$. There are two kinds of deviations between measured and predicted vibration levels. First, the vibration level seems to vanish for a deceleration corresponding to an α-value of approximately $0.5 \cdot 10^{-3}$ Second, looking at the measured characteristics, it seems more quadratic than linear with α, especially in the region below $0.7 \cdot 10^{-3}$. Above this limit the scaled maximal vibration level Ψ_{max} is proportional to the vehicle deceleration and the judder model is appropriate.

$$\Psi = \frac{\gamma e_{acc}}{\varepsilon}$$

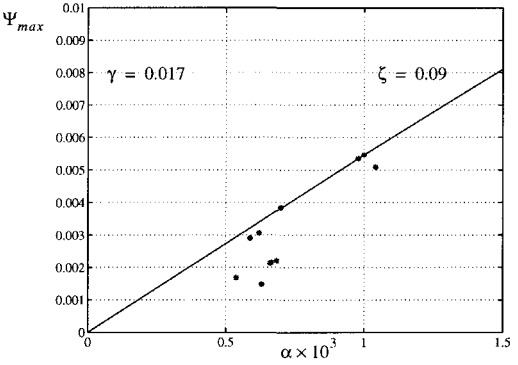

Figure 2. Measured and theoretical Ψ_{max} vs. α.

Possible explanations for the deviation for low decelerations are

1. The effect of ground contact, rolling resistance, aerodynamic drag and engine braking has been neglected.
2. The analysis postulated that BPV and BTV are proportional and that the proportionality constant is independent from brake pressure level, vehicle speed and so on.
3. The geometry of the model is not detailed enough. Especially non-linearities in for instance the hydraulic system must be considered.

The present paper analyses the effect of ground contact, rolling resistance, aerodynamic drag and engine brake.

2 ANALYSIS

A rotor-stator model from (9) and (10) has been completed with engine brake M_e and ground contact force F_f on the front axle, see fig. 3. The angle Φ is the "ideal" or vibration-free motion of the disc and wheel axle and Φ_C the corresponding ideal motion of the caliper. The vibration of disc and caliper are described by φ_D and φ_C respectively.

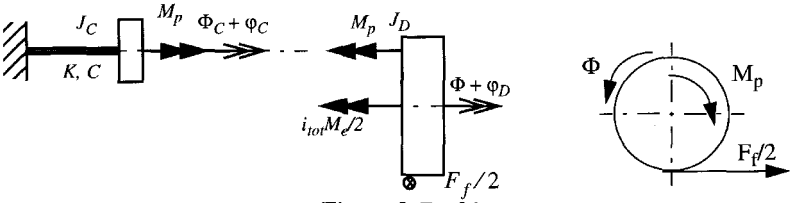

Figure 3. Braking system

If T denotes the braking time, the corresponding system of differential equations, DE, becomes

$$J_C(\ddot{\Phi}_C+\ddot{\varphi}_C)+C(\dot{\Phi}_C+\dot{\varphi}_C)+K(\Phi_C+\varphi_C)=M_p(t) \qquad 0<t<T$$
$$J_D(\ddot{\Phi}+\ddot{\varphi}_D)=R\cdot\frac{F_f(t)}{2}-M_p(t)-\frac{i_{tot}\cdot M_e(t)}{2} \qquad (1)$$

J_C and J_D are inertia moments associated with caliper and disc, K is the stiffness of the driven part of the system and C is the total viscous damping of that part. K and C are associated with the properties of the wheel suspension.

Let the brake torque M_p have a mean value M_0 and assume that there is a brake torque disturbance with amplitude εM_0. This brake torque variation, BTV, can be a result of DTV or dynamic effects. The only assumption is that the BTV can be described by a sinusoidal function with a frequency that is an integer multiple n of the instantaneous rotational speed of the disc. Then M_p can be expressed as

$$M_p(t) = M_0(t)+\varepsilon(t)M_0(t)\cdot\sin n(\Phi(t)+\varphi_D(t)) \qquad (2)$$

Then equation (1) can be rewritten as

$$J_C\ddot{\Phi}_C+C\dot{\Phi}_C+K\Phi_C=M_0 \qquad 0<t<T$$
$$J_D\ddot{\Phi}=R\cdot\frac{F_f}{2}-M_0-\frac{i_{tot}\cdot M_e}{2}=-J_D\Lambda \qquad (3)$$
$$J_C\ddot{\varphi}_C+C\dot{\varphi}_C+K\varphi_C=\varepsilon M_0\cdot\sin n(\Phi(t)+\varphi_D(t))\approx\varepsilon M_0\cdot\sin n\Phi(t)$$

where i_{tot} is the total gearing from engine to wheel. The approximation $\sin n(\Phi(t)+\varphi_D(t))\approx\sin n\Phi(t)$ is valid except immediately after braking starts. The contact force F_f is a function not only of the brake pressure (i.e. M_0) and deceleration Λ, but also of the rolling resistance F_{Ro} and the aerodynamic drag F_l.

Let the engine brake be approximated by a linear function of the vehicle speed v

$$i_{tot} \cdot M_e = C_e \cdot (v + \delta \cdot R\omega) \tag{4}$$

where C_i and δ can be generated from the engine map (with no throttle) for the specific engine.

For constant deceleration, the frequency sweep of the wheels is described by

$$\Phi(\tau) = \beta\tau - \frac{\alpha}{2}\tau^2 \tag{5}$$

where the dimensionless time τ and the parameters α and β corresponding to relative deceleration and relative initial speed are defined by

$$\tau = \omega t \qquad \omega = \sqrt{\frac{K}{J_C}} \qquad \alpha = \frac{\Lambda}{\omega^2} \qquad \beta = \frac{\Omega_0}{\omega} \tag{6}$$

ω is an eigenfrequency of the wheel suspension, Λ is the angular deceleration of the disc and Ω_0 is the angular speed of the disc where braking starts.

When introducing ground contact, rolling resistance, aerodynamic drag, and engine braking in the brake judder model shown in fig. 1 the brake torque M_0 is changes from $\alpha\omega^2 J_D$ (derived in (9)) to the expression

$$M_0 = J\omega^2\alpha_{red}(\tau) \tag{7}$$

where J_D is exchanged for J because of ground contact and α is exchanged for the reduced value α_{red}

$$J = \frac{k_f m R^2}{2} + J_D \approx \frac{k_f m R^2}{2} \qquad k_f = 1 - a + \frac{R\Lambda}{g} b \approx 1 - a \tag{8}$$

$$\alpha_{red}(\tau) = max(0, \alpha - \upsilon_0 - \upsilon_1 \cdot (\beta - \alpha\tau + \delta) - \upsilon_2(\beta - \alpha\tau)^2)$$

k_f is the portion of the total vehicle weight working on the front axle, m is the mass of the vehicle and the parameters a and b, defined in fig. 4, determine the position of the mass centre of the vehicle.The reduction terms υ_0, $\upsilon_1 \cdot (\beta - \alpha\tau + \delta)$ and $\upsilon_2(\beta - \alpha\tau)^2$ due to rolling resistance, engine braking and aerodynamic drag respectively.

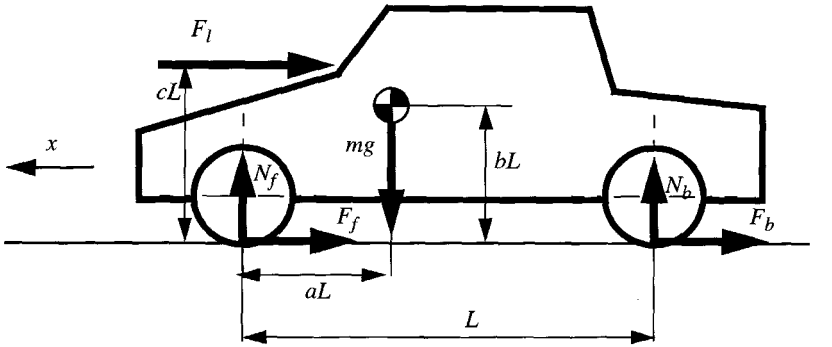

Figure 4. Forces on a braking vehicle

The parameters υ_0, υ_1 and υ_2 defined by

$$\upsilon_0 = \frac{fg \cdot k_f \cdot m}{2J\omega^2} \approx \frac{fg}{R\omega^2} \qquad \upsilon_1 = \frac{C_e \cdot R}{2J\omega}$$
$$\upsilon_2 = \frac{k_f(\rho_{air} \cdot c_w \cdot A_{cross} \cdot R^3)}{4J} \approx \frac{\rho_{air} \cdot c_w \cdot A_{cross} \cdot R}{2m} \tag{9}$$

where g is the gravity constant (9.8 m/s^2), R is the wheel radius and f is the coefficient of rolling resistance ($f \approx 0.013$ on asphalt). Further, for a normal size family car the cross section area $A_{cross} \approx 2\text{m}^2$, and shape factor $c_w \approx 0.5$. ρ_{air} is the air density, $\rho_{air} \approx 1.2\text{kg/m}^3$.

Now the differential equation for caliper vibration of equation (10) may be rewritten as

$$\varphi''_C + 2\zeta\varphi'_C + \varphi_C = \frac{\varepsilon}{\gamma}\alpha_{red}(\tau)\sin n\left(\beta\tau - \frac{\alpha}{2}\tau^2\right) \tag{10}$$
$$\varphi_C(0) = \varphi_C'(0) = 0$$

By use of the Laplace transform of equation (10), the solution can be written as

$$\varphi_C(\tau) = \int_0^\tau h(\tau - u) \cdot g(u)du$$
$$h(\tau) = \frac{e^{-\zeta\tau}\sin\kappa\tau}{\kappa} \qquad g(\tau) = \frac{\alpha_{red}(\tau)}{\gamma}\varepsilon \cdot \sin n\left(\beta\tau - \frac{\alpha}{2}\tau^2\right) \tag{11}$$

Then the formal solution of equation (10) may be written as

$$\varphi_C(\tau) = \frac{\varepsilon}{\gamma\kappa}e^{-\zeta\tau}\int_0^\tau \alpha_{red}(u) \cdot e^{\zeta u}\sin\kappa(\tau - u)\sin n\left(\beta u - \frac{\alpha}{2}u^2\right)du \tag{12}$$

where the parameters γ and ζ and the factor κ are defined by

$$\gamma = \frac{J_C}{J} \qquad \zeta = \frac{C}{2J_C\omega} \qquad \kappa = \sqrt{1-\zeta^2} \qquad 0 \le \zeta < 1 \tag{13}$$

In the previous model the parameter γ was defined as J_C/J_D, which here is a correspond to the special case when the vehicle mass is negligible. The constant κ is a factor which determines how much the eigenfrequency ω changes due to damping.The initial vibration speed (i.e. parameter β) does not influence the vibration level as long as braking starts over a certain limit (1.09 in this case).

By replacing the parameters group $A_0 = \varepsilon\alpha/\gamma$ with the time function $A_{red} = \varepsilon\alpha_{red}/\gamma$ in the corresponding expression derived by for the previous model (10) for the amplitude function e_{acc} will become

$$\begin{aligned} e_{acc} &= \sqrt{(-A_{red}(\tau) + a_0 + 2\zeta(a_0' - b_0 n\Phi'))^2 + (b_0 + 2\zeta(b_0' + a_0 n\Phi'))^2} \\ A_{red}(\tau) &= \frac{\varepsilon\alpha_{red}(\tau)}{\gamma} \\ \Phi(\tau) &= \beta\tau - \frac{\alpha}{2}\tau^2 \end{aligned} \tag{14}$$

The functions $a_0(\tau)$, $b_0(\tau)$, $a_0'(\tau)$ and $b_0'(\tau)$ are generated by solving

$$\bar{x}'(\tau) = P\bar{x} + \bar{q}_{red} \qquad \bar{x}(0) = \tag{15}$$

where

$$P = \begin{bmatrix} 0 & 0 & 1 & 0 \\ 0 & 0 & 0 & 1 \\ -p_1(\tau) & p_2(\tau) & -2\zeta & p_3(\tau) \\ -p_2(\tau) & -p_1(\tau) & -p_3(\tau) & -2\zeta \end{bmatrix} \qquad \bar{x} = \begin{bmatrix} a_0(\tau) \\ b_0(\tau) \\ a_0'(\tau) \\ b_0'(\tau) \end{bmatrix} \qquad \bar{q}_{red} = \begin{bmatrix} 0 \\ 0 \\ A_{red}(\tau) \\ 0 \end{bmatrix} \tag{16}$$

and the functions p_1, p_2 and p_3 are defined by

$$\begin{aligned} p_1 &= 1 - n^2(\beta - \alpha\tau)^2 \\ p_2 &= 2\zeta n(\beta - \alpha\tau) - n\alpha \\ p_3 &= 2n(\beta - \alpha\tau) \end{aligned} \tag{17}$$

3 RESULT AND DISCUSSION

By use of the equations (14), (15),(1) and (17) together the definition of α_{red} in equation (8) can be used to calculate the scaled amplitude function

$$\Psi = \frac{\gamma e_{acc}}{\varepsilon} \qquad (18)$$

as a function of time for various parameter combinations of parameters. Varying the deceleration parameter α when holding the others fixed. Then save the maximal value Ψ_{max} of each simulation, and put them together as vectors. The functions $\Psi_{max}(\alpha)$ are generated, one for each combination of the discrete value of the studied parameters υ_0, υ_1 and υ_2. Then the theoretical vibration-deceleration characteristics of fig. 5-7 are generated.

From equation (8) and (13)it follows that ground contact will change the parameter γ from J_C/J_D to J_C/J, where J is dominated by the vehicle mass term. This can explain why γ becomes so small when experimentally determined in a street-going vehicle. A stationary lab rig without ground contact of the wheel (such as a brake dynamometer) will result in a much higher γ-value. Then it is directly follows from equation (12) that the brake judder level will become much lower than in the vehicle.

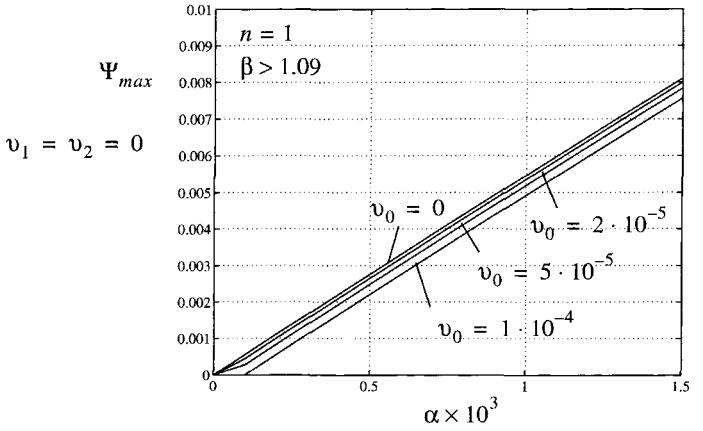

Figure 5. Effect of rolling resistance alone.

The introduction of rolling resistance, aerodynamic drag and engine braking have qualitatively the same effect. The straight line in vibration-deceleration characteristics is shifted downwards. The slope of the curve is unaffected; it is still a straight line, at least in most of the interesting region as seen fig. 5-7.

Quantitatively, the aerodynamic drag was found to have the greatest effect of the vibration-deceleration characteristics followed by engine braking. Rolling resistance at normal values ($\upsilon_0 \approx 5 \cdot 10^{-5}$ when $\omega = 2\pi \cdot 14$ rad/s and R=0.3m) had only marginal effect of the characteristics, at least in this example, see fig. 5

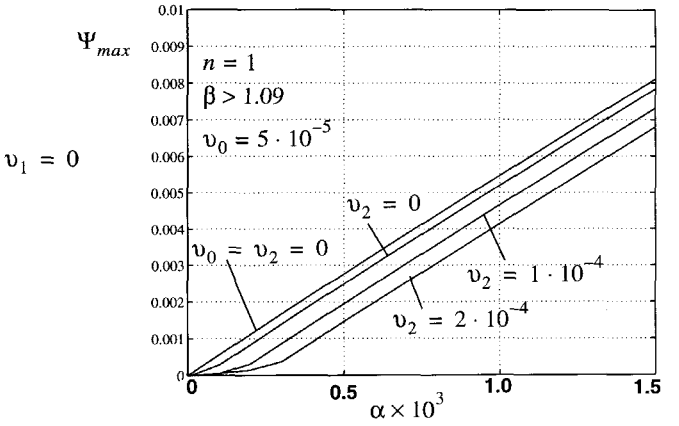

Figure 6. Effect of aerodynamic drag and rolling resistance

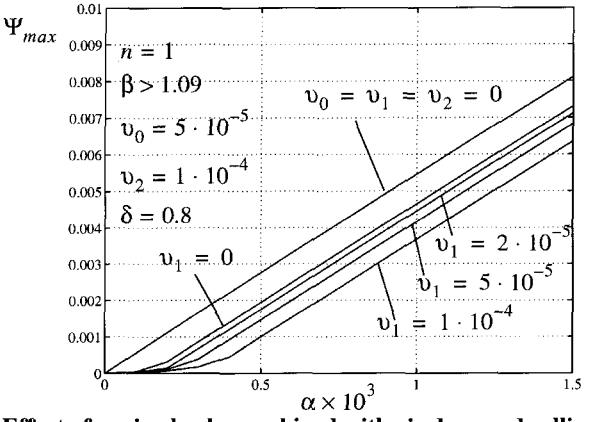

Figure 7. Effect of engine brake combined with air drag and rolling resistance.

4 CONCLUSIONS

- Ground contact will lead to that the parameter γ will become J_C/J instead of J_C/J_D where it is dominated by the vehicle mass term. This can explain why the experimentally measures γ becomes <<1.
- A stationary lab rig without ground contact of the wheel will not achieve the same vibration level as a street-going vehicle, since the γ-value will become much higher.
- Introduction of rolling resistance, aerodynamic drag, and engine brake to the judder model, cause a parallel shift of the vibration-deceleration characteristics.
- To understand the non-linearity of the measured vibration-deceleration characteristics further studies are needed.

ACKNOWLEDGMENTS

This work was carried out at Machine and Vehicle Design, Chalmers University of Technology, Göteborg, Sweden. It was supervised by Professor Göran Gerbert. Measurements were made at Chalmers on an automobile sponsored by Volvo. Financial support was provided by the Swedish Research Council for Engineering Sciences (TFR). Special thanks to Per Mattsson and Georgios Minos at Volvo Car for valuable discussions.

REFERENCES

1. Augsburg, K., Brunner, H., and Grochowicz, J. "Untersuchungen zum Rubbelnverhalten von Pkw-Schwimm-sattel-bremser", *ATZ Automobiltechnische Zeitschrift* 101, pp 22 -30, 1999.
2. Bosch, "*Automotive Handbook*", 3rd edition, SAE, ISBN 1-56091-372-X
3. Bosworth, R., "Investigations of Secondary Ride Aspects of Steering Wheel Vibration (Shimmy and Judder) using Taguchi Methodology", *Proceedings, AUTOTECH 89*, London, IMechE paper C399/9, 1989.
4. Crolla, D.A., and Lang, A.M., "Brake Noise and Vibration - The State of the Art," Vehicle Tribology, Tribology Series, No 18, pp. 165-174, Leeds, England, 1991.
5. Engel, H.G., Bachman, Th., Eichhorn, U., and Saame, Ch., "Dynamical Behaviour of Brake-Disc Geometry as cause of Brake Judder", *Proceedings, EAEC 4th International Conference on Vehicle and Traffic System Technology*, Vol 1, pp. 465-481, Strasbourg, France, 1993
6. Engel, H.G., Hassiotis, V., and Tiemann, R., "System Approach to Brake Judder", *Proceedings, 25th FISITA Congress*, Vol. 1, pp. 332-339, Beijing, paper 945041, 1994
7. Haigh, M.J, Smales, H., and Abe, M., "Vehicle Judder under Dynamic Braking caused by Disc Thickness Variation," *Braking of Road Vehicles*. pp. 247-258. London. I.Mech.E. paper C444/022/93., 1993
8. Inoue, H., "Analysis of Brake Judder caused by Thermal Deformation of Brake Disc Rotors", *Proceedings, 21th FISITA Congress*, Belgrade, pp. 213-219, paper 865131, 1986
9. Jacobsson, H., "Wheel Suspension related Disc Brake Judder", *Proc, ASME Design Engineering Technical Conferences*, Sacramento, California, 1997.
10. Jacobsson, H., "Analysis of Brake Judder by use of Amplitude Functions", *Proc, SAE Noise and Vibration Conference*, Traverse City, Michigan, SAE Paper 1999-01-1779 1999.
11. Kao, T. K., Richmond, J. W., and Douarre, A., "Thermo-Mechanical Instability in Braking and Brake Disc Thermal Judder; an Experimental and Finite Element Study", *Proceedings, The 2nd International Seminar on Automotive Braking, Recent Developments and Future Trends*, pp 231-263 IMechE, Leeds, UK, 1998.
12. Kim, M-G, Jeong, H-I, and Yoo, W-S, "Sensitivity Analysis of Chassis System to Improve Shimmy and Brake Judder Vibration on Steering Wheel.", *SAE Special Publications*, no. 1136, pp 59-70, 1996.
13. Stringham, W., Jank, P., Pfeifer, J., and Wang, A., "Brake Roughness - Disc Brake Torque Variation, Rotor Distortion and Vehicle Response," *SAE Transactions*, Section 6, pp. 1235-1247, SAE Paper 930803, 1993.
14. de Vries, A., and Wagner, M., "The Brake Judder Phenomenon", *SAE Transactions*, Section 6, Vol. 101, pp. 652-660. SAE paper 920554, 1992.

Brake Refinement – II

This page intentionally left blank

The use of high-speed ESPI and near-field sound pressure measurements to study brake-disc modal behaviour

C EDWARDS, N TAYLOR, D WILLIAMS, M DALE, and **C BUCKBERRY**
Land Rover Group Limited, Gaydon, UK
M REEVES
Scitek, Derby, UK

ABSTRACT

This paper discusses the findings of an experiment into disc brake squeal and the associated vibration modes present on the disc. Two techniques were used in the experiment; High-Speed ESPI (Electronic Speckle Pattern Interferometry) and Near-Field Sound Pressure Measurement.

The combination of these two techniques has allowed a mathematical model to be formulated that agrees with that proposed by others for brake rotor mode mobility and explains varying fringe rotation rates observed previously in holographic interferometry and thought to be experimental error. The mathematical model requires 2 modes of the same order to be present on the disc, but with different amplitudes, spatial or temporal separations. Sound field results and ESPI fringe rotation rates are presented along with predicted results from the mathematical model.

Sound radiation modelling results are also presented for a brake disc; these help to demonstrate why squeal can be so problematic.

1 INTRODUCTION

The much studied subject of brake squeal is becoming more important as vehicle customers demand more refinement. Brake squeal can occur under most braking conditions, although the exact conditions are dependent on the specific brake under study. Most disc brake squeal is characterised by a vibration mode on the rotor. Nowadays brake refinement is becoming an issue that has associated with it a very large warranty bill.

Historically brake squeal has been studied greatly by academia; many theories abound as to why squeal occurs, yet it still remains a problem today. One of the greatest problems is that a

brake changes its physical structure over time, mass and stiffness are lost due to wear, friction can change depending on pad history etc. Therefore a fix that was working can cease functioning in time, or perhaps make squeal even worse.

Traditional fixes for brake squeal include mass and stiffness modifications, lining material changes, the fitting of a noise fix shim to the pad etc. Mass and stiffness modifications are the cheapest method of fix in terms of piece cost, but these have to be implemented early in the design cycle if large tooling costs are to be avoided. Changing the lining material is problematic as any new material must meet the friction requirements, the vehicle manufacturers fade requirements and must have a better level of refinement. Noise fix shims are a very popular palliative, but they are very expensive and their performance can be degraded when the brake is subjected to high temperatures. All of the above means there is a need to be able to model brakes so that squeal problems can be identified and fixed before components are made. Currently refinement issues are dealt with on prototype cars and rigs; quite often the components being used are radically changed before volume production, which means work is repeated many times.

2 LITERATURE REVIEW

A large number of papers have been published which contain models describing brake squeal. Some authors have also used optical techniques to image the brake rotor vibrations during squeal generation in the hope of gaining greater insight. There follows a brief review of some of the most pertinent literature of the last few decades.

Up until the early 1960s it was assumed that brake squeal was due to variable dynamic friction. The first move away from this concept was made by Spurr in 1961 (1), the new idea involved a simple model of a double cantilever and constant friction. It was shown experimentally that such a system did stick-slip (or sprag-slip), however, the model was only explained qualitatively. Spurr's model did suggest that the friction level was a critical factor.

In 1963/64 Jarvis *et al* (2) showed that a constant coefficient of friction could be used to explain squeal generation. They showed that squeal arises from the geometry of coupling between components and suggested that it might be possible to design out the problem. Their model consisted of a cantilever beam whose end was loaded against the disc. The beam angle and load could be changed. They observed experimentally the possible existence of two simultaneous modes of vibration, which they attempted to include within their model by creating a non-rigorous proof.

In the 1970s a large amount of work was done on the modelling of brake squeal, one of the most notable authors was North (3). This paper reviewed previous theories and models, from the 1960s onwards, that had been put forward to explain brake squeal. North also put forward a new theory that owed its origins to the flutter of aircraft wings, the new theory was termed binary flutter. North realised that the two vibration modes were unnecessary for the model of Jarvis *et al*, however, they were necessary for the new binary flutter model. The binary flutter model was verified with experiment and it was found that small tweaks to measured stiffness values gave good correlation between the model and experiment, which used a real brake.

Millner (4) reiterated the theory that squeal arises from a geometrically induced or kinematic constraint instability of the elastic system. Millner used a 6 degree of freedom model that

incorporated the relevant parts of other theories. The model predicts what should happen when various factors within the brake system are changed for example caliper stiffness, pad friction etc. The paper discusses the correlation between theory and practice, and the practical implications of the model results. Millner states that use of mass and stiffness could improve system stability, but notes that as the pad wears the brake geometry changes and therefore squeal may return.

Lang *et al* (5) performed an experiment into squeal modes using a goods vehicle drum brake. The paper describes the rotor vibration as complex and draws comparisons with the findings of Jarvis *et al*. Using experiments it was determined that free-free modal analyses do not reliably predict squeal frequencies or propensity. Lang *et al* used a mode splitting technique to cure squeal problems, this requires knowledge of the rotor mode order so that the correct number of masses can be attached.

Matsushima *et al* (6, 7) modelled a couple of disc brakes, with different calipers, using finite element methods. The papers compare modelled brake squeal frequency with that of the actual brakes. The frequencies modelled are all below 5 kHz, at which point the theoretical and experimental results agree within a few hundred Hertz. The authors used the propensity index suggested by Millner to select which modelled frequencies matched the experimental frequencies. It appears that the authors have not verified the individual component frequencies before creating a complete model, if this had been done then it might indicate which factors are causing the difference between results, for example pad material, which is probably highly non-linear.

Felske *et al* (8) were one of the first groups to use holographic interferometry to view the vibration modes on a self excited disc brake. They present interferograms for two types of brake; a yoke and a fist type. The disc interferograms presented are self excited (Double Pulsed Holography) and artificially excited (Time Averaged Holography). The paper suggests that the audible noise from a brake system comes from the pad and caliper, and not the disc as the noise from this destructively interferes in air. This is at odds with our sound radiation models, which suggest it would be hard to design a better sound radiator. It is also surprising as the authors would have artificially excited modes on the discs, an experience that can be quite painful without ear defenders.

Using Double Pulsed Laser Holography, Fieldhouse *et al* (9) investigated a noisy disc and drum brake. A great deal of emphasis was placed on extracting as much useful temporal information as possible, this was achieved by linking sets of holograms together via use of a vibration trigger signal from a piezo electric crystal. The trigger allowed holograms taken tens of seconds apart to be formed into a time series. The problem with this approach is that the squeal amplitude and frequency may shift slightly. The plot of antinode position against time within the paper shows that the vibration on the disc is complex in nature, and that the deviation from the linear theoretical is a manifestation of the vibration. However, this was not realised by the author at the time, due to the possibility of triggering errors. The quality of the results is now easy to see when compared with the time resolved results from High-Speed ESPI.

3 THE TECHNIQUES

Traditional methods of measuring vibration, accelerometers, are impractical for measuring the vibration of a disc brake rotor because the flat faces of the rotor pass under the pads and the rotor edge passes close to the caliper, also the whole system is rotating. For the above reasons it is difficult to measure the vibration of a naturally excited brake disc, Double Pulsed Laser Holography has been an aid in the past but it does not provide a time resolved output, merely a "snapshot" in time. To produce a time resolved output of the vibration two techniques were used:

1. High-Speed Electronic Speckle Pattern Interferometry (ESPI).
2. Near-Field Sound Pressure Measurements.

ESPI or TV Holography produces output similar to Holographic Interferometry, except that the results are visible almost instantly and in the case of HSESPI the system is capable of 40000 frames per second.

The sound pressure measurements allow surface velocities to be gauged, as sound pressure is proportional to the surface velocity. Thus acceleration can be measured where a normal accelerometer could not be placed.

All of the work was carried out using a brake dynamometer to drive the brake under examination.

3.1 Brake Test Rig

The test rig uses a 7.5 kW electric motor driving through a 30:1 worm gear reduction box to provide high torques to drive the brake under test. The speed of the brake can be varied between 0-80 RPM, this is achieved using a Hitachi J300 IGBT Inverter. A pressure between 0-12 MPa can be applied to the brake under test. Temperatures are measured using a rubbing thermocouple with digital read out. Typical parameters used in squeal generation are 10-20 RPM, 10-20 MPa and 100-200° C. Figure 1 shows a typical disc brake system under test.

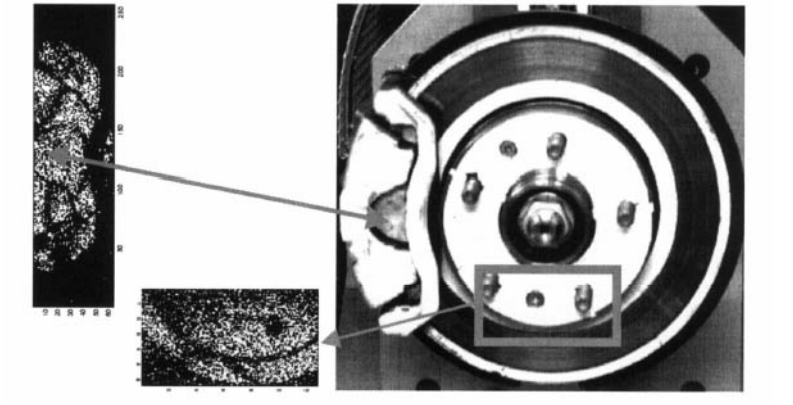

Figure 1. Brake under test on the dynamometer showing retroreflective tape and output from the HSESPI system.

3.2 High-Speed ESPI System

The High-Speed ESPI system consists of a Kodak 4540 high-speed digital camera and a 140 mW Continuum DPSS continuous wave, frequency-doubled (λ=532nm) YAG laser together with optics for object and reference beam formation and delivery. The camera lens was a Nikon 35-80mm, operated with an aperture of f/# = 16.

The brake disc and caliper, suitably coated with high-gain retroreflective tape, are shown in Figure 1. The tape was applied to the static components, and also to three areas on the disc itself. The top hat at the centre of the disc demonstrated very low vibration amplitudes, and was therefore not studied further. An 8mm wide annulus around the inner edge of the disc was coated with retroreflective tape, and this was found to show a vibration amplitude of between one and two interference fringes (approximately 0.25-0.5 microns) during naturally excited squeal. The vibration amplitudes at the edge of the disc were typically found to be too high for the present ESPI technique, causing significant phase averaging over the camera integration time of 37-55 microseconds. Therefore work concentrated on observing the inner annulus.

Example speckle correlograms are shown, Figure 1, for a 90° arc of the brake disc as well as the fixed brake components. Correlograms are the processed output from the ESPI system and can be interpreted the same as holographic interferograms. The curved, dark fringes in these images represent contours of the change in surface height between successive camera frames and visualise the instantaneous modal behaviour adopted by each component. Although the behaviour of the fixed components is important in squeal mitigation, the discussion here will be restricted to the modal behaviour of the disc itself.

3.3 Near Field Sound Pressure Measurements

The sound field generated by a brake disc in isolation excited with a sinusoidal input has been shown to have a distinct spatial structure in the near and far field. The relationship between surface displacement and near-field sound pressure is shown very clearly by Figures 2a and 2b.

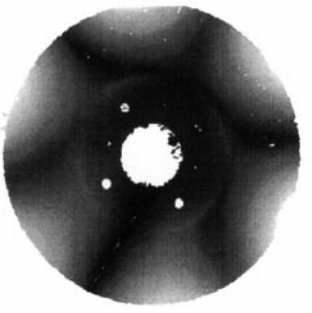

Figure 2a. Surface displacement of free-free disc.

Figure 2b. Average pressure contours (2dB per interval) 0.01m from surface of free-free disc.

The pressure along the nodal lines is ≥ 20dB lower than that at an antinode. This structure is also maintained at greater distances from the brake.

The sound field produced by the brake disc in its free-free condition has a very distinct structure. If the squeal mode of vibration of the brake disc under normal operating conditions were rotating around the disc then this rotation would be observed in the sound field. A measurement and analysis of the sound field under operating conditions would allow some inference of the mode of vibration of the brake disc.

When recording sound field pressures, the microphone array provides a signal proportional to the out-of-plane surface velocity. Thus, iso-pressure contours in the time-resolved sound pressure field are also out-of-plane iso-velocity contours. Sequentially subtracted, High-Speed ESPI correlograms display dark fringes which also represent contours of out-of-plane surface movement over the fixed frame period. Therefore, the fringes may also considered as surface iso-velocity contours and are directly analogous to the near-field sound pressure contours. If the interference fringes appear to translate or rotate in time, so too should the iso-pressure contours in the time-resolved sound measurements.

4 RESULTS AND MODELLING

The phenomena observed within the experiment required explanation, therefore the surface deformation of the disc was modelled. Once the deformations were obtained it was possible to model ESPI fringe patterns and sound pressure data, this allowed a number of vibration types to be validated against experimental results. It was also possible to predict sound radiation efficiencies using the deformations.

4.1 Brake Disc Investigated

A typical disc brake system exhibiting a 4^{th} diametral squeal mode at around 3kHz was investigated. The squeal could be induced at rotation rates between 3 and 40 RPM with a typical brake pressure of the order of 25 MPa. The temperature of the brake surface was approximately $140^{o}C$ at the time of squeal onset.

The disc modal behaviour visualised by ESPI and the near-field sound pressure measurements could vary considerably from one test to the next. Subjectively, one of two different spatial sound fields could be heard. The most commonly observed case appeared to have time-stationary minima where the noise was clearly less than at the loudest locations. This first case will be referred to as the "Complex Mode" or "Case 1". The second case, which occurred less frequently and had an apparently louder and more pure tone was accompanied by an apparent switching of the apparent sound source from one ear to the other every few seconds. This will be referred to as the "Standing Mode" or "Case 2". As expected, the microphone array measurements of time-resolved and RMS sound pressure showed significant differences in the two cases. In addition, the accompanying High-Speed ESPI movies showed a quite different disc modal mobility for the two distinct acoustic behaviours.

4.2 Mathematical Model of Squeal Modal Behaviour

Several candidate models of the disc modal behaviour were considered. These included a pure travelling mode and several waves generated by the mixing of two slightly different

frequencies. None of these waveforms were found to produce a near-field time-averaged sound pressure field of the correct form. The most successful description was the complex mode proposed by Jarvis *et al* (2). This description assumes the single frequency excitation of two identical diametral modes with a spatial and temporal phase shift between them.

The standing mode is just a special case of the complex mode, where only one of the two possible modes is excited at any time. Here we choose to simplify the two-dimensional surface vibration on a disc and approximate the behaviour around a single thin annulus as a one-dimensional wave with no damping. For the purposes of modelling and data presentation, the thin annulus at a single radius was unwrapped into a straight line of length 2π radians.

The undamped surface vibration due to two point excitation along the line, can be expressed in the general form:

$$S(\theta,t)=A_1 sin(\omega t+\tau_1)sin(\theta M+\alpha_1)+A_2 sin(\omega t+\tau_2)sin(\theta M+\alpha_2) \qquad \text{Eq. 1.}$$

Where;

S = Surface deformation;
t = Time, s;
θ = Disc position, rads;
M = Mode Order;
ω = Frequency, rads/s;
A_1, A_2 = Peak amplitudes;
τ_1, τ_2 = Temporal phase shift, rads;
α_1, α_2 = Spatial phase shift, rads.

For Case 1, a complex wave is generated by using:

$$A_1 = A_2,\ 0 < |\tau_1 - \tau_2| < \pi/2 \text{ and } 0 < |\alpha_1 - \alpha_2| < \pi/2.$$

For Case 2, a pure standing wave is generated by using:

$$A_1 = A_2,\ \tau_1 = \tau_2 \text{ and } \alpha_1 = \alpha_2.$$

It should be noted that different combinations of variable values can yield similar results to the variables above.

The instantaneous pressure field may be estimated by differentiation of the surface deformation with respect to time:

$$P(\theta,t) \propto \dot{S}(\theta,t) \qquad \text{Eq. 2.}$$

The locus of the iso-pressure contours has a one-to-one correspondence with the locus of the ESPI fringe orders as discussed earlier. Thus, if the ESPI fringes appear to rotate in one direction as time progresses, so too will the iso-pressure contours, including the maxima and minima, of $P(\theta,t)$. Further to this, the spatial variation of the RMS value of $P(\theta,t)$ should correspond to the spatial structure in the RMS sound pressure measurements.

Thus, it is possible to validate any model of the surface deformation against the observed ESPI fringe movement and both the observed sound pressure history and mean pressure field.

4.3 High-Speed ESPI, Near-Field Sound Pressure Measurements And Model Results

When the squeal was at its loudest and a pure tone was heard the ESPI correlograms, Figure 3a, showed a vibration mode on the disc that did not move around the disc's circumference. At the same time a structured sound field was present, Figure 3b, with high peaks and deep troughs. These results were easily modelled by assuming a standing vibration mode on the disc, this predicted ESPI fringes which are stationary in space and a sound field that has well defined structure, Figure 3c.

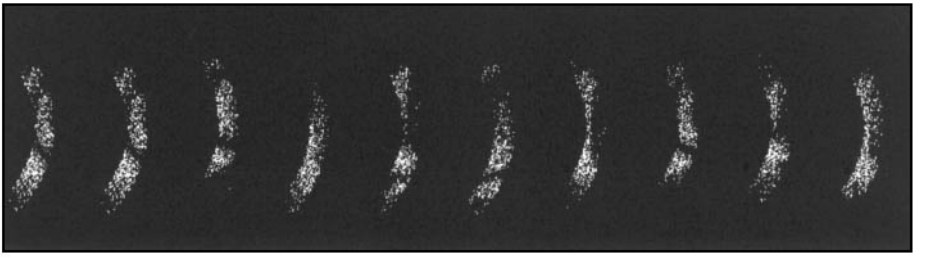

Figure 3a. Series of successive High-Speed ESPI correlograms for the standing mode, Case 2, showing only small changes in fringe location from one frame to the next. 18000 frames/sec. Correlograms show displacement between frames, not absolute displacement.

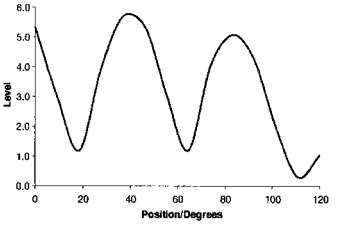

Figure 3b. Measured RMS sound pressure for Case2. 15-20dB spatial variations.

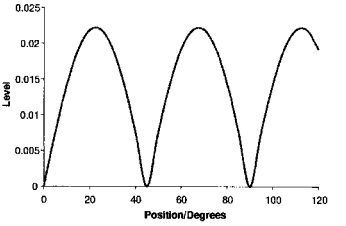

Figure 3c. Predicted RMS pressure field for Case2.

However, the standing wave is only observed occasionally. The ESPI correlograms usually show a rotating mode shape, Figure 4a. This rotating mode shape is accompanied by a sound field that has structure which is less well defined, Figure 4b. If a mode rotates, i.e. a travelling wave, then the RMS sound pressure should be a constant around the disc and this was not observed. It was only with the modelling of the vibration modes that a solution was found and validated. The solution to the problem is a complex mode, this predicts "apparent" fringe rotation and structure in the sound field, the predicted sound field structure is shown in Figure 4c.

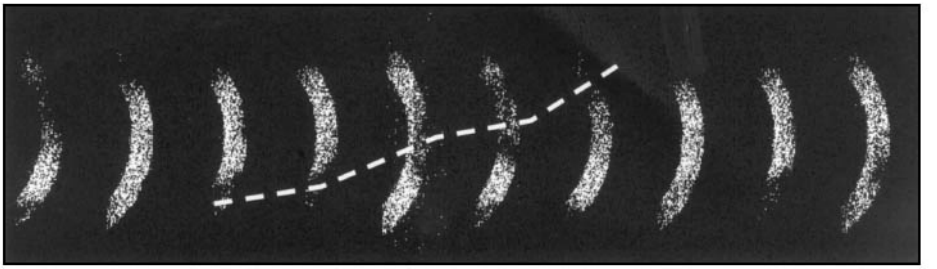

Figure 4a. Series of successive High Speed ESPI correlograms showing non-uniform fringe rotation in Case 1. 18000 frames/second. Squeal frequency 3kHz. Pattern repeats every 6 frames. Locus of one fringe order indicated by dashed line.

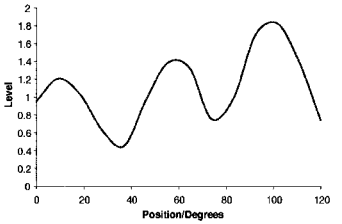

Figure 4b. Measured RMS pressure for complex mode, Case1. Spatial variations in range 6-11 dB.

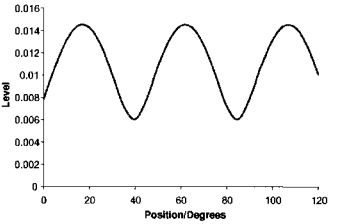

Figure 4c. Predicted RMS pressure for complex mode, Case1. Predicted variations of ~7dB.

The "apparent" fringe rotation that the complex mode predicts has a time varying rotation that can be seen in the sound pressures, Figure 5a, and in the ESPI fringes, Figure 5b. Non-linear rotations of rotor modes have been observed before using Double Pulsed Laser Holography, although they have not been explained (9), Figure 5c. The rotation rate that the complex mode predicts is shown in Figure 5d, it can be seen that the model agrees well with the experimental results.

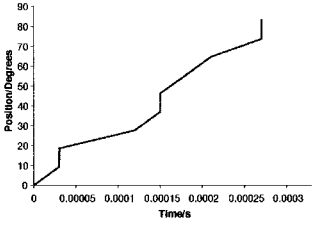

Figure 5a. Rotation rate of sound iso-pressure contours from measured time history.

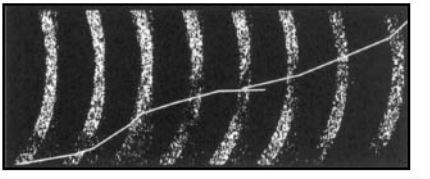

Figure 5b. Movement of ESPI fringes.

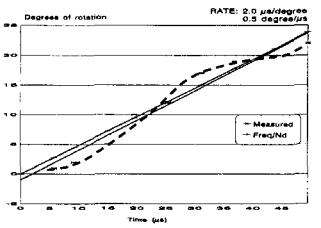

Figure 5c. Experimental fringe movement for diametral order 4 at 2750Hz. After Fieldhouse (9).

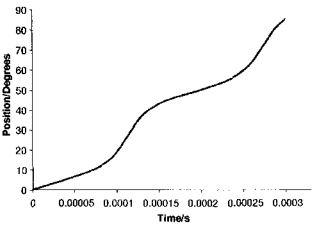

Figure 5d. Predicted fringe movement from complex mode theory for diametral order 4 at 3000Hz.

Using sound pressure modelling it is possible to calculate the average sound pressures at various distances from the disc. This requires knowledge of the rotor's mode order, vibration amplitude, frequency and vibration phase. Figure 6a shows the average sound pressure map over a hemisphere of radius 0.5m from the brake disc, the pressure map is for a standing 4th diametral mode whose frequency is 3.2 kHz and amplitude is 5 µm. There is structure around the hemisphere's circumference which reflects the mode order. Figure 6b shows a sound pressure map for a similar vibration, except that it is a pure travelling wave. Around the circumference there is no structure and therefore this type of vibration was not observed in the experiments. A complex mode would have similar structure to that shown in Figure 6a, but it would be less well defined. The existence of structure in the sound field relating to the disc vibration contradicts the views of Felske *et al* (8).

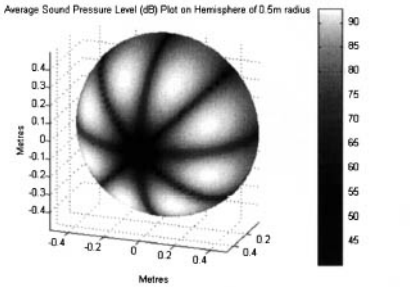

Figure 6a. Average sound pressure 0.5m from a disc, standing 4th diametral mode, 3.2 kHz, amplitude 5 µm.

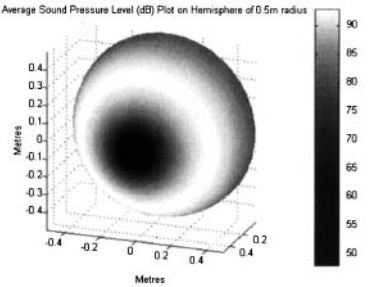

Figure 6b. Average sound pressure 0.5m from a disc, travelling 4th diametral mode, 3.2 kHz, amplitude 5 µm.

4.4 Sound Radiation Efficiency

Optimum efficiency (maximum energy transfer from vibration to sound or vice versa) is achieved when the plate is vibrated such that the wavelength of flexural waves in the plate is equal to the wavelength of acoustic waves in the air (alternatively the flexural wavenumber in the plate is equal to the wavenumber of the acoustic waves.). This is more commonly known as the coincidence or critical frequency of radiation f_c.

However, the flexural wavelength in the structure will match the acoustic wavelength in air over a frequency range when the projection of the acoustic wave onto the structure is considered (10).

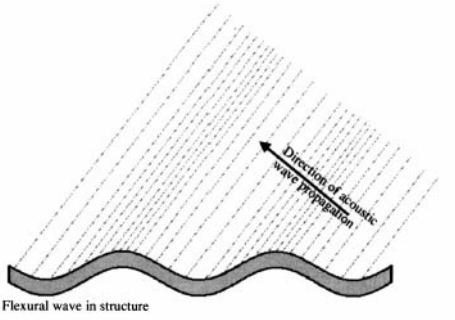

Figure 7. Acoustic wave radiated from a structure at a projected angle.

The projection of the acoustic wave onto the flexural wave in the structure is based on a $\sin(\phi)$ term where ϕ is the angle between the direction of acoustic wave propagation and the normal to the structure, Figure 7.

The result of this is that for a given structural mode of vibration e.g. 3 diametral mode of a brake disc the radiation efficiency of the disc will be dependent on the frequency at which this mode occurs. Figure 8 shows the radiation efficiency plotted versus frequency for a 3 diametral mode of a brake disc with a diameter of 0.26m.

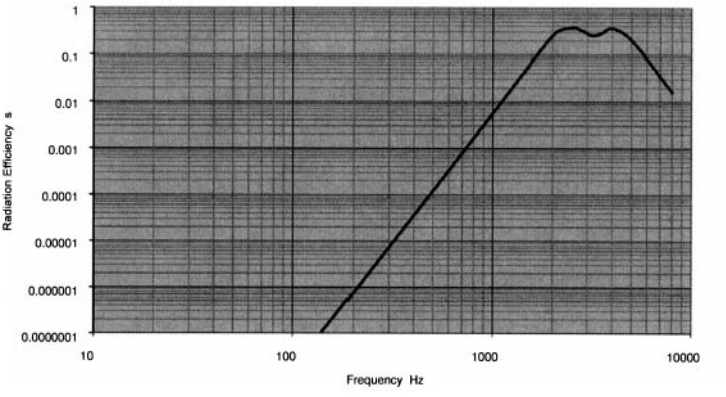

Figure 8. Radiation efficiency versus frequency for a 3 diametral mode of a brake disc (0.26m diameter).

The radiation efficiency is at a maximum from around 2000Hz to 5000Hz. This is typically the frequency range of vibration for a 3 diametral mode on most modern brake discs. A step change in efficiency would only be gained by reducing the frequency of vibration to ~1000Hz. However, this would impact on the integrity of the disc structurally and would not

help the overall situation as higher modes of vibration would then be in this frequency range. The other alternative is to move the 3 diametral mode of vibration above 5000Hz. This would be very difficult within the constraints of the package.

5 CONCLUSIONS

Two distinct modes of vibration of the brake disc were observed in this work. The most commonly occurring was the complex mode. This may be generated simply by the superposition of two diametral modes of the same order that have a spatial and temporal phase difference. A less frequently occurring standing mode corresponds to the excitation of just one of the two possible diametral modes.

In the more common form of the complex mode brake squeal, the mathematical description of the surface vibration waveform is able to reconcile the time averaged and time-resolved sound pressure measurements with the observations of High-Speed ESPI and Double Pulsed Holography. The ability of this waveform to predict the previously unexplained non-uniform fringe rotation rate in holographic work is further evidence that this is indeed the correct description for the majority of non-standing disc vibration modes under conditions of natural excitation.

The complex mode description of disc squeal is also in agreement with that proposed by others for brake rotor modes. This points to a possibly generic excitation mechanism for brake squeal in both disc and drum systems.

REFERENCES

(1) Spurr, R.T., "A Theory Of Brake Squeal". IMechE Auto Div Proc, No. 1, 1961/62, pp 33-40.

(2) Jarvis, R.P., Mills, B., "Vibrations Induced By Dry Friction". Proc Instn Mech Engrs, 1963/64, Vol 178, Pt 1, No 32, pp 847-866.

(3) North, M.R., "Disc Brake Squeal". IMechE, 1976, pp 169-176.

(4) Millner, N., "An Analysis Of Disc Brake Squeal". SAE Paper No. 780332, 1978.

(5) Lang, A.M., Schafer, D.R., Newcomb, T.P., Brooks, P.C., "Brake Squeal – The Influence Of Rotor Geometry". IMechE Paper No. C444/016, 1993, pp161-171.

(6) Matsushima, T., Nishiwaki, M., Masumo, H., Ito, S., "FEM Analysis Of Low Frequency Disc Brake Squeal (In Case Of Opposed Type Caliper)". SAE Paper No. 973020, 1997.

(7) Matsushima, T., Masumo, H., Ito, S., Nishiwaki, M., "FE Analysis Of Low Frequency Disc Brake Squeal (In Case Of Floating Type Caliper)". SAE Paper No. 982251, 1998.

(8) Felske, A., Hoppe, G., Matthai, H., "Oscillations In Squealing Disk Brakes – Analysis Of Vibration Modes By Holographic Interferometry". SAE Paper No. 780333, 1978.

(9) Fieldhouse, J.D., Newcomb, T.P., "Double Pulsed Laser Holography Used To Investigate Noisy Brakes". Optics And Lasers In Engineering 25, 1996, pp 455-494.

(10) Fahy, F. J., Sound And Structural Vibration, Radiation, Transmission And Response. Academic Press, 1985. ISBN 0-12-247671-9.

Noise investigations of a commercial disc brake using holographic interferometry

C A BEVERIDGE and **J D FIELDHOUSE**
School of Engineering, University of Huddersfield, UK

ABSTRACT:

The paper discusses the design and manufacture of a small-scale continuous drag dynamometer for noise testing a full size commercial vehicle disc brake. The rig has been carefully designed to replicate mounting of the brake as in the vehicle yet allow both the non-driven front wheels and driven rear wheels to be accommodated within the same structure. The design uses a 45kW AC motor as the prime mover, this being geared down to 30:1 using a mechanical reducer. The speed of the rotor is variable from zero to 100 r/min. A friction material with an artificially high coefficient of friction was used to promote noise. The whole body visual technique of holographic interferometry is used to investigate the modes of vibration of the principal component parts, mirrors being used to allow visual access to otherwise hidden areas. Selected examples of initial holograms are presented and discussed. The information obtained indicates that the vibrational characteristics of the commercial brake are similar to those of a car brake and that positive cross-correlation of information may be a possibility. An analysis of the pad/disc interface geometry, as used on car brakes, allows the probable instability frequency to be predicted, this being the frequency generated during the tests.

1 INTRODUCTION

Brake noise is merely an annoyance to drivers but this annoyance is reputed to cost vehicle manufacturers within Europe US$100 million a year in warranty claims. This cost is exacerbated when the additional costs of research undertaken by the brake and friction material suppliers are accounted for. It is not therefore an insignificant problem in terms of finance for the motor industry and a great deal of effort has been, and is being expended, in an attempt to understand and eradicate this phenomenon. High volume production vehicles receive greatest attention because of the cost implications and the concern that if complaints reach significant levels the reputation of the vehicle manufacturer may become threatened. The reason for the levels of complaints with cars is because the owners are often the drivers and it is a significant part of the assets of an individual. That is not the case with commercial vehicles, they are low volume production and the driver is often not the owner, nor is the vehicle likely to form part of the driver's status rating. Complaints in this class of vehicle are not therefore so forthcoming and are not considered a main priority regarding the vehicle

specification. As a consequence research regarding commercial brake noise may be regarded as minimal, this being reflected in the number of publications on the problem and of these the tendency has been focussed on drum brakes (1 - 4 typically)

The general acceptance of commercial vehicle brake noise is about to change. There is a growing awareness of environmental issues with all engineers and controlling bodies and commercial brake noise may be now considered an environmental pollutant. Commercial brake noise is more than an annoyance. It is verging on frightening if you happen to be a cyclist or pedestrian in close proximity to the brake and may even prove dangerous to an unwary driver who reacts aversely to the noise. Complaints will go beyond the driver and owner and legislation will be issued to ensure commercial brakes become quiet. The situation is already starting to change and the need for quieter commercial brakes is now being addressed.

Heavy commercial disc brakes are currently at a relatively infant stage and the use of industrial dynamometers has so far been mainly limited to performance and wear testing. Noise generation is usually fugitive in nature and the high cost of dynamometer testing cannot be justified without the guarantee of a positive result. In addition, the need to accommodate the brake to suit the dynamometer may raise criticism that it becomes too remote from the real situation. In-vehicle testing is clearly the best method but it is equally expensive and the information is often restricted because of instrumentation problems and therefore difficult to interpret meaningfully. There is therefore a need to test the brake on an economical facility that will replicate the mounting as in the vehicle and allow sensible information to be gathered. It is also not necessary to consider a commercial brake in isolation because it is little more than a larger version of a car brake. There is a need to call upon the vast amount of information accrued on car brakes (5 to 8) and to correlate this information with the data obtained from commercial testing.

It is the purpose of this paper to outline the foundation work undertaken in creating a small scale commercial brake testing facility and to present the very early results using the whole body visual technique of holographic interferometry.

1.1 Commercial Brake Research

There is very little published research into commercial brakes and it is generally accepted by industry that there is little information or knowledge regarding commercial brake noise. This is seen by the lack of publications in this area.

Investigations of self excited noise in commercial disc brakes are rare and generally only undertaken in response to customer/driver complaints. The investigation will terminate when a "noise fix" has been established and subsequent correlation of any information or findings is limited, if it exists at all. Because the investigations are only concentrated on a "noise fix" the work tends to be "job focused" and as a consequence research into the fundamental causes is superficial and limited. Since the work is customer related there is little dissemination of the results and few papers are available on any form of commercial vehicle brake noise and associated investigations. This is despite the audible magnitude of a noisy commercial brake, its affects on the environment and the anxiety caused to any member of the public in close proximity to it. As a result, the problems of brake noise with commercial vehicles continues with industry in general making little apparent movement towards improving the position.

Only a few concerned partners are sensitive to the issues and are prepared to investigate the problem and release information.

2 THE BRAKE DESIGN

Commercial disc brakes are different to car disc brakes in many respects. In more recent designs the disc is fixed using an alternative system to the usual method of bolting through a "top-hat" arrangement. The calliper and pad assembly is much larger in relation to the disc than a car brake, the calliper occupying a greater angular proportion of the disc in commercial brakes. In addition pressure is applied using a pneumatic applicator through a mechanical amplifier rather than hydraulic operation. As a consequence, noise fixes pertinent to car brakes often do not work on commercial brakes and it is the design differences that are quoted as the reason for their ineffectiveness. It must be also accepted that the extreme pressure and temperature conditions found on a commercial brake and the durability of car brake solutions often make them inappropriate for commercial vehicle installations. But the principle of operation of a commercial brake is similar to that of a car in that it has a calliper body housing the pads that are mechanically or hydraulically forced onto a rotating disc so the instability mechanism may show a relationship. To give an indication of size Table 1 gives a comparison between the commercial brake and a fairly standard car brake.

Table 1 – Comparison of brake sizes.

2.1.1 Brake	DISC – APPROX. DETAILS		CALLIPER	PAD
	MASS	DIAMETER	MASS	SURFACE AREA
Car	3 kg	220 mm	2.3 kg	2500 mm^2
Commercial	33 kg	435 mm	50 kg	19000 mm^2
Increase	11	2	22	7.6

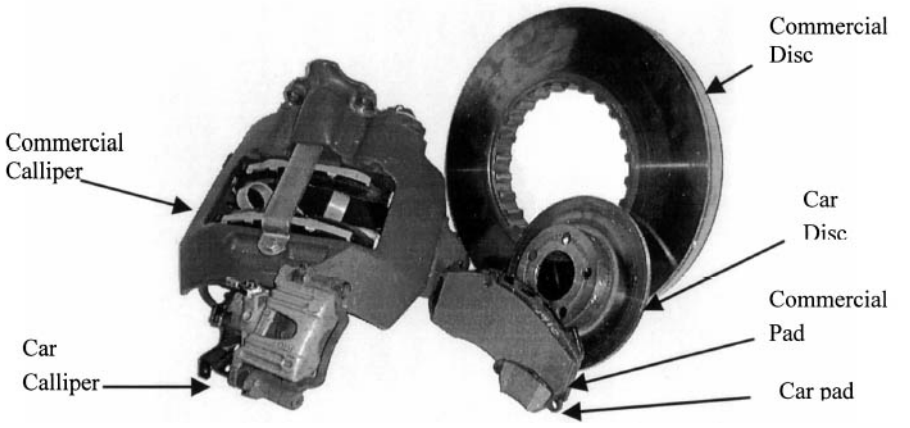

Figure 1- Comparison between a small car disc brake and commercial disc brake.

Figure 1 shows the two brakes arranged together to get a better appreciation of their size. The calliper is of the sliding fist type and is air actuated, rather than hydraulic, operating at a

maximum of 9 bar (0.9MPa). Although many similar components are used for the front and rear brakes there is a marked difference in their design. The front brake calliper is mounted horizontally over the disc and protrudes only a short way into the vehicle chassis to allow a smaller clearance arc when steering. It also has a vertically mounted brake cylinder since vertical space can be allowed for. However the rear brake calliper is mounted on its side trailing the disc with a greater intrusion into the chassis by the horizontally mounted brake cylinder, dictated by the suspension and axle design.

3 TEST RIG DESIGN

Several smaller test rigs have already been designed and built successfully at the University of Huddersfield and the knowledge gained from their operation has been used to help in the design of the commercial test rig.

The primary concern was that the rig should mimic the vehicle as near as possible and with no compromise regarding the existing brake design. It was only with close collaboration with the industrial partners that it was possible to build a test rig that would replicate the in-vehicle mounting of the brakes. There was a desire from all parties to ensure that both the front and rear offside brakes could be mounted on the test rig with the minimum amount of down-time. By careful design a rig was designed to accept both the offside and nearside brakes, so anticipating the inevitable need to confirm that the brakes on both sides of the vehicle behave the same.

3.1 Motor and Gearbox

The motor and gearbox selection was based on experience. It is known that brake noise is independent of vehicle speed and that noise is was most noticeable at slow speed – often the last few wheel revolutions before full stop. This low speed was in keeping with experiences with the vehicle and satisfies the preferred requirements of holographic interferometry. The drive selection was in keeping with the smaller rigs that had proved successful. A 45kW motor/gearbox combination using a 30:1 worm and wheel gearbox provided the necessary torque for brake testing yet sufficient speed for effective brake bedding. The whole unit is securely bolted to a concrete filled steel bedplate that also houses the test rig. An inverter controller allows a final drive speed of 0.5 to 100 r/min in intervals of 0.1 r/min, although most testing is conducted at 10 r/min as standard.

3.2 Test Rig Main Frame

To maximise the information possible from using the technique of holographic interferometry it was essential that the rig allowed a clear view of the brake and also allowed for the positioning of fairly large mirrors around the brake. In addition it was necessary to account for either the front or rear brake to be mounted, these being at 90^0 to each other, the front calliper being positioned horizontally whereas the rear calliper is mounted in the vertical plane. The different positions of the spring brake chambers, which actuate the calliper, also need to be accommodated, the combination of arrangements leaving little space for structural support. It is felt that the final design satisfies all requirements, this being shown in Figure 2.

Figure 2 – General view of test rig main frame.

The narrow stem that supports the hoop is necessary to provide clearance for the rear calipers, nearside and offside, and due to the large mass hanging off the hoop it has been fabricated from 60 mm steel plate. The flat platform to the rear of the rig is not used, but is an additional feature to allow the test rig to be re-used for other brakes or for extra equipment to be added.

3.3 Driveshaft

Standard vehicle parts were used throughout the test rig in order to satisfy the requirement of replicating in-vehicle mounting of the brakes. In particular the driven rear brake uses the original drive shaft with only minor modifications to allow coupling to the rig motor/gear unit. However since the front wheels are in effect driven by the road wheel, an alternative drive was necessary for this arrangement. This was achieved by using a driveshaft running though the wheel hub and bearings, which is then bolted onto the outer face of the hub using a drive plate as shown in Figure 3. This may be readily removed by pulling it through the wheel centre.

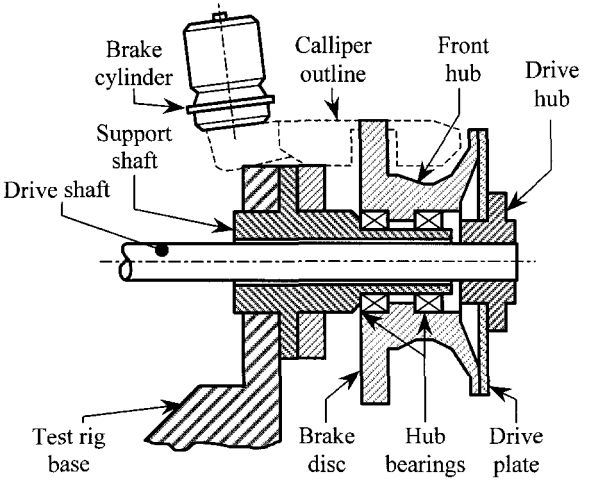

Figure 3 – Mounting of Driveshaft to front wheel assembly.

3.4 Front Brake

Figure 4 shows three views of the front brake as assembled on the test rig main frame. The views show the vertically mounted air actuator so positioned to reduce the clearance arc required when the vehicle is being steered.

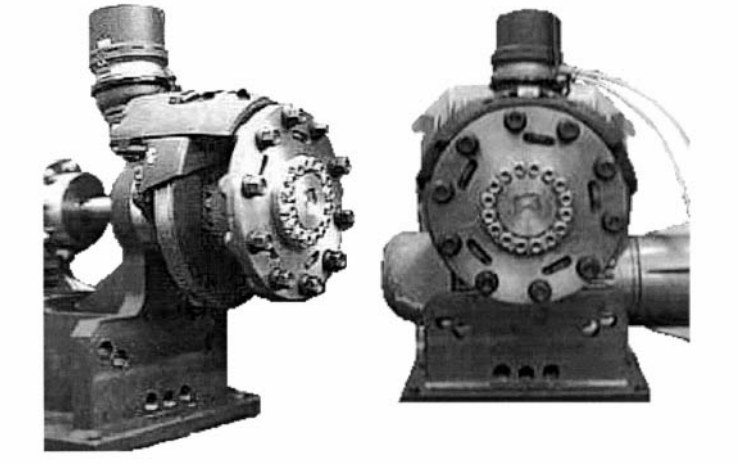

Figure 4 – General views of front brake mounting on rig

3.5 Rear brake

Figure 5 shows three views of the rear brake as assembled on the test rig. When compared to figure 4, it is seen how the rear brake intrudes into the vehicle, the air actuator laying along the rear axle.

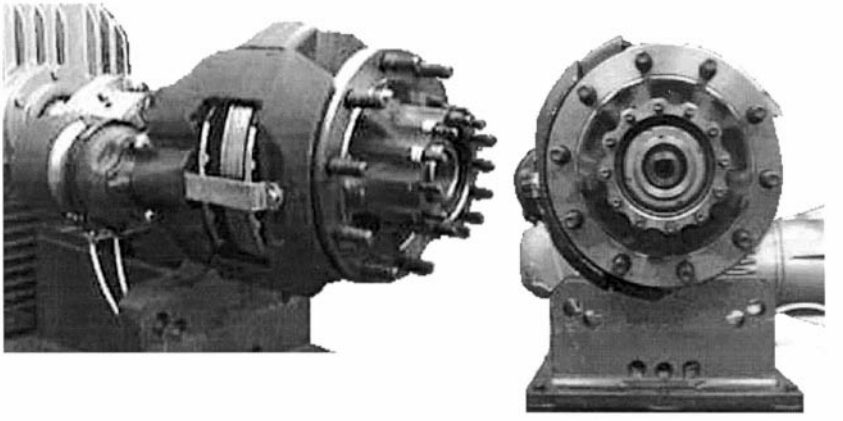

Figure 5 – General view of rear brake and air actuator mounting

3.6 Final Layout

The finished design has proved to be successful with only minor modifications. Additional equipment such as an air filter for the removal of dust and the mirror gantry have improved laboratory conditions. In particular the mirror gantry has enabled a secure set up of the mirrors required by the holographic teqhnique to maximise visual access as well as being used for secure attachment of other experimental equipment. Figure 6 shows the test rig layout with mirror gantry and dust extractor in position.

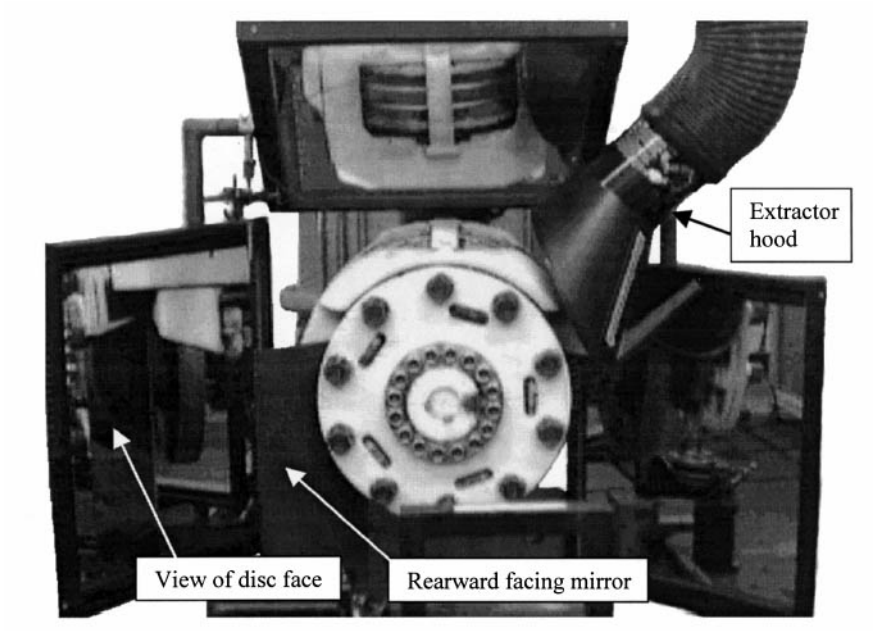

Figure 6 – General view of test rig showing arrangement of mirrors and dust extractor. Note rearward facing mirror that is viewed in left hand mirror to see disc face.

4 MODIFICATIONS

Even before construction of the test rig was started it was known that the wheel mounting flange on both the front and rear hubs would prevent a direct line of sight to the disc, therefore requiring mirrors to be used to view the disc vibration. Initial tests and holograms were carried out to determine to what extent the mounting face affected the noise characteristics of the system. Work on the front brake has shown that it appears to have no effect, and this can be seen in Figure 7. The lines on the front drive plate are due to the rotation of the disc. If vibration were present the lines would not appear parallel. This indicates that the flange is sufficiently

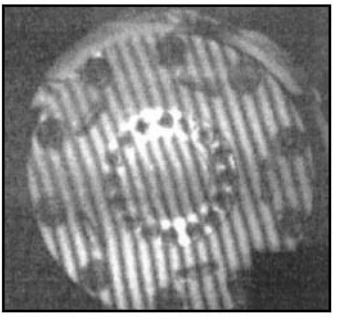

Figure 7 – Parallel fringes on front flange indicate no vibration.

removed from the source as to not affect the brake noise characteristics and its removal would not adversely affect the results. The test rig was designed with this in mind and the drive shaft is capable of rotating the front brake with or without the wheel-mounting flange. Figure 8 shows how this is accomplished and the reasons for removing the mounting flange.

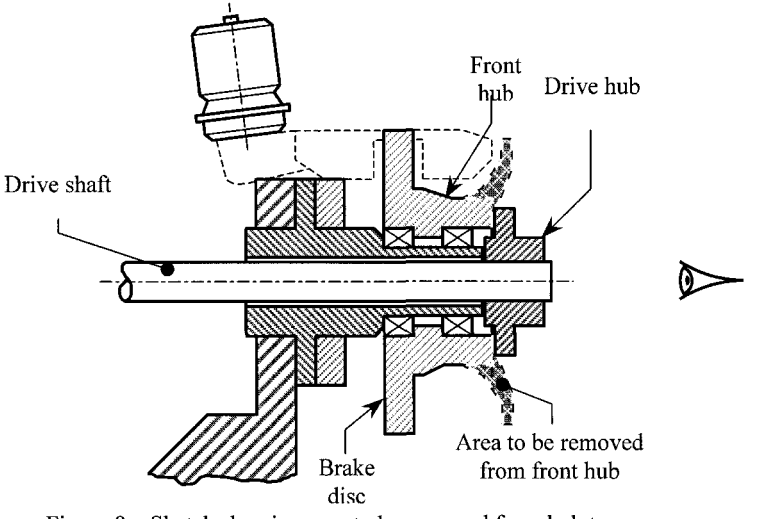

Figure 8 – Sketch showing area to be removed from hub to incease visual access to the disc without use of mirrors

5 RESULTS

5.1 Modal Analysis:

Modal analysis of the disc and pad was carried out in the free-free state by attaching piezo-electric crystals to the component faces in order to allow forced excitation. A sinusoidal charge was applied to the crystals using a B&K heterodyne analyser that allowed the frequency signal to be increased from zero to 20,000 Hz automatically. The heterodyne analyser was driven mechanically by a pen level recorder that gave frequency identification along the "x – axis" every 100 Hz. The disc and pad response to the input signal was detected using a secondary piezo-electric crystal mounted on the surface of the components (surface strain) and also using a microphone to detect the generated noise level. Both responses were recorded on the level recorder for subsequent analysis. With such an arrangement, the natural frequencies of the disc and pad were readily identified, Table 2. Selected holograms were taken to establish a basic benchmark for subsequent plotting of the disc characteristic as antinode pitch against frequency as shown in Figure 9. These holograms are shown in Figure 10 for the disc and Figure 11 for the pad. It has been found on car brakes that fixing of the disc effects the natural frequencies in the region of 8 %. Since angular location of the disc on the driveshaft is by spline, and axial by snap-ring retainers, it is anticipated the location effect on the disc natural frequencies would be minimal.

Table 2 – Frequency Response of Disc and Pads

Frequency Response of Disc		
Frequency (Hz)	Diametral Mode Order	Node Pitch Angle (degrees)
652	2	90
1700	3	60
3000	4	45
4500	5	36
6000	6	30
7800	7	25.7
9500	8	22.5
11300	9	20
15000	10	18

Frequency Response of Pad		
Frequency (Crystal) (Hz)	Frequency (Trace) (Hz)	Mode of Pad Vibration
825	1100	
1846	2000	
3978	4000	Bending
4612	4600	Bending
6220		
7185	7000	
7731	7800	
9305	9300	
17462		

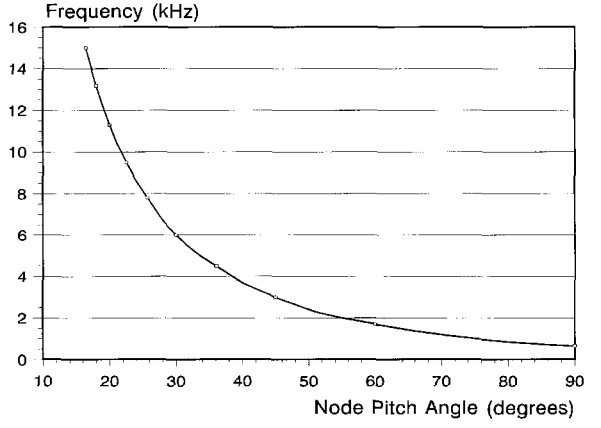

Figure 9 - Graph showing node pitch angle against frequency

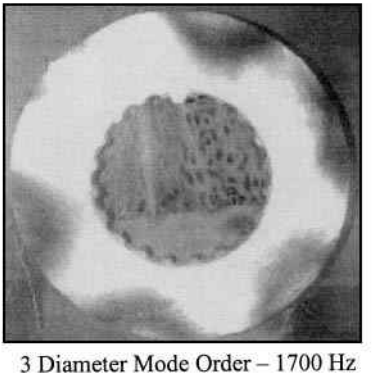

3 Diameter Mode Order – 1700 Hz

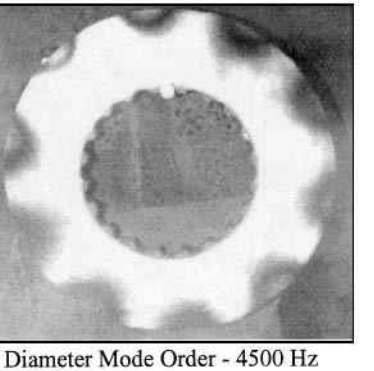

5 Diameter Mode Order - 4500 Hz

Figure 10 - Photographs of Reconstructed Holograms - Diametral Mode Shapes of Disc:

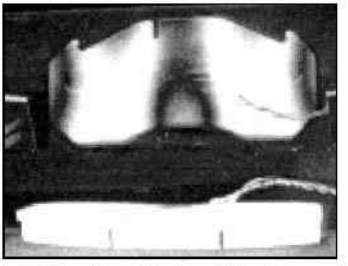

Bending Mode - 4000 Hz

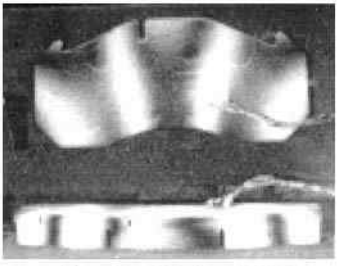

Bending Mode - 4600 Hz

Figure 11 - Photographs of Reconstructed Holograms - Mode Shapes of Pad

Regarding the disc, it is noted at this stage that the amplitude is very small, as seen by the single fringe on the disc face. Although it is appreciated that amplitude is related to energy input it is not expected that significant disc amplitude will be observed during noise generation - the physical structure of the disc (diameter and thickness parameters) would suggest a deformation in the region of $1/30^{th}$ that of a car disc for a given load.

5.2 Dynamic results

5.2.1 Experimental details

To record all the holograms a 100 mJ double pulsed ruby laser with pulse spacing variable between 1 and 999 μs and pulse duration of 30 ns was used. A 25 mm condenser microphone and spectrum analyser were used for frequency identification and a dual channel storage oscilloscope and mating printer used to record the laser pulses and associated brake frequency signals. Piezoelectric transducers were fixed to the finger pad backplate as a vibration reference signal. Temperature was detected using a non-contacting laser thermometer reading the surface temperature of the disc. Full details of the equipment may be found in earlier work (6).

5.2.2 Test procedure

A standard front brake was used for the initial tests although a friction material with a deliberately high coefficient of friction was used to promote noise. It was practice for the brake to be bedded on assembly to the rig before any tests were carried out. All testing would be preceded by a conditioning procedure which required warming the brake to a temperature in excess of 500°C before noise tests were undertaken. The disc speed was set to 10 r/min and brake air pressure to above 3 bar and gradually reduced to zero, the condition being allowed to stabilise at set intervals to provide the opportunity for noise to become established. The temperature was then allowed to fall about 50°C at the higher temperatures and the procedure repeated, in 10°C stages when the temperature was around 200°C. Once noise was obtained, it was possible to sustain the situation provided the conditions could be maintained. The thermal inertia of the brake provided relatively stable conditions. A selection of results is presented in Table 3. The principal generated noise frequency was in the order of 1550 Hz. In general this frequency was obtained at air pressures ranging from 0.18 MPa to 0.2 MPa. At lower pressures, the frequency would be slightly less – in the order of 1540 Hz. The difference may initially appear to be insignificant but the trend of frequency shift with pressure is a characteristic observed on car brakes and supports the proposal that frequency is related to disc/pad interface geometry. A lower pressure allows the antinode under the pad to

compress causing the free antinodes to expand and so the frequency reduces according to the disc characteristic (Figure 9). An analysis is undertaken in 5.3 and further details of this approach may be obtained in earlier work (8).

Table 3: Typical results from temperature/pressure tests.

Test Number	Temperature (deg C)	Pressure (Bar)	Frequency (Hz)	Noise Level (dBA)
1	180	1.85	1550	60
2	230	1.95	1550	60
3	300	2	1550	60
4	103	1.5	1540	60
5	120	1.5	1540	57
6	140	1.5	1540	54

5.3 Disc/Pad Geometric Considerations

An investigation to predict the probable instability frequency was undertaken using the disc characteristics as shown in Figure 9 and the pad/disc interface geometry details. A summary is shown in Figure 12. The pad effective length is considered to be 50 to 85 % of the full pad length (53° to 73°) and the disc antinode compressed angle under the pad is taken as 100 % to 60 % of the free antinode pitch angle. This criteria determines the limits for antinode angular pitch and pad angle in Figure 12.

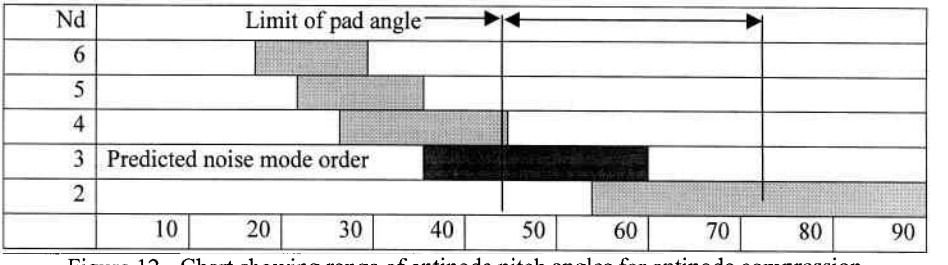

Figure 12 - Chart showing range of antinode pitch angles for antinode compression from zero to 60% of free mode angle for each disc mode order.

The geometric considerations as shown in Figure 12 predict an unstable 3 diameter mode order. This mode order would be most favourable because its starting range lies well within the effective length of the pad. The 2 diameter mode is a possibility but it requires excessive antinode compression and this is felt to be unlikely. Conversely the 4 diameter mode requires antinode expansion, although it may prove to be problematic if the effective pad length proved to be smaller than 50 % of the contact length. Figure 12 would infer a possible antinode pitch under the pad of between 44° and 60° which in turn equates to a disc free antinode pitch of 63.2° to 60°. Reference to Figure 9 provides the instability frequency of between 1500 and 1700 Hz – as found on the brake.

5.4 Dynamic holographic results

Random holograms were recorded of the brake generating noise with the laser pulse spacing set at half the period of detected noise frequency. The noise level was relatively low, in the region of 50 to 60 dBA. Figure 13 shows a general view of the brake with mirrors positioned to maximise visual information. This figure assists in orienting the observer with regard to the complete brake whereas Figure 14 provides a more detailed view as seen through the top mirror and describes the component parts involved.

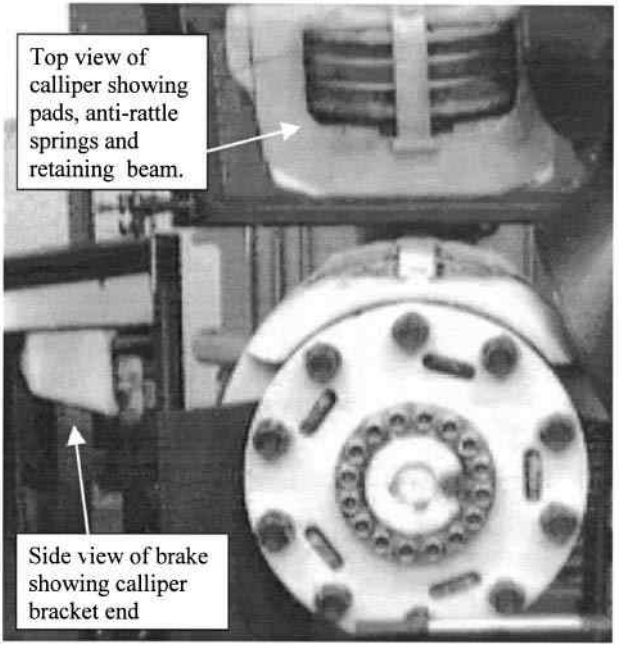

Figure 13 – General view of brake showing mirrors placed to allow top view of calliper and pads and side to view end of calliper and disc rim.

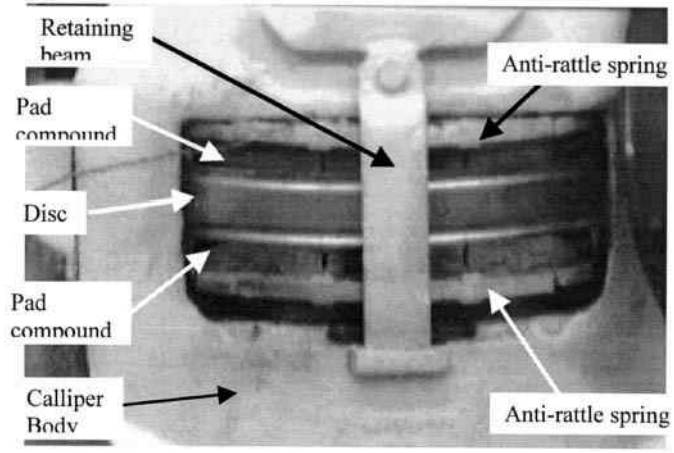

Figure 14 – Detail view of calliper through top mirror showing edge of disc, calliper body, pad compound, anti-rattle springs and retaining beam.

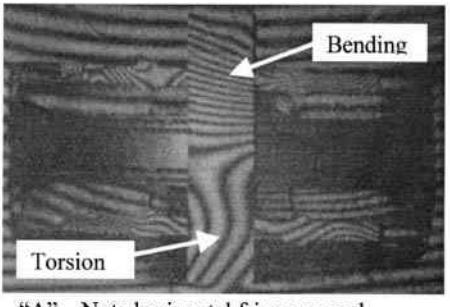

"A" – Note horizontal fringe on pad

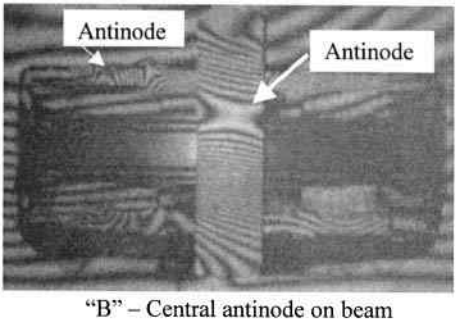

"B" – Central antinode on beam

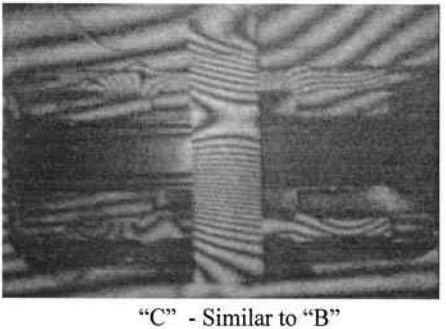

"C" - Similar to "B"

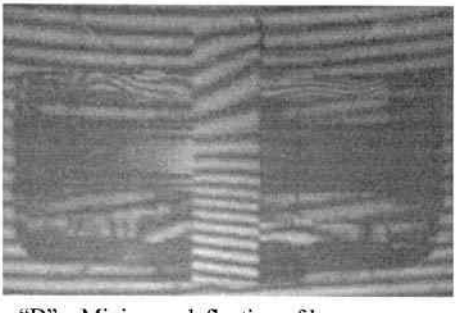

"D" – Minimum deflection of beam

Figure 15 – Typical modes of vibration of the calliper, pads, springs and beam - as described and seen through the top mirror in Figure 13.

6 DISCUSSION OF RESULTS

The holograms as seen in Figure 15 are individual non-time-related images of the brake generating noise at around 1540 Hz.

Disc: The complete image (not provided) does not show any diametral mode shape on the disc face but, as shown in the modal analysis, the amplitude will be fairly small and only one or two fringes would be expected. The rim of the disc, as seen in Figure 15, does not show the presence of fringes which indicates that the amplitude of vibration of the disc is extremely small, if present.

Pad Compound (Friction Material): In all views, the fringes on the pad compound are nearly parallel to the face of the disc and in some instances appear to be extensions of the fringes shown on the calliper. If the fringes were a continuation of the calliper fringes it could be concluded that the pad was moving in sympathy with the calliper. This may be the case at some parts of the cycle but a more detailed examination indicates that this may not be true at all times. In image "A" the left side of the lower pad shows fringes at about 20° whereas the calliper has parallel fringes. Again the right hand side of the lower pad in "B" and "C" has no fringes whereas the calliper shows parallel fringes. It is noted that the slight fringe angles as seen on the left hand side of both pads in "B" and "C" are parallel. This would indicate slight rotational movement of both pads. This type of movement would occur if the pads were moving with the disc face and a low amplitude rotating disc mode was passing between the pads.

Anti-rattle Springs: These clearly indicate a high amplitude of vibration of a complex nature. There is an arrangement of antinodes causes by bending and parallel fringes as a result of torsion. It would be necessary to record a series of time related holograms in order to fully understand the true mode of vibration.

Retaining Beam: The fixing of this beam would tend to restrict motion to bending but the angles fringes as seen in "A", "B" and "C" indicates torsion at the "clipped" (lower) end. Indeed the image shown in "A" indicates a bending mode at the bolted end and torsional at the lower end. The clear antinodes in "B" and "C" and the fringe intensities indicate a fixed bending mode of high amplitude. Again a series of time related holograms would be necessary to establish moving mode shapes and phase relationships. Image "D" shows the beam at minimum amplitude – note fringes at the bolted end are almost a continuation of the calliper fringes.

7 CONCLUSIONS

- Although the work is in its very early stages, there is evidence to show that the characteristics shown here may be cross-correlated with the observations as seen on cars. If this is the case, the extensive research carried out on cars may be directly relevant to commercial vehicles.
- In addition, it has been shown that the pad/disc interface geometry may be as relevant to commercial discs as for cars – the probable unstable frequencies may be predicted.
- Because the mode order of the disc is low, a 3 diameter mode order, and the amplitude is small, as inferred by the modal analysis, the pads do not exhibit significant bending or torsional modes. This may explain why noise fix shims do not appear to be effective on these types of brakes; they are not flexing sufficiently and the frequency is too low to provide adequate damping.

8 ACKNOWLEDGEMENTS

The authors would like to thank Volvo Truck Corporation, Meritor Automotive and BBA Friction for their support and their permission to publish this work.

9 REFERENCES

1. Suzuki Y, Ohno H "A Study on Drum-Brake Noise of Heavy-Duty Vehicle". Motor Vehicle Technology in the 80's – Needs and Resources, 1981, pp 287-292.
2. Peterson B. "Truck Noise – Planning an Effective Compliance Program". Controlling Truck Noise, 1981, pp 31-43.
3. Lang A.M. "An Investigation into Heavy Vehicle Drum Brake Squeal" PhD Thesis, 1994, Loughborough University of Technology.
4. Cornish R.H. Atkinson G.A. "An Investigation of Production Variability of Light Commercial Vehicle Noise". Road Vehicle Automation II, 1997, pp 191-197.
5. Fieldhouse J.D. "An Analysis of Disc Brake Noise using Holographic Interferometry". PhD Thesis, 1993, Huddersfield University.
6. Fieldhouse J.D. and Newcomb T.P. "The Application of Holographic Interferometry to The Study Of Disc Brake Noise" SAE International Congress and Exposition, Detroit. USA. Paper Number 930805, March 1-5 1993. Note: Paper also included in SAE publication "ABS/TCS & Brake Technology" Reference SAE SP - 953, pp 133 - 147.
7. Fieldhouse J.D. and Newcomb T.P. "Double Pulsed Holography Used to Investigate Noisy Brakes" *Optics and Lasers in Engineering* - special issue No 25, Volume 6 entitled "Optical Sensors for Automotive Applications" December 1996 ISSN Number 0143-8166(95)00094-1, pp 455 – 494.
8. Fieldhouse J.D. "A Proposal to Predict the Noise Frequency of a Disc Brake Based on the Friction Pair Interface Geometry." 1999 SAE Brake Colloquium and Engineering Display. SAE Paper number 1999-01-3403.

This page intentionally left blank

Improving comfort of friction brakes

R HOLINSKI
Dow Corning GmbH, Wiesbaden, Germany

ABSTRACT

A test machine has been designed to detect brake squeal and judder of friction brakes. It was found, that this device shows good correlation to comfort measurements during field testing. This new tester has been used as a tool to develop antinoise additives for friction brakes.

Technology of surface treatment of graphite has been developed which changed the tribological performance of graphite entirely. Friction coefficient is no longer dependent on humidity. Difference between static - and dynamic friction has been minimised, which results in reduction of vibration during sliding friction. When polarised graphite is added to brake lining formulations, comfort of braking is improved by reduction of squeal noise and roughness. Several European brake lining manufacturers are using these additives in brake lining formulations to improve comfort of braking.

1. INTRODUCTION

Friction brakes of vehicles were always subject to improvement in cost and performance. Brake rotor material never changed because this was very cost effective and showed good heat resistance. To meet the ever increasing requirements concerning brake performance the challenge was always to modify the formulation of the brake composite. The most important performance parameters in a friction brake were safety related issues like fading and friction stability. These issues were addressed first. Also service life of brake components was prolonged substantially by formulation work on composites (1).

In recent years comfort of braking became an important concern. The trend towards weight saving resulted in smaller brake pads, which was accomplished by an increase of friction coefficient to keep braking efficiency at the same level.

A lot of effort and money is spent to improve comfort of braking by secondary measures. In order to dampen vibrations, which travel from frictional interfaces through the composite and the back plate to the brake piston, various separating layers are applied to the back plates of brake pads. Lubricating greases and pastes dampen vibrations but have a limited life time of a few thousand kilometers. Foils and lacquers last much longer. But eventually these films lose their flexibility at the contact area between brake piston and back plate and brake noise will be noted again. The most costly and most effective solution is the application of a metal shim along with the use of expensive high temperature stable greases.

The application of various secondary measures for brake noise reduction or elimination is a sign of growing demand of car drivers for comfort of braking. On the other hand manufacturers of brake systems and cars do not trust, that comfort of braking may be achieved by primary measures only.

2. WHY DO VIBRATIONS OCCUR ?

In a friction brake, surfaces of organic composites and a cast iron rotor are in sliding contact. A discontinuity of friction is caused by the difference of static friction and dynamic friction. The higher the friction coefficient the higher the difference between both types of friction. These micro stick slip effects result in brake comfort problems at various frequencies from low frequency judder to high frequency squeal (2).

Stick slip is a well know phenomenum in tribology, which occurs primarily at low speeds during sliding contacts. Again stick slip is explained by the difference of adhesive friction and dynamic friction (3). Friction altogether can be lowered at low sliding speeds by the application of solid lubricants like Molybdenum Disulphide. Thereby the difference between static - and dynamic friction is reduced and stick slip is eliminated.

In friction brakes coefficient of friction must not be lowered but the gap of both forms of friction has to be minimised preventing the occurance of vibration. In order to achieve this goal, vibration of friction brakes needed to be detected in a test machine.

3. A VIBRATION DETECTING TEST PROGRAM

In order to investigate frictional properties of composites a simple friction lining tester was built consisting of a cast iron disc and three composite segments. In this arrangement the rotor is not rotating but stationary and three composite segments rotate and slide against the rotor surface. Recorded is disc temperature and friction force (Figure 1). Since the rotor is stationary, vibrations being generated during sliding friction can be detected by attaching a piezo sensor to the disc. Acceleration is amplified and recorded. This signal is analysed further in a frequency analyser ranging from 0 to 20.000 Hertz.

For detection of vibration various tests were performed during continous braking at different speeds, different pressures and different disc temperatures. After this screening the test parameters were selected to be: Speed 500 RPM at a constant disc temperature of 200°C by heating the rotor. Over a 6 hour test program the pressure was changed from 40 N/cm² to 5 N/cm² (Figure 2). During the test the acceleration signal and the analysis of frequency was recorded. It was of vital importance to find out if there is any correlation between the acceleration signal during dry sliding of composites against the stationary disc and the brake noise in an actual braking procedure of a car.

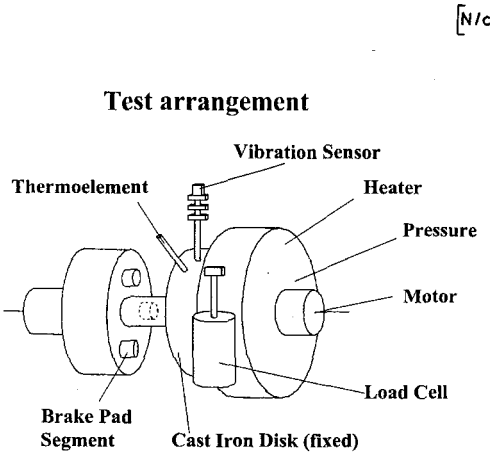

FIG.1 - SKETCH OF FRICTION LINING TESTER

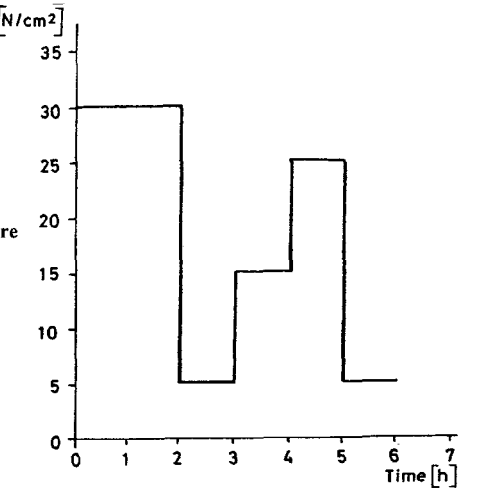

FIG. 2 - CHANGE OF SPECIFIC PRESSURE DURING A SIX HOUR TEST RUN

4. CALIBRATION OF THE TEST METHOD

To calibrate the test method a number of brake lining manufacturers supplied us with brake pads, which have been tested for noise in the field. Two drum linings of different formulations were evaluated. Formulation A with a high noise level showed an average acceleration signal of 37 g, while the brake lining B with lower noise level had a signal reading of 20 g (Fig. 3).

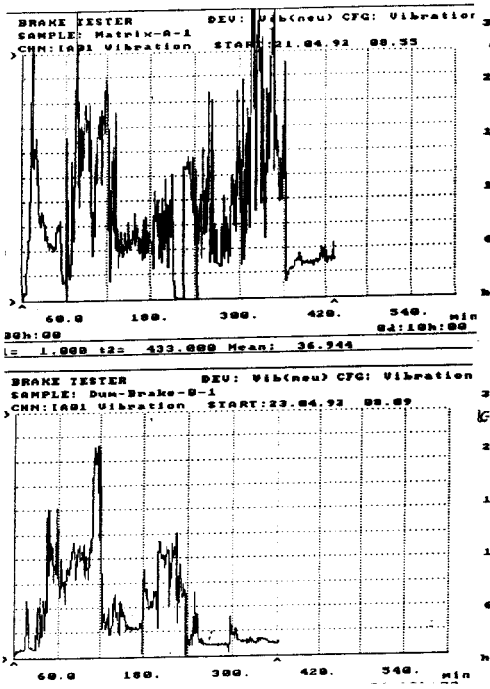

FIG. 3 - RECORDING OF VIBRATION OF TWO DRUM LININGS.
TOP: A: HIGH NOISE LEVEL
BOTTOM: B: LOW NOISE LEVEL

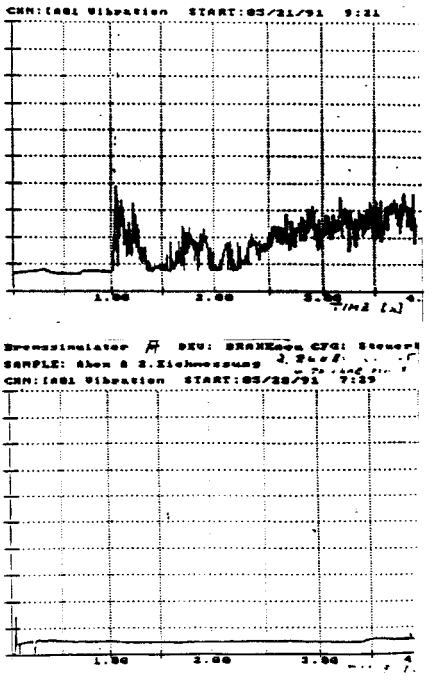

FIG. 4 - RECORDING OF VIBRATION OF DISC BRAKE PADS
TOP: NOISE RATING 3
BOTTOM: NOISE RATING 8

A passenger car pad of a high noise level showed almost no vibrational signal during the first hour of testing. After this running-in period vibration increased sharply and stayed high throughout the test (4). The test pad A with a low noise rating had a low acceleration signal throughout the entire test and no peaks (Fig. 4). It is well known, that surface chemistry of brake linings change during initial brakings (5, 6).

Driving a small passenger car braking noted was a high level of brake squeal during braking at low speeds and low pressures. The brake pads of the front axle were tested for vibration under described test device. A low level of acceleration was detected in this case which

indicated no comfort problem. Listening closely to the brake squeal of the small car, it was noted that squeaking occured at the rear drum brakes. Inhouse tests of these drum linings revealed high level of vibration.

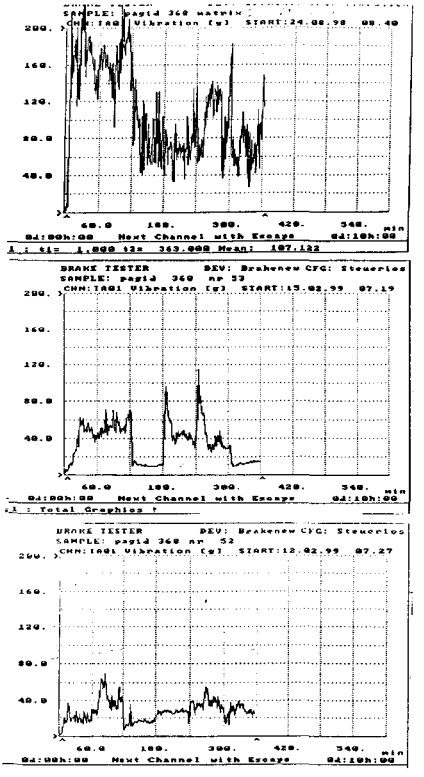

Testing numerous brake composites with known comfort levels revealed, that there is a reasonable correlation between vibration of the inhouse tester and noise during car braking. It has been found imperically, that the addition of Molybenum Disulphide powder to brake lining formulations reduces noise of friction brakes (5). Tested was a brake lining formulation without any additives during a 6-hour-test-program. From Fig. 5 it can be seen, that this brake lining matrix had a very high level of vibration (top). The addition of 7% Molybdenum Disulphide of a purity of 95% to the brake lining formulation reduced vibration significantly. Vibration is further reduced by the addition of 7% MoS2 of a purity of 98%. Again this is in line with field results. This correlating test procedure was the prerequisite for development of a noise reducing additive.

FIG. 5 - RECORDING OF VIBRATION OF BRAKE COMPOSITES
TOP: BASE MATRIX
MIDDLE: MATRIX CONTAINING 7% MOS2 (95%)
BOTTOM: MATRIX CONTAINING 7% MOS2 (98%)

5. DEVELOPMENT OF NEW SOLID LUBRICANT TECHNOLOGY

One of the key raw materials in friction linings is graphite. However, this material can only be used in brake lining formulations in limited quantities, since the friction coefficient changes with humidity. In a humid environment or in the case of brake pads at lower temperatures friction is imparatively low. At higher temperatures water is evaporating and dry graphite presents a very high friction coefficient. The problem of wet sensitivity in brakes is caused primarily by graphite.

Dry graphite has poor adhesion to substrates and poor film formation. Molybdenum Disulphide, however, has good adhesive properties and good film forming ability. These

properties can be explained by the polar surface of MoS2 lamellae, which is caused by a small molybdenum atom of high polarity. Since graphite is only an element the lamella surfaces have no polarity. By special surface treatment of graphite particles have been coated with inorganic compounds. Such treatments with metal molybdates, -phospates, -sulfates, and -sulphides change their tribological properties of graphite entirely. Friction coefficient is no longer dependent on humidity, load carrying capacity is increased and wear reduced (7). Dry lubricating ability is greatly improved since polarised graphite has under pressure very good adhesion to substrates and good film forming ability (Fig. 6).

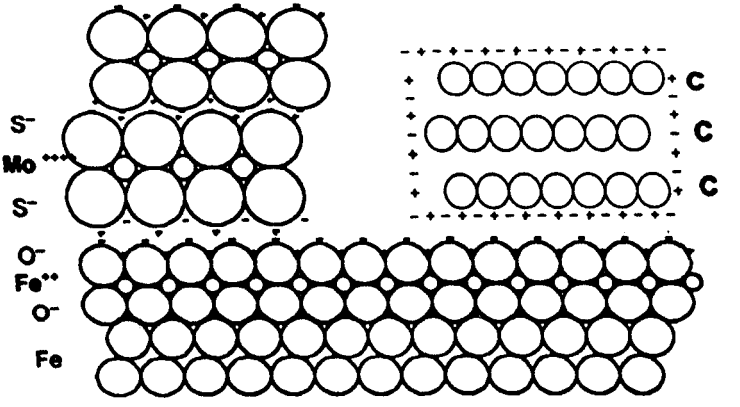

FIG. 6 - MOLYBDENUM DISULFIDE AND POLARISED GRAPHITE ON A METAL SURFACE

6. POLARISED GRAPHITE AS ANTINOISE ADDITIVE

When polarised graphite was added to a brake lining matrix it was found, that during dry sliding against a disc vibration was greatly reduced. Level of vibration has been minimised by the type of polarisation (Fig. 7). Tests were performed only at disc temperatures of 200°C. It should be ascertained if vibration is kept also low at high braking temperatures. On the friction lining machine tested were also brake pads at higher temperatures and during go and stop conditions. Temperature recording of this tests is given in Fig. 8 Top. Initially the matrix shows a low level of vibration during the running-in procedure, however, vibration increases sharply after 40 minutes of continous braking. After running-in there has been a formation of transfer layers on the metal rotor and a change of chemistry in the friction layer of the brake composite. This change of friction interfaces resulted in an increase of vibration. Initially this temperature was about 150°C. At higher interface temperature vibration stayed at a high level. Also during the cold run after hot run vibration still is high. The same brake lining formulation containing 7% of polarised graphite showed a very low level of vibration at low and high frictional temperatures. Also after the hot run vibration stayed low (Figure 8 Bottom).

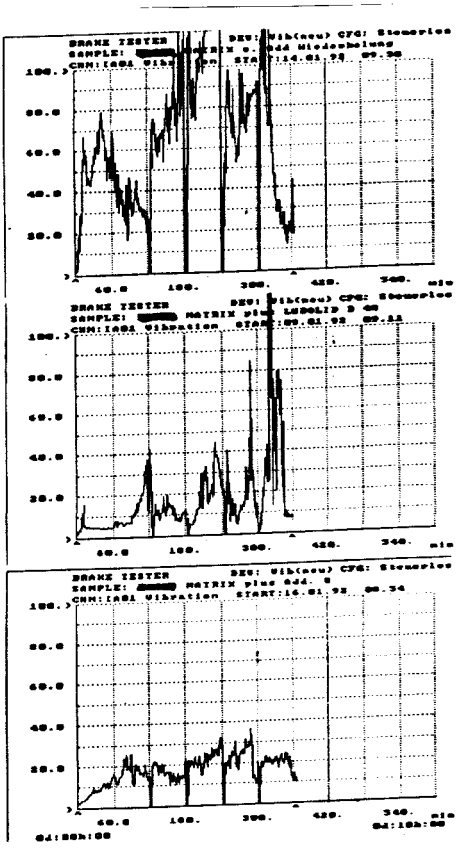

FIG. 7 - RECORDING OF VIBRATION OF FRICTION LININGS

TOP: BASE MATRIX

MIDDLE: MATRIX CONTAINING 7% POLARISED GRAPHITE TYPE A

BOTTOM : MATRIX CONTAINING 7% POLARISED GRAPHITE TYPE B

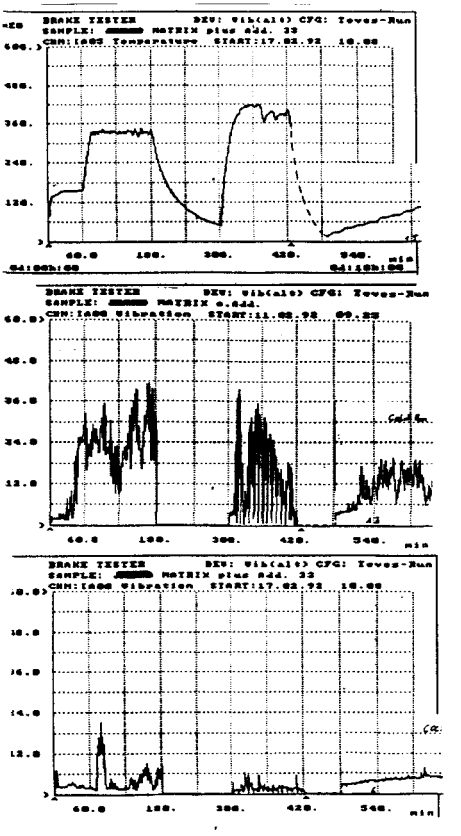

FIG. 8 - TESTING OF FRICTION LININGS AT VARIOUS TEMPERATURES.

TOP: RECORDING OF DISC TEMPERATURES

MIDDLE: RECORDING OF VIBRATION OF MATRIX

BOTTOM :RECORDING OF VIBRATION OF MATRIX CONTAINING 5% ADDITIVE

Polarised graphite as an additive in brake linings reduced fluctuation of friction during the braking procedure. Recording of friction force during continuous braking showed greatly reduced scatter of friction, although friction was not reduced (Figure 9). This may be also an indication, that polarised graphite reduces the difference between static and dynamic friction.

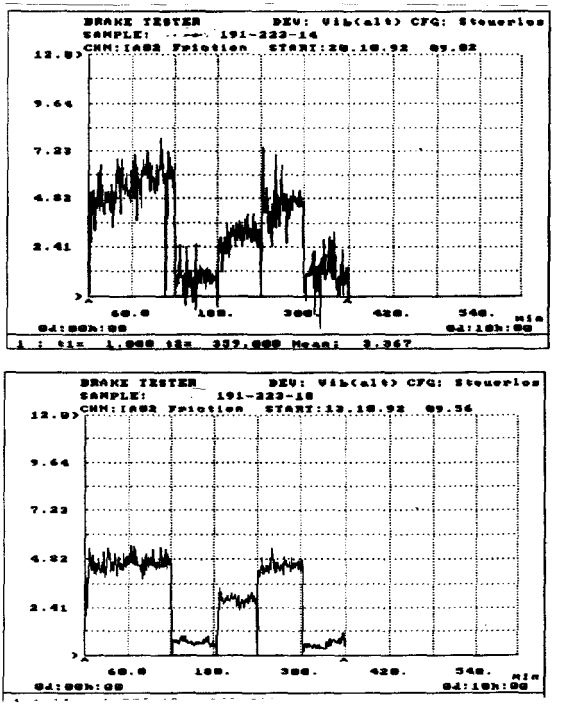

FIG. 9 - RECORDING OF FRICTION FORCE DURING CONTINUOUS BRAKING AT VARIOUS PRESSURES
TOP: MATRIX
BOTTOM: MATRIX CONTAINING 7% OF ADDITIVES

7. FIELD RESULTS

Additives based on polarised graphite technology were tested by friction lining manufacturers in noisy brake lining formulations. Results from noise test machines revealed that these additives reduced low frequency vibrations and high frequency noise. This was confirmed by field tests. It was found that an addition of 3,5% to 7% of polarised graphite in a brake lining formulation improved comfort level by 3 points on a noise scale ranging from 1 to 10. In this noise scale 1 means a high noise level and 10 means no noise. Various brake pad manufacturers use products based on polarised graphite in place of lead sulphide to improve comfort of braking.

This work demonstrates that by a simple test device a method was established which has a good correlation of vibration generated during dry friction of composite surfaces against the cast iron rotor to noise occuring in a friction brake. Using this test facility antinoise additives were developed which reduced micro stick slip by reducing the difference between static - and dynamic friction. These findings were confirmed in the field. This work demonstrated, that comfort of braking can be improved by primary measures.

9. LITERATURE

1. Holinski, R.: Tribologische Anforderungen an Reibbeläge von heute und morgen. Paper at 10th Intl. Coll. Tribology, Ostfildern, Germany, Jan. 1996

2. Borchert, T. „Dynamical Behaviour of Disc Brake Pad" presented during the 9th annual brake colloquium Oct. 13, 91 in New Orleans.

3. Severin D., „Der Reibbelag, das unbekannte Wesen", presented at a Conference at Bad Nauheim, Sept. '91

4. Holinsky, R.: „The Interface in Dry Frictional Systems". SAE Conference, New Orleans, 1994.

5. Jacko, M.G.: „Physical and chemical changes of organic disc pads in service" Wear, 46 (1978), 163

6. Wirth, A., Eggleston D., Whitaker R.:"A fundamental tribochemical study of the third body layer formed during automotive friction braking" Wear 179 (1994), 75 - 81

7. Schiefer, H.M; Kubczak, G.V.: „Controlled friction additives for brake pads and clutches"; SAE paper 790717; Automotive Engineering, June 1979.

8. Holinski, R; Jungk. M.: „New Solid Lubricants as Additive for Greases - „Polarised Graphite". ELGI Annual General Meeting, June 13-15, 1999, Oslo.

This page intentionally left blank

Summary of the brake noise recommended practice draft developed by the US working group on brake noise

J K THOMPSON
Link Engineering Company, Plymouth, Michigan, USA

1. ABSTRACT

The new brake noise test procedure that has been developed by the US Working Group on Brake Noise is presented. This procedure is described in detail with a step-by-step description of the actual measurement procedure. Careful attention is paid to the similarities and differences between this new procedure and the AK procedure already in use by many organizations. A key difference from the AK procedure is the inclusion of a series of deceleration stop modules. Acknowledging the success of the AK procedure, this specification also incorporates drag modules.

2. INTRODUCTION

Automotive brake noise is a matter of considerable concern among consumers, the automobile manufacturers, and the braking industry. Consumers' perception of problem brake noises may range from mild annoyance to an urgent concern when the noise is thought to indicate a malfunction of the braking system. Despite much progress in identifying and rectifying brake noise issues, they continue to be a major problem whether judged by warranty claims, reported to be in the hundreds of millions of dollars, or the number of papers published on the subject.

Although there are numerous publications and a great deal of effort devoted to understanding and correcting brake NVH (Noise, Vibration, & Harshness) issues, there is still not a high fidelity model of the NVH source. References [1-3] provide some insight into the brake NVH state-of-the-art. There do not appear to be models that can predict brake NVH performance before prototypes are built and tested. The existing models have provided considerable insight in the product development process and are often used for resolving noise problems. However, they are not yet capable of predicting absolute NVH performance. Therefore, brake

NVH testing remains an important part of the braking system and vehicle development processes.

At present there is no globally recognized brake NVH test procedure. There has been a European Working Group (AK or Arbeitskreis Gerausch) in existence for some time. This group has developed a test procedure that is being used by some organizations. The US Working Group was established to develop and promote a brake noise test procedure for the US that would be in harmonization with global test practices. This group, like that in Europe, is composed of automobile manufacturers, braking system suppliers, and friction material suppliers. The goal is to develop a laboratory screening procedure that would highlight the vast majority of potential high frequency noise issues for disc brake systems.

There is clearly a need for a global test standard. Both braking system sourcing and applications are global. Consistent methods of performance evaluation are necessary to be used throughout the industry. Currently, variations in testing exist among automakers, brake system suppliers and even among local facilities of a particular brake supplier. No single test procedure will guarantee common data and evaluations. A global procedure is a start from which more comprehensive practices and specifications can be developed. What follows is a summary of the current status of the activities of the US Working Group and the test procedure currently under review.

3. BRAKE NVH TESTING

Brake noise may occur under a wide range of vehicle operational conditions. It is well known that brake noise is a function of a wide range of parameters including: temperature, humidity, speed, application pressure, temperature history, vehicle dynamics, and various brake dynamic properties. Neither the AK nor the US Working Group procedure attempts to replicate the wide range of vehicle operational conditions or potential brake noise issues. These initial attempts at a test procedure are directed at quantifying high frequency noise, above 900 Hz, since this noise is less dependent on vehicle characteristics. Noise in this frequency range is often referred to as "squeal." Lower frequency brake noise may be dependent on suspension and vehicle structural dynamics. Even above 900 Hz, suspension dynamics are important and must be considered in the test set-up.

The intent is not to measure all possible vehicle operations that may generate squeal noise. Instead, the goal is to provide a screening procedure that is highly sensitive to brake-squeal potential. It is not required that this test procedure model the exact details of the noise generation mechanism in actual vehicle operation. In fact it is more important that the procedure clearly distinguish often-subtle performance differences between brake designs than provide a completely faithful prediction of on-vehicle sound levels and frequencies.

A dynamometer test procedure known as AK Noise has been developed by the European working group. This procedure follows the lines of the drag mode test procedures with an optional extension to in-stop braking. In the US, the more common approach is to use in-stop mode procedures emphasizing the replication of vehicle road test. Drag mode tests consist of constant speed operation with the brake applied. Constant speed is typically maintained by use of an electric motor. In-stop modules consist of decelerating the rotor from some initial

speed to a complete stop by brake application. Actual or simulated inertia is used to insure that such a stop is typical of actual vehicle operation.

The US Working Group was founded to address the need for a global standardization of NVH dynamometer tests. A global NVH matrix has been developed that combines drag mode and deceleration mode tests. This procedure was presented to the US Working Group in February 1999 [4].

Based on the AK noise and in-stop modules, the matrix contains 25 sections and 1917 brake applications. The new procedure is currently being considered as a draft for the SAE J2521 Recommended Practice [5]. This procedure owes much to the previous development of the AK procedure. This prior work is gratefully acknowledged. There are several variations from the AK procedure that will be described in the subsequent sections.

This draft of SAE J2521 contains deceleration stop modules beyond the requirements of the AK procedure. These modules were added to provide noise measurements under operational conditions more representative of normal vehicle usage. In addition, these modules provide frictional interface conditioning more like that found in typical operation.

By having both Drag and Deceleration Stop modules, this procedure provides a more thorough evaluation of potential performance. The low speed Drag module is seen as an extreme case where frictional coefficients are at their highest and damping is at its lowest. The Deceleration Stop module is not as extreme, but it better represents at least one aspect of typical operation. Therefore, it is felt to be a more conservative noise evaluation. It is anticipated that users may develop acceptance criteria based on whether noise is seen in both the Deceleration Stop and the Drag modules or in only one.

Another difference in the draft test protocol is that friction characteristics are measured after each Deceleration Stop module and before each Drag module. Thus, one has a record of friction characteristics that may be related to noise measured in the Drag and Deceleration Stop modules.

The current status of this procedure is that it is currently under review by members of the US Working Group and the Society of Automotive Engineers. Although there are many test procedures being used for brake noise testing, this protocol provides a comprehensive screening process. Unlike other procedures, it is not intended to simulate typical vehicle operation. The goal of this procedure, using low speed drags and full-stop sequences, is to highlight potential noise issues that may be experienced in typical vehicle operation.

4. DRAFT PROCEDURE

What follows is a description of the procedure as it currently stands. Where there are open issues or alternative approaches being considered, they are pointed out in this discussion.

4.1 Procedure's stated goal

The stated goal of the procedure is shown in its entirety below.

"This matrix describes the test conditions and steps to investigate the influence of pressure, temperature and velocity on the NVH behavior of disc brakes. This matrix is intended to replicate vehicle tests to get a fair comparison for different brake corner components."

It is assumed that the procedure will be run on a dynamometer in a laboratory test environment. As for the correlation with vehicle tests, there is limited data for such a comparison at this point. It has been suggested that a future activity for the Working Group would be to conduct vehicle and dynamometer tests to establish if there is such a correlation. Since this procedure is intended to screen for potential noise issues, vehicle correlation is not easily defined.

4.2 Test apparatus definition

The minimum drive power required for the test apparatus is defined as 60 kW or 80.5 horsepower. The maximum needed is dependent on the torque capabilities of the brakes being tested. The maximum speed for testing is defined as 100 km/h or 62 mi/h. The procedure also notes that inertia flywheels, inertia simulation, or a combination of the two may be used in this test procedure. It is noted that the system must be capable of providing torque levels of at least 1500 Nm or 1106 ft-lb. The brake actuation pressure must be at least 40 bar or 580 lb/in^2. The test system must be capable of reversing the direction of rotation.

4.3 Environmental requirements

The working group did not feel that it was necessary to require the use of full environmental control. There was no clear consensus as to environmental specifications. Therefore, the control of temperature and humidity in the environment of the brake is optional. Cooling air must be provided to the brake. Airflow must be controlled such that it is not so high as to blow away wear debris or create noise above the background limit of 60 dB (A). It is believed that brake wear debris may be part of the noise generation mechanism, and therefore, should not be artificially removed. The allowable cooling air temperature is within the range from 10 to 40°C or 14 to 104°F. The relative humidity of cooling air may range from 20% to 90% and is recorded. It is recognized that some may wish to control the environmental conditions and the cooling air temperature and humidity more closely than specified here to improve measurement repeatability or to represent particular conditions of concern.

4.4 Measurements

The location of the microphone for noise measurements is specified as shown in Figure 1. The transducer must be 10 cm outboard from wheel hub face and 50 cm above and perpendicular to the centerline of the axle.

The placement and orientation of the microphone are critical to obtain consistent results that permit the comparison of brake design changes. Since the wavelength of important brake noise may be as small as 20 mm, a small change in location of even a few centimeters from test to test can lead to significant differences in measured sound levels.

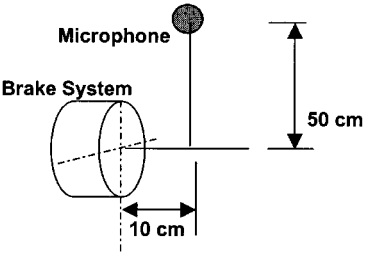

Figure 1 – Microphone Orientation

It is anticipated that many testers may utilize additional microphones, accelerometers, or laser Doppler vibrometers in such a test program.

Although the use of these transducers is not described specifically, this procedure provides a framework that permits such additions.

Noise measurements are specified to have the same duration as the brake application for all test sequences. Therefore, noise measurements are made throughout the test sequence. For the purposes of this test, noise signals are to be acquired with a high pass filter centered at 0.9 kHz. The upper measurement frequency is specified as 17 kHz. The goal of this specification is to eliminate low frequency noise issues whether from the braking system or the test apparatus. Furthermore, a minimum spectral resolution of 800 lines is specified.

As a screening test, it is required that all measurements be made in a peak hold mode where the highest peaks in the spectrum are captured during the sampling or test period. In line with this specification, it is required that measurements be done in the "Fast" mode or the equivalent sampling configuration. All data should be recorded in an A-weighted format. No data need be recorded if the sound level is below the threshold of 70 dB (A). The goal is to capture the highest noise levels during each procedural step to insure that all potential noise issues are highlighted.

The maximum permissible background noise level is 60 dB (A) above 0.9 kHz. The goal is to insure that the ambient level is sufficiently lower than the brake noise level.

4.5 Temperature measurements

The recommended practice in this procedure is to measure temperature using infrared measurement on the in-board face at the outside diameter of the disc. Infrared measurements are preferred since they avoid potential noise generation by contact thermocouples and structural changes when embedding thermocouples. Temperature measurements using thermocouples are still permitted as a non-preferred option.

It is recommended that redundant temperature measurements should be made to prevent accidental overheating. This requirement was added due to the concern that the effects of an inaccurate temperature measurement could be more than simply incorrect data. In the extreme case, the brake could be overheated to component failure.

4.6 Brake operations – modeled on AK noise test procedure

4.6.1. Operating conditions

A brake snubbing operation from 80 km/h to 30 km/h (see Figure 2) under different braking pressures is performed during the bedding program. The braking time, t, is a result of the test rig inertia or is adapted to match the desired vehicle configuration.

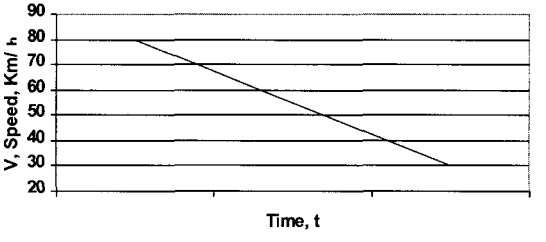

Figure 2 – Braking Operation

4.6.2. Drag operation (constant speed brake applications)

In order to evaluate brake noise, brake drag operations are performed according to the following braking pressure ramp shown (Figure 3). The increase of the brake pressure is 1 bar per second from P_n (normal mean value) -2.5 bar to P_n+2.5 bar at the same speed. The total braking time is 10 seconds. Before the brake drag operation, the temperature of the rotor is

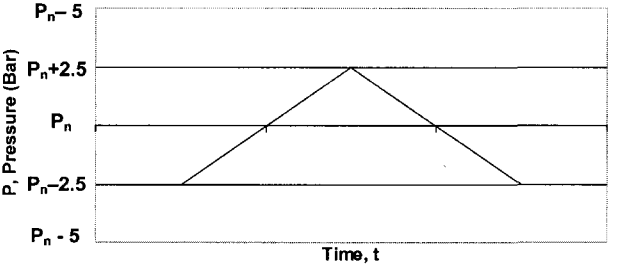

Figure 3 – Braking Pressure Ramp

adjusted to the prescribed value by warming up or cooling down. A single set of tests will be run at 3 km/h.

4.6.3. Stop braking operations

Another portion of the noise evaluation is to perform deceleration tests. The brake is applied to reduce the speed from 50 km/h to 0 km/h as shown in Figure 4 with defined normal pressure. The braking time is either obtained from the test rig inertia or adapted to match the

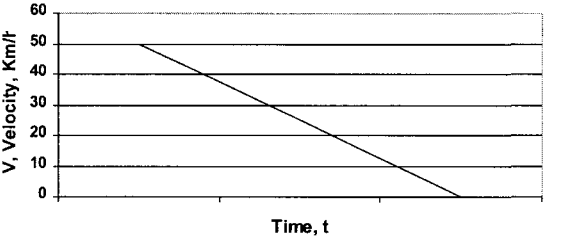

Figure 4 – Stop Operation

desired vehicle configuration.

4.6.4. Warm-Up operation

If the temperature decreases below the initial temperature of the next braking condition, brake warm-up is required by a brake drag operation at 50 km/h with a 20 bar braking pressure until the required initial braking temperature is reached.

4.6.5 Intermediate Conditioning and Warm-Up Operation

This operation is designed to provide conditioning and warm-up between the end of the drag cycle and the beginning of the forward-backward section. A series of stops are executed to warm-up the brake to 150 °C while also providing conditioning.

5. TEST MATRIX – SEVERAL SECTIONS MODELED ON AK TEST PROCEDURE

The test matrix is described in the following sections.

5.1 Main test matrix

Section 1 – Break-In (According to AK Noise Procedure), Section 1 (30)

Cycle	# Of Applications	Initial Speed	Final speed	Pressure (bar)	Initial Temp.
1.1	30	80 km/h	30 km/h	30	100 °C

Section 2 - Bedding (32) – (As defined in AK Master) – Section 2

Cycle	# Of Applications	Initial Speed	Final speed	Pressure (bar)	Initial Temp.
2.1	32	80 km/h	30 km/h	15, 30, 15, 18, 22, 38, 15, 26, 18, 34, 15, 26, 15, 22, 30, 46, 26, 51, 22, 18, 42, 15, 18, 46, 26, 15, 34, 22, 18, 30, 18, 38	100 °C

Optional Section 3 - Friction Characteristic Value After Break-In (6) – (As defined in AK Master) – Section 3

Cycle	# Of Applications	Initial Speed	Final speed	Pressure (bar)	Initial Temp.
3.1	6	80 km/h	30 km/h	30	100 °C

Section 4 - Drag Module (266)

Cycle	# Of Applications	Initial	Speed	Pressure (bar)	Initial Temp.
4.1	14	3 & 10 km/h	(Alternate)	0, 30, 5, 25, 10, 20, 15	50 °C
4.2	Same	Same		Same	75 °C
4.3	Same	Same		Same	100 °C
4.4	Same	Same		Same	125 °C
4.5	Same	Same		Same	150 °C
4.6	Same	Same		Same	175 °C
4.7	Same	Same		Same	200 °C
4.8	Same	Same		Same	225 °C
4.9	Same	Same		Same	250 °C
4.10	Same	Same		Same	300 °C
4.11	Same	Same		Same	250 °C
4.12	Same	Same		Same	225 °C
4.13	Same	Same		Same	200 °C
4.14	Same	Same		Same	175 °C
4.15	Same	Same		Same	150 °C
4.16	Same	Same		Same	125 °C
4.17	Same	Same		Same	100 °C
4.18	Same	Same		Same	75 °C
4.19	Same	Same		Same	50 °C

Section 5 – Intermediate Conditioning and Warm-Up Module (24)*

Cycle	# of Applications	Initial Speed	Final speed	Pressure (bar)	Initial Temp.
5.1	12	50 km/h	0 km/h	30, 5, 25, 10, 20, 15	100 °C
5.2	Same	Same	Same	Same	150 °C

* Run 2 stops for each pressure.

Section 6 - Backward/Forward (50)

Cycle	# of Applications	Initial	Speed	Pressure (bar)	Initial Temp.
6.1	10	-3, 3 km/h	(Alternate)	0, 20, 5, 15, 10	150 °C
6.2	Same	Same		Same	125 °C
6.3	Same	Same		Same	100 °C
6.4	Same	Same		Same	75 °C
6.5	Same	Same		Same	50 °C

Section 7 – Deceleration Module (108)*

Cycle	# of Applications	Initial Speed	Final speed	Pressure (bar)	Initial Temp.
7.1	12	50 km/h	0 km/h	30, 5, 25, 10, 20, 15	50 °C
7.2	Same	Same	Same	Same	100 °C
7.3	Same	Same	Same	Same	150 °C
7.4	Same	Same	Same	Same	200 °C
7.5	Same	Same	Same	Same	250 °C
7.6	Same	Same	Same	Same	200 °C
7.7	Same	Same	Same	Same	150 °C
7.8	Same	Same	Same	Same	100 °C
7.9	Same	Same	Same	Same	50 °C

* Run 2 stops for each pressure. For example, 5 bar at 50 °C for 3 stops. Then run 10 bar at 50 °C for 1 stops. Continue this for the remaining pressures. Do this for all 9 cycles.

Section 8 - Friction Characteristic Value After Break-In (6)
-Repeat Section 3 Above

Section 9 - Drag Module (266)
-Repeat Section 4 Above

Section 10 – Intermediate Conditioning and Warm-Up Module (24)
-Repeat Section 5 Above

Section 11 - Backward/Forward (50)
-Repeat Section 6 Above

Section 12 - Deceleration Module (108)
-Repeat Section 7 Above

Section 13 - Friction Characteristic Value After Break-In (6)
-Repeat Section 3 Above

Section 14 - Drag Module (266)
-Repeat Section 4 Above

Section 15 – Intermediate Conditioning and Warm-Up Module (24)
-Repeat Section 5 Above

Section 16 - Backward/Forward (50)
-Repeat Section 6 Above

Section 17 - Deceleration Module (108)
-Repeat Section 7 Above

Section 18 - Friction Characteristic Value After Break-In (6)
-Repeat Section 3 Above

5.2 Optional test matrix – noise after fade recovery
Sections 19-25 are optional. The noise data from these sections will represent the squeals generated after severe fade and recovery.

Section 19 - Temperature Fade Module (15)

Cycle	# of Applications	Initial Speed	Final speed	Deceleration (g)	Pressure (bar)	Initial Temp. (°C)
19.1	15	100 km/h	0 km/h	0.4	160	100, 215, 283, 330, 367, 398, 423, 446, 465, 483, 498, 513, 526, 539, 550

Section 20 - Recovery (18)

Cycle	# of Applications	Initial Speed	Final speed	Pressure (bar)	Initial Temp.
20.1	18	80 km/h	30 km/h	30	100 °C

Section 21 - Drag Module (266)
-Repeat Section 4 Above

Section 22 – Intermediate Conditioning and Warm-Up Module (24)
-Repeat Section 5 Above

Section 23 - Backward/Forward (50)
-Repeat Section 6 Above

Section 24 - Deceleration Module (108)
-Repeat Section 7 Above

Section 25 - Friction Characteristic Value After Break-In (6)
-Repeat Section 3 Above

6. SUMMARY

The automakers and brake suppliers continue to work toward improving brake NVH performance. Without an effective method to analytically predict NVH performance during development, testing is a critical component of the development process.

At present there is no globally recognized brake NVH test procedure. There is clearly a need for a global test standard. Both braking system sourcing and applications are global. Consistent methods of performance evaluation are necessary to be used throughout the industry.

There has been a European Working Group (AK or Arbeitskreis Gerausch) in existence for some time. They have developed a noise test procedure that is in limited use. The US Working Group on Brake Noise has reached the stage where a draft procedure has been developed. Several major components of this procedure have been drawn for the AK test protocol. Due to common practice in the US and the experience of some members of the Working Group, this protocol includes a series of deceleration noise tests.

6. REFERENCES

1. Wallaschek, J., Jach, K-J, Mody, PA, "Survey of the Present State of Friction Modeling in the Analytical and Numerical Investigation of Brake Noise Generation," *Proceeding of ASME Vibration Conference, 1999 ASME Design Engineering Technical Conference* Las Vegas, 1999, ASME, 1999.
2. Rhee, SK, Tsang, HS, and Wang, VS, "Friction –Induced Noise and Vibration of Disc Brakes," *Wear*, Vol. 133, P 39, 1989.
3. Abendroth, H, "Advanced/Progress in NVH Brake Test Technology," *Proceedings 16th Annual SAE Brake Colloquium and Engineering Display*, SAE P98-327, PP 21-32, 1998.
4. Blaschke, Peter and Rumold, Walter, "Global NVH Matrix for Brake Noise – A Bosch Proposal," SAE 1999-01-3405, 1999.
5. US Working Group on Brake Noise, "Draft Disc Brake Dynamometer NVH Matrix," SAE J2521 Draft, 2000.

Materials and Modelling

This page intentionally left blank

CAE prediction and experimental verification of maximum temperature of cool running 72 curve fin brake rotor design

A R DAUDI
Hayes Lemmerz International, Ferndale, Michigan, USA
M NARAIN
Optimal Inc, Novi, Michigan, USA

ABSTRACT

Hayes Lemmerz's 72 curve fin brake rotor design, was analyzed using CAE tools to predict the temperatures after braking. A cool running brake rotor design, was developed by shaping the cast iron material of equal mass into shapes that would receive the heat generated by 100 to 0 kph braking, and conduct, convect and radiate the heat away from the brake plate, so that the brake plate temperature does not rise significantly. In previous publications (1,2,3,4 and 5) several fin numbers (42 vs. 72), shape (straight vs. curve), geometries (air inlet angle 90 vs. 45, air outlet angle 90 vs. 110) and brake plate attachment to fins (outboard brake plate vs. both outboard and inboard brake plate attached symmetrically to hat section) were examined to find the 72 curve fin brake rotor design to have the highest airflow velocity.

FEA (Finite Element Analysis) was used to verify structural strength, and Fluent CFD software was used to find the highest airflow velocity rotor and its thermal film coefficient. The magnitude of solid-fluid heat transfer at the metal-fluid interface, is in a highly turbulent range. Abaqus software received these thermal film coefficients and predicted the temperature of rotor. Dynamometer test of the 72 curve fin rotors was compared to the CAE predictions. The predicted temperatures on brake plate center and hat area matches the dynamometer thermocouple temperature readings. These 72 curve fin rotors were tested on LACT (Los Angeles City Traffic) vehicle test and showed 50°C (122 °F) cool running capability. Hayes Lemmerz now has the CAE software to reasonably predict the maximum brake temperature for vehicles with known brake load and given brake design.

1. INTRODUCTION

High temperature of vehicle brake structure as shown in Figure-1, during braking operation have created the four big brake customer complaints as seen by the brake warranty costs.

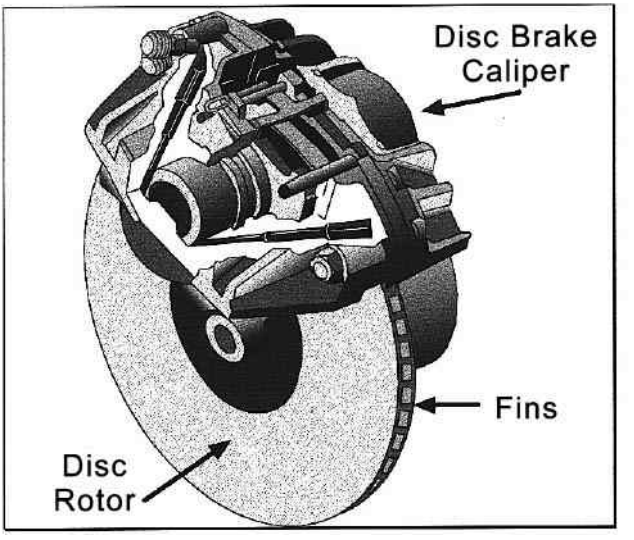

Figure 1 – Vehicle Brake Structure

High temperature causes large brake rotor and pad/caliper distortions. High lateral runout and thickness variations of rotor creates noisy brakes. High temperature of brakes causes accelerated corrosion of the cast iron rotor causing more NVH problems of brakes. High temperature of rotor causes excessive brake pad wear and thus reduces pad life.

The brake component and system suppliers are developing new technologies to win over new business based on a better designed brake rotor/drum/caliper/pad assembly. The brake industry needs a change in their status quo culture. The pace of technology change is an essential element that Brake Component Suppliers must consider. Enormous advances in technology are needed to successfully and permanently solve these re-occurring brake problems. The solutions have to be reliable, efficient, safe and affordable. No supplier can claim innovation leadership for long - so opportunities need to be grasped quickly.

Hayes Lemmerz, has created an analytical tool that could correctly predict the brake temperature reached on the brake dynamometer thermal capacity test and vehicle thermal capacity test during LACT (1,2,3,4 and 5) . In this paper, a detailed analysis of a cool running design of rotor known as "72 curve fin design" is presented showing the lowering of the maximum temperature by 50°C (122 °F). This drop in temperature was predicted by the CFD/Thermal Analysis Computer Program. Both the dynamometer and vehicle tests confirmed the 50°C (122 °F) drop in maximum temperature during heating and cooling cycles of tests.

The objective of this paper is to predict the transient temperature distribution in two different brake rotor designs using CAE (Computer Aided Engineering) techniques. Figure-2A and 2B, shows the first brake rotor is the current WIN126 design and the second rotor is the HLI proposed design.

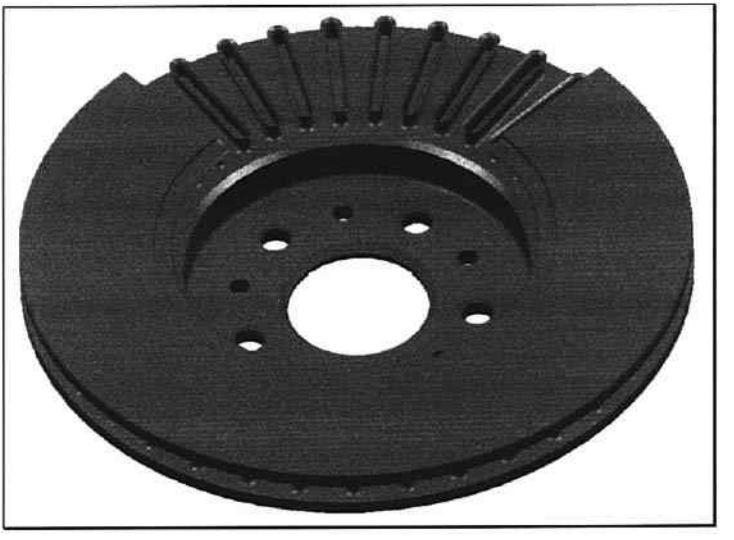

Figure 2A WIN126 37 Straight Fin Rotor

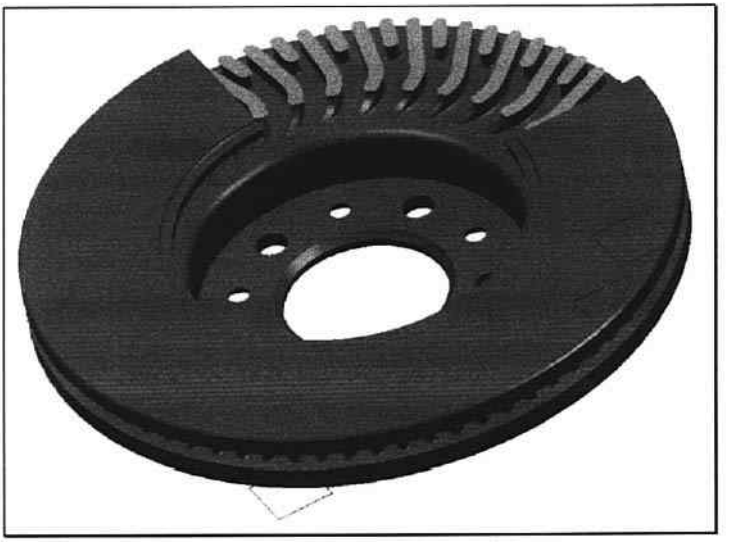

Figure 2B HLI Proposed 72 Curve Fin Rotor

The WIN126 design has 37 straight fins and the HLI design has 72 curved fins. First, steady state conjugate heat transfer analysis is performed using CFD (computational fluid dynamics) to determine the heat transfer coefficients at the solid-fluid interface. Then, the heat transfer coefficients are transferred as boundary conditions to the solid model and FEA (finite Element Analysis) is used to perform transient temperature calculations in the rotor. Fluent is used for the CFD analysis and the Abaqus is used for the FEA.
The CAE results show that the HLI proposed design is 90°C (194°F) cooler than the current WIN126 design after 25 stops. The HLI design has 11% more flow through the rotor than the current WIN126 design. The temperature results from CAE are compared with the dynamometer test data and vehicle test data. The vehicle test data shows that the HLI design is 50°C (122°F) cooler than WIN126 design. Dynamometer test data shows that the HLI design is 70°C (158°F) cooler than the WIN126 design. The absolute temperatures of rotors predicted by CAE are about 300 °C higher than those measured by tests. The reasons for these discrepancies are due to zero heat flow assumed across the hub/spindle area. As future improvement Hayes Lemmerz is adding a subroutine to take in account heat lost through hub and spindle area and correlating it to actual dynamometer data. The results will be published in another paper.

2. OBJECTIVE

The objectives of this paper are :
(1) To evaluate and compare the temperature distribution and airflow of the WIN126 and HLI proposed brake rotor design using CAE techniques.
(2) To compare CAE predicted rotor temperature with the experimental data to assess the effectiveness of assumptions and the methodology used in the current CAE analysis.

3. METHODOLOGY

3.1 CAE PROCESS

The CFD and FEA meshes are created in the solid (rotor) and fluid (air) region. Steady state conjugate heat transfer CFD analysis is performed to obtain flow and temperature distribution in both the solid and fluid region. The heat transfer co-efficient are extracted from the CFD results and used as boundary conditions for the transient heat transfer FEA. The FEA is used to predict transient temperature distribution because it reduces the computational time significantly and further analysis can be done to predict thermal stresses and distortion, which cannot currently be done in CFD.

3.2 GEOMETRICAL MODELING

Figure-3 shows the three-dimensional computation domain for the CFD analysis for the WIN126 brake rotor design.

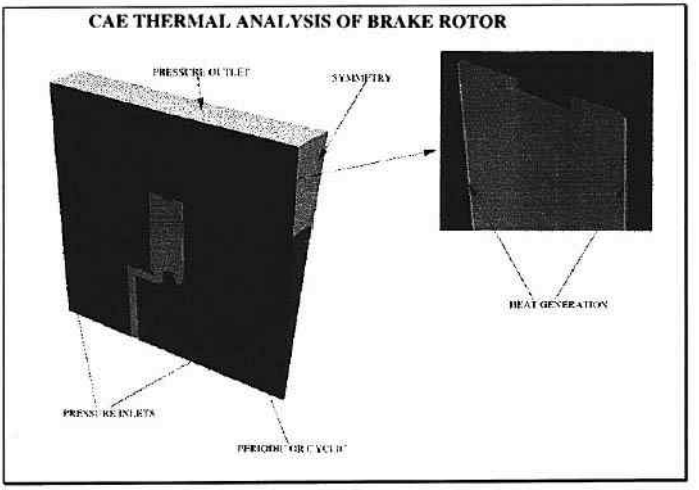

Figure 3 Computational Domain and Boundary Conditions for CFD

The computational mesh for the CFD analysis is created from the IGES data provided by HLI. Only one pair of fins is considered for this analysis, because all the fins have the same shape and the flow is assumed to be steady state. Inlet and outlet sections are added upstream and downstream of the rotor, where the boundary conditions are imposed, as shown in Figure 3. The CFD mesh for the WIN126 and HLI rotor designs is shown in Figure 4.

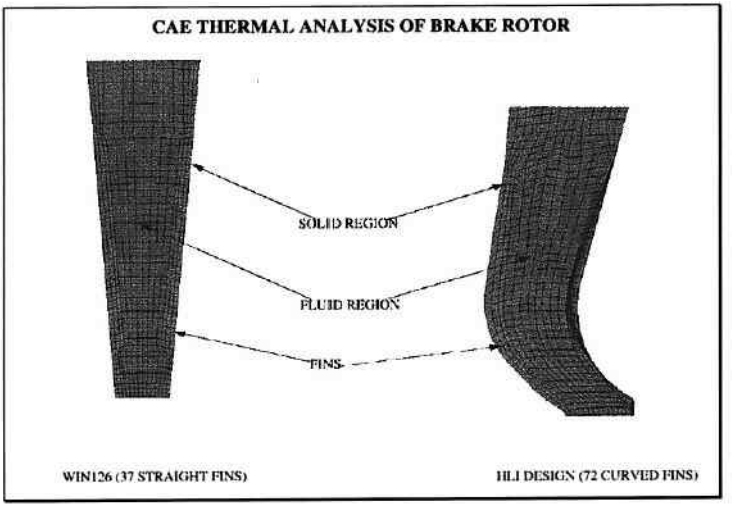

Figure 4 Mesh in the Region of Fins for WIN126 Design

The mesh is created both in the solid (rotor) and fluid (air) regions for the conjugate heat transfer CFD analysis. The mesh for the FEA analysis is extracted from the CFD mesh in the solid region.

3.3 ASSUMPTIONS

To obtain results in a reasonable period of time, the following assumptions were made in the CAE analysis.

a) The rotor is rotating with a constant steady speed.

b) The airflow is at steady state.

c) Heat transfer coefficient ("h") is dependent on the airflow velocity only. "h" does not change with time.

d) The frictional heat generated by brake pads is distributed uniformly over the whole surface area of the rotor.

e) Flow is incompressible (density of air is constant).

f) K-Є model is used to represent turbulence. Standard wall functions are used at the wall.

g) The heat loss by radiation is neglected.

h) Heat is removed by airflow (convection heat transfer) only.

I) The model does not include knuckle and other components of the brake corner assembly. The model includes the rotor only.

3.4 CFD AND FEA MODELING

Fluent is used for this CFD analysis. Fluent numerically solves the generalized Navier-Stokes equations. The Navier-Stokes equations describe most of the fluid flow and heat transfer phenomenon. Fluent is a finite volume based CFD software. To obtain the velocity field, temperature and pressure field in Fluent, the continuity, momentum, energy and turbulence equations are solved. The governing equations are solved in a rotating frame of reference. Abaqus by HKS is used for the transient heat transfer FEA. In the FEA, the conduction equation is solved to obtain the transient temperature field in the rotor.

3.5 BOUNDARY CONDITIONS

3.5.1 CFD

Boundary conditions need to be provided at the faces of the computational domain. Refer to Figure 3 for the location of the boundary conditions. Atmospheric temperature and pressure boundary conditions are applied at both the inlet and the outlets. The brake rotor is rotating at 670 RPM corresponding to a vehicle speed of 100 kph. At the inlet, turbulence intensity of 5% and mixing length scale of 0.01 meter is used. No-slip velocity boundary condition was used at the surface of brake rotors. Periodic boundary conditions are used at either side of the wedge of the brake rotor computational domain. Symmetry boundary conditions are used for the remaining regions.

In the steady state conjugate heat transfer analysis, the heat generation boundary condition is imposed on a thin strip of cells near the rotor surface. This is done to simultaneously simulate both the heat generated by the braking process and heat loss from the brake cheeks of the rotor by the outside air. The heat generation per unit volume used in the CFD analysis is $3x10^8$ W/mm^3. This is an average value to obtain a maximum steady state temperature of approximately 800°C (1472°F). The exact value of heat generation is not important because the objective of the CFD analysis is to predict the heat transfer coefficient and not the exact temperature. It is also assumed that the heat transfer coefficient does not change with time and is dependent on the flow field only.

3.5.2 FEA

Cyclic boundary conditions are used at either side of the wedge of the brake rotor. Heat flux boundary conditions are imposed on the cheeks of the rotor that are exposed to the pads. The

heat transfer boundary conditions are transferred from the CFD model. For the transient heat transfer, FEA uses the heat generation parameter as follows : (provided by HLI dynamometer data)
Initial Temperature=68°C
Braking 100 kph to 0 kph =5.7 seconds
Ramp=32 seconds
Heat generation during braking=0.98 W/mm^2

3.5.3 TRANSFER OF HEAT TRANSFER BOUNDARY CONDITIONS
The following approach is used to transfer heat transfer boundary conditions between the CFD and FEA model:
1. Write out the heat transfer co-efficient from Fluent in Patran format. The reference temperature is the air inlet temperature of 27°C. The Patran file includes the shell at the walls and the corresponding "h" value at the face.
2. Write out the mesh for the solid region from ICEM and transfer it to Hypermesh. Impose constant "h" boundary condition of the surfaces exposed to the airflow.
3. Write Abaqus deck from Hypermesh.
4. Use Matlab to modify the Abaqus input deck with the "h" values from the Patran file.

3.6 MATERIAL PROPERTIES
The following material properties were used for both design analyses:
3.6.1 AIR
Density = 1.164 kg/m^3
Viscosity = 1.824e-5 kg/m-s
Conductivity = 0.0261 W/m-K
Specific Heat = 1012 J/kg-K
3.6.2 ROTOR
Density = 6950 kg/m^3
Conductivity = 0.046 W/m-K
Specific Heat = 452 J/kg-K

4. RESULTS AND DISCUSSIONS
The steady state CFD results for temperature and heat transfer co-efficient on the brake rotor surface are shown in Figure 5 and Figure 6 respectively.

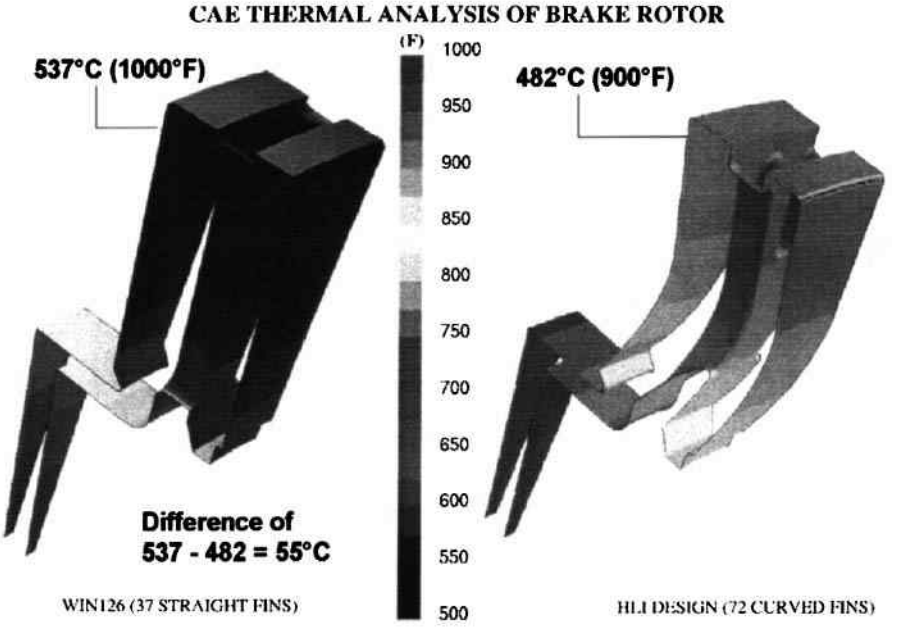

Figure 5 Temperature Contours

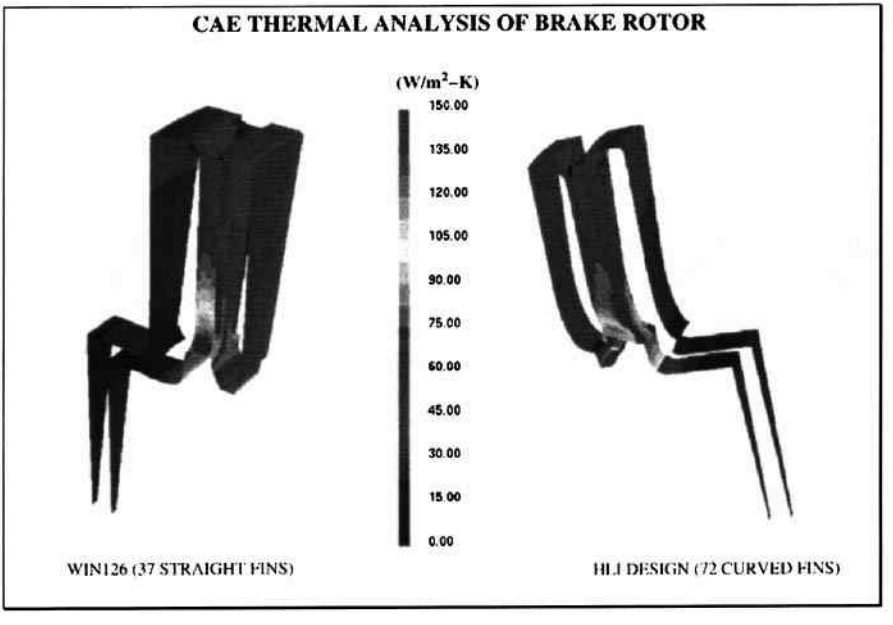

Figure 6 "h" Distribution Contours

Figure 7 shows the airflow distribution on mid-plane through the rotor for both designs.

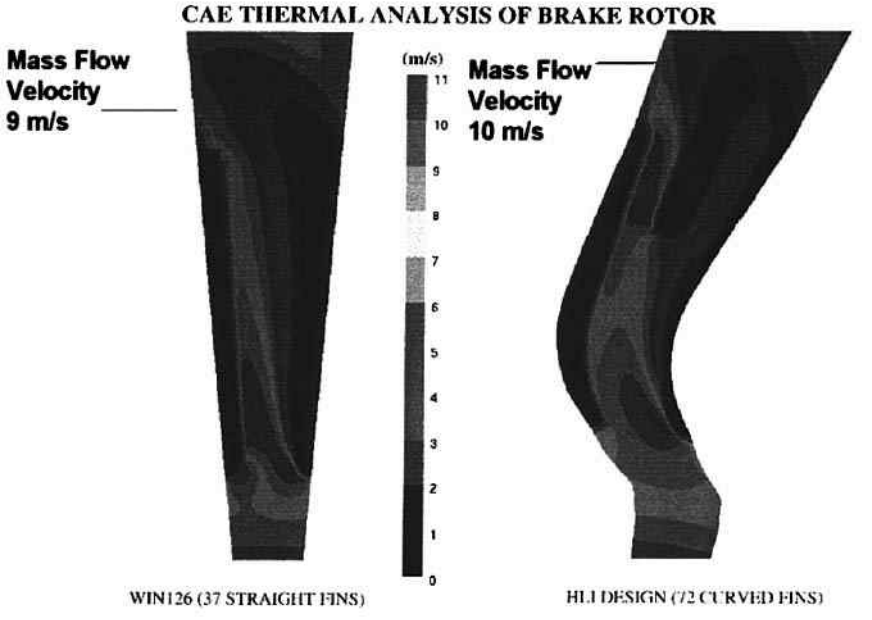

Figure 7 Relative Airflow Velocity Contours

The scooping action of the curved fin design increases the airflow through the rotor. The airflow through the 72 curved fin HLI rotor is 11% higher than that for the 37 straight fin WIN126 rotor. From the airflow distribution, it can be seen that the channel on the right is not filled completely. About 50% more air flows through the left channel as compared to the right channel. The heat transfer from the curved fin design can be further improved by redesigning the fins to have more flow through both passages. This can be accomplished by changing the fin angles and increasing the length of the short fin.

The maximum temperature in both the rotor designs from the transient heat transfer FEA analysis is shown in Figure 8A.

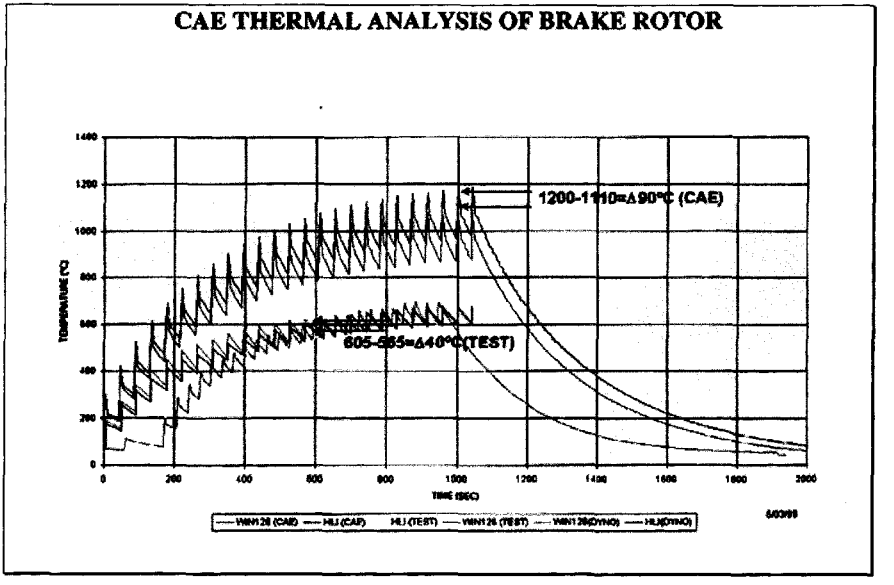

Figure 8A CAE, Dyno and Vehicle Testing Temperature Data

This figure shows the HLI design is 90°C (194°F) cooler than WIN126 design after 25 stops. This improved cooling can be attributed to the increase in heat transfer co-efficient resulting from improved airflow for HLI design. Figure 8A, 8B and 8C also includes the maximum temperature from the dynamometer and vehicle testing.

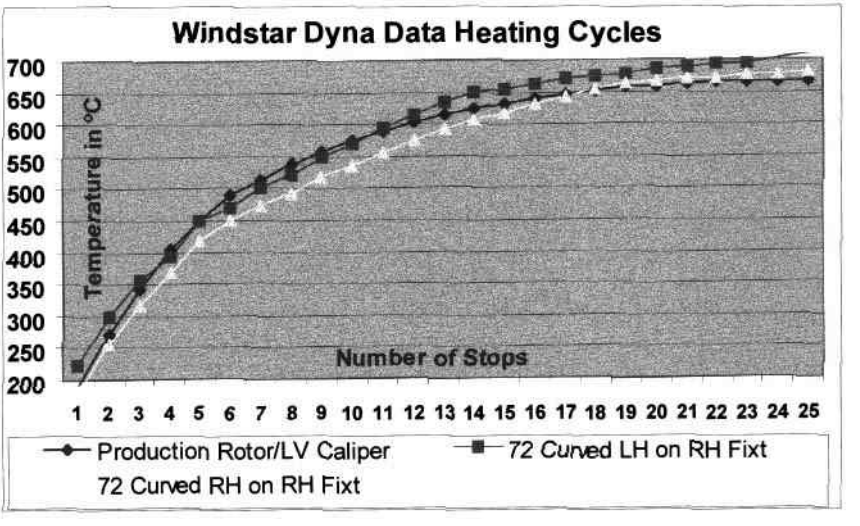

Figure 8B – Windstar dynamometer test – temperature vs no. of stops graph

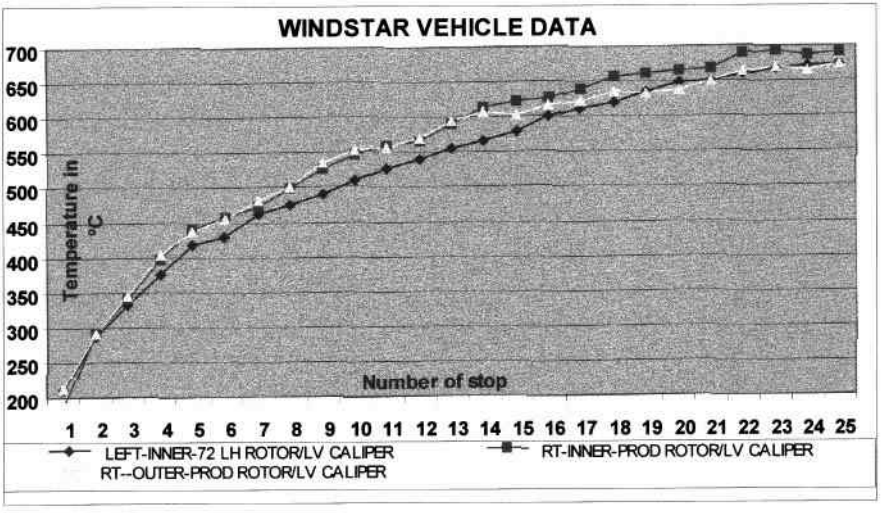

Figure 8C – Windstar vehicle test – temperature vs no. of stops graph

In the dynamometer testing data, the maximum temperature difference of 40°C (104°F) occurs after 13 stops. The temperature difference after 13 stops from the CAE analysis is 60 °C (140°F). The CAE analysis correctly predicts the temperature difference trends corresponding to rotor design changes, but on the other hand, the temperature after 25 stops for CAE is 300 °C higher than the testing data. The testing data temperature peaks earlier than the CAE data. This difference could be attributed to:

1. Thermal mass of hub and other components in the corner assembly.
2. Heat loss due to radiation.
3. Heat loss to the knuckle or axle due to conduction.
4. "h" may change with time.
5. "h" may be under-predicted by the wall-functions in the low velocity regions on the cheeks and the recirculation zones around the fins.

Figures 9 to 14 show the temperature distribution from the FEA for 1st, 10th and 25th stops.

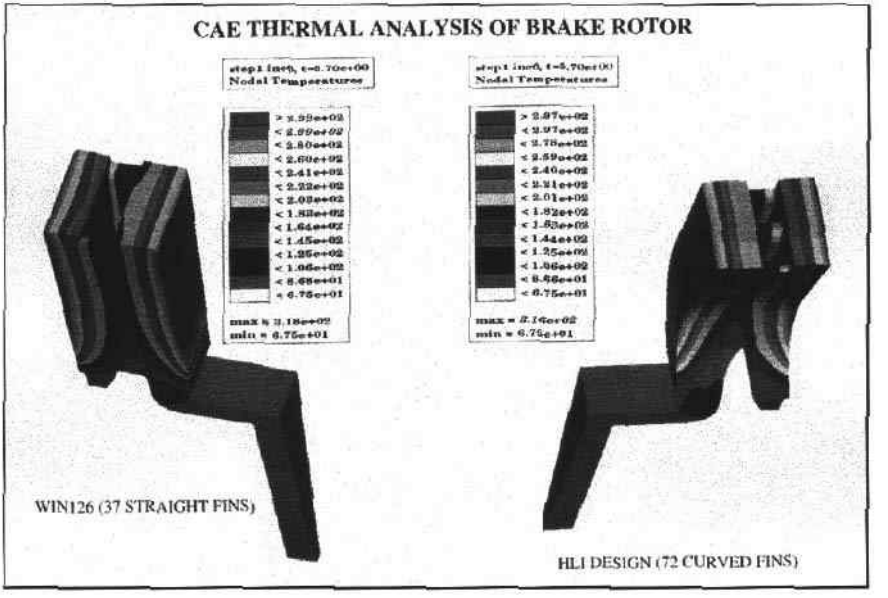

Figure 9 Temperature Distribution at the end of 1st Heating *Period*

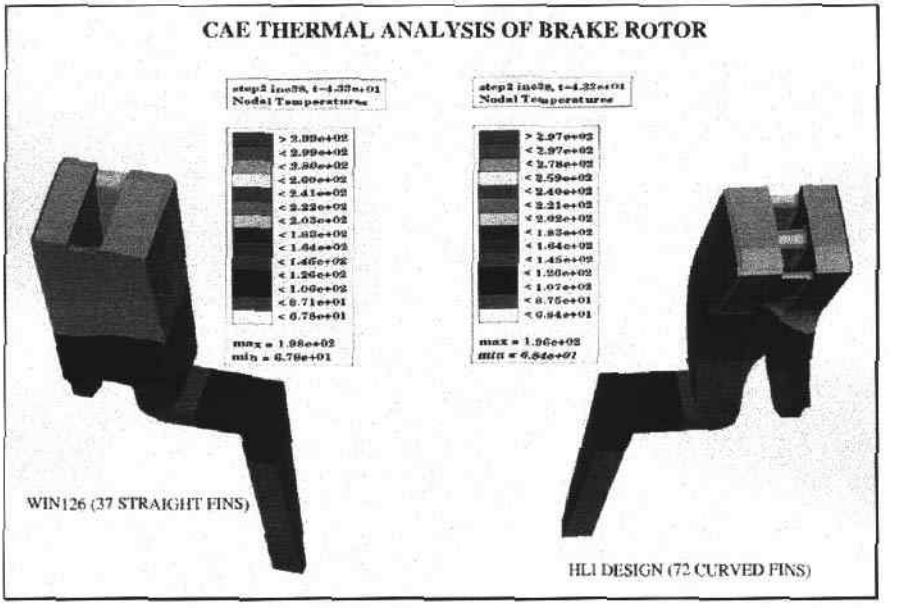

Figure 10 Temperature *Distribution* at the end of 1st Cycle

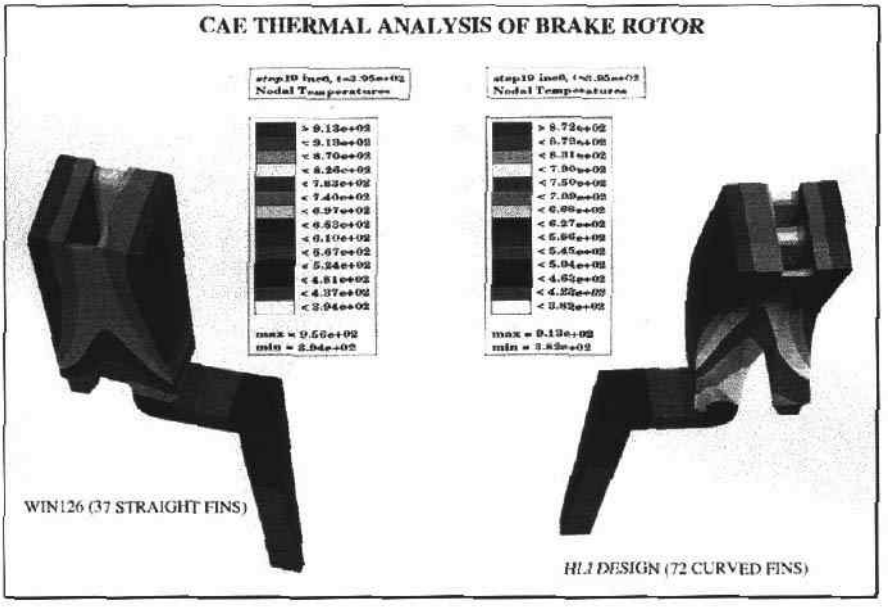

Figure 11 Temperature Distribution at the end of 10[m] Heating Period

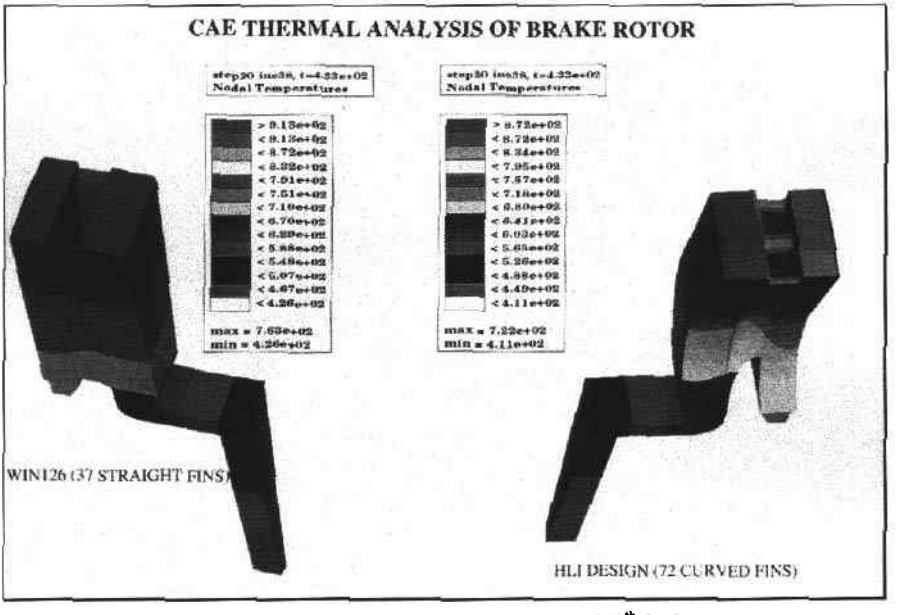

Figure 12 Temperature Distribution at the end of 10[th] Cycle

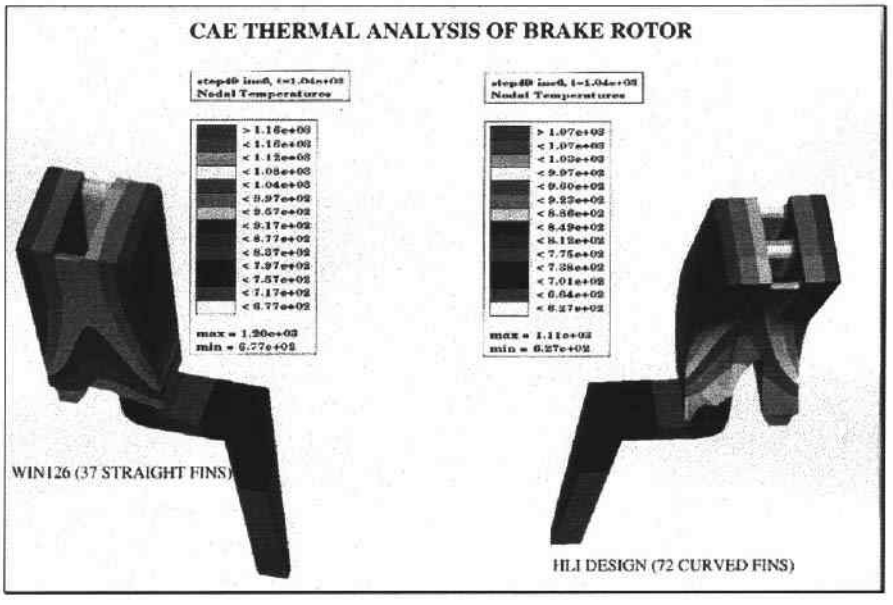

Figure 13 Temperature Distribution at the end of 25th Heating Period

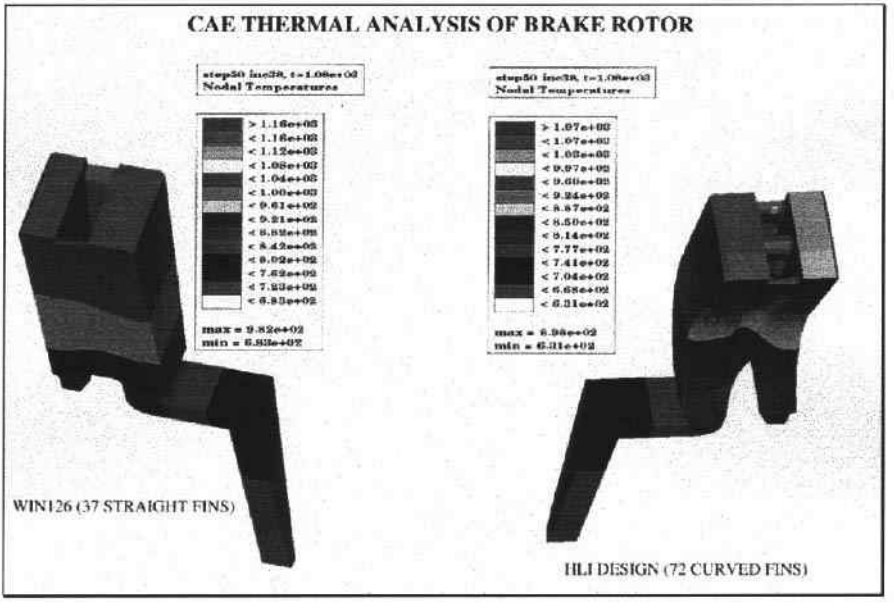

Figure 14 Temperature Distribution at the end of 25th Cycle

5. FUTURE WORK

The CAE process applied in this paper correctly predicts the temperature difference trends corresponding to brake rotor design changes. Additional efforts are needed to improve the correlation of the absolute temperature in the rotor. Following is a list of tasks that can be attempted to improve the temperature correlation:

1. Include more details of the corner assembly in the FEA model to account for the thermal mass.
2. Apply the radiation model.
3. Change boundary conditions to include the effect of heat loss due to conduction.
4. Use advanced two-layer K-Є model to predict the "h" value more accurately.
5. Determine "h" as a function of time and/or temperature for FEA analysis.

6. CONCLUSION

1. The airflow rate through the 72 curved fin HLI rotor is 11% higher than that for the 37 straight fin WIN126 production rotor.
2. The increase in airflow rate in the 72 curve fin proposed HLI rotor design has lowered the maximum rotor temperature by 60°C (140°F) after 13 stops, compared to an equal mass production rotor with 37 straight fin design.
3. Dynamometer test show 40°C (104°F) drop in maximum temperature in 72 curve fin rotor design after 13 stops, compared to an equal mass production rotor with 37 straight fin design.
4. Vehicle test show 50°C (122°F) drop in maximum temperature in 72 curved fin rotor after 13 stops, compared to an equal mass production rotor with 37 straight fin design.

REFERENCES

1- Anwar R. Daudi and Wes E. Dickerson, "Disc Brake Rotor Design for increased Airflow", 15th SAE Brake Colloquium, October 8, 1997

2- Anwar R. Daudi, Wes E. Dickerson and M. Narian,"Hayes Increased Airflow Rotor Design", Page 127, Automotive Braking, Professional Eng. Publishing Ltd., London, UK 1998

3- Anwar R. Daudi, "Hayes High Airflow Design Rotor for Improved Thermal Cooling and Coning", SAE #982248, 1998

4- Anwar R. Daudi, "72 Curved Fins and Air Director Idea Increases Airflow through Brake Rotors", SAE 1999-01-0140, March 1-4, 1999

5- Anwar R. Daudi, "72 Curved Fin Rotor Design Reduces Maximum Rotor Temperature", SAE 1999-01-3395, October 10-13, 1999

This page intentionally left blank

Finite element prediction of inelastic strain accumulation in cast-iron brake rotors

S KOETNIYOM, P C BROOKS, and **D C BARTON**
School of Mechanical Engineering, The University of Leeds, UK

ABSTRACT

This paper reports the results of detailed thermo-mechanical finite element analyses of cast iron brake rotors under repeated high-g braking conditions. The thermal analysis allows for heat loss from the vanes in a back-ventilated disc design as well as heat transfer to other parts of the brake assembly. The cast iron material properties required for the non-linear structural analysis are generated by mechanical tests on samples cut from the brake disc. The material model allows for the variation of flow stress with temperature and for the different yield properties in tension and compression. The finite element results indicate regions of high plastic strain accumulation which may lead to disc crazing and/or cracking and enable comparisons to be made between back- and front-vented rotor designs.

1. INTRODUCTION

The competing demands for smaller and lighter brake discs together with greater performance expectations for passenger cars have heightened concerns over the integrity of brake rotors under severe braking conditions. In particular, it is recognised that repeated severe brake applications under high speed autobahn driving conditions may lead to thermal cracking of brake rotors due to inelastic (plastic) cyclic strain accumulation. It is very desirable to be able to compare alternative designs and materials at the pre-prototype stage by developing computer models of the brake thermal performance and structural integrity. Ultimately however any new design of brake rotor must be validated for each vehicle by on-vehicle testing.

With the advent of commercially available software packages, it was evident that finite element (FE) analysis represented the most appropriate and convenient method of simulating brake rotor performance on the computer [1]. Different approaches to the thermal modelling of disc brakes were described by Sheridan *et al.* [2] whilst Bailey *et al.* [3] used thermal imaging results as input to FE simulations of the rotor thermal distortions. There have been a

number of attempts to predict the structural integrity of brake rotors based on FE thermal stress analysis [3-5]. However, these have tended to use a simple elastic material model or standard von Mises plasticity relations that do not accurately reflect the complex yield and hardening behaviour of cast iron. This paper describes work that attempts to remove some of the inaccuracies and uncertainties surrounding previous structural analyses by adopting a more rigorous approach to modelling the mechanical properties of cast iron.

The particular brake rotor chosen to demonstrate the technique is a back-vented high carbon disc developed by Rover Cars. The paper first describes the heat transfer analysis of this rotor under severe autobahn stop conditions. The mechanical property tests on samples cut from the Rover brake disc are then outlined. The results generated are used to derive the parameters of a temperature-dependent plasticity model, which allows for the different yield properties of cast iron in tension and compression. Finally, the application of this material model to the thermal stress analysis of the back-vented rotor is described and compared with the results for a corresponding front-vented design in terms of the likely propensity for thermal cracking. The commercial FE package ABAQUS, well known for its non-linear capabilities, was used throughout.

2. INITIAL FINITE ELEMENT ANALYSIS OF RD1 BRAKE DISC

The purpose of the analysis is to predict the temperatures and corresponding thermal stresses in the brake disc when the vehicle is subjected to sudden high speed stops as can occur under autobahn driving conditions. The particular cycle chosen for the simulation involved braking the vehicle from an initial velocity of 48 ms^{-1} (108 mph) to 16.7 ms^{-1} (37.5 mph) at a constant deceleration of 0.7g with the brake rotor at an initial uniform temperature of 80 °C. The vehicle is subsequently accelerated up to the same initial velocity and the rotor allowed to cool again to 80 °C before the cycle is repeated up to 7 times.

In order to accurately simulate both the thermal and structural response of the back-vented rotor, a 15.65° segment of the brake disc and hub was modelled using solid finite elements as shown in Figure 1. Note that one complete long vane and two half short vanes have been included in the model which, with appropriate boundary conditions, allows for the cyclic symmetry that exists in the disc (i.e. this segment is repeated 23 times to give the complete brake disc).

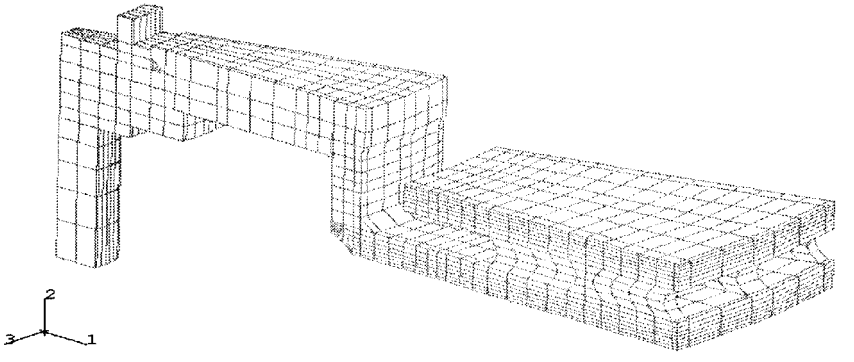

Figure 1: Finite element model of 15.65 ° segment of back-vented disc and hub

For the thermal analysis of the brake application, a uniform heat flux is applied over the two rubbing surfaces of the disc using the formula:

$$Q = \frac{X_f K_p K_i K_d V Ma}{n_p A}$$

where X_f = proportion of braking due to front wheels (0.725)
K_p = proportion of heat to disc (0.95)
K_i = correction factor due to vehicle inertia (1.1)
K_d = correction factor due to drag force (0.726)
V = instantaneous velocity (ms^{-1})
M = vehicle mass (1990 kg)
a = deceleration (0.7 g)
n_p = number of pads on front axle (4)
A = total rubbing surface area per pad (0.0392 m^2)

The parameter values shown in parenthesis were either supplied by Rover or taken from other similar studies [7]. Note that no account is taken of radial or circumferential heat input variations due to non-uniform interface pressure distributions or relative velocities (a fully coupled thermo-structural analysis was considered outside the scope of the present work).

Heat loss from the model during braking and the subsequent cooling period occurs by convection and radiation from all free surfaces. Heat transfer coefficients were calculated according to the formulas and factors presented by Grieve *et al.* [7] which take account of the variation of cooling airflow with vehicle velocity. This approach has been shown to give accurate results compared with experimentally measured rotor temperatures. The density of the cast iron rotor was taken as 7165 kg/m^3 whilst the conductivity and specific heat were assumed to vary with temperature as per standard reference data for high carbon cast iron.

Results of running the thermal simulation are illustrated in the temperature contour plot at the end of the first brake application shown in Figure 2. It can be seen that the maximum temperature approaches 400 °C with the outboard cheek running slightly hotter than the inboard side due to the longer conduction path on this back-vented design even though the heat has had little time to penetrate into the neck or top-hat section of the disc.

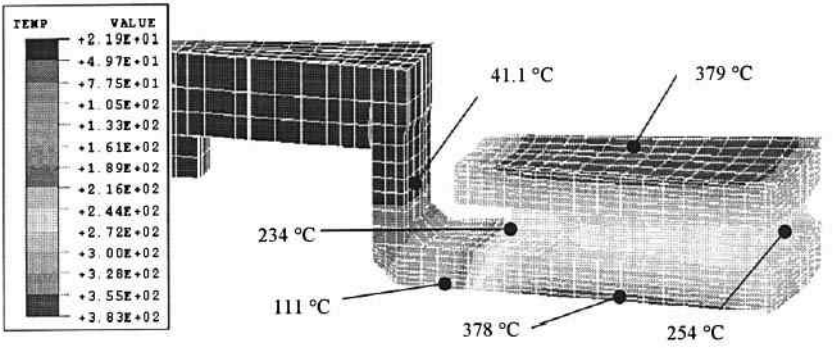

Figure 2: Contour plot of temperature at end of first brake application for back-vented disc

In order to estimate the magnitude and direction (i.e. tension or compression) of the thermal stresses arising from the predicted non-uniform temperature distributions a linear elastic stress analysis using the same brake rotor finite element model was carried out for each time step of the thermal analysis. The Young's modulus and Poisson's ratio of the cast iron disc were assumed to be 116 GPa and 0.26 respectively. Only thermal stresses were considered, the mechanical loading due to the pad normal pressure and surface traction being insignificant in comparison. The maximum elastic von Mises stress predicted at the end of the first brake application was 517 MPa which is much higher than the yield stress of cast iron at this elevated temperature. Therefore a non-linear elasto-plastic stress analysis coupled to a realistic rotor material model is required to accurately predict plastic strains that may be the precursor to rotor cracking.

3. MECHANICAL PROPERTY TESTS

In order to accurately determine the stress-strain response of the rotor material as a function of temperature and direction of loading, dumb-bell test specimens were machined from a Rover disc as indicated in Figure 3.

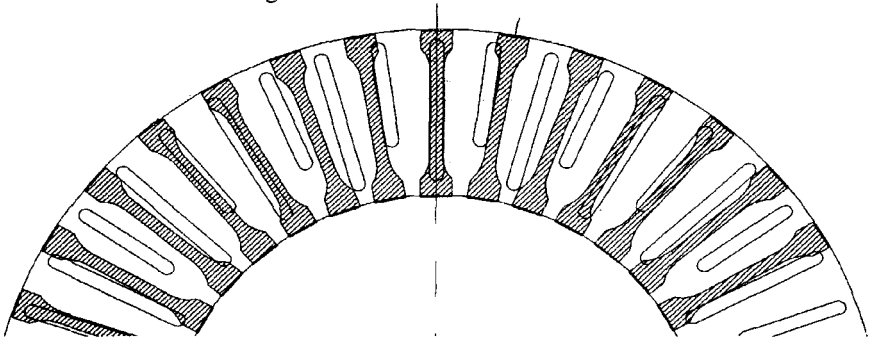

Figure 3: Test specimens cut from Rover disc brake

All specimens were loaded monotonically in either tension or compression in a Dartec servo hydraulic test machine at a constant load rate of 300 Ns^{-1}. In addition to room temperature tests, an induction heating coil with temperature feedback control from an infra-red pyrometer was used to maintain the gauge length of specimens at elevated temperatures of 300, 350 or 400 °C throughout the duration of a test (unfortunately it proved impossible to maintain a stable gauge length temperature of less than 300 °C using the induction heater system). Samples tested at room temperature were fitted with strain gauges in order to effectively calibrate the crosshead displacement transducer of the Dartec so as to give an accurate measure of the strain in the specimen gauge length. This calibration was assumed to be maintained at elevated temperature i.e. the compliance of the Dartec and its fixtures was assumed to be unaffected by changes in the temperature of the specimen gauge length. Specimens were loaded to failure in tension and up to a strain of 0.01 in compression. Separate specimens were used for each test to prevent damage accumulation from previous tests affecting the results.

No evidence of necking or buckling was seen in any of the specimens so the measured loads and crosshead displacements were converted to true stress and true strain respectively making the usual constant volume assumption for plastic deformation. The resulting true stress-strain curves are shown in Figure 4. It can be seen that the response in tension is quite different to that in compression, with the true stress at a given strain in the former regime being much lower due to the opening of voids around the graphite flakes. Also the rate of reduction of true stress with temperature in both tension and compression is particularly significant as the temperature is increased above 300 °C.

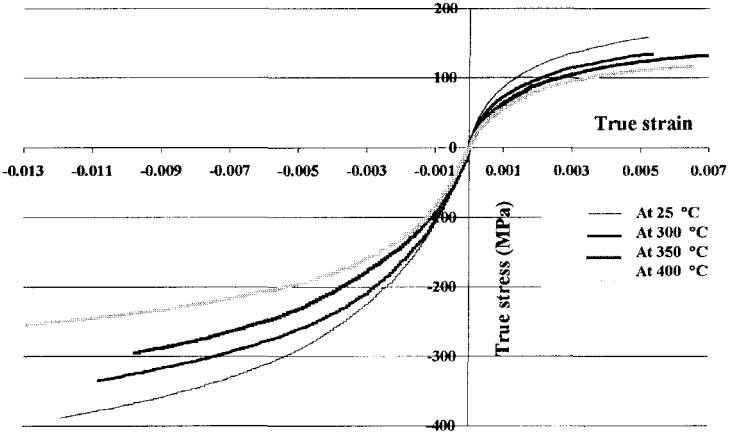

Figure 4: True stress-true strain curves for Rover cast iron disc material

4. INELASTIC FINITE ELEMENT ANALYSIS OF ROVER BRAKE DISC

ABAQUS Version 5.7 [8] contains a special elasto-plastic cast iron material model that allows for the different yield properties in tension and compression. The former assumes a Rankine (maximum principal stress) failure criterion and the latter the standard von Mises yield criterion. Which criteria to use depends on the mean of the three principal stresses acting at a point: if this is positive, then the tensile criterion is used; if the mean is negative, then the standard von Mises compression criterion is invoked. The inelastic material properties derived above were incorporated in this material model by simply reading in true stress-true strain data points at different temperatures for each mode of loading i.e. tension or compression. The code then linearly interpolates between these data points to give the inelastic stress at any strain or temperature.

The thermal stress analysis detailed above was rerun using the same input temperatures but with the newly derived temperature-dependent properties for the cast iron rotor. Contours of von Mises stress and equivalent plastic strain in tension and compression at the end of brake application are shown in Figure 5. Stresses are now much reduced compared with the elastic results due to yield and the consequent accumulation of plastic strain. Corresponding results at the end of the first cooling period show a residual stress distribution and permanent plastic

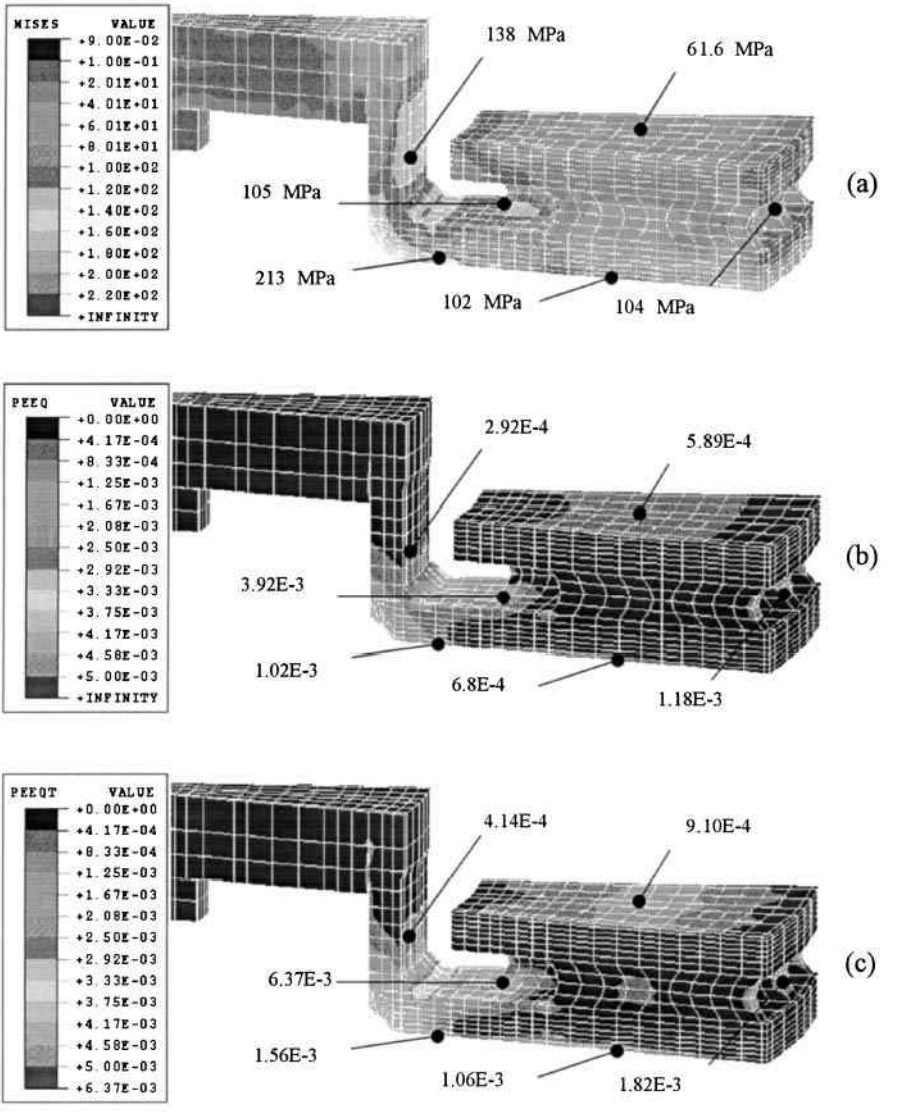

Figure 5: Results of inelastic finite element analysis at the end of first brake application for back-vented disc: (a) von Mises stress, (b) equivalent plastic strain in compression, (c) equivalent plastic strain in tension.

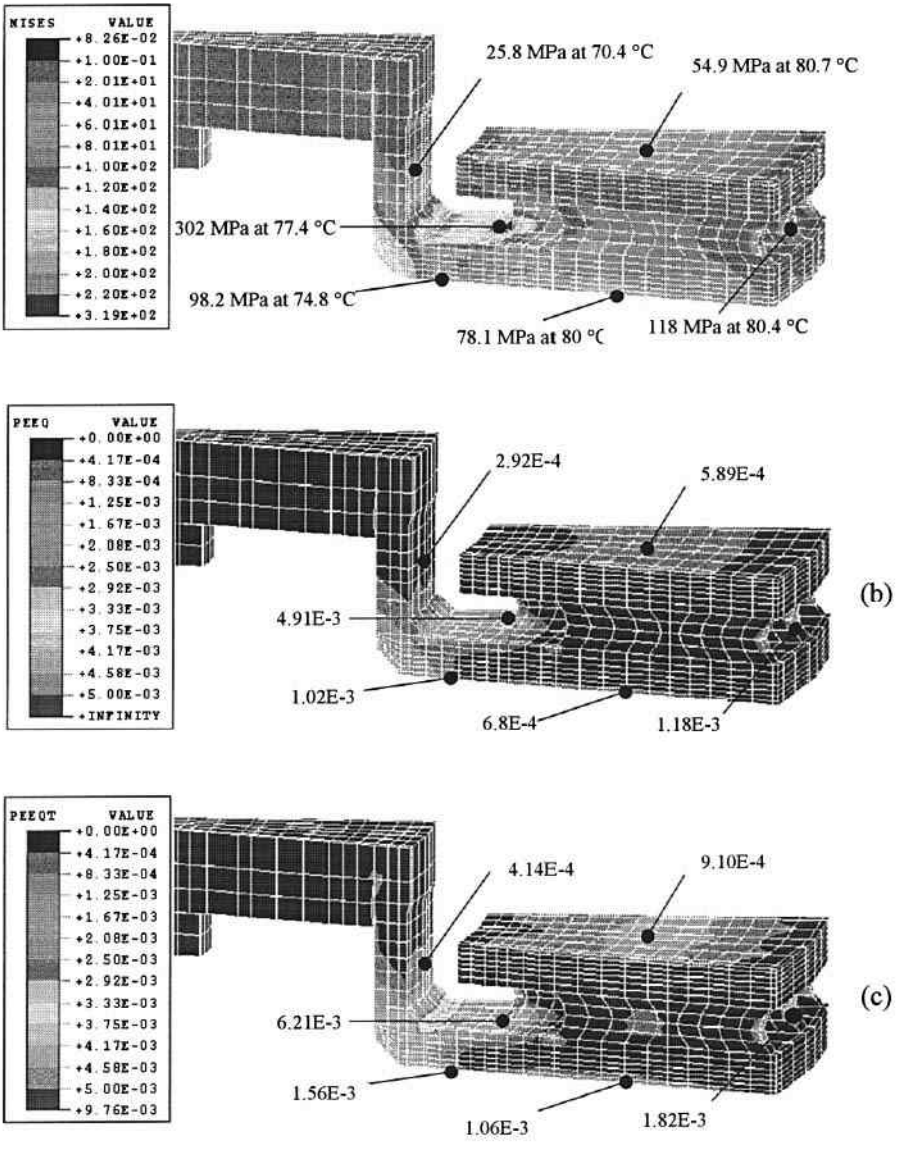

Figure 6: Results of inelastic finite element analysis at the end of first cooling period for back-vented disc: (a) von Mises stress, (b) equivalent plastic strain in compression, (c) equivalent plastic strain in tension.

straining of the rotor even though the temperature has now fallen to a uniform 80 °C, Figure 6. The effect of further braking cycles was to slowly increase this residual plastic strain. For example, the maximum tensile plastic strain (element centroid value) in the neck of the rotor was 2.29×10^{-3} at the end of the second cycle compared to 2.26×10^{-3} at the end of the first. Whether these relatively large (but localised) tensile strains would actually lead to rotor cracking depends on the low cycle fatigue properties of the cast iron which were not investigated as part of the present project.

As an interesting point of comparison the thermal and inelastic stress analyses were repeated for an equivalent front-vented disc design. In terms of the finite element model, this was achieved by simply axially translating the hub and top-hat sections and re-attaching the neck of the latter to the outboard check of the disc. Thermal boundary conditions were kept the same despite the fact that airflow through the rotor vanes might be affected by this change of geometry. Predicted temperatures were somewhat different for the front-vented design, with the inboard cheek now running slightly hotter. However, thermal deformations and stresses were affected much more due to the change in the thermal expansion bending moment acting about the neck of the disc. For example, the deformed shape for the front-vented design at the end of the first brake application indicates a much greater degree of "coning" compared with the corresponding back-vented results, Figure 7. Comparison of the von Mises stress and plastic strain contour plots for the front-vented design in Figure 8 with those for the back-vented rotor in Figure 5 reveals that maximum thermal stresses and strains are significantly lower for the former. It seems therefore that the back-vented design gives better dimensional stability (less "coning") but may be more prone to thermal cracking under extreme braking conditions due to the higher inelastic strains.

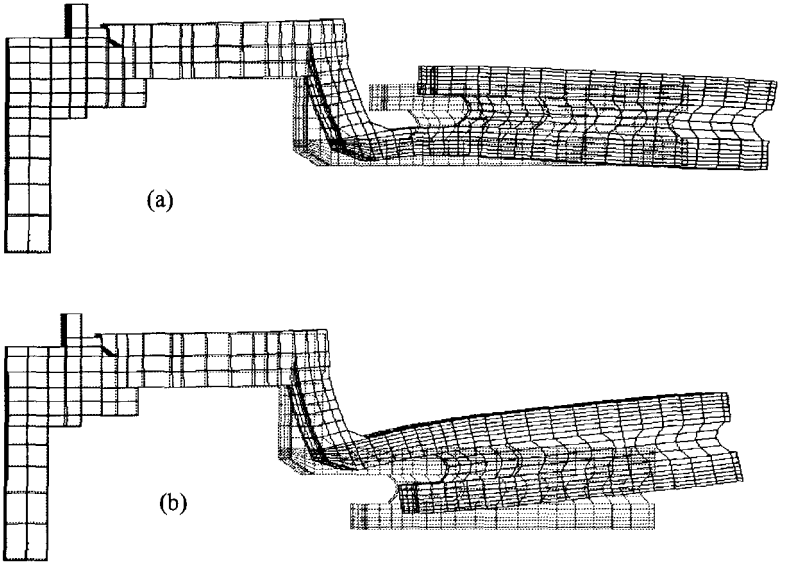

Figure 7: Deformed shapes at the end of first brake application: (a) back-vented disc brake, (b) front-vented disc brake

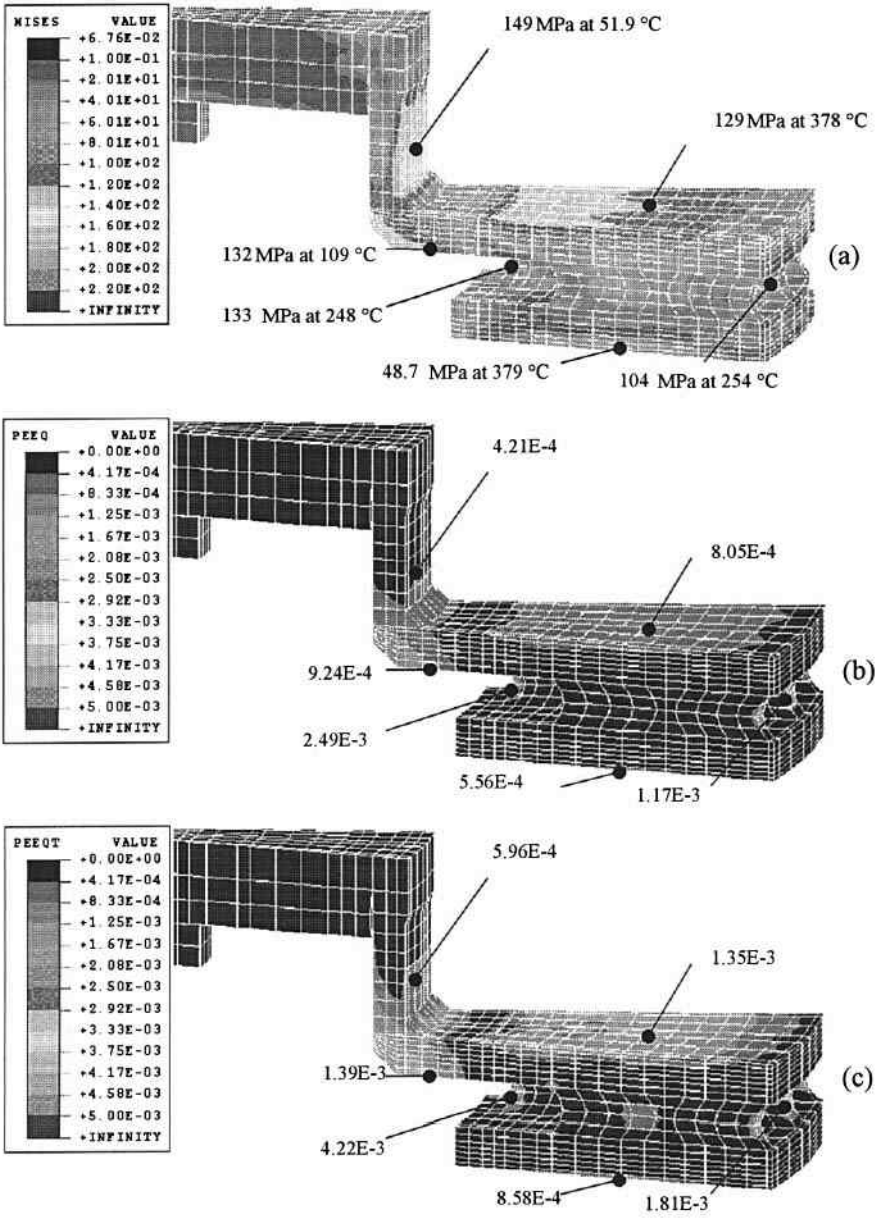

Figure 8: Results of inelastic finite element analysis at the end of first brake application for front-vented disc: (a) von Mises stress, (b) equivalent plastic strain in compression, (c) equivalent plastic strain in tension.

5. CONCLUSIONS

Cyclic plastic strain accumulation within a disc brake rotor can be estimated by means of thermo-structural inelastic finite element analysis. However, as well as being temperature dependent, the yield properties of cast iron are quite different in tension and compression. Based on new mechanical property test data derived from actual brake rotor castings, a material model that accurately allows for these effects has been derived and applied to the analysis of both back-vented and front-vented disc designs. The results can be used to indicate the relative propensity for thermally-induced cracking of each design.

6. ACKNOWLEDGEMENTS

The authors would like to acknowledge the assistance of Rover/BMW in providing relevant information and sample brake discs. The first named author is also grateful to the Thai Government for providing the scholarship which enabled him to complete this work as part of his PhD.

7. REFERENCES

[1] **Schwartz, H W, Harrter, L L, Rhee, S K and Byers, J E.** 'Evaluation of Gray Iron Brake Discs for Trucks by Thermal Modeling', SAE 751013, 1975.

[2] **Sheridan, D C, Kutchey, J A and Samie, F.** 'Approaches to the Thermal Modeling of Disc Brakes', SAE 880256, 1988.

[3] **Bailey, T P, Buckingham, J T and D'Cruz, A H.** 'Optimisation of Brake Disc Design Using Thermal Imaging and Finite Element Techniques', Autotech, 1991.

[4] **Fukano, A and Matsui, H.** 'Development of Disc-Brake Design Method Using Computer Simulation of Heat Phenomena', SAE 860634, 1986.

[5] **Medonos, S.** 'Study of Structural Behaviour of Ventilated Brake Disc', SAE 831316, 1983.

[6] **D'Cruz, A H.** 'Surface Crack Initiation in Ventilated Disc Brakes under Transient Thermal Loading', Paper C382/05, IMechE, 1989.

[7] **Grieve, D G, Barton, D C, Crolla, D A and Buckingham, J T.** 'Design of a Lightweight Automotive Brake Disc using Finite Element and Taguchi Techniques', Proc. Instn. Mech. Engrs, 212, Part D, 1998.

[8] **ABAQUS, Version 5.7**, Hibbitt, Karlsson & Sorensen, Inc., 1997

Investigation of CV rotor cracking test procedures

H ABENDROTH and **T STEFFEN**
Honeywell Bremsbelag GmbH, Glinde, Germany
W FALTER and **R HEIDT**
WABCO Perrot Bremsen GmbH, Mannheim, Germany

SYNOPSIS

Brake rotor cracking problems achieve increasing importance for heavy commercial vehicles. Existing test procedures are typically very time-consuming, predominantly empiric, and their results are subject to controversial discussions. Based on the analysis of established crack test procedures, field analysis has been started for both road-load data and crack failure patterns. Possible programme modules are investigated by FEA and experiments using new thermal methods of investigation.

A new method of crack testing was successfully demonstrated, allowing short term crack-prediction on dyno. The development of superior crack test procedures on the basis of field data and scientific tools appears indispensable. A first draft for a future crack test procedure is proposed, inviting the braking community to join on-going development efforts.

1 INTRODUCTION and PROBLEM DESCRIPTION

In the course of the development of brakes, rotors and friction material for heavy commercial vehicles, cracking problems are becoming increasingly important. The goal of dynamometer tests is the prediction of brake rotor crack occurrence and ultimately its avoidance in the field. Since there are no agreed representative road-load profiles available, existing dyno-test procedures are based on experience or (less desirably) best guess. Test results can be contradictory because of the test procedures not sufficiently reflecting reality in the field. Successfully destroying brake rotors on dyno in the shortest time possible can lead to misleading results. It is very common that a specific brake and rotor design successfully passes procedure A and fails procedure B, not mentioning the influence of different dyno's and their varying cooling conditions etc.
Other test procedures try to get closer to reality; however, for economic reasons they all must try to condense the time for rotor cracking. The challenge is to develop a common, broadly-accepted test procedure for rotor cracking, sufficient to predict lifetime of the disc. Failure mechanisms must be examined, allowing efficient optimisation of the system brake / rotor / friction material.

2 KEY POINTS OF INVESTIGATION

2.1 Analysis of existing rotor cracking test procedures

2.1.1 Bedding and interface conditioning

There are test procedures which start the main programme with green pads, some bedding instructions are rather vague, and some are very accurate, including friction monitoring. There is an apparent need to introduce normal brake applications among the sections designed to develop cracking, in order to maintain a more realistic rotor / pad friction-interface.

2.1.2 Cooling

Cooling also has a major influence on both the test duration and cracking itself. Test procedures reflect the well-known problems of defining cooling and exhaust conditions due to the layout of the dyno. The air volume coming out of the cooling duct needs to be defined, as well as the position of the parts to be tested. The same is true for the cooling speed between the brake applications.

2.1.3 Rotor temperature measurement

The rotor should never be weakened by drilling holes for thermocouples. Therefore predominantly rubbing thermocouples are used at present. The use of non-contact temperature measurement is critical due to changing outputs caused by material transfer from pad to rotor. The development of robust, non-contact temperature-measurement systems appears desirable (multi-target systems with different wave-lengths).

2.1.4 Main cracking test procedures

Todays cracking test procedures contain snubs, braking-to-rest, drag braking and a mixture of them.

2.1.4.1. Crack test procedures on the basis of braking-to-rest applications

Initial speeds vary from 60 to 90 km/h with typically high pressure and correspondingly high torque (deceleration). The number of required brake applications varies from 50 to 2000. The energy input typically is low; however, high brake performance mainly causes high loads at the rotor surface.

2.1.4.2 Crack procedures with snubs

Typical speeds are: 140 to 60 km/h, 130 to 80 km/h with up to 600 brake applications at decelerations between 2.5 and 3.5 m/s^2.

The energy input here is higher, however braking intensity is lower than above.

2.1.4.3 Drag-mode crack test procedures

We see up to 500 drag braking applications of 40 sec at speeds around 85 km/h with a deceleration of 1 m/s^2.

Energy input is very high due to the duration of the brake application, intensity rather low. That causes heating of the entire brake rotor.

2.1.4.4 Mixed test procedures

Such procedures contain brake applications for adjustment, heavy-duty snubs and braking-to-rest applications, combined with drag braking.

In order to come closer to reality, a mixed test procedure indeed makes sense, however the definition of modules, sequence and occurrence will need a considerably larger amount of information from road driving.

2.2 Analysis of data from the field

2.2.1 Investigation of representative road-load data relevant to cracking

Representative road-load cycles for performance, lifetime prediction, NVH and rotor cracking are perennial challenges of test departments.

In all respected vehicle test departments, basically similar questions arise. Problems concerning those road-load cycles are well-known. Discussions typically end up with the statement that more efforts of all people involved in brake system development appear highly desirable and not just those of an individual company. There is a specific deficiency of road-load data in the area of commercial vehicles.

Within the scope of the project the following strategies are envisaged:

- gather the statistically most common "normal" brake applications, which are expected to be between 0.5 and 1.5 m/s^2 deceleration.
- gather road-load data from customers who are known to have consistently major rotor crack problems; an additional selection criterion will be the specific crack pattern.

2.2.2 Analysis of rotor crack patterns

We typically find two different basic rotor crack patterns, which also can occur on one rotor: Radial cracks and grid-shaped cracks: see fig.1

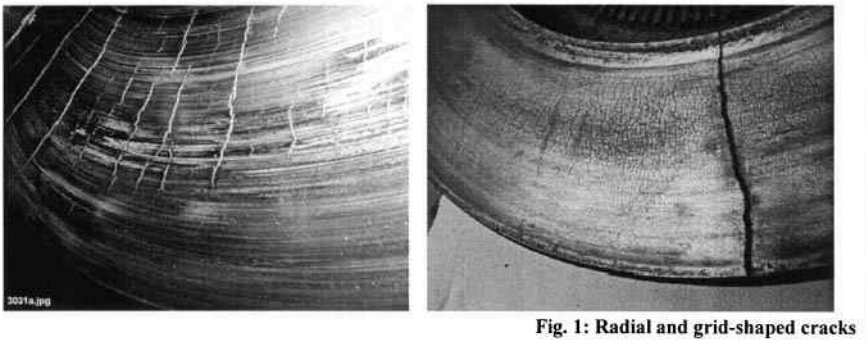

Fig. 1: Radial and grid-shaped cracks

The left picture shows cracks generated on dyno, the disc shown in the right picture comes from a vehicle.

Analysis of representative crack patterns in the field, their correlation to specific brake systems, related vehicles and their load profile has started. Again for this item, in order to get a broad database, the involvement of some more brake groups is necessary.

2.3 Theoretical investigation of the rotor cracking mechanism

2.3.1 Reasons for the appearance of rotor cracks

If analysis and improvement of cracking behaviour is required, the analysis of the reasons for cracking and its mechanism is required first. As is well-known, cracking is a result of alternating loads: if the limit of fatigue strength is reached, the first crack appears. So we have to concentrate on the relevant alternating loads in a brake system and on the fatigue strength of cast iron.

The load comes from different temperatures in the disc. These different temperatures lead to stresses in the disc caused by the restriction of expansion. The alternation of these loads comes from heating and cooling and from different temperature distributions from one brake application to the next. These temperature distributions might be very uneven (see fig. 2) and the hot and cold regions on the surface can change to the opposite from brake application to brake application.

Mechanical loads, such as pressure and friction force, do not have such an influence on cracking, because the tension in the disc caused by mechanical loads is less than the tension caused by uneven temperature distribution.

In addition to the tension in the disc, there is a loss of material strength of the disc at elevated

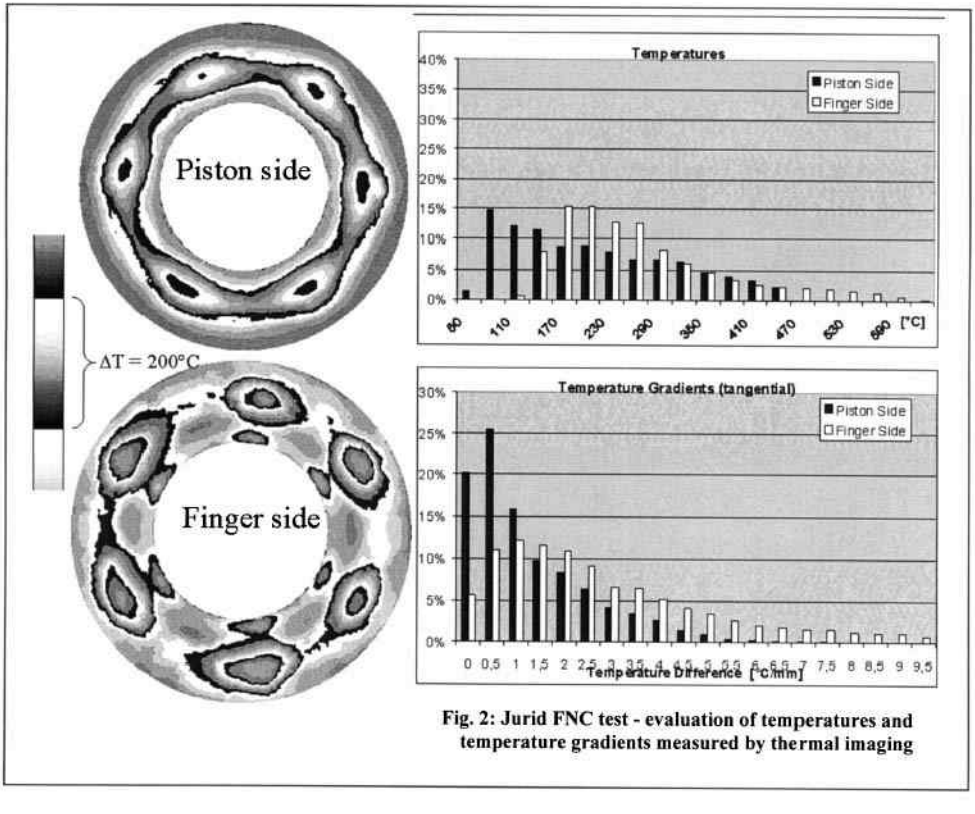

Fig. 2: Jurid FNC test - evaluation of temperatures and temperature gradients measured by thermal imaging

temperatures. The combination of these factors leads to cracks after a certain number of brake applications.

2.3.2 Variables for the analysis of crack test procedures

With this knowledge, the temperature levels, the temperature differences and the number of brake applications for a crack test procedure were analysed. One example for an evaluation of the Jurid FNC test (Fast Non-destructive Crack Test) is given in fig.2. This test was first published at the 17th Annual SAE Brake Colloquium 1999. It is known that the cracks that destroy the disc mainly are orientated radially and so must be caused by tension in tangential direction. That was why the temperatures and temperature differences per unit of length in the tangential direction for both sides of the disc were analysed. The main idea behind this new test was that it was not necessary to have cracks in the disc to evaluate the probability of cracking.

This example shows the temperatures and temperature gradients for the piston and finger side of the disc. The differences between each gray scale value of the thermal-imaging pictures of the disc are 40°C. One can see that the temperature levels (1st diagram) on both sides are nearly the same, but the temperature gradients (2nd diagram) show a higher average temperature gradient on the finger side than on the piston side. This result is repeatable with succeeding brake applications and correlates with the first appearance of cracks on the finger side.

2.3.3 Reasons for different crack behaviour

Besides the influence of material and geometry of the disc, there are influences of various other parameters:

The caliper: the higher crack probability on the finger side, for example, is influenced by an uneven pressure distribution in tangential direction which is caused by the geometry of the piston(s), of the finger side and of the whole caliper. (The influence can be demonstrated by FEA.)

The friction material: during cracking tests at constant torque, a pad material with a lower friction coefficient needs higher pressure. This leads to a more even pressure distribution on the disc, especially if the disc is slightly uneven. So the temperature distribution is more uniform too, and the tension is reduced. An example from FEA is shown in fig. 3. This is a simulation of two different pad materials with different friction levels. The development of the temperature during one revolution is nearly the same for both types if the disc is even. But if the disc is slightly uneven (1 µm), the temperature increase of the deformed region is higher when it comes into contact with a pad material with a higher friction level. The temperature distribution on the friction ring will be more uneven and the tension in the disc will be higher. So the crack probability is higher, too.

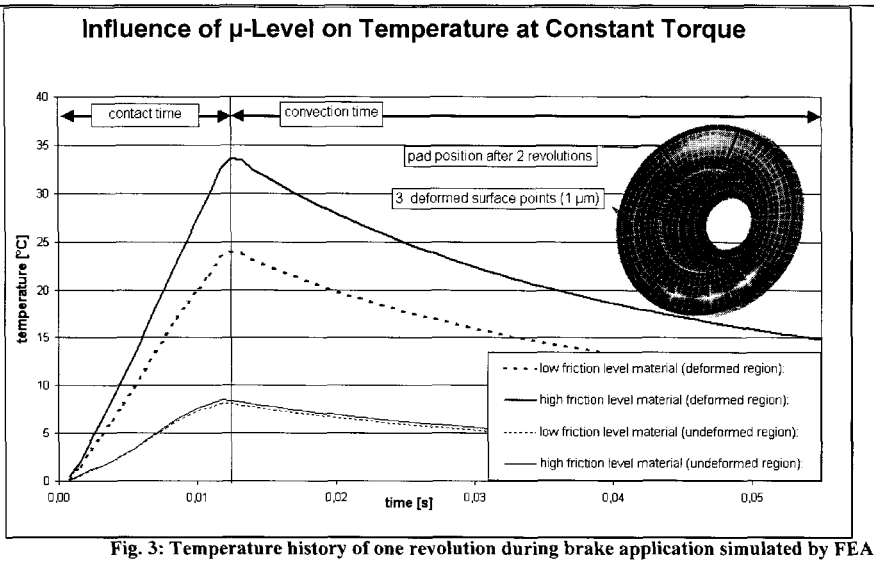

Fig. 3: Temperature history of one revolution during brake application simulated by FEA

Nearly the same relationship is valid if the temperature dependency of the material leads to lower friction levels at elevated temperatures. This also leads to a lower crack probability.

In our presentation to the 17th Annual SAE Brake Colloquium 1999, we showed that some other pad material properties also exert influence on crack behaviour.

2.4 Theoretical and experimental investigations of modules for a future crack test procedure

In a pre-study for a future draft cracking test procedure, some typical modules are being investigated theoretically and experimentally.

2.4.1 Braking modules to be investigated

Parameter	Bedding	Adjusting brake application	Heavy-duty brake application	Drag braking 1	Drag braking 2
Number of stops [-]	**50**	**2**	**2**	**5**	**5**
Initial velocity v_i [km/h]	**60**	**130**	**130**	**85**	**85**
Final velocity v_e [km/h]	**30**	**80**	**80**	**85**	**85**
Deceleration a [m/s^2]	**1,5**	**3**	**4,5**	**1**	**0,5**
Braking time t_{Br} [s]	**5,6**	**4,6**	**3,1**	**40**	**60**
Specific energy input [J/kg]	**104**	**405**	**405**	**944**	**708**
Specific power [W/kg]	**18,75**	**87,5**	**131,25**	**23,6**	**11,8**
Factor of intensity [-]	**1,8**	**2,16**	**3,24**	**0,25**	**0,17**
Initial temperature [°C]	**250**	**100**	**100**	**80**	**80**

The above-mentioned "factor of intensity" shows the relation of specific power to specific energy. Always considering the total value of the energy input, one can draw a conclusion in which way the disc is loaded. Obviously it is useful for instance to compare the drag mode brake applications to the other ones from 130 to 80 km/h.

Between the different kinds of brake applications to be investigated a module which prevents a "geometrical" bedding has to be inserted. The same type of brake applications as in the bedding module was chosen, but with a higher initial temperature of 300°C to increase the wear at 10 stops.

To evaluate the different kinds of brake applications the temperature and temperature gradient distribution by FEA were calculated and the FNC test evaluation for the temperature and temperature gradients in tangential direction was used. The combination of both leads to a three-dimensional stress distribution which causes the cracks.

2.4.2 Theoretical investigation of crack modules:
Calculation of temperature and stress development of modules

To combine the keynotes that are mentioned in 2.3 and 2.4.1, one must take a look at the calculated temperature distribution for different kinds of brake applications. There are

differences in both energy and power transfer into the disc. The result is a different temperature distribution during and at the end of the brake application for each kind of brake application. This leads to different stresses in the disc, which will cause the cracks.

A thermo-mechanical FEA model of the disc was built up, in order to calculate the temperature distribution in axial direction and the stresses and tensions in the disc at every moment of the brake application. The heat flow is calculated from the power transfer, the time from the expected braking time at constant deceleration. After that, the results for the different brake applications were evaluated with regard to crack probability.

To compare the different types of brake applications, high-power braking on the one hand and drag braking on the other, one must first focus on the temperature distribution of each kind of braking. Fig. 4 shows the temperature distribution of the heavy-duty brake application and of the drag brake application 1 after a braking time of nearly the same energy input. Because of the high power input of the heavy-duty brake application the temperatures on the friction surface are higher than of the drag brake application. The differences of the calculated temperatures between heavy-duty and adjusting as well as between drag braking 1 and 2 are negligible.

To evaluate the tension in the disc, the temperature gradients per unit of length in axial direction were calculated. The results are shown in fig. 5. The gradients of the same types of brake applications are nearly the same, but the gradients of the high-power-input brake applications are about 5 times higher than those of the drag brake applications.

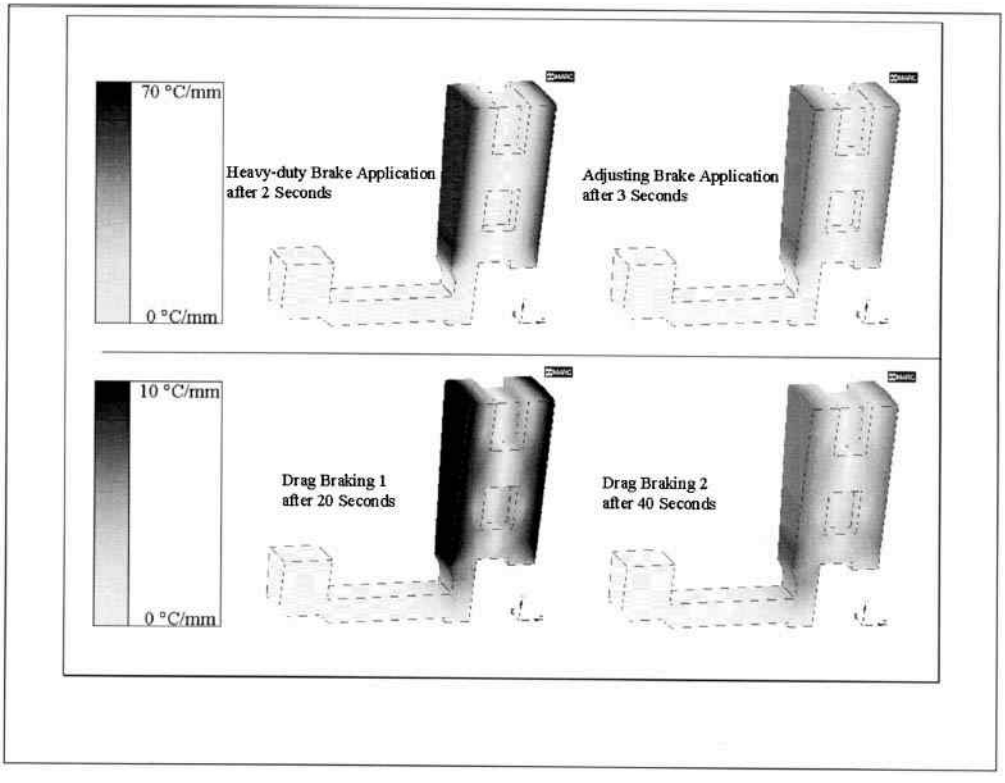

2.4.3 Experimental investigation of crack modules

The crack modules described were put together in a test procedure and ran on dyno. Dynamic temperature recording and evaluation were done as described in Section 3. The time for one complete cracking-cycle was two hours!

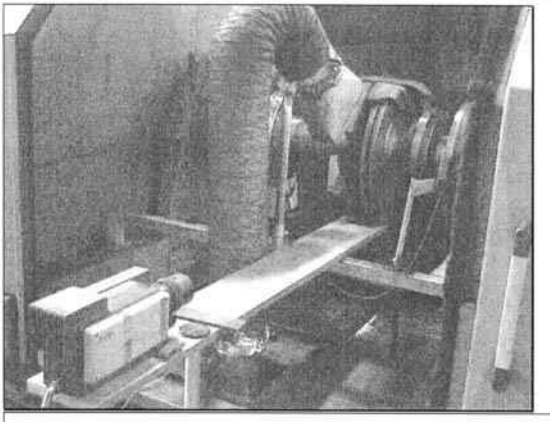

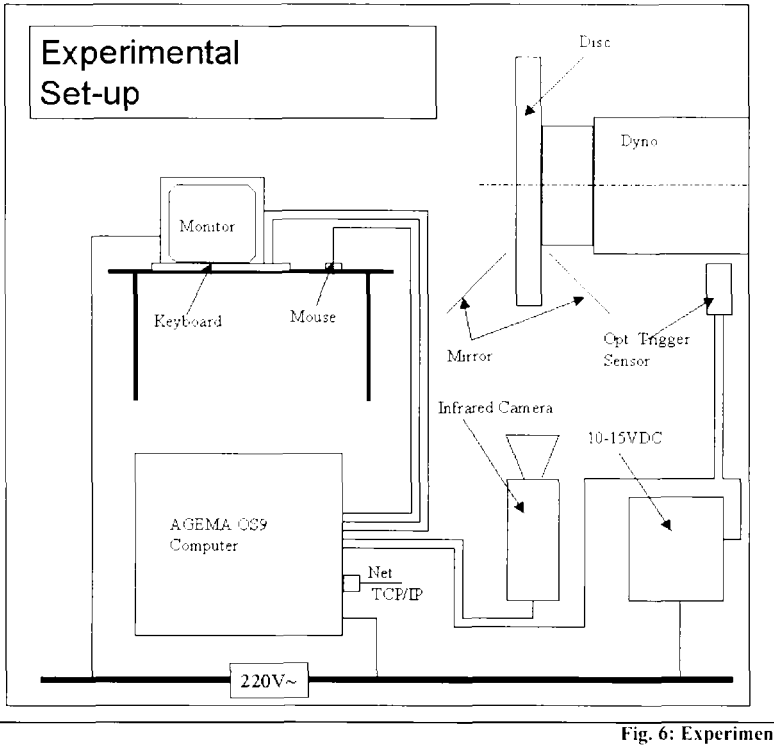

Fig. 6: Experimental Set-up

Two different friction materials were tested. The friction material "A" is known to be very "aggressive". Friction material "B" is the improved material with a lesser probability of inducing disc cracking. Fig. 6 shows the diagram "Crack Length vs. Stop Number" from this test.

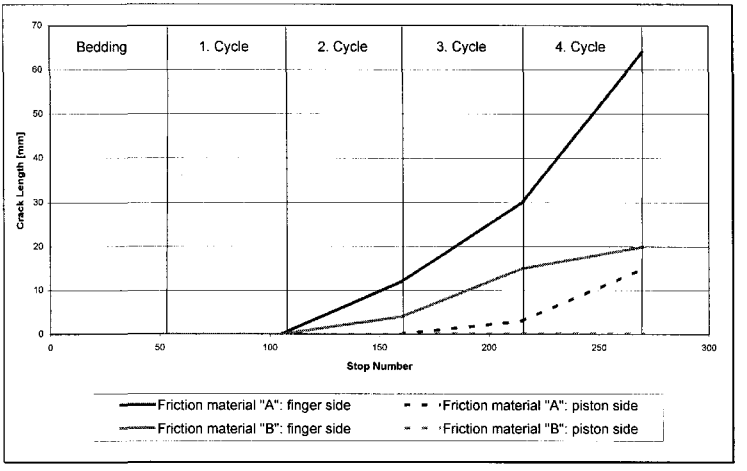

Fig. 7: Crack length development of different friction materials

This result correlates with the experience from the field and with former long-lasting crack tests.

All crack-relevant brake applications of the different types of brake applications were measured by thermal imaging. The starting times for measurement of the different brake application were:

heavy-duty braking:	2 seconds
adjusting braking:	3 seconds
drag braking 1:	20 seconds
drag braking 2:	40 seconds

The following table gives the summary of the FNC test evaluation of this investigation.

Results from Jurid FNC test				
	friction material "A"		friction material "B"	
	average temp. gradient: piston side [°C/mm]	average temp. gradient: finger side [°C/mm]	average temp. gradient: piston side [°C/mm]	average temp. gradient: finger side [°C/mm]
heavy-duty braking	2,07	2,45	2,50	1,97
adjusting braking	1,89	2,70	2,85	1,89
drag braking 1	1,82	3,18	1,23	1,67
drag braking 2	1,71	2,67	1,41	1,66

The average temperature gradient for each kind of brake application gives evidence of the thermal stresses in tangential direction and, in combination with the temperature gradient in axial direction, of the three-dimensional stress distribution which leads to cracking. Comparing the results of the different friction materials and different types of braking, it has to be accentuated that the highest average temperature gradient is the one of friction material "A" on the finger side. This correlates with the results from the crack test (see fig. 7).
The average temperature gradient seems to be a very good value for the evaluation of crack probability especially for the drag brake application. A representative overview of the different friction materials and the different types of brake applications is given in figs. 8 and 9.

In 2.4.2. of this presentation it is demonstrated, that the calculated temperature distribution in the disc is more even for the drag brake applications than for the high energy brake applications. The temperature distribution on the disc surface is quite different from this. In fig. 8 there are two representative examples for different temperature distribution for drag braking (right picture) and for high-power brake application (left picture).

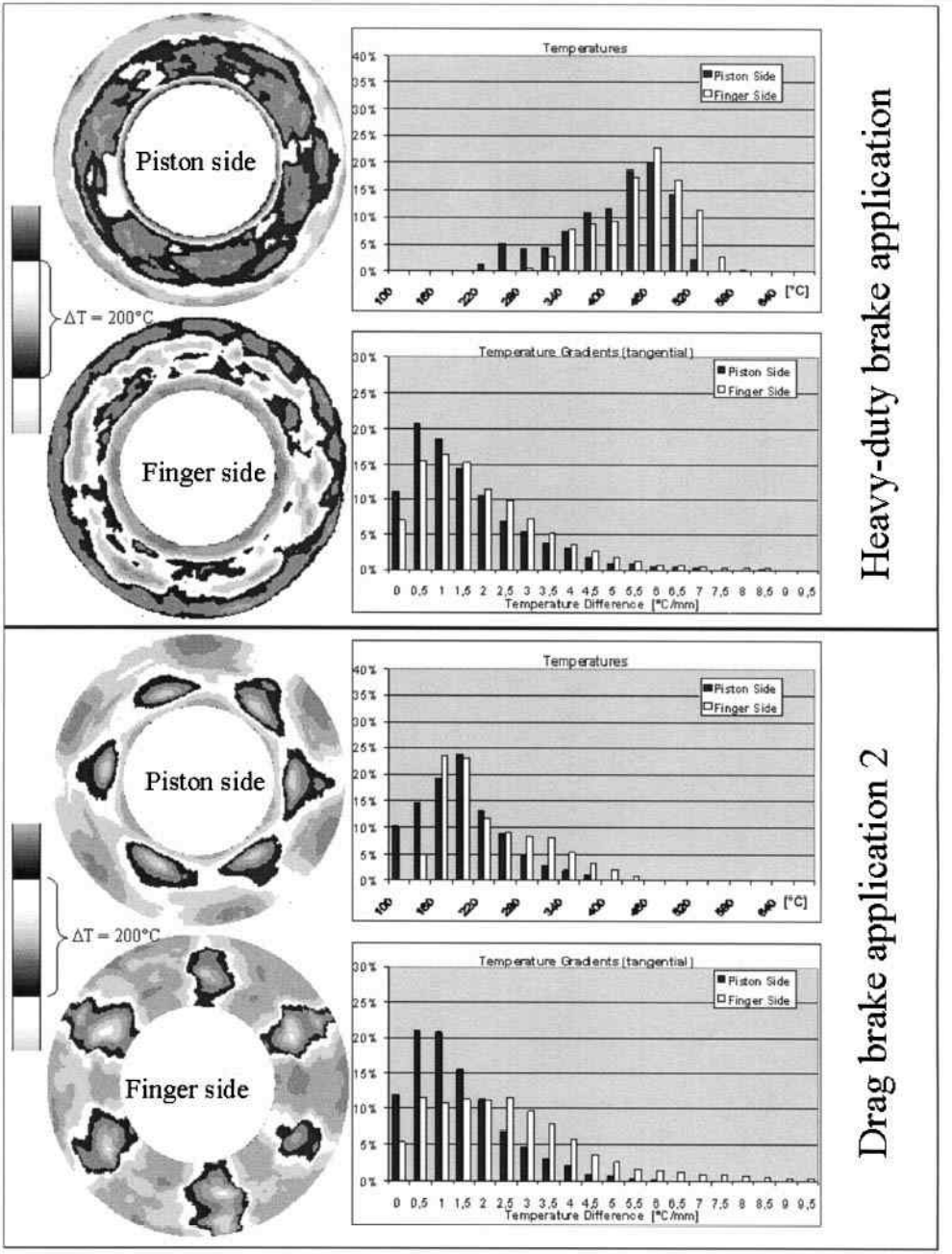

Fig 8: Comparison of different brake applications friction material "A"

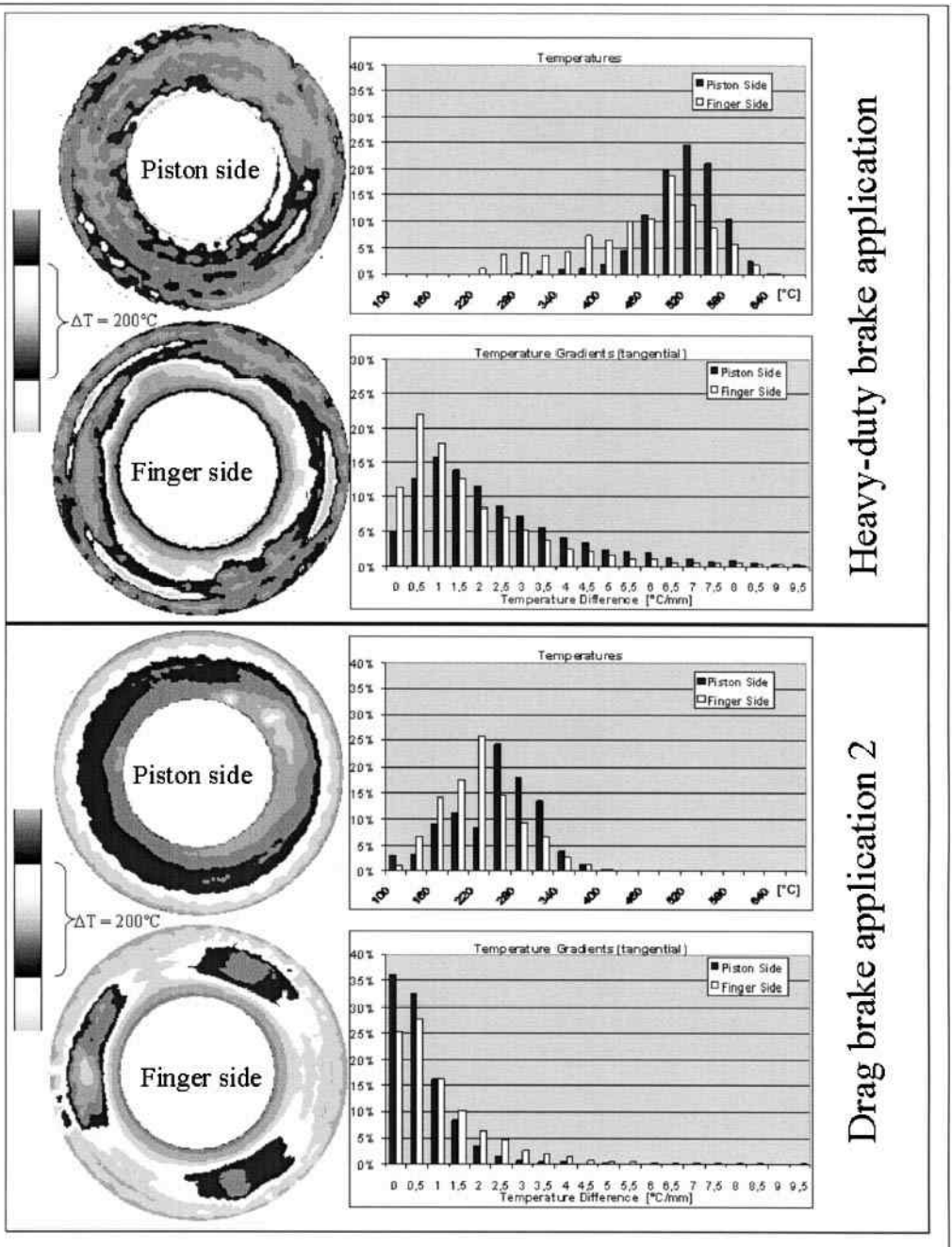

Fig 9: Comparison of different brake applications friction material "B"

3 CONCLUSIONS / SUMMARY

The recommended approach to develop rotor cracking test procedures includes
- collection and analytic evaluation of field data
- FE calculations
- methods of dynamic thermal rotor investigations

The proposed alternating structure of the test procedure shows numerous positive effects:
- the crack pattern generated on dyno resembles the one known from the vehicle
- occurence of obvious differences in lifetime of the disc when testing different types of friction material
- huge profits in testing time (all the tests ran less than 10 hours!)
- applying a suitable relationship of drag-mode and high-power brake applications amongst friction interface conditioning realistic road-loads are reflected

Drag-mode and high-power brake applications expose the brake rotor to different loads: The alternation of high temperature gradients in axial and tangential directions leads to alternating stresses which weaken the material. This is the reason why cracks appear so quickly.

The characteristics of the friction material exerts a large influence on crack probability. The effects can be visualised e.g. by FNC test evaluation.

Correlation was established between FE calculation and practical tests. Accordingly computer-aided optimisation of rotor cracking test procedures is possible.

The basic idea of predicting crack probability without having to wait for actual crack occurrence on the rotor is realised. Dynamic thermal measurement also allows fast differentiation of several friction materials.

4 OUTLOOK

In order to complete necessary investigations for a new, common rotor cracking test procedure, gathering of a large amount of field data will be necessary.

Validation of the new crack test procedure has to be done on dyno with different brake systems, passing through several optimisation cycles. Results must be compared with test results from the field.
The question to be answered is whether it is necessary to run the test procedure in the classic way until failure of the brake rotor, or whether short tests according to the Jurid FNC method are a more economical approach.

Because of the volume of related work to do and the intention to create a broadly-accepted standard, the involvement of as many brake test groups as possible appears desirable. Models for organisation and co-ordination need to be discussed.

Some other aspects to be considered are combined test procedures on the basis of road load simulations, also looking at wear, friction, NVH and rotor cracking, as under discussion in the passenger car brake area.

Initial dynamometer and laboratory evaluations of thermally sprayed aluminium brake discs

R HECHT BASCH, J FASH, R HASSON, T DALKA, and **R McCUNE**
Ford Research Laboratory, Ford Motor Company, Dearborn, Michigan, USA
R KAUFOLD
Alcoa Technical Center, Pittsburgh, Pennsylvania, USA

ABSTRACT

A compact inertia brake dynamometer was used to evaluate the performance of a new lightweight brake disc. These lightweight discs are fabricated by first sand casting a standard aluminum alloy and rough machining. A durable, mixed metal/metal-oxide coating is then applied to the disc rubbing faces using a two-wire arc thermal spray process. Lastly, the part is finished turned. These thermally-sprayed aluminum discs, described in US Patent 5,884,388, may offer a low cost solution to reducing the weight of brake components.

For this study, prototype ventilated rear discs were manufactured to the same geometry as a current model rear brake. Dynamometer tests of the thermally-sprayed aluminum brake discs and baseline gray cast iron discs were carried out at an inertia value of 25 kgm^2. The same friction material, a commercially available low metallic, was used to test both types of discs. Test procedures performed included a friction stability assessment, a thermal capacity simulation, and a simulation of the Auto Motor und Sport (AMS) magazine stopping distance test. The thermally-sprayed aluminum discs and the gray cast iron baseline discs exhibited similar behavior in the friction assessment, with the only major trend variation observed being that as hydraulic line pressure increased, friction increased with the thermally-sprayed aluminum discs but decreased with the gray iron ones. The thermal capacity fade test showed that the two types of rotors exhibited similar in-stop temperature rise, and the thermally-sprayed aluminum discs stayed slightly cooler. The maximum temperature achieved at the end of the 10^{th} stop was 455 °C for the coated aluminum and 475 °C for the gray cast iron. These initial dynamometer test results are encouraging, especially considering that the friction material used was designed for gray cast iron. Laboratory corrosion testing in humidity chambers was also performed. The results show that thermally-sprayed aluminum brake discs may offer a lightweight alternative to currently available disc and drum materials.

1. INTRODUCTION

Reducing vehicle weight without compromising performance is a primary objective of many automotive manufacturers in order to improve fuel economy and reduce vehicle emissions. The possibility of reducing the un-sprung rotating mass in a vehicle has led to many investigations of aluminum metal matrix composites (Al MMC's), carbon-carbon and lightweight ceramic composites for brake disc applications. These types of materials also offer the potential of lower brake operating temperatures, and are currently being used successfully in limited applications in racing and for the car enthusiast market. The primary reason why advanced lightweight materials are not more widely used in high volume passenger vehicle applications is their prohibitively high cost. Lightweight materials also typically require specially formulated friction materials that may differ from linings available for commercial passenger cars, adding more cost and time to brake system development.

The high cost of complex lightweight materials, such as Al MMC's, is due to the raw material cost being significantly higher than traditionally used gray cast iron, and more importantly, the high cost of manufacturing the components. For example, machining ceramic particulate reinforced metal composites is very difficult; hence efforts are made to produce near net-shape parts. Preform and infiltration steps to produce ceramic-ceramic composites take hours longer than traditional manufacturing processes, adding cost. In order to address the high cost of manufacturing advanced materials, several investigations had been made into using these low cost manufacturing technologies to produce lightweight discs: sand casting and thermal spraying. For example, in US Patent 5,407,035, a lightweight disc with a durable, wear-resistant coating applied to the surface, is fabricated by sand casting an aluminum or magnesium disc and then using electric arc spraying to apply and create an iron-based graphite composite coating.(1) For racing applications, thermal spray technology has been used to apply ceramic coatings to Al MMC discs to achieve higher friction.(2) In the work discussed in this paper, the goal was to develop a brake disc that would yield the same weight reduction as Al MMC's with a significantly lower cost penalty compared to gray cast iron. In order to further save cost, ideally the disc rubbing surface would be compatible with existing passenger car friction materials, such that new friction formulations would not have to be developed and complexity in the passenger car aftermarket would be avoided.

For this paper, we performed a series of brake dynamometer tests to assess the friction and thermal stability of an aluminum-based lightweight disc. These thermal spray-coated aluminum discs, described in US Patent 5,884,388, may offer a low cost solution to reducing the weight of brake components.(3) Alcoa fabricated the prototype discs evaluated here by first sand casting the component from a standard aluminum alloy (A319) and then rough machining. Next, a modified saw tooth pattern was machined by turning onto the disc rubbing faces of the cast disc. The saw tooth pattern is designed such as to create mechanical locking with the applied thermal-spray coating. A durable, composite metal/metal-oxide coating is then applied to the disc rubbing faces using two-wire arc thermal spray. Lastly, the parts are finished turned.

The ideal situation is to develop a coating that is both compatible with existing friction materials, and meets all brake system performance requirements. In order to be effective, a disc rubbing face coating must have good wear resistance, good high-temperature stability and

thermal conductivity, good adhesion to the underlying disc, and good machinability. The coating must also have a solution potential similar to that of the underlying material in order to prevent galvanic corrosion at the interface. Finally, the coating must possess a coefficient of thermal expansion similar to the disc material to prevent delamination during rapid temperature changes induced during extreme braking. For this investigation, a coating produced by two-wire arc spraying, one wire of commercially-pure 1100 aluminum and one wire of 305 stainless steel, was applied to the discs. The thermal spray process produces a coating consisting of mixed metal alloy particles and their respective metal oxides from the feedstock wires. At this time, this particular coating is believed to address the principal issues of friction performance and corrosion resistance.

2. TESTING DETAILS

For this study, prototype ventilated rear discs were manufactured to the same geometry as a current model vehicle rear brake. The same rear lining material was used for testing both the gray iron current production discs and the thermally-sprayed aluminum (TSAl) discs; this commercially available lining is a typical low metallic content rear lining. The vehicle and brake system characteristics are listed in Table 1. Dynamometer tests of the thermally-sprayed aluminum brake discs and baseline gray cast iron discs were carried out on a Link single-sided, compact inertia brake dynamometer with servo-hydraulic control, capacitance displacement probes, and slip-ring thermocouples mounted in the inboard and outboard disc plates. The proper inertia value to simulate the energy input to the rear discs in this particular vehicle was determined by analysis of previously generated vehicle test data. From temperature data recorded during a thermal capacity vehicle test, the rear disc temperature rise was compared to that seen on the dynamometer simulation of the same test on a baseline gray cast iron disc. An iterative process was used to establish the most representative inertia value that yielded disc temperature correlation between vehicle and dynamometer. A 25 kgm^2 inertia value was used for all subsequent dynamometer testing.

Table 1 – Vehicle and brake component geometries

Vehicle/Brake Attribute		
Total vehicle weight	3743	kg
Rear weight	1546	kg
Rear disc outer diameter	256	mm
Rear disc inner diameter	180	mm
Rear disc thickness	18	mm
Swept area	1041	cm^2
Lining contact area	127	cm^2
Caliper piston diameter	43.5	mm

3. DYNAMOMETER TEST RESULTS

A dynamometer simulation of a vehicle brake thermal capacity test was performed on baseline gray cast iron discs and subsequently on the TSAl discs. This test consists of 15 stops from 96.6 kph (60 mph) at 0.4 g, with 25 seconds in between stops. Tests were run with and without dynamometer cooling air on. The thermal capacity fade tests showed that the two types of rotors exhibited a similar in-stop temperature rise of about 50 °C with and without cooling air. When the dynamometer cooling air was turned off, both types of rotors exhibited a maximum temperature around 200 – 210 °C for stops #8-15. However, with the dynamometer cooling air turned off, both discs had a substantially higher maximum temperature at the end of each stop, but the TSAl discs stayed cooler. For example, at the end of the 15th stop, the cast iron baseline disc was 337 °C, while the TSAl disc was only 297 °C. The inboard plate temperatures for these dynamometer tests are shown in Figure 1.

Since the TSAl discs performed so well on this fade test, it was decided to subject them to a more stringent thermal performance evaluation, an AMS test simulation. The AMS vehicle test consists of 10 stops from 60 mph at 0.9 g performed consecutively, i.e. as soon as the vehicle achieves 60 mph again, the next stop is initiated. For our dynamometer simulation with this particular vehicle, an 8 second interval between stops was used. The disc temperature results from this very extreme test are shown in Figure 2. As seen in Fig. 2, the maximum temperature achieved at the end of the 10th stop was 455 °C for the coated aluminum and 475 °C for the gray cast iron rotor. We observed at the end of these tests (during the last 2 stops) that the TSAl disc coating began to glow red with heat. The coating did not, however, delaminate from the underlying disc. Scoring was observed on the rubbing faces of both types of discs, but on the TSAl disc there was an unusual banding pattern. It appears that some of the coating material from the disc rubbing face transferred onto the lining during this AMS simulation.

It should be noted that a dynamometer simulation of the AMS vehicle test likely results in a higher energy loading of the rear disc than an actual vehicle test would. For example, there is no form of brake distribution on a brake dynamometer; the dynamometer is programmed to stop with a certain deceleration rate and for a constant inertia. A vehicle also experiences a weight shift during stopping which would further load the front brakes and ease up on the rears; again, this does not happen on a dynamometer. For these reasons, we feel that the AMS dynamometer simulation conducted here was an aggressive test, addressing a worst-case scenario.

Following these high energy input tests, such as the thermal capacity and AMS dynamometer simulations described above, cooling curve data was collected to compare the gray cast iron and TSAl discs' cooling performance. Cooling performance can be characterized by heating the disc to a high temperature and then measuring the temperature as a function of time during cooling. The temperature decreases exponentially and the experimental data can be fit with the following equation,

$$T(t) - T_{amb} = (T_o - T_{amb}) \times e^{bt} \qquad (1)$$

where: T_{amb} = ambient temperature, T_o = maximum temperature, T(t) = temperature at time t, and b = the cooling coefficient. This cooling coefficient, b, incorporates both the effect of rotor thermal mass and the effect of convective cooling. Typical values of b range from –0.002 (poor) to –0.005 (good).

The cooling coefficients measured for the gray cast iron and the TSAl discs were virtually the same. Data was collected from both the inboard and outboard plates as the discs cooled from 400 °C to 40 °C, and this data was fit to Eqn. (1) using a 15-point moving averaging technique. The values of b for both types of discs were approximately –0.0003, an initially surprising result. Measured values are included here in Table 2.

Table 2. Calculated cooling coefficients

	Cooling coefficient, b
Gray cast iron, OB plate	-0.00284
Gray cast iron, IB plate	-0.00301
Thermally-sprayed Al disc, OB plate	-0.00281
Thermally-sprayed Al disc, IB plate	-0.00300

Since the mass of the TSAl disc is half that of the gray cast iron disc (1.9 kg vs. 4.0 kg), the thermal mass or thermal capacity of the TSAl discs is less than that of the gray iron ones. For the same change in temperature, the gray iron discs have more stored thermal energy to dissipate. It appears that improved convective cooling for the gray cast iron discs plays a significant role in the cooling behavior of this disc design.

A Ford Motor Company proprietary friction assessment test procedure was used to evaluation the friction performance of the TSAl discs paired with the current production, rear disc, low metallic friction material. This test procedure consists of approximately 100 burnish stops and 100 stops to assess pressure, temperature and speed sensitivity, as well as fade performance and recovery. Burnish stops are performed from an initial brake temperature (IBT) of 80 °C at 0.25 and 0.15 g deceleration. The temperature sensitivity stops, initiated at a range of IBTs from 50 to 300 °C, are performed from 100 kph to 0 kph at 0.4 g. The series of pressure sensitivity stops from 80 kph are performed at pressures from 10 to 100 bar. The fade test section consists of 15 stops from 100 to 0 kph at 0.4 g, with a 60 second cooling interval between stops. For each stop, the initial temperature, average pressure, average torque and average friction are plotted together.

The friction assessment dynamometer test was performed on two baseline gray cast iron discs and two TSAl discs; new hardware was used for each test. Data from three test sections are shown in Fig. 3. The left hand vertical axis is friction coefficient, and the right hand axis is pressure and disc temperature. The graph includes the average friction coefficient, average hydraulic pressure and the initial brake temperature. Results from both test runs are plotted together. It was observed that the duplicate runs for the gray cast iron exhibited consistent frictional performance throughout all sections of the test, except the green performance and bedding stops. The TSAl results also exhibited consistency between duplicate test runs, as shown in Fig. 4. However, some difference was observed in the average friction per stop

recorded during the fade stops for the TS Al tests, as seen in Fig. 5. One test had friction coefficients of approximately 10% less than the other test in the fade section.

Example friction data for both the TSAl and the baseline disc are plotted together in Fig. 6, providing the most noteworthy result of this testing. The TSA1 discs and the gray cast iron discs exhibited similar behavior in the friction assessment, both in the trend and the magnitude of the average friction coefficient. The only variation in friction trend observed between the two disc types occurred later in the test procedure during additional pressure control stops; as hydraulic line pressure increased, friction increased with the thermally sprayed aluminum discs but decreased with the gray iron ones. Overall, the frictional performance of the TSAl discs was remarkably similar to that observed for gray cast iron. This performance suggests that friction materials developed for gray cast iron discs may possibly be compatible with the rubbing face coating on the TSAl discs. This easy material substitution offers the opportunity for reduced development cost and time for the lightweight discs.

4. MATERIAL PROPERTIES

In order to facilitate future modeling of the new TSAl lightweight brake, we measured several material properties important for understanding the thermal-mechanical response of a brake disc to energy input. The properties, listed in Table 3, are measured heat capacity, thermal diffusivity, and density; thermal conductivity was calculated from these measured quantities. Also included in Table 3 are handbook values for the coefficient of thermal expansion, and the component weight.

Table 3 – Material property comparison

Properties	**[units]**	**Gray Cast Iron**	**Aluminum 3XX Alloy**	**Thermally Sprayed Coating**
Heat capacity, 100 °C	[J/g °C]	0.5	0.92	0.616
Density	[g/cm^3]	7.1	2.8	5.02
Thermal diffusivity, ambient	[cm^2/s]	0.172	0.75	0.058
At 100 °C		0.145	0.85	0.063
Thermal conductivity, 100 °C	[W/m °C]	51.5	219.0	19.4
Thermal expansion	[1/°C x 10^{-6}]	12	24	
Disc weight	[kg]	4.0	1.9	

Improved corrosion resistance compared to gray cast iron is an advantage typically cited for new, advanced non-ferrous-based materials proposed for brake components. As a preliminary assessment of the TSAl disc and coating corrosion resistance, several traditional humidity chamber and salt bath corrosion test procedures were performed on TSAl discs mounted to the production hub, and with friction pads lightly clamped onto the disc faces. These preliminary tests of the composite-coated disc using a salt-fog cabinet and accelerated proving ground simulation schedule did not result in any delamination or apparent loss of bond strength of the thermally-sprayed coating, nor did such tests lead to accelerated corrosion of the coating region in comparison to that observed visually on the base aluminum of the disc. Corrosion, in terms of measurable surface product, was, however, accentuated for an artificial crevice region created by securing the pad materials to opposing surfaces of the disc. Such crevice effects were not observed on a cast iron disc included in the test sequence for comparison. Further corrosion testing will be aimed at alternative brake pad materials, although the materials chosen for this study represented the baseline pad materials currently in use in the comparable gray-iron based disc brake system.

Early benchtop thermal studies of the composite coating material conducted in association with thermal property measurements suggest that an upper temperature limit may be encountered due to the onset of solid-state reactions between the constituent metals of the coating. The dynamometer tests reported in this work stayed below this upper thermal limit estimated to be in the 500-600°C range. Such aluminothermic, solid-state reactions have been observed in other material systems and may ultimately limit or degrade mechanical properties if such reactions are allowed to proceed.

5. SUMMARY

The initial dynamometer test results are encouraging, especially considering that the friction material used was designed for gray cast iron, and no component re-design was performed. It was observed that the TSAl discs performed reasonably well on dynamometer simulations of the AMS test; the maximum temperature achieved during this simulation remained below the recommended operating temperature for these aluminum-based discs, as well as below the final temperature of the gray cast iron discs. A friction assessment showed remarkably similar trends between the TSAl and the baseline discs. Corrosion tests revealed a possible adverse reaction between the mixed metal-metal oxide coating and the low metallic linings. However, it was demonstrated that a lightweight alternative to gray cast iron discs can be manufactured by low cost technologies, and it may be possible to create wear surface that is compatible with existing lining formulations, a potential reduction in development cost and time.

There are several questions that need to be addressed during future research and development of these thermally-sprayed aluminum discs. It is still yet to be determined if the long term durability and thermal-mechanical performance of TSAl discs are sufficient for passenger car applications. The performance of the thermally-sprayed Al discs during long term high energy input tests, such as a mountain drag simulation, needs to be evaluated. It also appears that additional investigation into the corrosion resistance and potential material interactions is necessary.

REFERENCES

[1] G. Cole, et al, Composite Disc Brake Rotor and Method of Making, US Patent Number 5,407,035, April 18, 1995.
[2] K. Harrison and M. Dorfman, "Thermally Sprayed Coatings for Lightweight Brake Rotors," SAE Technical Paper Series, SAE 1999-01-0139, 1999, pp. 1-8.
[3] E. Patrick, et al, Method for Manufacturing a Friction-Wear Aluminum Part, US Patent Number 5,884,388, March 23, 1999.

FIGURES

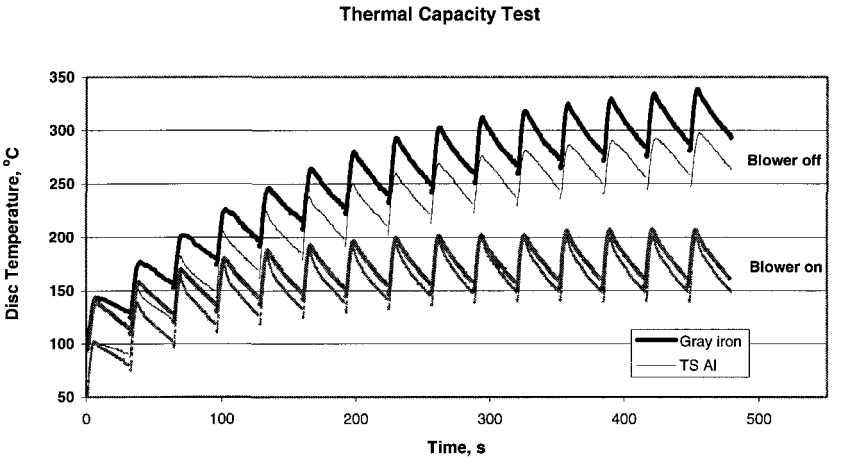

Fig. 1. Inboard disc plate temperatures measured during 15 stop thermal capacity brake dynamometer tests. In-stop temperature rise is similar for both gray cast iron (baseline) production discs and TS Al discs. Disc temperature is influenced by the use of dynamometer cooling air.

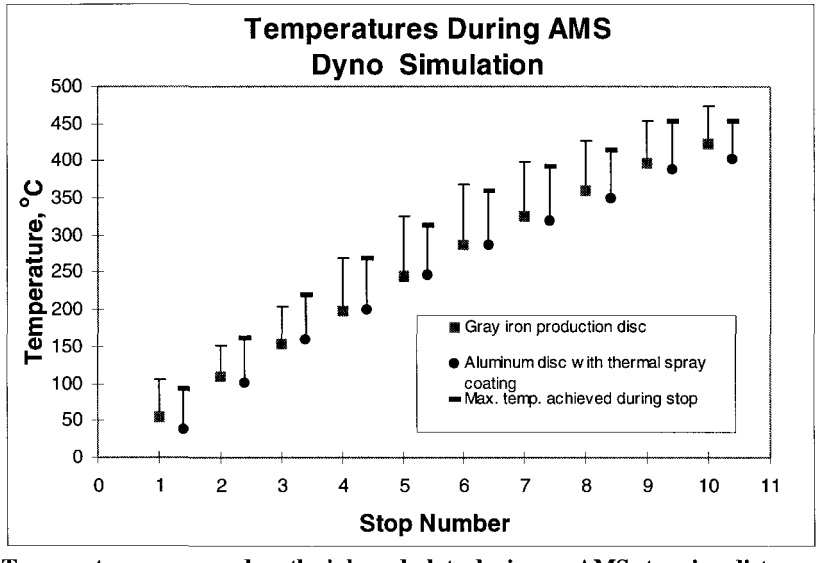

Fig. 2. Temperatures measured on the inboard plate during an AMS stopping distance test simulation; initial and final brake temperatures for each stop are shown.

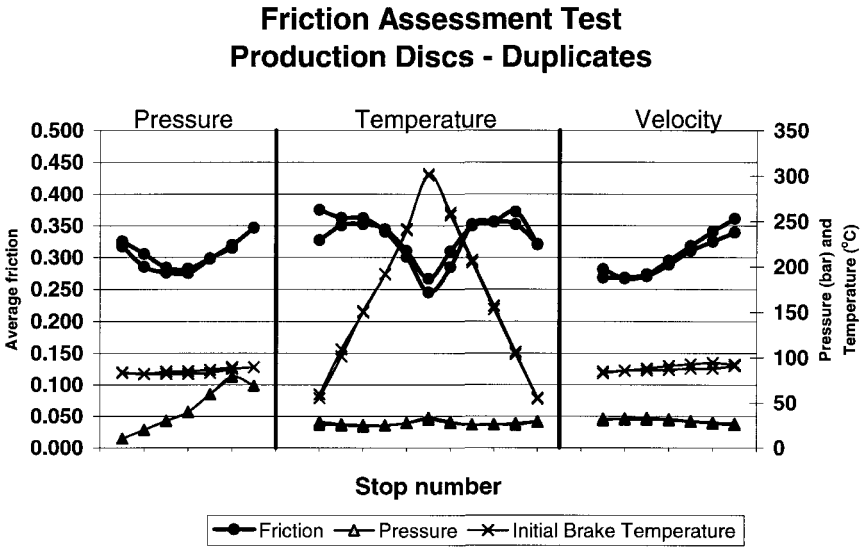

Fig. 3. Friction assessment results from three test sections. Average values of the friction coefficient, hydraulic pressure and initial brake temperature are plotted for each stop. Data from two duplicate test runs of production discs are shown together here.

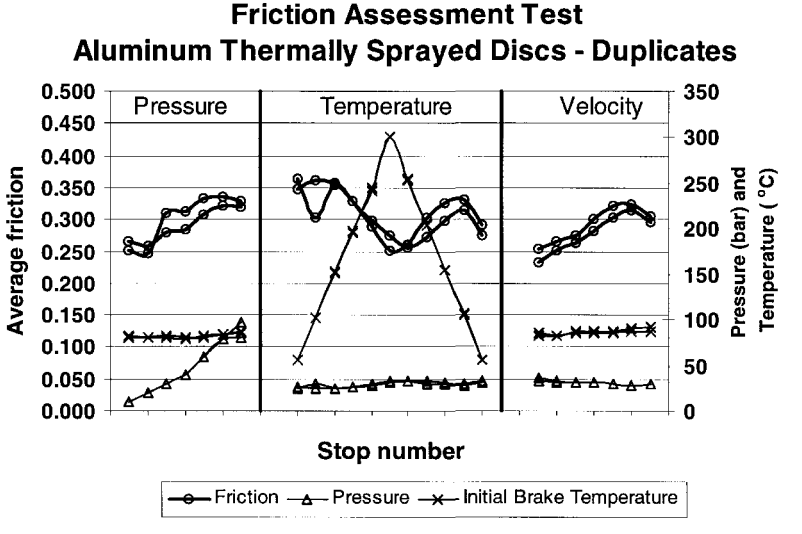

Fig. 4. Example of friction assessment test data for two duplicate TS Al discs.

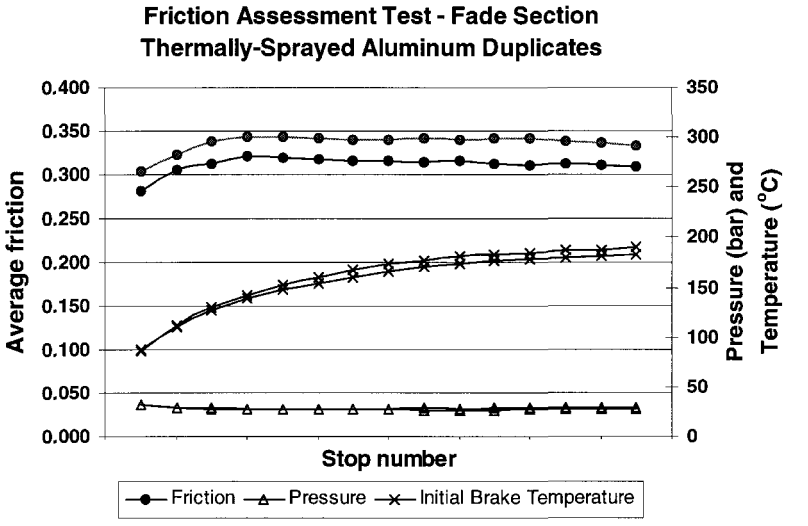

Fig. 5. Average friction coefficients vary by approximately 10% between duplicate tests of TS Al discs.

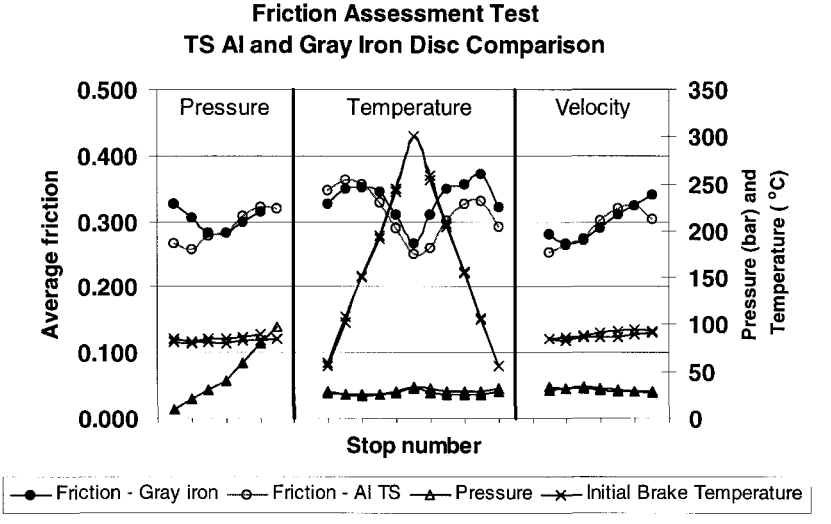

Fig. 6. Comparison of test results from one gray cast iron disc and one TS Al disc. Friction coefficient trends are similar.

This page intentionally left blank

Thermally sprayed surface coatings suitable for use in automotive brake and clutch applications

A WIRTH and **S McCLURE**
Materials Research, Institute School of Engineering, Sheffield Hallam University, UK
D ANDERSON
Plasma Coatings Limited, Tideswell, UK

ABSTRACT

Problems associated with the use of cast iron components in automotive friction braking/clutch systems, namely corrosion, uneven wear, distortion and in the worst cases structural failure have been overcome using thermally conducting coatings. The thermally sprayed coatings are composites of ceramic particles dispersed in a metal matrix. The coatings have good thermal conductivity, excellent corrosion and wear resistance with high energy absorption and heat dissipation. Careful selection of the friction material allows adequate friction levels to be generated over a wide range of operating temperature with the minimum levels of friction couple wear and disc cracking.

1. INTRODUCTION

Cast iron components are fulfilling an important role in automotive friction braking/clutch systems mainly due to their relative cheapness and ease of manufacture. Unfortunately parts manufactured in this material are susceptible to corrosion, uneven wear, distortion and in the worst cases structural failure. Probably the most serious problem encountered with cast iron brake components on light vehicles is DTV (disc thickness variation) brake judder, (1-3).
DTV judder arises from variation in torque output during braking as a consequence of uneven wear of the disc, ovality of the drum, non-uniform coverage of the transferred layer, and/or differential corrosion.
Distortion and structural failure generally occurs after prolonged operation or heavy-duty service and is more likely to occur with heavy vehicle components. However, the move towards extended warranty periods could mean vehicle manufacturers may have to pay greater attention to the effects of corrosion, uneven wear, distortion and structural failure as additional quality issues when using cast iron.
In this paper we demonstrate the qualities of metal matrix composite coatings to enhance

the performance of cast iron components and consider their possible use as a method for increasing the operating temperature of lightweight braking/clutch components.

2. MATERIALS AND EXPERIMENTAL PROCEDURE

The initial stages of the investigation to determine the friction performance of the thermally sprayed coatings were conducted using a copper rich coating "A" on substrates of cast iron, see table 1, and commercially pure aluminium. The performance of the coating was assessed by rubbing against a number of experimental and commercially available friction materials in a F.A.S.T. (Friction Assessment Screening Test) (4). For comparison purposes the same friction materials were also rubbed under identical conditions against the substrate cast iron. Two modes of testing were used, constant clamping force and constant friction force. In the former, a constant pre-set pressure is applied to the lining specimen. The friction force will alter to

Table 1 Chemical composition of cast iron discs used in F.A.S.T. experiments

Carbon	3.30 - 3.50
Manganese	0.60 - 0.90
Silicon	1.80 - 2.10
Sulphur	0.12 max.
Phosphorus	0.15 max.
Nickel	0.60 - 0.70
Chromium	0.15 - 0.25
Molybdenum	0.20 - 0.30

compensate for any variation in the coefficient of friction. In this mode, velocity, work done and disc temperature are not constant between each test so comparisons between tests is difficult. In the latter, the clamping force and the friction coefficient will vary in a reciprocal relationship. Consequently if the friction coefficient were to drop for some reason during the test (e.g. fade) the clamping force would increase to compensate. Where the friction force and test run time remain constant between tests, then the distance travelled by the specimen will be the same (constant velocity).

From the equation-

$$W = F \times S$$

Where W is the work done opposing the friction force F, and S is distance travelled, it follows that the work absorbed during each test will also be constant. Hence for near identical discs and ambient conditions the temperature rise of the disc should follow the same pattern. The values used in this investigation unless otherwise stated were 2.67 bar in constant pressure mode and 5.33 bar in constant friction force mode. The duration of each test was 90 minutes. Carefully comparing the results from each test mode gave a good indication of the repeatability of the machine. A "Work Bench" computer package was used to simplify data processing and

acquisition. Data values were collected at 0.01-second intervals and averaged out over 60 seconds producing 90 points for each 90-minute test. The scheme for data acquisition is illustrated in figure 1.

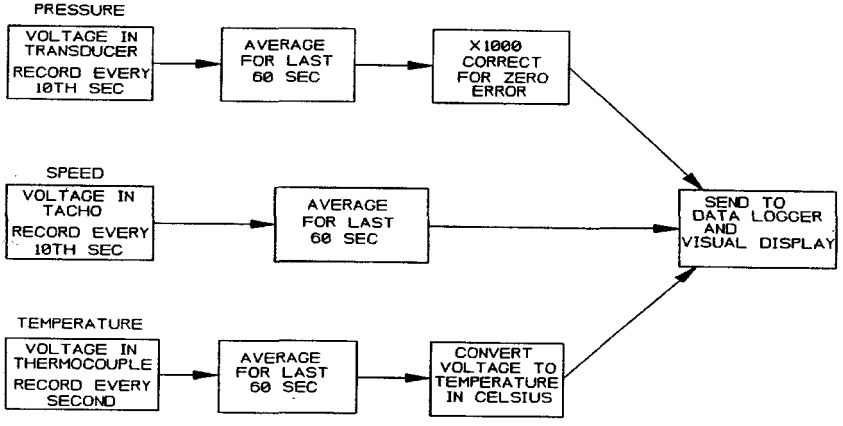

Figure 1. Schematic illustration of "Work Bench" programme for data acquisition

Because previous work (5,6) highlighted the relationship between friction performance and transfer film chemistry the nature of each transfer film was studied using methods described elsewhere (7).

After consideration of the data obtained from the F.A.S.T. work several friction material compositions were chosen as suitable candidates for manufacture into light car brake pads for dynamometer testing. The friction characteristics of each of these materials were assessed against a ferrous rich coating "B" and the original coating "A" both on cast iron, together with coating "A", on commercially pure aluminium and also against cast iron for reference. After bedding the materials were subjected to a variety of dynamometer test schedules that ensured the friction couple was subjected to a rigorous test. E.g. speed sensitivity tests were carried out from 160 k.p.h to 5 k.p.h. starting at 100 °C using pressures in the range 10 to 80 bar, the 300 °C performance was determined using 10 to 80 bar in increments of 10 bar to reduce speed from 80 k.p.h. to 30 k.p.h. Bulk disc temperatures were measured using either an embedded or a rubbing thermocouple. Extensive analysis of the dynamometer generated transfer films is currently underway. This data bank is not yet as extensive as with the F.A.S.T. generated films.

3. RESULTS AND DISCUSSION

3.1. Small scale testing

Typical examples of the extensive F.A.S.T. data acquired using constant pressure and constant friction mode are shown in figures 2 and 3 respectively. The majority of the friction materials examined showed similar trends when rubbed against the different counterfaces. In general terms all the friction materials when rubbed against the coating "A" whether on cast iron or the aluminium substrate produced increased final friction levels with less fade and lower overall wear of the counterface and friction material. The initial friction coefficient was generally lower with the coated materials. Visual inspection of the counterfaces during the test revealed the

coated discs did not produce a clearly defined transfer film as quickly as on the cast iron counterfaces. One other significant difference highlighted during this investigation was with one particular group of friction materials that initially "faded" badly against cast iron but showed no significant reduction in friction performance when rubbed against coating "A" on both the aluminium and cast iron substrates. This difference is illustrated in figure 4. The information contained in this illustration highlights the importance of ensuring selection of the appropriate friction material for the opposing counter face. The magnitude of the decrease in friction coefficient in this group of friction materials increases with increasing size of abrasive in the friction material. The differences in transfer film chemistry are shown in the energy dispersive x-ray spectral data illustrated in figures 4b and 4c. Detailed examination of this data shows, in line with expectations, that the transfer film formed on the cast iron is iron oxide rich whereas it is copper oxide rich after rubbing against coating "A". Studies of the transfer film formed on the cast iron surface immediately before and after the sudden change in friction coefficient indicate a significant change in the composition of the iron rich oxides. The results of this investigation, using sophisticated x-ray photoelectron spectroscopical methods will be reported elsewhere.

3.2. Dynamometer and vehicle testing

At the present time vehicle testing has been restricted to examining the performance of coating "A" on an aluminium substrate and cast iron although plans are in hand to commence testing of the ferrous coating "B" on cast iron. Coating "A" on the aluminium substrate performed extremely well on a lightweight concept car fitted with front discs and rear drums. However because of the confidential nature of the data the authors are not permitted to reveal details other than to comment that four wheel locking was achieved during emergency brake application without servo assistance.

During dynamometer testing of coating "A" on the aluminium substrate when the simulated unladen weight was kept below 1000 kg the coating performed extremely well. Figure 6a shows the condition of the disc after extensive dynamometer testing. Increasing vehicle gross weight to 1500 kg, gave satisfactory friction performance provided the coating substrate interface temperature did not exceed 525 °C. Above this temperature localised interface melting occurred with the formation of a "mushy" aluminium-copper alloy phase (fig 5). As a consequence of the low melting point alloy formation arising from excessive energy input, delamination of the coating occurs as illustrated in figure 6b. Plans are now in hand to increase the unladen kerb weight at which coating "A" on the aluminium substrate can operate by using coated ventilated discs.

Coating "A" on a cast iron performed more than adequately during vehicle trials using a Dax Rush Cosworth 4x4 vehicle. The vehicle, licensed for use on the public highway, was fitted with specially formulated brake pads to operate against coated discs installed on both front and rear axles. Figure 7a shows the proud owner with the trophy awarded for finishing first overall in the Clark Motor Group Midlands Hill Climb Championship during the 1999 season. Unlike dynamometer testing where much higher temperatures are reached and can cause stress relief cracking of the coating, as illustrated in figure 7b, the vehicle discs remained in excellent condition throughout the 1999 season. Figure 7c shows the condition of the outer face of the front offside disc at the end of 1999 season. Previous work has shown a similar coating also performs extremely well when used for clutch pressure plates, see figures 8a and 8b (taken from reference 8).

The most encouraging data gathered to date in this investigation has been the dynamometer information obtained from the friction testing of the ferrous coating "B" on ventilated cast iron discs. Table 2 summarises some of the information obtained from the dynamometer study and compares the data from coating "A" on cast iron together with information obtained from testing

against a ventilated cast iron disc. A change of fibre type in the friction material from type 1 to type 2 is responsible for producing friction levels similar to cast iron but with reduced pad and disc wear compared with cast iron and will form the basis for further vehicle testing. Although stress relief cracking of the coating is still evident in the ferrous coating, spalling should not occur since preliminary work undertaken to date indicates the cohesive strength of the coating is lower than the adhesive bond strength. Work is now being undertaken to evaluate the process parameters which will, we hope, reduce and eventually prevent stress relief cracking.

Table 2 Comparative performance of coatings "A" and "B" on ventilated cast iron discs against ventilated cast iron disc for same dynamometer regime.

Disc Material		Coating "A"	Coating "B"	Coating "B"	Cast Iron
Friction Material		Type 1	Type 1	Type 2	Type 1
Average μ	New	0.30	0.25	0.23	0.40
	Bedded	0.39	0.36	0.42	0.53
	Before Fade	0.33	0.33	0.41	0.49
	After Fade	0.40	0.35	0.46	0.45
Average	Pad (m.m.)	0.72	0.45	0.50	1.07
Wear	Disc (m.m.)	0.11	0.01	0.03	0.09

4. CONCLUSIONS

This investigation has provided encouraging data that indicates that thermally sprayed metal matrix coatings can be used to great effect to enhance the life of cast iron components in automotive braking applications. Friction materials producing similar or better friction performance than seen when paired with cast iron have been found to produce lower disc and pad wear when rubbed against specific ferrous coatings. The challenge now is to produce a cost effective coating free from stress relief cracking that will appeal to the whole of the automotive industry rather than niche markets such as sports car racing and the luxury end of the market.

5. REFERENCES

1. M.J. Haigh, H. Smales and M. Abe. "R.T.V. – A Friction Material Designers View". S.A.E. Paper No. 933070, S.A.E. 400 Commonwealth Drive, Warrendale, PA 15096, 1993.
2. A. de Vries and M. Wagner, "The Brake Judder Phenomenon". S.A.E. Paper No. 920554, S.A.E. 400 Commonwealth Drive, Warrendale, PA 15096, 1992
3. K. Vukolov, B. Tron and P. Buonfico. "Brake Vibration and Disc Thickness Variation D.T.V.)" Second International Seminar on Automotive Braking Leeds 1998 ISBN 1 86058 131 5 pp. 77-84.
4. A.E. Anderson, S. Gratch and H.P. Hayes. "A New Laboratory Friction and Wear Test for the Characterisation of Brake Linings". S.A.E. Paper No. 670079, S.A.E. 400 Commonwealth Drive, Warrendale, PA 15096, 1967.
5. A.Wirth and R. Whitaker. "An Energy Dispersive and Imaging X-ray Photoelectron Spectroscopical Study of Transfer Film Chemistry and its Influence on Friction Coefficient". J. Phys. D; Appl Phys. 25 (1992) A38-A43.

6. A.Wirth and R. Whitaker. "Characterisation of Transfer Films formed on Grey Cast Iron used in Automotive Braking Systems". Proc. Eurotrib 93, Budapest, Vol. 1,1993, pp.341-350.
7 A.Wirth, R. Whitaker, S. Turner and G. Fixter. X-ray Photoelectron Spectroscopy "Characterisation of 3rd Body Layers formed during Automotive Friction Braking". J. Electron Spectroscopy and Related Phenomena 68 (1994) 675-683.
8. Plasma Coatings Limited Application Data Bulletin "HIPAC COATINGS"

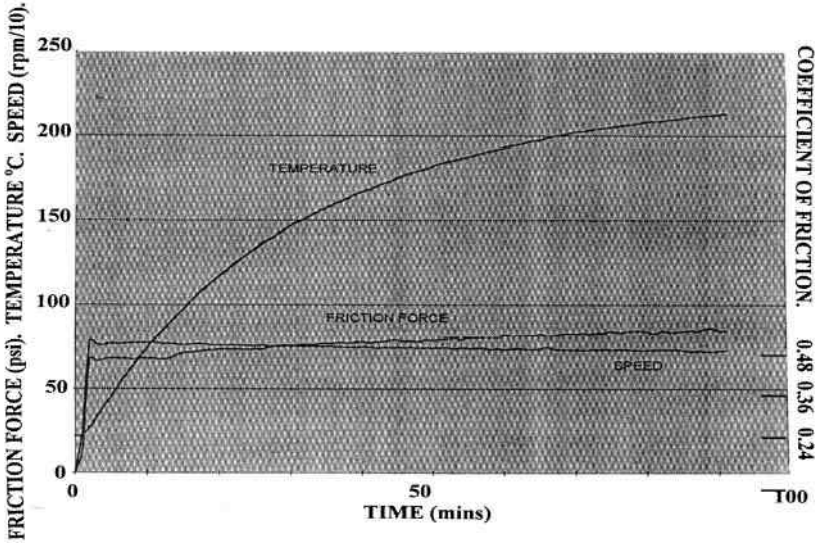

Figure 2: Friction coefficient versus temperature data acquired using 2.67 bar constant pressure.

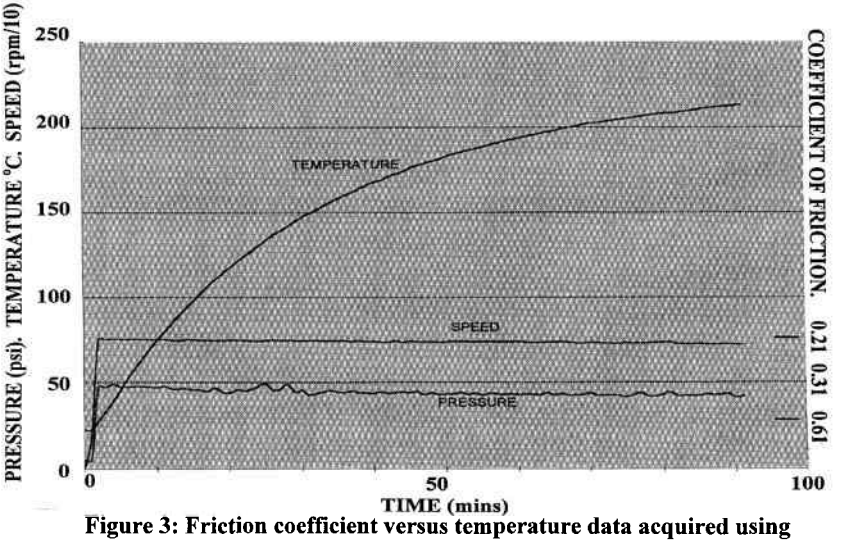

Figure 3: Friction coefficient versus temperature data acquired using 5.33 bar constant friction force.

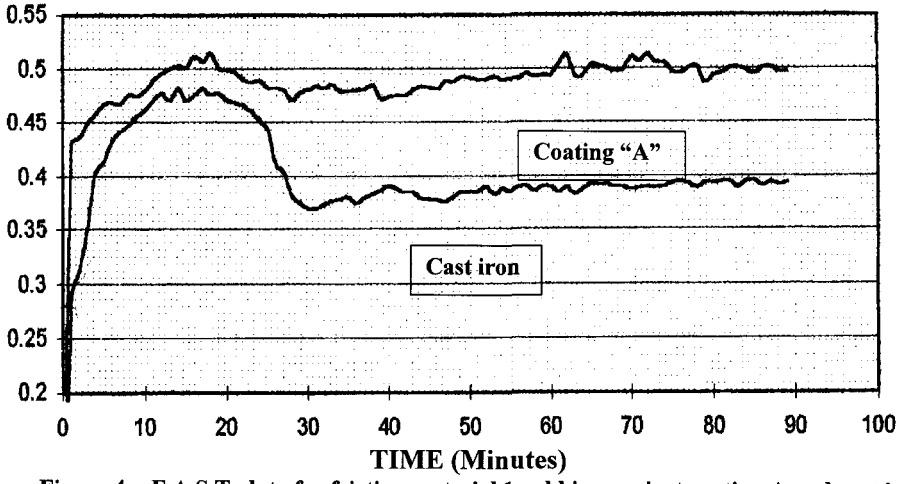

Figure 4a: F.A.S.T. data for friction material 1 rubbing against coating A and cast iron

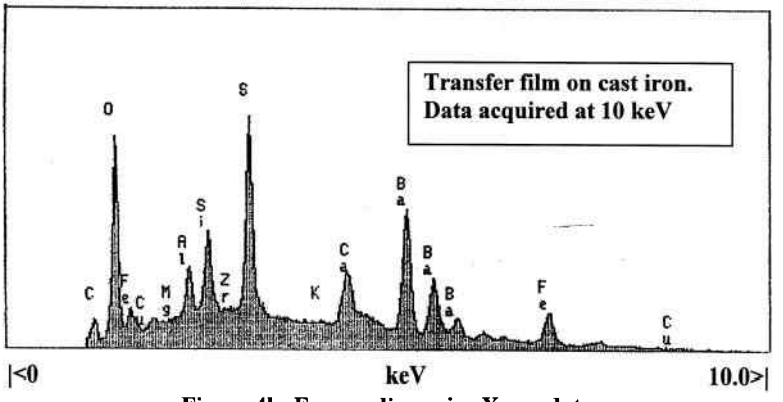

Figure 4b: Energy dispersive X-ray data

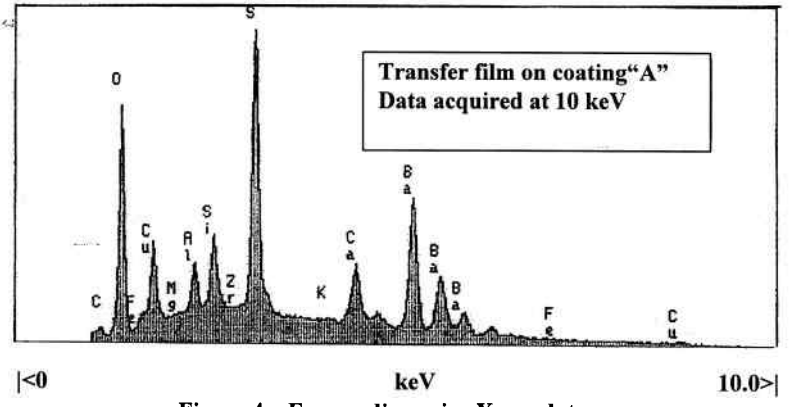

Figure 4c: Energy dispersive X-ray data

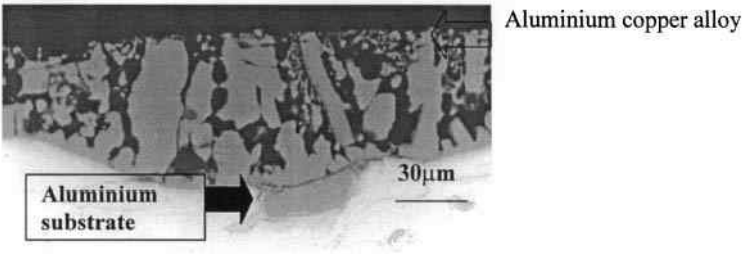

Figure 5: Scanning electron micrograph illustrating nature of aluminium-copper alloy

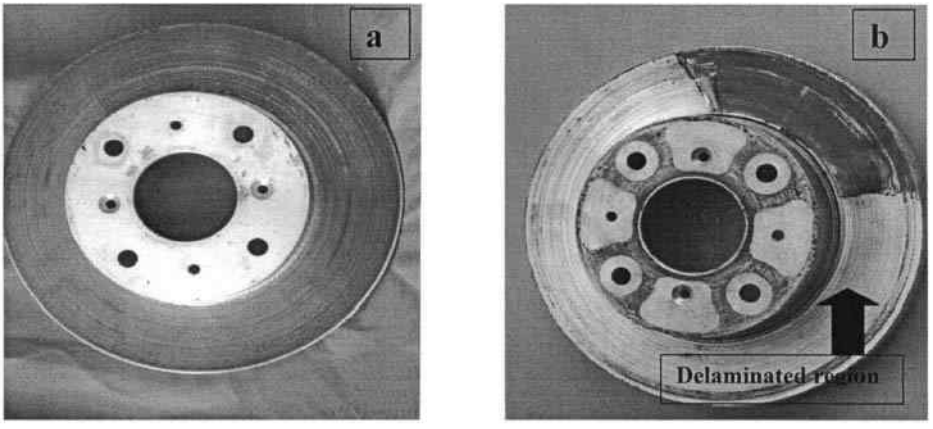

Figure 6: Solid aluminium discs with coating "A" showing satisfactory friction film generated on the coating at temperatures below 525 °C (fig 6a) but delamination of the coating from the substrate occurs at interface temperatures above 525°C (fig 6b).

Figure 7a: Dax Rush Cosworth 4x4 fitted with cast iron disc brakes with coating "A". winner of Midland Hill Climb Championship 1999 season.

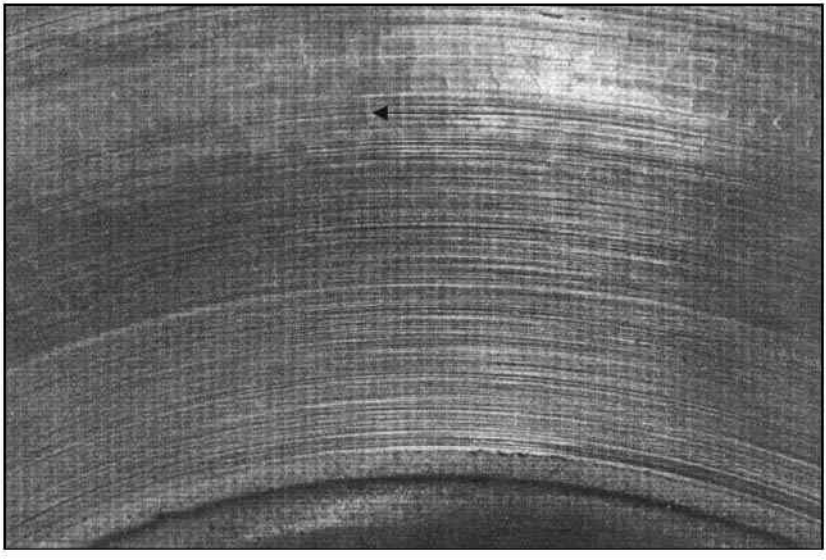

Figure 7b: Stress relief cracking, arrowed, of coating "A" on cast iron after subjecting to excessive thermal cycling during full scale inertial dynamometer testing.

Figure 7c: Condition of coating "A" on outer surface of front offside disc of Cosworth powered Dax Rush hill climb car after a full racing season.

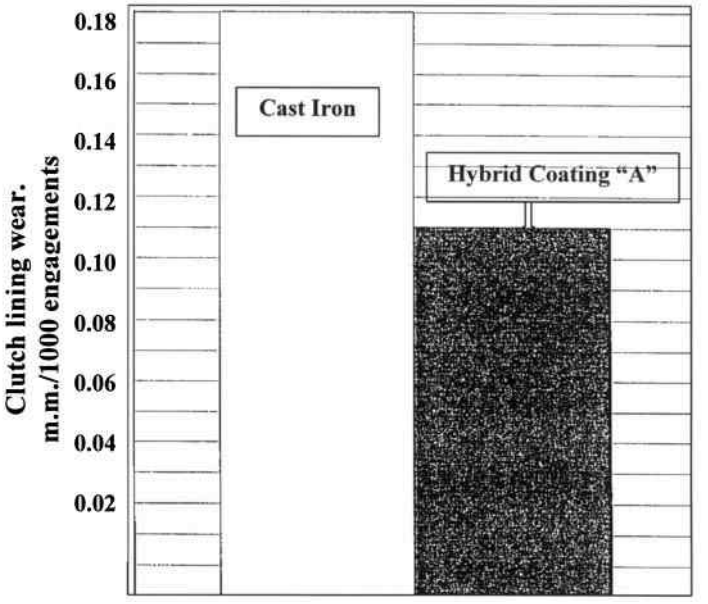

Figure 8a: Comparative data for clutch lining wear in an auto clutch assembly for cast iron and cast iron covered with material similar to coating "A", (Ref 8).

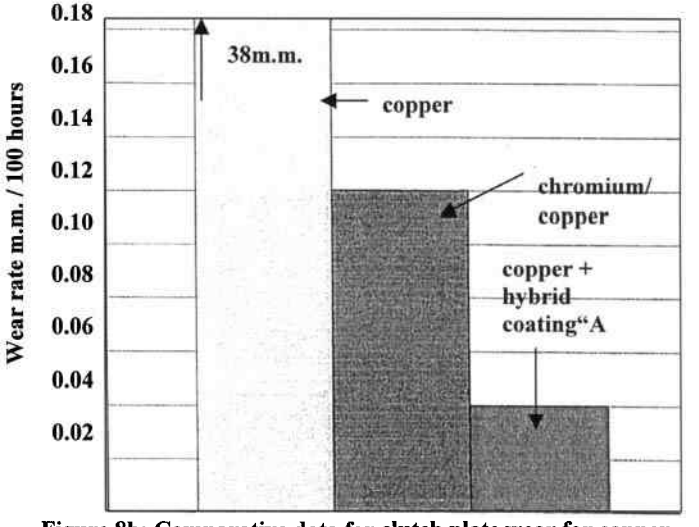

Figure 8b: Comparative data for clutch plate wear for copper, chromium/copper and copper with material similar to coating "A", (Ref 8).

The role of engineered cashew particles on performance

B B PALMER
Palmer International Inc., Worcester, Pennsylvania, USA
M H WEINTRAUB
M.H.W. Limited, West Bloomfield, Michigan, USA

Synopsis: This paper provides the reader with information on the use of cashew based materials in friction formulations. Through a study performed on a dynamometer, the role of cashew is discussed, with particular attention paid to wear and friction performance. Further discussion is provided on the many types of cashew particles that are commercially available in an attempt to clear up the "mystery" of cashew.

1. INTRODUCTION

Over the years, friction materials have evolved from simple formulations containing approximately eight ingredients to complex composites with as many as twenty ingredients. The evolution is due in large part to increased customer requirements, as well as new vehicle designs and governmental regulations.

Today, the expectation for noise and judder free friction materials, while maintaining a good pedal feel, is truly worldwide. As the supply of these materials lags behind the ever-increasing demand, formulators work under significant pressure to create higher performing products. Since formulators often are involved with resolving issues on current materials, little time is left to do basic research.

This paper describes the role of cashew particles in both a practical and fundamental manner. The study will also examine performance characteristics of wear and friction, as measured on a brake dynamometer.

Cashew particles have been used in friction materials for many years, yet its role in the formulation is not particularly clear. This may be due to use of the term "cashew particles" in a generic sense. In reality, there are many types of "cashew particles" that can affect friction material performance in several ways. Wear improvement, noise reduction, and influence on compressibility are three examples of parameters that can be affected by the selection of a particular type of cashew particle.

Cashew particles range from lower temperature brown particles to higher temperature blacks. Using cashew, inorganic lubricants or abrasive fillers can be encapsulated to create a flexible matrix.

2. BACKGROUND

Cashew particles have their basis in CNSL (Cashew Nutshell Liquid), which is a by-product of the cashew nut industry. Cashews are grown primarily in India and Brazil, but may also be found in several other countries located within approximately ten degrees of the equator.

Cashews are grown within a shell, although most people have never seen the shell. CNSL is contained within the soft honeycomb structure of the shell. Pictures of cashew trees and nuts are shown in Figures 1 – 3.

Fig. 1
Cashew Tree

Fig. 2
Cashew Tree Fruit

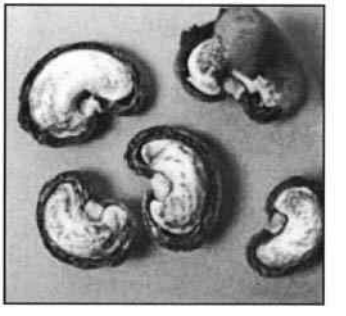

Fig. 3
Cashew Nut

3. CASHEW OIL PROCESSING

Since raw CNSL contains the homologue of the chemical that causes poison ivy, handling of the material is done under controlled conditions. Several processes are used to extract the oil from the shell, including heating, solvent extraction, and steam distillation.

Specific combinations of temperature, pressure, and catalyst are used to polymerize the oil to yield a type of cashew particle. The utmost control is required in processing to produce consistency and quality of the particles.

The use of proprietary catalysts and the addition of other materials create the wide range of cashew particles commercially available. The "Engineered Particles" chemically react or bond cashew with various abrasives, lubricants or fillers. Encapsulating of high gravity and small particle size materials in cashew help to eliminate separation or fall out during friction material mixing.

4. CASHEW PARTICLE STRUCTURE

The structure of the basic forms of cashew particles is shown in Figures 4 and 5. The brown type is cross-linked with a loose network of bonds, as compared to the interlocking network of the black particle by the use of furfural and other catalyst. The furfural becomes part of the network with a greater degree of hydrogen bonding.

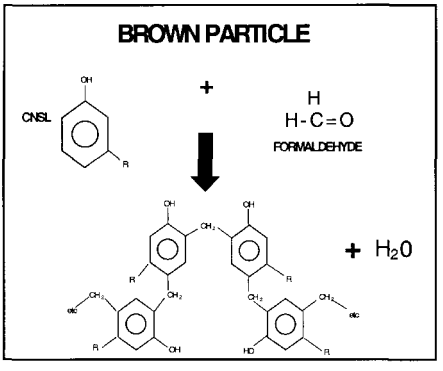

Fig. 4
Brown Cashew Particle

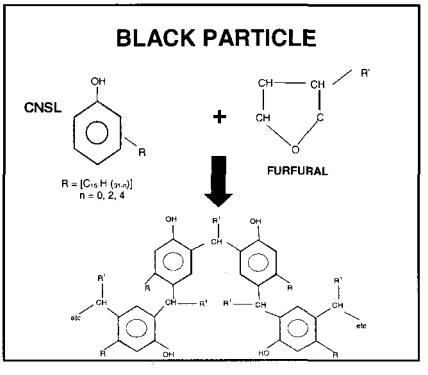

Fig. 5
Black Cashew Particle

Using tools such as GC-Mass Spec and FTIR (Fourier Transfer Infrared Analysis), information on the degree of cross-linking, decomposition, and reactivity can be obtained. The FTIR shows hydrogen bonding and its relationship to oxygen, carbon, and nitrogen in the matrix.

An FTIR analysis of CNSL is shown in Figure 6. Figure 7 shows an FTIR analysis of a typical brown (called 3400-1) and black (called 6250-1) particle. The brown particles exhibit a large absorption of the C=OH group (wave numbers at 3500 and from 900 to 1500). The black particles exhibit less hydroxyl bonding, and a greater degree of C-H bonding, which results in a higher decomposition temperature.

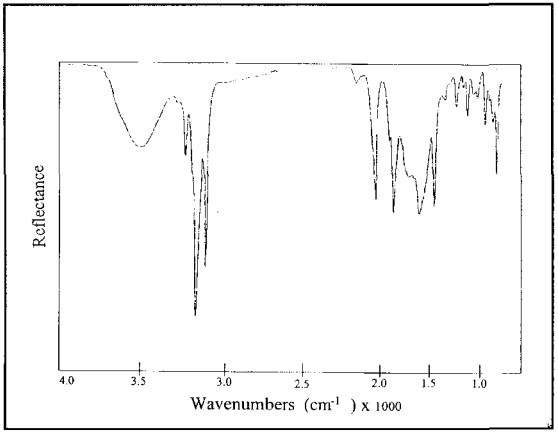

Fig. 6
Fourier Transfer Infrared Analysis
of Cashew Nutshell Liquid

Fig. 7
Fourier Transfer Infrared Analysis
of Brown particle (3400-1)
with Black Particle (6250-1)

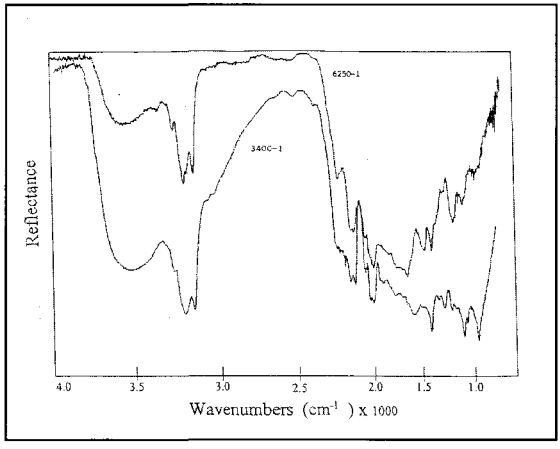

5. CASHEW PARTICLES

Three distinct particles were selected for detailed study. These particles exhibit a wide range of thermal resistance. The Thermal Gravimetric Analysis (TGA) for each is shown in Figures 8, 9, and 10.

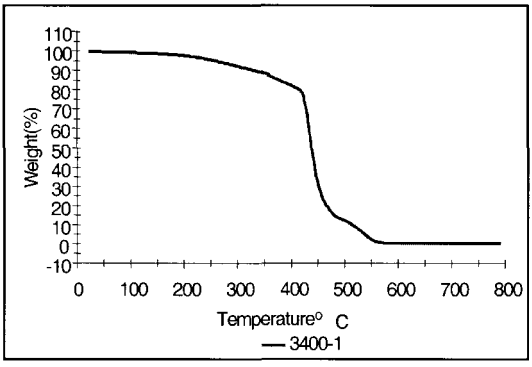

Fig. 8
Thermal Gravimetric Analysis in Air of Cashew 3400-1

Fig. 9
Thermal Gravimetric Analysis in Air of Cashew 6001-1

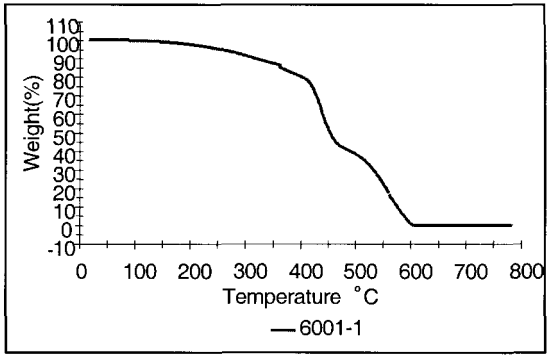

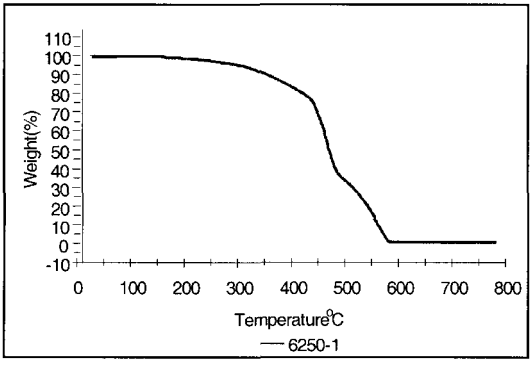

Fig. 10
Thermal Gravimetric Analysis in Air of Cashew 6250-1

The curves were run in air and show weight loss of the particles as a function of temperature. At around 450 °C, the 3400-1 exhibits a 75% weight loss, the 6001-1 shows a 60% weight loss and the 6250 a 40% weight loss. The performance difference of these particles is due to differences in polymerization sequences and catalysts used when processing.

As shown in figure 5, the addition of furfural to both 6000 series particles, 6001-1 and 6250-1, has added to the molecular structure, which in turn has a two-fold effect. First, the cross-link network is tightened due to increased hindrance to movement caused by the space taken by the furfural. Second, the furfural molecule brings inherent thermal resistance to the cashew particle. The resulting 6000 series black particles have a higher hardness and better thermal performance than would be expected from brown cashew particles (i.e 3400-1).

Based on the TGA results, the brown particles would be more appropriate in friction materials where brake temperatures do not become excessive. For those higher temperature applications, black particles should be considered.

However, it is important to remember that the synergy with the other ingredients in the formulation should always be considered to determine not only the type, but the amount of cashew particle to use.

6. FRICTION MATERIAL PROPERTIES

Many cashew particles can also have a positive effect on friction material processing. Engineered cashew particles assist with flow properties within the mold. Other cashew particles aid in the overall distribution in the mix and improvements in preforming.

Regardless of formulation type (NAO, semi-met, etc.), cashew particles influence almost all of the physical properties of friction materials – including compressibility, porosity, specific gravity, shear strength, and hardness.

For example, a special modified partially cross-linked cashew that has a controlled shrinkage with temperature is utilized to promote internal porosity in the friction material. Porosity has been directly correlated to certain types of noise. The thermal expansion and contraction helps to minimize hot spotting by distributing the load on the surface. The mechanism of how and why cashew particles assist with performance is based in part on the rate of thermal expansion and contraction. This is illustrated in Figure 11.

- Thermal Expansion / Contraction helps to distribute the load on the surface.
- The wear rate of cashew on the surface is a type of pulsation on a micro-basis.
- Improves the overall wear.
- Minimizes hot spotting propensity.

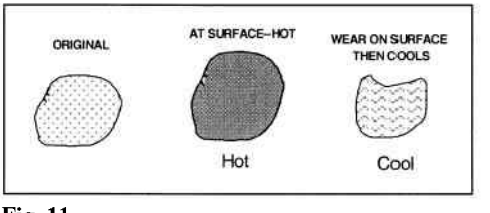

Fig. 11
Cashew Characteristics

As the rubbing surface increases in temperature, the cashew expands so that the surface,

on a microscopic basis, tends to expand. As these resulting high spots tend to wear and no longer remain in contact with the surface, there is a cooling effect, and the cashew in a micro basis, contracts. This cycle is repeated and the contact asperities will tend to move at a more rapid rate with cashew then without. This phenomenon has been examined by visualization techniques. This is only part of the mechanism attributed to cashew particles.

Compressibility as a function of noise is shown in Figure 12.

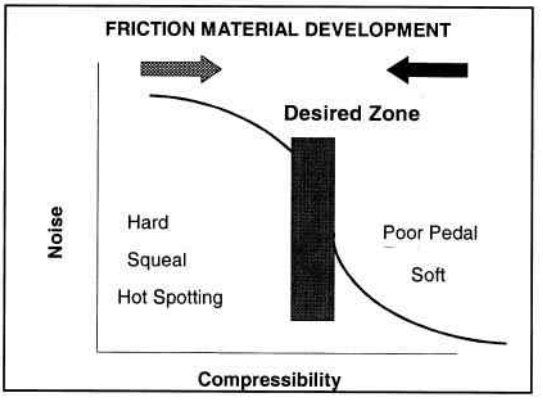

Fig. 12
Compressibility of Friction Material and Noise

Generally, the desired zone is a narrow band and if there is deviation to either side, customer complaints may result. For example, if the compressibility is too high, the customer could complain of a soft pedal. Different engineered cashew particles are being used to modulate compressibility in the friction material compounds. Generally, the higher temperature and harder particles are used for the high performance friction materials.

With respect to noise, not only is porosity one of the factors, but internal damping of the friction material maybe the major factor. The use of modal analysis is used to develop new type of Engineered Cashews Particles. Both semi-metallic and low or non-steel friction material laboratory formulations are used for comparative modal analysis.

7. FORMULATIONS

To examine the influence of cashew particles on performance, an NAO and a semi-met formulation were compounded at a friction material facility, using standard production techniques. The samples were molded in a Ford Taurus shape for 4.5 minutes at 150 °C and post cured for 8 hours. For the NAO formulation, the cashew particles were added at two different levels - 4% and 8%, with the baseline having no cashew.

For the semi-metallic formulation, the baseline contained 2% and 6% cashew levels. Four different cashews were compared. The formulations are not intended for customer approval or to reflect any formulations used in the industry. They are for the sole purpose or determining the attributes of the various cashews. The formulations are shown in Tables I, and II.

TABLE I
NON ASBESTOS ORGANIC (NAO)

RAW MATERIALS	BATCH WEIGHT	WEIGHT PERCENT	BATCH WEIGHT	WEIGHT PERCENT
PHENOLIC RESIN	8	8 %	8	8.00%
BARIUM SULFATE	17	17.00%	14	14.00%
RUBBER	4	4.00%	4	4.00%
KEVLAR	2	2.00%	2	2.00%
ULTRAFIBE II	18	18.00%	18	18.00%
FIBROX	20	20.00%	20	20.00%
ZIRCON	2	2.00%	2	2.00%
ZINC SULFIDE	2	2.00%	2	2.00%
CALCIUM FLUORIDE	2	2.00%	2	2.00%
COPPER	6	6.00%	6	6.00%
VERMICULITE	8	8.00%	8	8.00%
GRAPHITE	6	6.00%	5	5.00%
EXTENDOSPHERE SG	1	1.00%	1	1.00%
*CASHEW PARTICLES	4	4.00%	8	8.00%
TOTAL	100%	100.00%	100%	100.00%

TABLE II
SEMI-METALLIC 2% AND 6% CASHEW

RAW MATERIALS	BATCH WEIGHT	WEIGHT PERCENT	BATCH WEIGHT	WEIGHT PERCENT
PHENOLIC RESIN	8	8.00%	8	8.00%
BARIUM SULFATE	8	8.00%	6	6.00%
RUBBER	4	4.00%	4	4.00%
ULTRAFIBE II	3	3.00%	3	3.00%
ZIRCON	4	4.00%	4	4.00%
ZINC SULFIDE	2	2.00%	2	2.00%
CALCIUM FLUORIDE	2	2.00%	2	2.00%
VERMICULITE	6	6.00%	6	6.00%
GRAPHITE	6	6.00%	6	6.00%
CASHEW PARTICLES	2	2.00%	6	6.00%
STEEL FIBER	35	35.00%	33	33.00%
SPONG IRON	20	20.00%	20	20.00%
TOTAL	100	100.00%	100	100.00%

8. PERFORMANCE

8.1 Friction Material Wear

The AK standard dynamometer procedure was used for the evaluation. For illustration purposes, the life of the material, rotor wear and friction levels will be examined.

Figure 13 shows the overall wear rates for the NAO formulation after completion of the

AK procedures and Figure 14 for the SM.

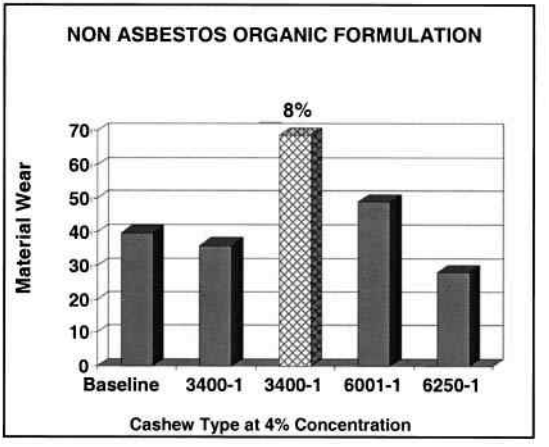

Fig. 13
AK Standard Test

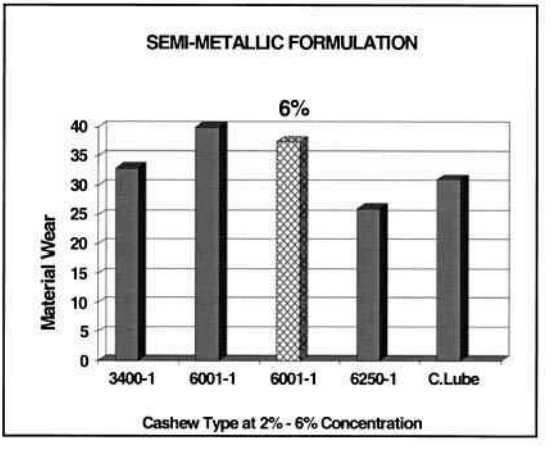

Fig. 14
AK Standard Test

Even though the AK procedure is not specifically designed for wear, it is a reasonable guideline to examine trends. For the NAO formulation, at an 8% concentration of the brown particle (low temperature), the life of the material decreased compared to the baseline. There was a slight improvement in life at the 4% concentration with the brown, and the high temperature black particle showed the most improvement in life. For the SM formulations only the black particle shows a difference. The baseline and the 3400-1 are almost identical.

Figure 15 shows the influence of cashew on rotor wear for the NAO. In all cases, cashew improves the rotor wear.

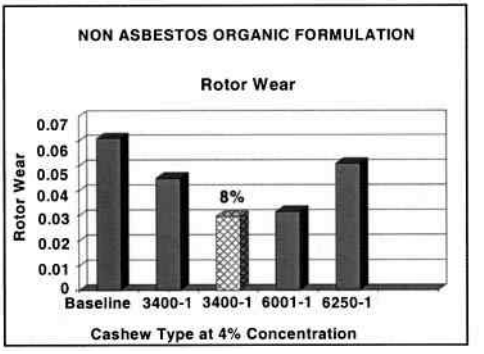

Fig. 15
AK Standard Test

8.2 Speed Sensitivity

Figure 16 and 17 show three sequences of the AK procedure for the NAO and SM formulations

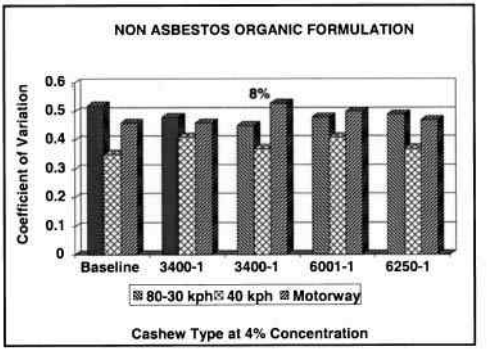

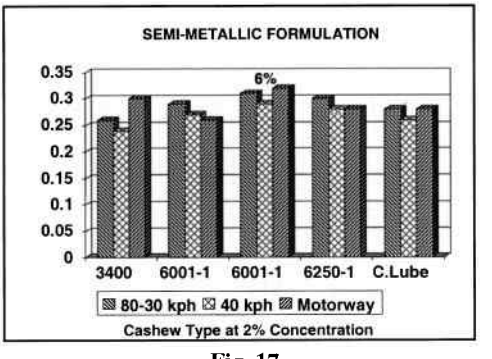

Fig. 17
AK Standard Test

For the NAO formulations (Figure 16), it is interesting to note that cashew tends to decrease the speed sensitivity of the material and the 6001-1 black particles show an increase friction level in the motorway sequence. In fact, at the 40-kph sequences, independent of the cashew type, there is a trend of increased friction. For this NAO formulation, 6001-1 may be the best selection while slightly sacrificing wear improvement. If the criterion were longer life, the 6250 would be the best choice.
For the semi-metallic formulation, the cashew content was examined at a 2% level based upon typical usage in some production formulations. In this case, for interest, a new generation of particle was examined. It is a type of compounded cashew lubricant. Figure 17 shows the friction material wear rate as a function of the type of cashew.

The baseline and 3400 were almost identical in all respects, except the specific gravity was lowered. The life of the material slightly decreased for the other particles. Again, the cashew tends to improve the speed sensitivity of the friction materials. There is less variation in speed using the 6000 series. However, at the 6% level of the 6000-1, there is a higher friction level obtained. For this semi-metallic formulation, the cashew lubricant and the 6250 look the best overall.

Just this small experiment illustrates the complexity of selecting a cashew friction particle.

9. FUTURE PLANS

The following properties will be examined to understand the mechanisms involved:

- How do the various cashew particles correlate to brake squeal?
- What is the role of cashew particles in the relationship to low frequency noise—creep-groan and dynamic groan?
- What is the mechanism for the decrease in moisture sensitivity of the friction material?
- What is the role of new cashew particles on low temperature and cold molding of friction materials?

10. CONCLUSION

Cashew particles tend to:

- Improve the life of the friction material and brake rotor
- Minimize friction variation as a function of temperature and speed
- Influence friction material friction properties
- Influence the rubbing interface

THE CASHEW PARTICLE TYPE SHOULD BE SELECTED BASED UPON THE FORMULATIONS AND CUSTOMER NEEDS

This page intentionally left blank

Multi-criteria optimization in the design of composites for friction applications

D M ELZEY
Department of Materials Science and Engineering, University of Virginia, Charlottesville, USA
R VANCHEESWARAN
Cornell University, Ithaca, New York, USA
S MYERS and **R McLELLAN**
Carlisle, Motion Control Industries Inc., Charlottesville, USA

ABSTRACT

The performance of composite materials is determined by the selection of constituents, their relative volume fractions, and their shape, orientation and distribution. In many cases, the performance-defining attributes of such heterogeneous materials may be predicted (to some level of useful accuracy) by means of micromechanics analyses, which account explicitly for some or all of these design variables. By then identifying an objective function, which is a weighted sum of the performance-defining attributes (PDA's), the micromechanical models may be used to track the position of the overall performance in a *n*-dimensional performance space as changes in constituent selection and relative volume fractions are made. This paper discusses the application of optimization techniques to efficiently search the performance space appropriate for friction materials, leading to optimal composite designs. In particular, component selection is seen to be a combinatorial optimization problem which can be addressed by the *simulated annealing* technique [S.Kirkpatrick et al, Science, 220 (4598), 671, 1983]. The simpler problem of volume fraction optimization is solved using sequential quadratic programming. This *design of materials* approach, in which structure-property relations are coupled with multi-criteria optimization, promises to accelerate the development of improved friction materials.

NOMENCLATURE

α	coefficient of thermal expansion (CTE)
a_{ij}	intrinsic material properties
C	composite cost per unit volume
ε_{ij}	strain tensor (local)
E	energy
ϕ_i	shape factors for second phases
f,v	volume fractions
F	friction coefficient

G	shear modulus
J	friction material objective function
k	thermal conductivity, Boltzmann's constant
k_i	weighting factors defining relative importance of performance attributes
K	bulk modulus
l	micromechanical length scale
l_m	typical microstructural length scale
L	typical macroscopic length scale
M	specified friction material constituents
MST	Materials Selection Tool
N	total number of available material choices
N_{cx}	combinatorial optimization with x unspecified constituents
$N_{c(x\text{-}p)}$	combinatorial optimization with x-P unspecified constituents
N_{cM}	combinatorial optimization with M unspecified constituents
$N_{c(M\text{-}P)}$	combinatorial optimization with M-P unspecified constituents
OFM	optimal friction material
p	probability
P	user-specified constituents
P_l, PDA	performance defining attribute
θ_{ik}	interfacial properties (i^{th} constituent, k^{th} property)
RVE	representative volume element
σ_{ij}	stress tensor (local)
s_j^m	smoothing functions between dilute and non-dilute approximations
T	temperature (local)
t	time
V	bounds on volume fraction
W	dimensionless wear rate
x_k	position vector
m, p	subscripts: matrix and reinforcing phases
cra, abr, adh	subscripts: cracking, abrasive, adhesive (friction and wear mechanisms)
cer, met, pol	subscripts: ceramic, metallic, polymeric

1. INTRODUCTION

Composite materials are attractive whenever an application requires a set of properties or performance specifications which cannot be satisfied by a monolithic material. Examples of composites include bamboo, fiberglas, polyurethane foam and concrete. Composites are often favored because of their increased range of microstructures (and hence property combinations), which can be tailored to suit the needs of a particular application. Structural and most biological materials (e.g. wood, leather, cork, bone, skin tissue) occurring in nature are composites because no single-phase material is available which could satisfy, in an optimal way, the various demands placed upon it by the application. Friction materials in the braking systems of automobiles, trucks, buses, and aircraft are also composites for this reason.

Automotive and heavy vehicle friction materials typically consist of a dozen or more different constituents, combining polymeric, metallic and ceramic phases. Their performance characteristics include wear rate, coefficient of friction, strength, stiffness, coefficient of thermal expansion, thermal conductivity, density, cost and environmental impact. However, while it is taken largely on faith that each constituent uniquely influences each of these performance character-

istics, and therefore the overall performance of the braking material, it is not known if current friction materials represent an optimal design, or how far they may be from an optimum. Could the same or improved performance be obtained using only five constituents? How much of each constituent should be incorporated? What should the shape, orientation and distribution of the constituents be? These are all questions regarding the design of the friction material, which using the current trial-and-error approach to materials development, are virtually unanswerable. With some 80,000 potential raw material constituents to choose from, and a literally infinite number of designs possible based on selection of volume fraction, shape, orientation, etc., an alternative approach is needed if such questions are ever to be addressed.

A *design of materials* approach to the development of improved friction composites has been applied which combines micromechanics models with multi-criteria optimization (1). Micromechanics models relate the intrinsic properties and volume fraction of each constituent to the overall (composite) performance. Such models have been successfully developed for predicting a wide range of performance-defining attributes (e.g. stiffness, strength, thermal conductivity, toughness, etc.) for composites consisting of polymer, metal and ceramic matrices reinforced with particles, whiskers or continuous fibers (2-4). An objective function is identified which is a weighted sum of the performance-defining attributes (PDA's); models relating the selection and volume fraction of a composite's constituents to each PDA are then used to track the position of the overall performance (objective function) in a n-dimensional performance space. Optimization methods are then applied to search efficiently for a composite design maximizing overall performance or to indicate refinements having the most favorable impact on braking performance. Micromechanics modeling of friction composite performance has been presented in a previous paper and is therefore only briefly reviewed here. We then describe optimization techniques that have been applied to aid in the design of improved friction composites.

2. FRICTION MATERIAL PERFORMANCE MODELS

Consider a brake lining of typical dimension, L, subjected to an arbitrary loading with resulting distributed stress, strain and temperature fields, $\sigma_{ij}(x_k)$, $\varepsilon_{ij}(x_k)$ and $T(x_k)$. A smaller volume element of the composite having length scale, l, is identified which is small enough so that gradients in stress, strain and temperature can be neglected, yet larger than the typical microstructural length, l_m. Micromechanics analysis is then applied to this representative volume element (RVE) to predict its properties in terms of the properties, shape and volume fraction of the constituents.

For the purpose of comparing one composite with another to see which performs better, we are less interested in the actual distributions of stress, strain and temperature within the brake pad or lining than in the performance of representative volume elements subjected to uniform (i.e. single-valued) fields. As mentioned previously, friction materials are required to satisfy a number of performance objectives; these performance-defining attributes of a friction composite are strongly determined by the choice of constituent materials, each of which has a set of intrinsic properties (stiffness, density, thermal conductivity, etc.) which make it either more or less suited for use in braking applications.

Performance-defining attributes may also be distinguished according to whether they are surface or bulk attributes. In this context, friction and wear are surface performance attributes while all others are defined for the bulk. Micromechanics models for surface attributes may take into account microstructural changes occurring near the sliding surface due to the high temperatures and shear stresses acting there. In this region of altered microstructure and proper-

ties, evolution models are needed which track time-dependent changes in microstructure given the initial (bulk) structure and the braking history.

A given micromechanics model may be valid over a wide range of material properties and second phase volume fractions, but a change in the geometry of the second phase, say from spherical particulate to fibrous, invalidates the model. Thus, if second phase geometry is changed, a different micromechanics model must be used. A change in model may also be required as the volume fraction of second phase is changed. For low volume fractions, second phase particles are far apart and behave as though isolated. This case, which is sometimes referred to as the "dilute limit", simplifies the development of a micromechanics model since particle interaction effects may be neglected. As the volume fraction increases, such interaction effects become more severe and must be accounted for if the model is to remain acceptably accurate.

The micromechanics models are represented by a set of equations of the form

$$P_l = P_l[f_i, a_{ij}(T, t), \varphi_i, \theta_{ik}(T, t), p] \tag{1}$$

where P_l is the lth performance defining attribute, f_i are the constituent volume fractions, φ_i describes the shape of discontinuous phases (fibrous, particulate, etc.), a_{ij} represents the jth intrinsic material property of the ith constituent, θ_{ik} are the interfacial properties of the ith constituent with the matrix, T is the temperature, p is the applied pressure and t is time. The temperature- and time-dependence of the performance attribute enters through the intrinsic material and interfacial properties, a and θ. Time-dependence allows microstructural evolution (e.g. recovery, precipitation, grain growth, etc.) to occur within the various phases and their interfaces. When applying models of the form given by Eqn. (1), it is assumed that no change in mechanism occurs and that the model may be valid only over a limited range of constituent volume fractions.

3. MULTI-CRITERIA OPTIMIZATION

Once a set of suitable micromechanics models relating the friction material's composition to performance have been identified, the models are coupled with an optimization algorithm to search for "optimal" composite designs. The optimal composite is one for which a scalar objective function containing a weighted set of performance defining attributes (PDA's) for the brake composite is minimized. Figure 1 is a flow chart showing the sequence of problems that may be considered: combinatorial optimization methods are needed if some or all of the composite constituents are unspecified, otherwise the problem reduces to finding the optimal set of volume or weight fractions. Thus the optimization problem can be broken down into the two sub-problems of optimal composition and optimal selection. Referring to Fig. 1, the optimal composition sub-problem seeks to find the relative volume fractions of a set of M (specified) brake lining constituents that drive the lining's performance attributes to a desired goal state. The performance attributes are computed using the micromechanics models represented by Eqns. (1). The solution to the volume fraction optimization problem is referred to as an optimal friction material (OFM).

The optimal selection algorithm searches for new materials selections for composite friction materials leading to improved performance. Assuming a database of N materials from which to choose, several combinatorial optimization problems arise, depending on the number of constraints to be applied. In order of increasing complexity, these are as follows:

1. The number constituents (M) is known and a subset (P) of the constituents are specified.
2. The number constituents (M) is known, but none of the constituents are specified.
3. The number of constituents is not known, but a subset (P) of the constituents are specified.
4. The number of constituents is not known and none of the constituents are specified.

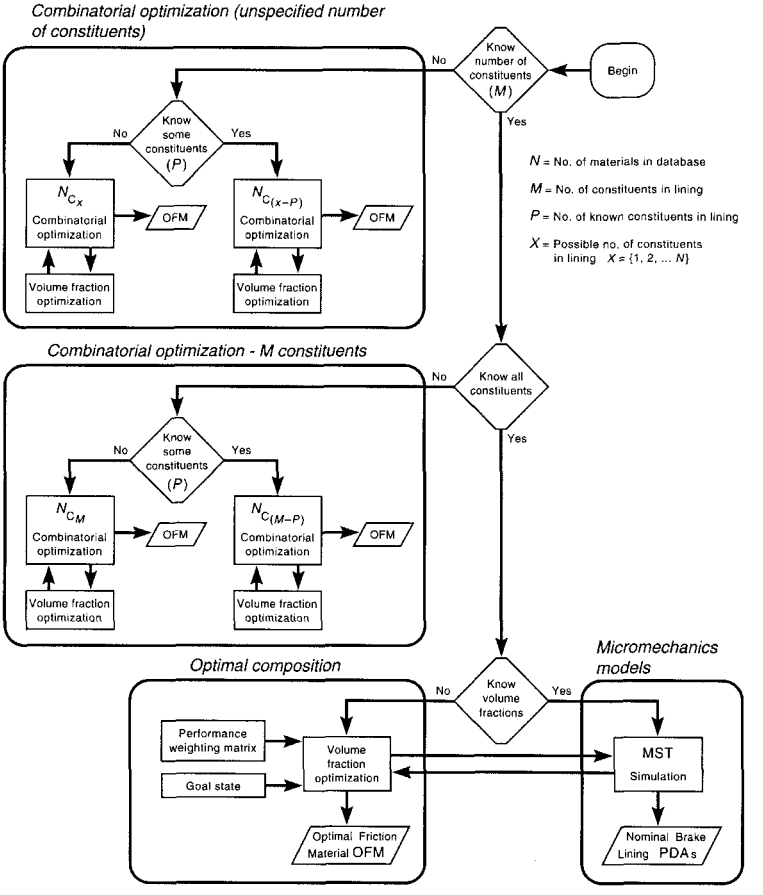

Figure 1. Decision-tree indicating the combinatorial (materials selection) and constrained (volume fraction) optimization problems associated with friction material design.

In each case, friction material design optimization entails first selecting a set of constituents and then solving the volume fraction optimization sub-problem. The materials selection that gives the best overall performance will be chosen as the optimal friction material. The following two sections describe composition and materials selection optimization in greater detail and present examples of their application.

3.1 Volume fraction optimization

Given a set of friction composite constituents, what should the relative fraction of each constituent be to optimize the composite's performance? This *optimal composition* problem is solved by minimizing a user-defined performance function, thereby driving the performance defining attributes (PDA's - e.g. wear, friction, cost, CTE, shear stiffness, ...) to a user defined goal state. Each PDA is computed as a function of the set of materials selected (and their associated physical, thermal and mechanical properties) and their volume fractions. In this problem, the decision variables are the constituent volume fractions. The optimal overall performance is found by minimizing an objective function, J, expressed as

$$J = k_1(W^g - W)^2 + k_2(F^g - F)^2 + k_3(C^g - C)^2 + k_4(k^g - k)^2 + k_5(\alpha^g - \alpha)^2 \quad (2)$$

where W is the dimensionless wear rate, F is the friction coefficient, C is composite cost per unit volume, k and α are the thermal conductivity and expansion coefficient, respectively, and k_i are weighting factors determining the relative importance of each performance attribute. The superscript 'g' designates goal-state values. The objective function is minimized subject to the following constraints:

$$\sum_{i=1}^{N} f_i = 1 \quad (3)$$

i.e. that the constituent volume fractions sum to one. Also performance models:

$$\{W, F, C, k, \alpha\} = \left\{ W_{cra} + W_{abr} + W_{adh}, \sum_j (s_j^f F_{abr}) + F_{adh}, \sum_i f_i C_i, \right.$$

$$\left. \sum_j s_j^k k(f_i, k_m, k_p, shape, packing), \sum_j s_j^\alpha \alpha(f_i, \alpha_m, \alpha_p, K_m, K_p, G_m) \right\}$$

and inequality constraints: $\underline{V}_{cer} \le \left(\sum_{j=1}^{N_{cer}} f_{cer_j} \right) \le \bar{V}_{cer}$, $\underline{V}_{met} \le \left(\sum_{k=1}^{N_{met}} f_{met_k} \right) \le \bar{V}_{met}$;

$$\underline{V}_{pol} \le \left(\sum_{l=1}^{N_{pol}} f_{pol_l} \right) \le \bar{V}_{pol} \quad (4)$$

are needed, where the s_j^m in the performance models are switching functions that allow a smooth transition between the dilute and non-dilute approximations, and V_{cer}, V_{met} and V_{pol} are bounds on the fractions of ceramic, metallic and polymeric materials, respectively. Subscripts m and p are used to indicate matrix and reinforcement.

A constrained sequential quadratic programming (SQP) algorithm is used to solve the optimal composition problem given by Eqs. equation (2) - equation (4) which drives the PDA's towards their goal states. The first equality constraint ensures that the volume fractions sum to unity. The second equality constraint guarantees that the performance models are satisfied. The inequality constraints are user-defined soft constraints limiting the amount of each material class (i.e. polymeric, metallic, or ceramic). In addition to the set of constituents, friction material operating conditions (i.e. applied braking pressure and temperature) must be specified.

As an example of the application of the constrained SQP algorithm to the composition problem, consider the following set of specified lining constituents: a phenolic matrix containing glass fibers and particulate graphite, cast iron, brass and nylon. The performance function for the system is given by equation (2) with the goal states chosen as $W^g = 0$, $F^g = 1$, $C^g = 0$, $k^g = 1$, and $\alpha^g = 0$ and the PDA weighting factors $\{k_1, k_2, k_3, k_4, k_5\}$ given by $\{1,1,1,0.1,0.1\}$. The relative fraction of each material class is bounded as follows: $0.05 \le v_{cer} \le 0.49$, $0.05 \le v_{met} \le 0.4$ and $0.05 \le v_{pol} \le 0.7$.

The computed optimal composition is found to be: phenolic: 0.55, glass fiber: 0.0443, graphite: 0.0057, cast iron: 0.4, brass: 0.0 and nylon: 0.0. The optimization did not choose brass or nylon primarily because of their relatively high cost. The metallic phases are chosen over the ceramics because of their high fracture toughness, which strongly affects the wear rate due to microcracking. Cast iron is favored due to low cost, reasonably good wear resistance and high thermal conductivity.

The sensitivity of the friction material's performance attributes to small perturbations in composition can be explored by perturbing the volume fraction of a particular constituent about the optimal composition. Increases or decreases in the relative fraction of the given constituent are offset by changes in the matrix fraction only. Figure 2 shows the effect of varying the amount of glass fiber. Each PDA is normalized by it's optimal value to show the relative effects of changing composition. Wear, cost and thermal conductivity are sensitive to changes in glass fiber content, while the CTE and friction level are relatively unaffected. The wear PDA exhibits a nonlinear inverse relation with the amount of glass, which because of its relatively high hardness, reduces the rate of abrasive wear. It is interesting that the friction PDA shows a local maximum at the optimal point. High hardness materials tend to lower friction while in the lining, but when fractured, or pulled out, they create abrasive particles which enhance frictional sliding resistance due to microplowing, an effect also captured by the micromechanics models.

3.2 Materials selection optimization

Determining the combination of (M) constituents from among a set of (N) possible materials providing the greatest performance is a combinatorial optimization problem. The number of possible combinations of M materials chosen from a set of N materials (e.g. a database) where $M \le N$ is given by:

$$ {}_N C_M = \frac{N!}{M!(N-M)!} \tag{5} $$

As a result, the number of possible materials combinations to be considered for even a very modest database may preclude an exhaustive search for a combination providing optimal performance. For example, if a set of six constituents were selected from a database containing only eighteen materials, Eqn. (6) indicates there would be 18,564 possible constituent combinations. Combinatorial optimization problems are also encountered for example in the scheduling

of large job shops and in the optimal placement and routing of devices on microprocessors. The methods developed for solving these problems are distinguished on the basis of the search method used deal with the large number of discrete combinations. The friction composite design tool incorporates the simulated annealing method (5,6), so called because of its analogy with the thermally activated annealing of metals. A significant advantage of the simulated annealing method (as opposed to steepest descent and conjugate descent methods) is its ability to look beyond the local landscape while searching for a minimum.

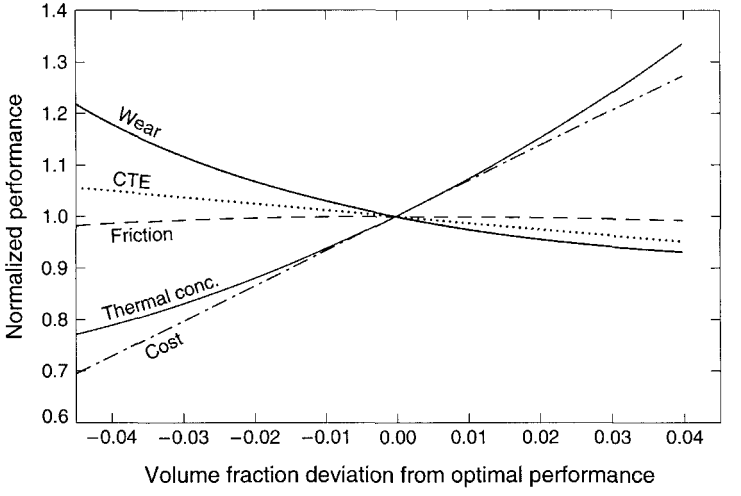

Figure 2. The influence of variations in composition about the optimal can be explored for each performance defining attribute, as shown here for the case of glass fiber in a phenolic matrix composition.

To solve the problem of material selection using simulated annealing, a set of M constituents is first selected. Calling this selection, v_c, the optimal composition problem is solved and the resulting optimal objective function is $f^*(v_c)$. According to the annealing analogue, this result is regarded as an energy, $E_1 = f^*(v_c)$, in which increasing energy equates to decreased performance. Next, one of the constituents in v_c is randomly replaced by another material from the database, resulting in a new composition, v_n. The optimal composition for this new selection is $f^*(v_n)$, corresponding to energy, $E_2 = f^*(v_n)$. In analogy with thermally activated processes such as annealing, the probability that a system will change from the current to a new configuration is given by a Boltzmann distribution:

$$p = \exp\left[\frac{-(E_2 - E_1)}{kT}\right] \tag{6}$$

where k is Boltzmann's constant and T is the absolute temperature.

Using this equation we find that if $E_2 < E_1$, this probability is greater than unity, and in this case the probability of accepting the change is arbitrarily assigned to 1 and hence the new selection becomes the current selection. On the other hand, if $E_2 > E_1$ then the probability is less than unity and will therefore be accepted only part of the time, i.e. the new selection, v_n, is accepted

only if it's probability is greater than a random number between 0 and 1. Initially, the fictitious temperature is high, making it probable that a higher energy (lower friction material performance) will be accepted. As the temperature is reduced (according to the formula, $g(t,T) = (T*0.9^t)$ where t is time), the probability of accepting a higher energy state correspondingly reduces. Reducing the annealing temperature has the effect of decreasing the probability of acceptance of material selections when $f(v_n) > f(v_c)$ (i.e. the new selection is worse than the old selection).

This simulated annealing algorithm emulates the annealing process and thus initially (when the simulated annealing temperature is high) searches over a very large search space and as the temperature drops, the algorithm reduces the material selection search space and in so doing will have a better chance of finding the global minimum.

As an example of the simulated annealing method applied to constituent selection, consider a set of six metallic, six ceramic and six polymeric materials, from which a set of six materials are to be selected as constituents for a friction composite. In addition to limiting the total number of constituents making up the composite, we specify that there can be no more than two selections from the polymer class, two from the ceramic class and two from the metallic class. This results in a problem that has $3 \times {}_6C_2 = 3375$ possible material selections. The optimal composition sub-problem for each case is the same as that formulated in Section 3.1. The weights for each of the performance criteria are $\{k_i\} = \{1,0,0,0,0\}$ so that only wear rate is considered while ignoring other performance attributes.

Figure 3 shows the evolution of the simulated annealing search process as a function of time. Initially when the annealing temperature is high (Fig. 3b), the performance function (i.e. the total wear rate, Fig. 3a), oscillates between about 0.005 and 0.02. As the temperature drops, the oscillations fall off significantly and it is clear that the minimum value of the performance function is captured.

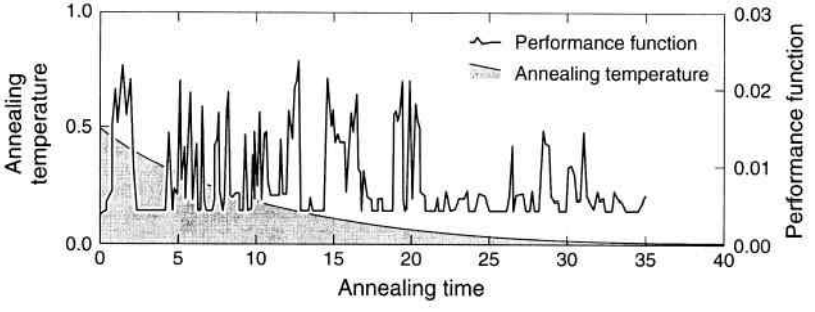

Figure 3. Simulated annealing optimization in which the only performance attribute considered was the wear rate; as the fictitious annealing temperature is reduced, the algorithm gradually focusses in on an optimal materials selection which minimizes wear rate.

For this limited database, it seems there are many good material selections and the simulated annealing algorithm finds these local minimum wear selections very early on in the process. However, if the database were increased in size, the material selection terrain would be much more varied and the search for a global minimum more difficult. The contributions of the dif-

ferent wear mechanisms to the total wear performance can also be tracked if desired. For the given materials database and constraints, the optimal composite proposed by the simulated annealing method was milled fiber glass ($f = 0.2$) and zinc alloy ($f = 0.29$) in a nylon matrix ($f = 0.51$).

The foregoing example illustrates the complexity of the optimal materials selection problem and the importance of reasonable constraints. In an n-dimensional space whose coordinate axes correspond to the various performance criteria, each raw material in the database represents a point. The composite micromechanics models allow arbitrary combinations of any number of these materials to reach other points within the performance space. The simulated annealing algorithm does not guarantee a global optimum, but as with any search among a large selection of possible outcomes, reasonable results can be obtained by judiciously constraining the search space. In addition, simulated annealing can be repeated using the same constraints, but with varying cool-down cycles to obtain a more refined solution.

4. CONCLUSIONS

The design of friction materials is treated as a multi-criteria optimization problem in which the overall (weighted) performance of a friction composite is tracked in an n-dimensional performance space. Minimization of the objective function is achieved by a combinatorial optimization method (*simulated annealing*), which considers the influence of composite constituent selection as a design variable, and a sequential quadratic programming method, which considers the influence of the relative fractions of each constituent. Micromechanics models used here to relate the composite's microstructural design (choice of composite constituents and their relative volume fraction, shape, orientation, etc.) to overall performance have been introduced in a previous paper. This *design of materials* approach allows the materials development engineer to focus R&D efforts more efficiently and to realize application-specific design of new friction materials.

REFERENCES

1. D.M. Elzey, R. Vancheeswaran, S.W. Myers and R.G. McLellan, "Intelligent Selection of Materials for Brake Linings", to be published, SAE proceedings (2000).
2. R.M. Christensen, Mechanics of Composite Materials, John Wiley and Sons (New York) (1979).
3. A.M. Brandt, *Cement-Based Composites: Materials, Mechanical Properties and Performance*, Chapman and Hall (New York) (1995).
4. J.Aboudi, *Mechanics of Composite Materials: A Unified Micromechanical Approach*, Elsevier (New York) (1991).
5. S. Kirkpatrick, C.D. Gelatt and M.P. Vecchi, *Science* **220**, 671 (1983).
6. W.H. Press, B.P.Flannery, S.A.Teukolsky, W.T.Vetterling, *Numerical Recipes: The Art of Scientific Computing*, Cambridge University Press (Cambridge, UK), pp.326-334 (1989).

Composite materials in transport friction applications – a critical UK industry review

R H MARTIN and **S BOWRON**
Materials Engineering Research Laboratory Limited, Hertford, UK

ABSTRACT

This paper summarises the findings of a DTI funded review into the use of composite friction materials in the transport industry. The document proposes areas requiring research and development work to promote the use of composite friction materials in bulk applications. The friction materials industry in the UK is described along with the current practices of the industry in testing composite friction materials. Discussion is included on key areas for future development, identified by industry for test methods, standards and analysis techniques.

1 INTRODUCTION

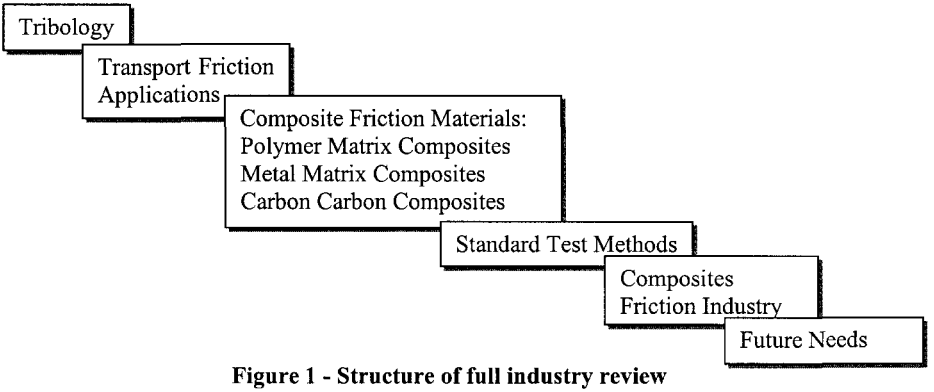

Figure 1 - Structure of full industry review

An industry review was written as one part of the UK Department of Trade and Industry (DTI) Composite Performance and Design (CPD) Programme (1). The CPD programme started in August 1997 and ended in July 2000. The aims of the programme were to maintain and develop the existing UK infrastructure relating to the performance, testing and design of components made from composites.

There exists a number of test methods used by the industry for the characterisation of composite friction materials and components. However the nature of these tests varies greatly between industries and even between companies in the same field. The aim of the review, was to highlight the test methods that are currently in use and to define requirements for

developments of these test methods to further increase the use of composite friction materials in bulk transport applications.

The tools used to develop the review included technical literature research, industrial investigations, market surveys and industrial liaison. To further identify industry needs, an industrial advisory group was established. This group comprised representatives of different sectors in the industry. A public workshop was held in conjunction with the Leeds University Brake Network (Brakenet) where representatives from across Europe were invited to attend and describe their testing approaches.

An outline of the review is shown in Figure 1. The review describes some of the basic principles of tribology and the application of friction materials in transport applications (brakes: caliper, pad-on-disc, disc-on-disc; and clutches). This paper summarises the work ongoing and future needs to increase the use of these materials in the UK. Example references are given in this paper. Further references and a Bibliography are given in the Review.

2 COMPOSITE FRICTION MATERIALS

Friction rotor components manufactured from composites have been introduced to the transport industry primarily because of their good specific properties (2). Composite friction rotors have the capability to withstand the mechanical and thermal loads demanded of them whilst offering dramatic weight reduction relative to components made from traditional materials. Reduction in component weight offers a number of distinct advantages for transport industry applications, such as performance, handling, and energy efficiency.

Increasingly stringent automotive, rail and aerospace emission standards and escalating customer expectation have made the reduction of vehicle weight a key issue for the associated industries. In the aerospace industry, any reduction in aircraft weight reduces the necessary fuel load and therefore improves the economics of flight. For Concorde, the introduction of carbon-carbon composite (CCC) friction materials significantly reduced the operational costs of supersonic transatlantic flights (3). However, the economies of weight saving are only realised with long cruise parts of the flight profile in sub-sonic commercial aircraft. For short haul airliners the additional cost of CCC braking systems may not be recuperated.

Most automotive vehicles still used traditional polymer matrix composites (PMCs) and cast iron friction couples. However, environmental factors coupled with government legislation are leading to an increased drive towards lightweight vehicles. These environmental and economic factors are increasingly driving the production automobile manufacturers to reduce component weights with the US manufacturers predicting vehicle weight reductions in excess of 5% by 2007. Heavy components such as cast iron or steel brake rotors and clutch plates are an obvious target for weight reduction and have resulted in the introduction of composite friction material components such as aluminium metal matrix composites (MMCs) (4).

For the rail industry, emergency stops in high speed trains such as the French TGV or the Japanese "Bullet Train" result in very high energy transfer and resulting high temperatures. The move to high temperature friction materials is of vital importance. High speed trains typically have four vented discs and the necessary calipers for each axle. The sum of all the brake components accounts for approximately 20% of the bogie mass and therefore reduction

of the mass of brake components is of significant advantage. The combination of good opportunities for weight reduction and a tolerance of high operating temperatures means that reinforced ceramic matrix composites (CMCs) are an appropriate technology for railway friction applications (5).

3 THE UK FRICTION INDUSTRY

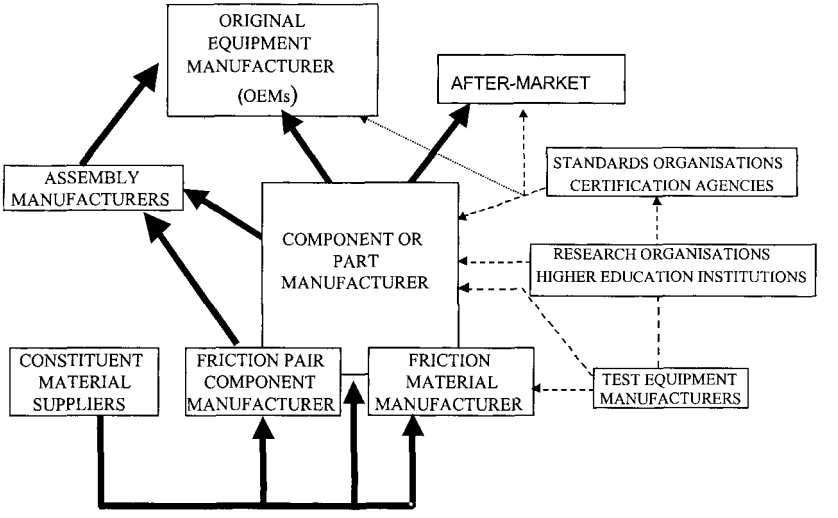

Figure 2 Representation of the UK composite friction material supply chain.

3.1 A national survey of the industry

To identify what aspects of the industry are considered the 'state of the practice' in terms of testing of composites as friction materials, a national survey was conducted. The objectives of this survey were to identify the following:

- Company information & industrial position.
- Involvement with composite friction materials.
- Testing/qualification procedures used (and associated shortcomings).
- Friction materials, applications and tests.
- Future developments in research and development needs.

Over 100 companies in the Supply Chain, Figure 2 were contacted. Over 50 of these organisations returned a completed questionnaire.

As a result of the market survey some conclusions on the nature of the transport friction industry were made. A summary of those findings, as they relate to testing and development is given below.

- The majority of end users for the friction system (car manufacturers, racing teams, railway coach builders, etc.) have minor interest in the details of the development of friction materials. They procure the brake or clutch assembly as a complete specified unit and expect it to be pre-qualified and supported by the supplier.

- Material suppliers to friction component manufacturers have a diverse client base and may know little about their material's contribution to the friction component (especially as in the case of a brake pad where the material may be interacting with up to 25 other materials from other suppliers).

- The majority of knowledge on the development of composite friction materials therefore lies with the friction material and component manufacturers.

- Similar testing schedules are used industry-wide. Often (although not always) a specimen test is conducted, followed by a component test and then a vehicle test. Difficulties in relating the specimen test to the component test, the component test to the vehicle test, and the vehicle test to the real service conditions were common.

- Performance assessment techniques were considered adequate by some. There was a strong consensus that prediction of component life was inadequate. Work is required at the formulation stage.

- The companies surveyed made limited use of finite element analysis (FEA) techniques and little attention is paid to the tribological mechanisms involved. Computational fluid dynamics (CFD) is used by some of the rotor manufacturers to increase airflow. Many saw the potential for combining FEA and CFD to gain more accurate temperature predictions.

- There was found to be no clear consensus regarding the future testing and R&D requirements. However, lower costs, reduced time-scales and improved reliability and accuracy were all stated as important requirements for future test development. Important issues to be considered for future R&D were considered to be test standardisation and improved performance.

- Confidentiality in the formulation of the friction materials is paramount. The business was regarded as highly competitive both nationally and internationally. For the racing teams a lead in the braking and clutch technology has profound influence on the results from different racing teams. Therefore, formulation information was regarded as proprietary.

3.2 Technical visits and industrial advisory group

From the responses of the national survey, selected companies were visited to gain a better understanding of the issues involved with the use of composite materials in friction applications. Following these visits an Industrial Advisory Group (IAG) was established with representatives from the different sectors of the transport industry. Because the vested interest in R&D and test development lies with the component manufacturer, only these organisations were included in the IAG. The organisations were:

- AP Borg and Beck & AP Racing
- Dunlop Aviation
- European Friction Industries

- Federal Mogul Light and Heavy Vehicles
- Lucas Varity Heavy Vehicle Braking Systems – Now Meritor HVBS
- SAB Wabco and Federal Mogul-Railway Division
- Wichita (Warner Electric)

4 STANDARDS AND MATERIALS TESTING

The procedure for composite friction material selection and verification was similar for all companies, Figure 3. Initial material selection is based on desirable physical, chemical and mechanical properties that are appropriate to the application requirement. These test methods are often based on national or international standards. For the systematic tribological evaluation of materials, the tests are usually developed by the company or sometimes the end user. Testing programmes often involve a high degree of iteration to produce optimum friction materials. Therefore the cost to develop and characterise new materials is largely empirical and expensive.

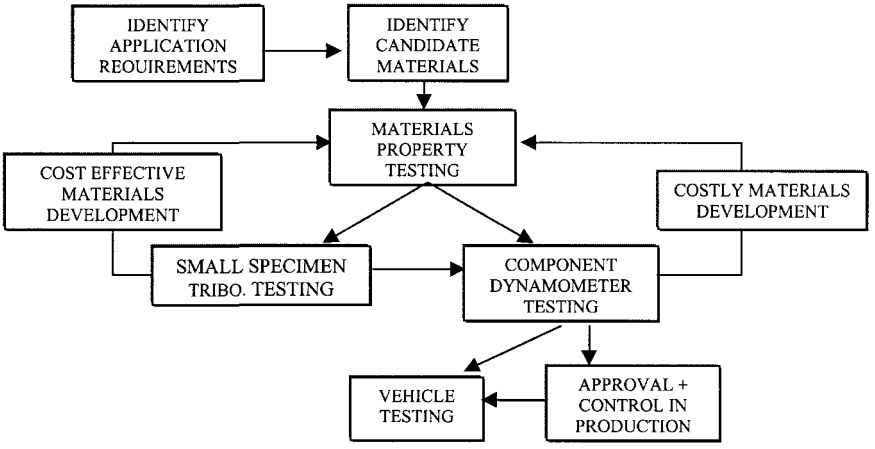

Figure 3 Developing a new friction material

Table 1- Properties of friction materials considered for design

Physical properties:	Mechanical properties:	Other properties:
▪ Density	▪ Tensile Strength	▪ Machinability
▪ Thermal conductivity	▪ Compressive Strength	▪ Processability
▪ Porosity	▪ Flexural Strength	▪ Corrosion
▪ Specific heat	▪ Shear Strength	▪ Judder & Vibration
▪ Coeff. of expansion	▪ Stiffness	▪ Squeal & groan
▪ Thermal shock resistance	▪ Hardness	▪ Environmental impact
▪ Melting/softening point	▪ Impact behaviour	▪ Emission and debris
▪ Swelling	▪ Compressibility	▪ Health and safety
	▪ Toughness	▪ Smell
	▪ Damping capacity	

4.1 Materials testing

To evaluate friction materials, a complete physical, chemical and mechanical characterisation should be carried out before a tribological evaluation. The testing of brakes involves evaluation over the widest set of conditions in order to locate flaws and behavioural inconsistencies. A list of material characteristics that should be considered is given in Table 1. Many of these properties have ISO or other national standards to measure these properties. This was not seen as an area in need of development.

4.2 Tribological testing

Tribological tests are concerned with the identification of the friction and wear properties of the friction pair. Brake friction and wear characteristics are sensitive to material composition effects, temperature, rubbing speed, pressure, and prior usage history. The overall brake design and contact geometry, the removal of wear debris and the environment also have major effects. All of these factors must be considered in a complete tribological characterisation of the friction material pair. Any friction peaking or fade effects must also be characterised.

Initial tribological testing is often carried out using small scale constant torque or constant pressure test machines. The constant torque friction test concept allows a standard comparison between different friction materials tested, by adjustment of the normal load on the sample. The same output torque is achieved which is independent of the friction level. The constant pressure friction test concept allows a standard comparison between samples of friction material tested, since the normal force is held constant, thus allowing measurement of braking torque and coefficient of friction.

Small scale tests are used to reduce the costs associated with the development of new friction material systems. These tests are not intended to replace full scale testing or indeed to fully characterise a friction material but are instead meant to act as an initial screening stage for material selection. There are a number of small scale test machines currently used by the friction industry. Some are based upon standard test methods while others have been developed in-house by individual companies. These tests are set-up to provide a comparison between potential material systems. With this form of test programme, care must be taken to ensure that the relationship between small and full scale tests is fully understood to ensure that the correct material systems are selected for further examination, for the correct reasons.

4.3 Full scale tests (dynamometers and vehicles)

In many instances small scale tests are not conducted and full scale tests on dynamometers are used for the initial stage in the evaluation of friction materials. This is because of the poor correlation between small scale tests and dynamometer tests. In addition, for many applications it is the minimisation of judder and noise that are paramount. These can only be determined with full scale tests. Therefore, duplication of actual service conditions as far as possible in the laboratory environment is desirable to enable the best prediction of the field performance of the friction materials. Brake dynamometers are designed to simulate the braking conditions of vehicles. Most inertial brake dynamometers evaluate full size components in the braking system.

For each transport method the final test is the complete system test that includes the brake. This is generally carried out on a test vehicle and is usually the final approval stage once the materials and braking system has been finalised.

5 RESEARCH REQUIREMENTS

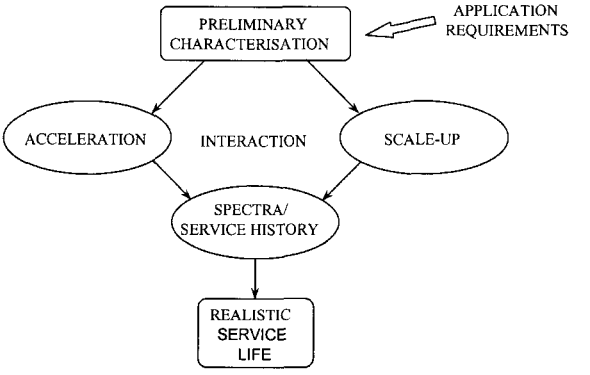

Figure 4 Research requirements for the testing of composite friction materials

From the information gathered, further research needs were identified in the use of small scale testing so that it could be more meaningfully scaled up to give more realistic information, such as wear, NVH and judder relevant to the braking system. This is illustrated in Figure 4. With new materials such as CCCs and CMCs, there is need to better understand how the physical properties and microstructure effect the tribological properties. This can be carried out on a small scale and, once understood, physical properties can go a long way to evaluating materials for use as friction materials. Small specimen tribological tests offer the opportunity to conduct rapid testing and development of materials prior to the manufacture of a full scale component. This approach leads to savings of cost and time and permits faster materials development.

5.1 Characterisation

The application requirements for the friction material must first be considered. Each specific component type has a unique set of conditions over which it is required to operate. For example, the range of temperatures, pressures and sliding velocities that a component must operate at can be summarised as in Figure 5. Evaluating the application requirements for each component type is essential to the process of developing new testing procedures that will be useful to aid in the transition of technology between industries.

While some of the basic material properties discussed above are useful for screening purposes there is a need for increased understanding in relating these basic material properties to the tribological properties of the friction pair. This knowledge does not exist extensively for the 'new materials' such as CCCs, CMCs or MMCs. Knowledge of this relationship could also be improved even for 'traditional' PMC/cast iron friction couples. By gaining an understanding of this relationship, material selection to meet a customers' needs would be simplified. The effect the transfer film, or surface morphology, has on the tribological properties and the mechanisms by which the surface morphology is formed and altered must be understood. For

tribological properties it is necessary to generate 'maps' showing the tribological behaviour of these materials against different parameters to aid in materials selection, see Figure 6. Through this process surface morphology should be tracked.

An understanding of the effects of processing on the material and its tribological behaviour would also allow friction materials to be optimised through processing. While this information is useful in screening or ranking materials there is some difficulty relating tests of this kind to the behaviour of larger components and the effects of scale up must be researched.

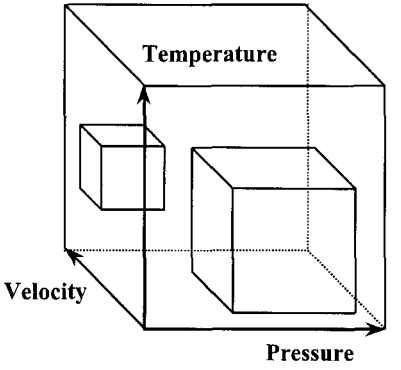

FIGURE 5 Range of parameters

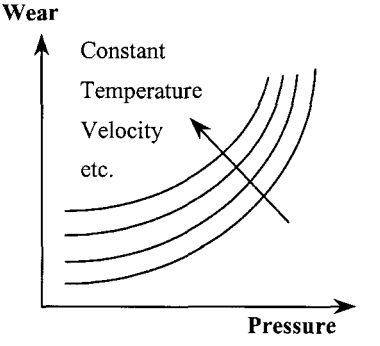

FIGURE 6 Tribological maps

5.2 Scale-up

Once the understanding of how physical properties relate to tribological properties is improved, the need to identify how this understanding can be scaled-up is required. As in all engineering applications the issues of scaling up coupon data to in-service data is non-trivial. Often, smaller coupons have to be made separately or in a different manner to full scale components. Flaws and inclusions in the material dominate mechanical properties such as strength. As the volume of the material increases, the probability of a significant flaw being present in the material increases thereby reducing the apparent strength. The same may apply to the tribological properties and the transfer film, both of which may be effected by flaws and inclusions in the friction material.

Perhaps of more significance is the change in heat transfer and air flow around a reduced sized pad compared to an actual brake pad applications. Further the effect of the shape (circular, square, etc.) of the reduced coupon and the effect of the edge may all play a role in complicating scale-up procedures.

Currently, the friction materials industry only run scaled tests such as wear tests for commercial reasons. For their customers and to meet legislation, it is the performance of the vehicle that is paramount. For commercial aircraft, stopping is the only requirement that is legislative. For automobile brakes NVH and anti-judder can predominate over wear properties. For automobile clutches the road duty levels supplied by the customer which are specific to the vehicle dictate performance.

5.3 Accelerated testing

With the possible exception of automobile racing, it is impractical to test friction materials for their full expected life. Various acceleration methods are used by industry. These include changes in temperature, longer running schedules or reduced distance road load data. There is a general lack of knowledge with regards to acceleration of test methods industry wide. A truncated schedule is often used and extrapolated. Confidence in this extrapolation would require an accelerated testing methodology to be developed.

The term 'accelerated testing' can include a variety of methods. The effect of mechanical load can often be emphasised by increasing the load, applying it more rapidly or cycling the load on and off. Changes to the material properties such as ageing, swelling, embrittlement, etc. can often be accelerated by increasing the parameters that are responsible for the physical or chemical change in property, such as temperature or oxygen content. For example, a given interface under given loading conditions experienced oxidation dominant wear. Increasing the oxygen content of the immediate atmosphere may increase the wear rate of the specimen without changing the nature of the wear mechanism itself.

The fundamental rule for accelerating any test is that the acceleration parameters must not change the mechanism being measured. For frictional applications, the prime concern is to reproduce the frictional interfaces that dominate the response but in a shorter time period. Increasing (or decreasing) the severity of the test temperature, pressure, sliding speed, environmental conditions, etc. may also be means to accelerate the degradation mechanism of interest.

5.4 Spectra and service history

The previous two sections on scale-up and accelerated tests largely cover basic tribological properties under uniform loads. For these data to correlate to dynamometer or vehicle data, the move to take this information one step further to spectra or real service history data is required. Service spectra is often unique and confidential to individual OEMs. There have been moves to develop harmonised specifications such as AK Eurospec for the Automobile Industry, but these may never replace individual OEM requirements. Therefore, the scaled down machines must also allow computer control to simulate the service spectra.

5.5 Research co-ordination in the UK

There are efforts to co-ordinate the various activities within the UK with regards to the friction industry. The British Friction Materials Council (BFMC) represents the UK friction industry at regulation level. They are road transport and phenolic/formaldehyde pad focused. Hence they do not deal with advanced composite rotors. The recently initiated Brakenet organised by Leeds University and sponsored by the EPSRC, has the remit to co-ordinate R&D efforts in automobile braking between universities, RTOs and companies. This is seen as an important step towards coordination.

6 CONCLUDING REMARKS

Recent development necessitated by environmental and technological interests has over the past 30 years seen the introduction of fibre reinforced polymer matrix composites. These materials often comprise of a fibrous yarn such as glass, aramid or carbon in a phenolic resin binder. Other 'ingredients' are included to improve friction performance. These materials

now form the bulk of friction material usage. Their properties are reasonably well understood by the manufacturers. However, there are still applications, such as the replacement of asbestos based brakes in the light aircraft industry, that may require further demands on this grade of material. There will always be a drive to reduce cost and increase life and performance in these materials which is where most effort is now placed.

Higher energy dissipation applications produce demands that cannot be met by polymer based composite friction materials. This has presented the need to introduce CCCs and CMCs. While the former has been in the aircraft industry for decades its introduction into motor racing is more recent. Introduction of CCC into production vehicles or heavy good vehicles still appears a long way off. The high cost and poor cold wet friction properties will restrict their use in production automobiles for many years. CMCs are a promising new material and further tribological knowledge on them is required. Most data generated to date remains company confidential. Early indications are that they may be the only material of choice, despite the current cost, in some high energy braking, e.g. high speed trains.

As part of the move to lighter vehicles, composites have also seen applications in the rotors or discs in vehicles. The use of MMCs to replace the heavier steels and cast irons has made a successful move into the production car industry. The ability to use conventional polymer based pads and coatings on the reinforced aluminium pads has been an advantage for this material. However, the cost still is higher than regular rotors so they have mainly been utilised on higher performance cars.

The move for the original equipment manufacturers (OEMs) to require warranty and liability demands to the component supplier has resulted in a need for the composite friction material supplier to better understand the performance and life of their product. This is now mostly achieved through full-scale tests on dynamometers because of the lack of confidence from small scale tests. This is an expensive method of developing materials and still provides only an extrapolation of service life.

7 REFERENCES

(1) Composite materials in transport friction applications - A critical industry review, July 1999, Materials Engineering Research Laboratory, Hertford, SG13 7DG, UK.

(2) **Bijwe, J.**, Composites as friction materials: Recent developments in non-asbestos fibre reinforced friction materials – A review, Polymer Composites, June 1997, Vol. 18, No. 3.

(3) **Fisher, R.**, Carbon-carbon brakes for aircraft, Middleton, D. H. (Ed.), Composite Materials in Aircraft Structures, Longman Scientific & Technical UK (1990), pp. 336-340.

(4) **Denholm, M. J.**, Aluminium metal matrix composites rotors and drums - A future trend, in Barton, D. C. and Haigh, M. J. (Eds.), 2nd International Seminar on Automotive Braking - Recent Developments and Future Trends, Leeds, UK, 14-15th May 1998, Professional Engineering Publications, London and Bury St. Edmunds.

(5) **Hubbard, D.A.**, New materials in railway braking – The next generation, Barton D.C. (Ed.), Advances in Automotive Braking Technology, Mechanical Engineering Publications, London and Bury St Edmunds (1996).

Braking Systems and Vehicle Performance

This page intentionally left blank

Measured benefits of the exhaust pressure modulator valve (EPMV) used for retardation of commercial vehicles

L ROWLEY and **I BATES**
WABCO Vehicle Control Systems, Leeds, UK

SYNOPSIS

The paper discusses some of the general claims made regarding the benefits of fitting exhaust braking devices. It then goes on to report specific vehicle testing carried out to substantiate these claims. Advantages in the areas of foundation brake usage and compressor on-load times are examined after commercial vehicle testing. The paper focuses on the use of the exhaust pressure modulator valve (EPMV) during urban running. Comparisons to other retardation devices are also made.

1 INTRODUCTION

With almost ten years of design and development invested, the EPMV is today, a commonly seen part on the modern commercial vehicle. Now a mature product, the users are reaping the savings and benefits inherent to this method of endurance braking. The EPMV is a technology enhancement of the conventional butterfly exhaust brake (CEB) and a patented WABCO Automotive device. The EPMV differs from the CEB in the design and function of the butterfly mechanism. In the CEB, the butterfly is simply a balanced valve that restricts the exhaust flow as much as is physically possible without creating seizure. Its fixed orifice creates a linear increase in engine back-pressure with speed, up to the engine manufacturer's safety limit at maximum overrun condition. See figure 1 (Ref. 1). The primary benefit of the EPMV can also be seen on this same graph; this being the greater back-pressure (and therefore braking) at lower engine speeds. The design aspect that creates this advantage is primarily the offsetting of the butterfly centre relative to its axis of rotation as shown in figure 2. When the butterfly is closed, the exhaust pressure generated between the engine and the EPMV, reacts on the butterfly, resulting in a torque at the axis. This torque then reacts against the output of a pneumatic actuating cylinder. When the butterfly torque becomes sufficient to

overcome the actuator cylinder load, the butterfly opens slightly. This venting maintains a pressure balance that can be clearly seen in figure 1. This design of valve is often referred to as Variable Orifice Valving.

With this increase in engine back-pressure at lower engine speed clearly visible, the main driver for developing these devices becomes clear. Furtherfore, the EPMV brings additional benefits, making it even more attractive to the vehicle manufacturer and user. Not only does the EPMV carry over the benefits of the CEB listed below (2):

- Increase in brake lining life.
- Reductions in tyre wear.
- Reduction in fuel consumption.
- Reduction in running times. Particularly in extremely mountainous conditions.
- Engine life extension due to the cushioning effect of back-pressure in the overrun condition.
- Reduction in driver fatigue.

The EPMV also increases these advantages due to the inherent superiority in braking performance; more than double the retardation across the full engine speed range offered by the CEB (1). Other benefits, above and beyond those offered by the CEB, include additional functionality and flexibility. These are due to the design and configuration of the EPMV and control system employed. See figure 3. The introduction of a proportional pressure valve allows the varying of the pneumatic actuator input pressure to directly proportionally vary the maximum back-pressure generated. This means that the EPMV can be used for functions other than braking. i.e. lower actuator input pressure at idle could accelerate engine and cab warm-up by generating around 2 bar gauge back-pressure. Looking at figure 1 it can be seen that to generate this level of back-pressure with a CEB, the vehicle would need to maintain higher exhaust flow equating to circa 650 r/min. An idle speed for a modern commercial vehicle is typically 500 r/min.

A by-product of this same function is the improvement of white smoke emissions on warm-up. This is largely due to the simple fact that fuel combustion improves with cylinder wall temperature. Therefore by retaining heat in the cylinder, more of the fuel is burnt and less is exhausted as 'white smoke' and fuel economy is improved as a result. Again, the same activity performed by a CEB would demand a higher engine speed. Another benefit of the EPMV function is its ability to protect the engine against potentially damaging excess pressures during engine over-run conditions. Short-term overspeeds of up to 25% are possible with a laden vehicle using the CEB to control long descents (1).

Some of these claims have been substantiated in the past and almost all have been regularly realised and reported by users. In this paper it is intended to analytically prove and quantify some of these benefits by studying controlled vehicle journeys with a 'typical' vehicle on a 'typical' urban route.

2 VEHICLE TESTS

2.1 Test Procedure

The basic objective of the testing was to compare the brake and compressor usage on similar test runs. The first run analysis was performed using the standard EPMV set-up, the second

with the EPMV permanently switched off. This, ideally, was to be the only difference between the runs. The vehicle was instrumented to record the relevant inputs and outputs of the vehicle's individual devices. The difference in the data for the two runs illustrated the benefits given by the EPMV. The main areas of interest were how often and to what extent the foundation brakes were used and also how often the compressor was on load. From these readings actual physical savings could be extrapolated relating to the claims made in section 1. One thing to note at this point is that although benefits were expected to be seen, it was also recognised that these would be almost worst case benefits due to the nature of the route selected; the route being an urban cycle further described in section 2.2. In terms of route types to emphasise the benefits of the EPMV, a list of routes from worst to best would be as follows; motorway, urban, hilly, and finally, mountainous.

2.2 Vehicle Preparation

The vehicle selected for this testing was a 38T tractor semi-trailer combination with a 12 litre turbocharged 6 cylinder diesel engine. The trailer was, however, only loaded to the reduced all up weight of 32T.

Instrumentation was added to the tractor to allow the following test parameters to be measured:

- Controller Area Network bus details of engine speed & road speed.
- Front brake chamber pressure.
- Rear brake chamber pressure.
- Compressor delivery pressure.

These items were then continuously recorded while on the runs at 150μs intervals.

It is important to note here that at no point was the actual braking performance of the EPMV being measured. This had been done more than once in the past and duly reported. What is of interest here is the control of the EPMV. In this instance it can assumed that the WABCO unit installed was only a single signal device providing just the one level of back-pressure, this being nominally 6.5 bar gauge. The operation of the EPMV was foot-brake synchronised. i.e. the foot pedal has an integral switch that signals the EPMV prior to the foundation brakes being applied.

2.3 Urban Route

The full route details can be found in appendix A. The main points to note are that the route is 75.3km in length set in the heart of West Yorkshire. Although West Yorkshire is quite hilly, the route takes the main 'A' roads that follow the valleys. It is estimated that over the full route no more than 200m change of altitude is experienced. The route does not take in any motorways but does use dual carriageways for a limited time at certain points.

2.4 Vehicle Runs

Attempts to make the runs as similar as possible were reasonably successful in that the runs were made at the same time of day, on weekdays of the same week in similar weather conditions using the same driver. The full run details can be seen in Appendix B.

3 RESULTS AND ANALYSIS

The pressure readings of the brake chambers and compressor delivery were, as described earlier, logged against time. Focus was confined to two distinct areas. The first is depicted in figure 4. This shows the two different sets of front brake chamber pressures set against the same time scale. Only a sample of the total data recorded is shown here for clarity. Depicted here, in real terms, is the number of times the front brakes are actuated and the effort used. This, after further analysis would provide a measured difference in foundation brake usage with and without the EPMV. To do this, the sums of the pressure measurements for each of the runs were compared. The results show that over the run the front brake chambers were used 14% less when the EPMV was employed.

The second area of interest, compressor activity, is shown in figure 5. Again this is a sample graph showing the main elements. The output pressure of the compressor is logged against time. This is then describing how much work the compressor is performing. The pressures are summed as before and the full results show a 9% reduction in compressor work (cumulative pressure generated). This figure confirms the fact that much less air usage occurs when the EPMV is employed in comparison to foundation brakes only.

Further analysis has been conducted to compare the work done by the brakes. The method of performing this comparison is to multiply the working pressure on the brakes (measured brake chamber pressure less threshold pressure) by the vehicle road speed. The threshold pressure is pressure required in the brake chamber to overcome the inertia in the brake mechanism; seal friction, pull of spring loads etc. A nominal value of 50kPa was used. This gives a general figure for work done by the brake linings.

Brake lining life can now be extrapolated for each run type and compared. The results can be seen in figure 6, where the average work done at the front brakes is given for runs with the EPMV on and off. The results show a 43% reduction in work done by the front brakes when the EPMV is employed. The difference when compared to the simple brake usage is due to the number of applications made under the threshold pressure and the function of the EPMV to reduce the use of foundation braking effort.

4 CONCLUSIONS

The benefits in foundation-brake usage and compressor on-load times are very much dependant on the circumstances in which they were measured. To this end, it can be stated that, when compared to the list of historical claims shown in section 1, these savings are reasonable for the urban route performed. The reductions seen in the foundation brake usage and work done at the brakes can be read directly across into brake lining wear and also the less tangible area of driver fatigue. The reduction in compressor work has a direct effect on fuel economy. It can be considered that the average commercial vehicle compressor would create a 3% parasitic loss when on load (3). Any reduction in this would be advantageous. i.e. 0.3% increase in fuel economy due only to reduced compressor on-load times. Maintenance frequencies and, therefore costs would also be realised due to the 9% reduction in compressor loading. This fuel saving, for reduced compressor on-load times, would recoup the cost of fitting an EPMV to a 12 litre commercial vehicle running, typically 2000 hours a year in around 18 months (3).

Although these benefits are substantial in themselves, the use of the EPMV is made even more attractive if different methods of retardation are also compared. The majority of the benefits quoted, both historic and measured, are as applicable to the other retardation devices, to varying degrees, as they are to the EPMV. (brake lining life, fuel economy, driver fatigue, etc.) As legislation demands retardation capability which necessitates an additional retarding device on heavy commercial vehicles (4), a selection of device becomes necessary. Other properties then become critical. i.e. weight, package size, cost and braking effectiveness. Figure 7 (Ref. 5) compares various devices used for retardation. The EPMV has almost 60% of the retardation power of the device with the best retardation (the electromagnetic-type) for 10% of the cost and 5% of the weight and size.

The benefits of the other devices must of course be considered for the individual application. For instance foundation brake usage can be reduced to almost zero in some urban bus applications if an electro-magnetic or hydro-mechanical device is employed. This could make the more expensive devices very attractive when maintenance time and costs are considered. Also the engine head brake is being more commonly designed-in to new engine developments. This obviously reduces the weight and cost when compared to a retro-fit device. All things considered, with the multi-functionality it exhibits, (Cab warm-up, emissions reduction) the EPMV is an enticing choice for the general population of endurance brake applications. Except in specialist applications, the size and expense of the electro-mechanical and hydro-dynamic devices only becoming viable for use in the medium to highly mountainous regions (6).

5 REFERENCES

1 RG Baines, Exhaust Brake Retarders, IMechE Conference Paper 1993
2 HB Smith, Exhaust Brakes, IMechE Conference Paper 1974
3 AH Beck, et al, Developments in Compressed Air Management for CV Braking Systems, Brakes 2000 Conference Paper
4 Braking Regulations, ECE Regulation 13 Annex 5 Page
5 AJ Day, Braking of Road Vehicles, University of Bradford 1998
6 Prof.C Von Glassner, Braking of Road Vehicles, Memorial Lecture University of Bradford 1998

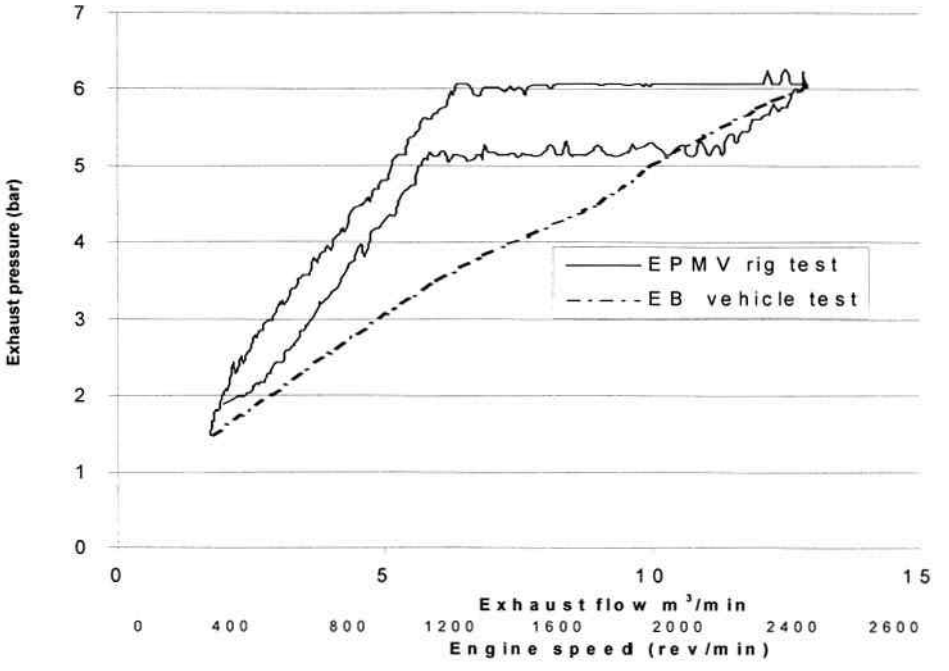

Figure 1 **EPMV and CEB Back-pressure Generation**

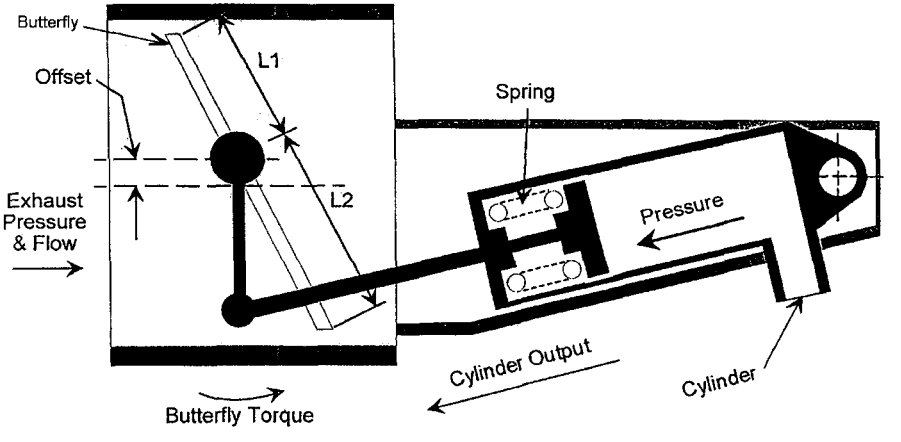

Figure 2 **Schematic of the EPMV Function**

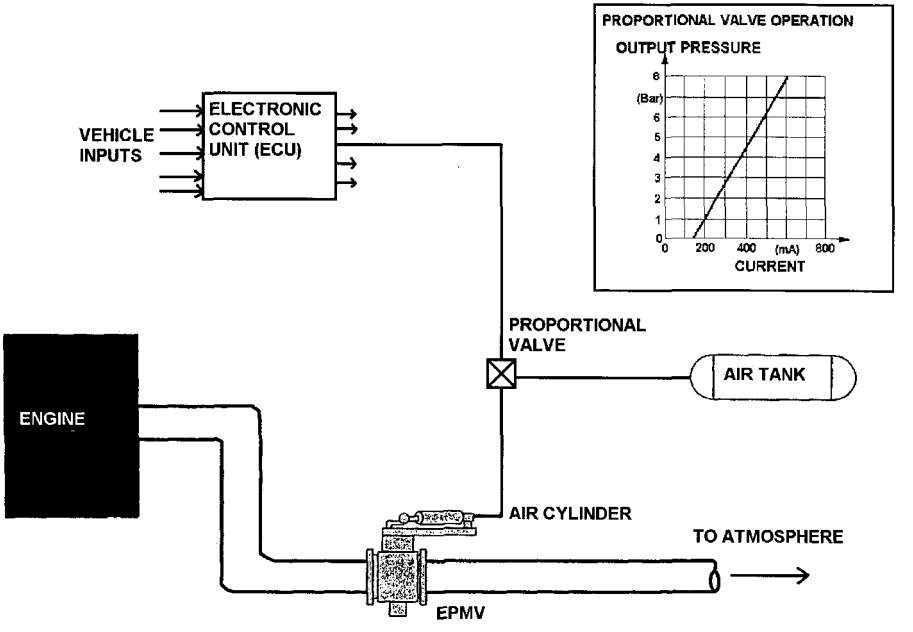

Figure 3 **Schematic of the EPMV Control**

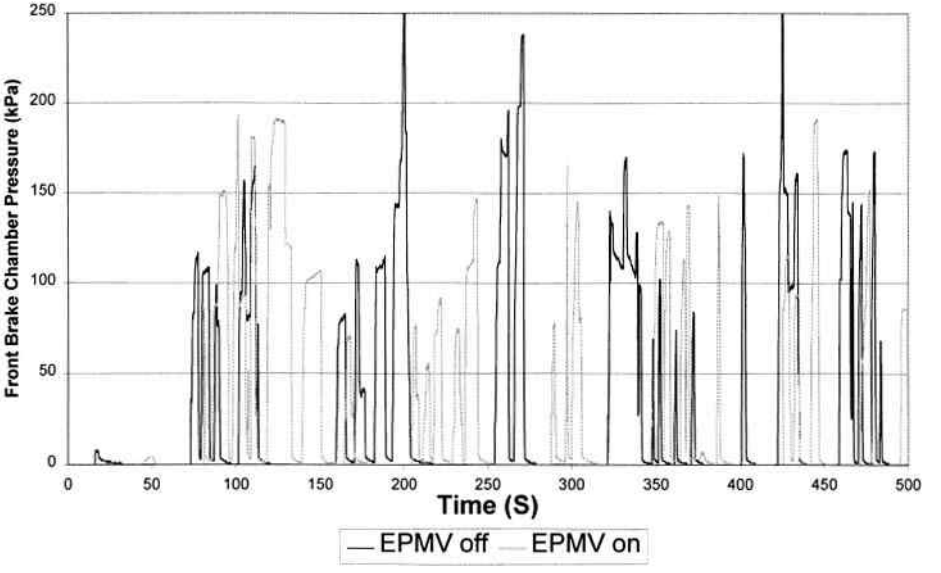

Figure 4 **Recorded Front Brake Chamber Activity**

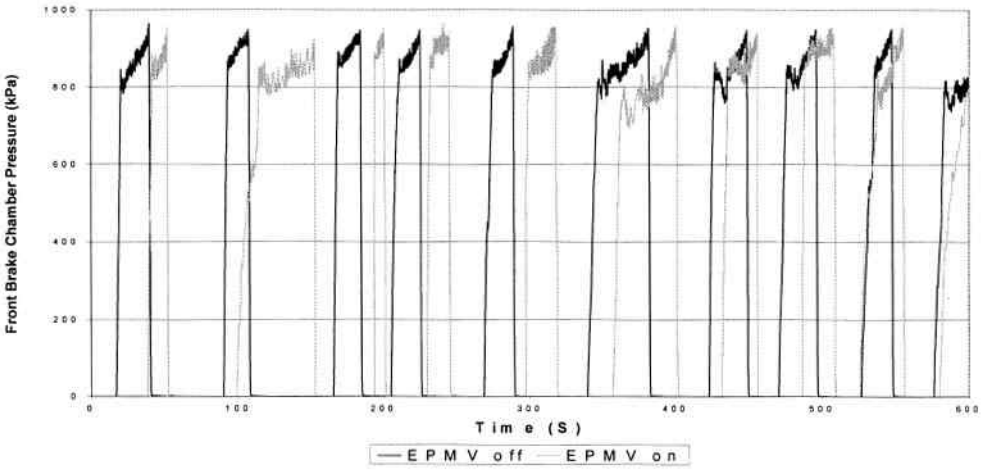

Figure 5 Recorded Compressor Activity

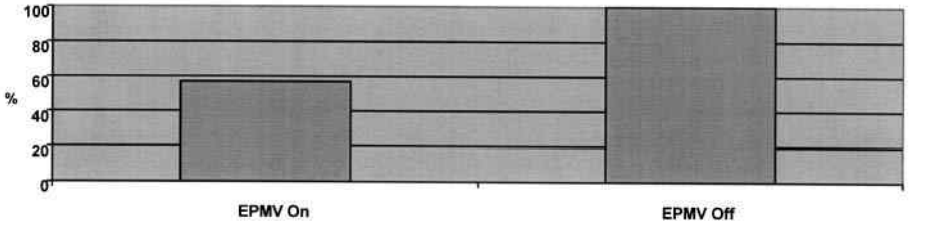

Figure 6 Comparison of Work Done by the Front Brakes

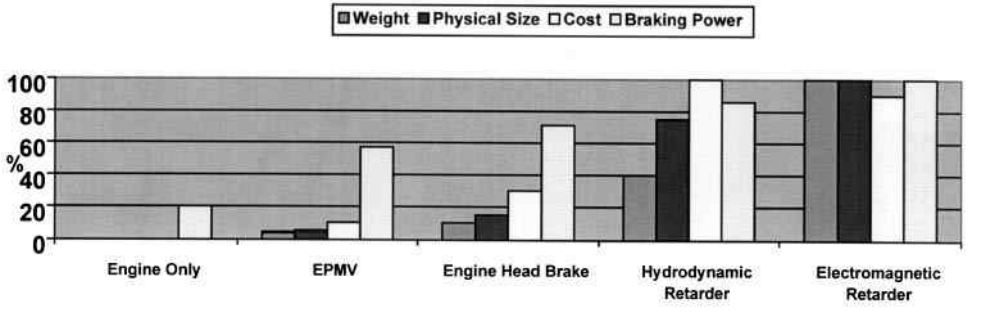

Figure 7 Comparison of Retardation Devices Neglecting Foundation Brakes

Urban Route			
Junction and Direction	**Take Road Number or Name**	**Towards**	km Reading
Start	A650	J28 of M62	0.0
Roundabout	A653	Leeds / Airport	1.0
Straight on / left fork	A6110, Leeds Outer Ring Road	City Centre + Leeds + Airport	3.9
Roundabout (M621)	A6110, Leeds Outer Ring Road	City Centre + Leeds + Airport	6.0
Roundabout	A6110, Leeds Outer Ring Road	Bradford	10.3
Slip Road	A647	Bradford	10.8
Roundabout / left filter lane	A647	Bradford	14.3
Traffic Lights, right	A650	City Centre North + Keighley + Skipton	19.0
Slip Road, sharp left	Canal Road	Foster Square Retail + City Centre North	20.0
Traffic Lights right fork	A6181, Hamm Strasse	Foster Square Retail + City Centre North	20.1
Traffic Lights, right	Manningham Lane	Manningham + Frizinghall (HGV Diversion Route)	20.6
Traffic Lights, Straight on	A650	Keighley	21.7
Traffic Lights, Straight on	A650	Skipton	24.3
Roundabout	A650 (Dual Carriageway)	Skipton + Keighley	31.9
Roundabout, U Turn	A650	Bradford	35.4
Traffic lights, Left Filter Lane	A6181, Hamm Strasse	Foster Square Retail (HGV Diversion Route)	49.7
Traffic Lights, left	Canal Road	Wakefield (A650)	50.2
Traffic Lights, right	A650	Wakefield	50.4
Traffic Lights, Straight on	A650	Brighouse & Huddersfield	51.3
Traffic Lights, right fork	A641	Brighouse & Huddersfield	51.6
Traffic Lights, left	A641	Brighouse & Huddersfield	52.3
Slip Road / Roundabout	A638	Dewsbury	54.9
Roundabout (M62 & M606)	A638	Dewsbury, Heckmondwike	58.2
Traffic Lights, sharp Left	A638, Dewsbury Ring Road	Wakefield	68.2
Traffic lights, Left Filter Lane	A653	Leeds, M62	68.5
Roundabout	A650	Bradford, WABCO	74.2
End		Total	75.3

Appendix A Urban Route Summary

Run 1 Information	
Comments	EPM on Automatic
Vehicle Description	12 litre 4x2
Weight	32 tonne
Date	24/8/98
Route	Urban
CAN Nodes connected	Engine
Conditions	Sunny
Start Time	13:20
Finish Time	15:25
Start km	287275
Finish km	287340
Ambient Air Temperature	19.6°C
Ambient Air Relative Humidity	43%
Battery Voltage	24

Run 2 Information	
Comments	EPM off
Vehicle Description	12 litre 4x2
Weight	32 tonne
Date	26/8/98
Route	Urban
CAN Nodes connected	Engine
Conditions	Fine
Start Time	13:20
Finish Time	15:15
Start km	287710
Finish km	287775
Ambient Air Temperature	19.5°C
Ambient Air Relative Humidity	48%
Battery Voltage	24

Appendix B Run Information

Testing of ABS operation in stand conditions

A GAJEK
Institute of Automobiles, Cracow University of Technology, Poland

ABSTRACT

The paper presents the results of tests of antilock braking systems (ABS) carried out on the fast rotating roller stand with inertial mass. The results of braking tests for passenger cars on the homogeneous surface and on the surface with changing adhesion coefficient have been presented. Qualitative and quantitative parameters for diagnostic assessment of ABS operation have been proposed.

1. INTRODUCTION

So far diagnostic control of ABS during exploitation has included only current examination of electronic and electrical parts. It is realized by the selfmonitoring system integrated with the electronic control unit ECU and by control devices (diagnostic testers) in stand conditions. This diagnostic system checks electronic and electrical elements. Mechanical and hydraulic parts are not controlled currently. Up to now, the routine, periodic vehicle brakes inspection does not include checking the ABS operation as a total unit, which would allow us to examine the effect of ABS operation (to check wheels speed at time of braking). It is an important problem, because the interaction between electrical and mechanical parts decides the correct operation of ABS. The kinetic method of brakes control in stand conditions gives possibilities to examine the ABS operation as a total unit (2,3,4). The results of ABS tests on that kind of stand and analysis of ABS operation are presented below.

2. PRINCIPLE OF STAND CONTROL

Fig. 1 shows the scheme of the diagnostic stand. The tested car is driven on the four units of the stand. Each unit consists of driving drum 2 connected with inertial mass 7 (front), 8 (rear)

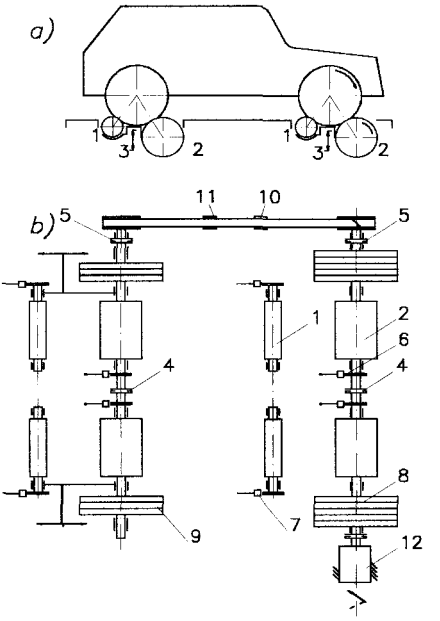

Fig. 1. Scheme of the test stand: 1- support rollers, 2- driving drums, 3 - system of car lifting and blocking support rollers, 4, 5 - electromagnetic clutches, 6 - drum speed sensors, 7 - support rollers speed sensors, 8, 9 - inertial mass front and rear wheels, 10, 11 - transmission (toothed belt and belt stretcher), 12 - electrical drive

and support roller 1. Rear units can be shifted exactly to the wheel base of the tested car. Inertial masses are divided into front and rear units in 2:1 ratio, corresponding to average brake distribution for passenger cars. Setting of drum 2 and support roller 1 (roller higher than drum) and direction of rotations prevents the car wheels from being thrown out from the stand and keeps them in contact with rollers and drums. The stand is equipped with a system for lifting the car and blocking support rollers for safety of drive on and drive out from the stand.
During the test the electromagnetic clutches and toothed belt connect four units into one set. There is a possibility to follow the test on disconnected units, but in that case different conditions of braking are simulated for front and rear wheels.
Car wheels with driving drums, inertial mass and support rollers are driven by electric motor 12. When the speed of the car wheels is about 45....50 km/h, electromagnetic clutch uncouples the drive and the brakes are intensively applied. Car wheels and rotating elements of the stand are braked until they stand still. During braking the peripheral speed of the drums (it meets the speed of the car) and peripheral speed of the rollers (as the speed of the braked wheels) are measured. The measured parameters are automatically transferred to computer.
The investigation has shown that because of small mass of the roller and its moment of inertia over dozen times smaller than the car wheel, the slip between wheel and support roller is near zero. It allows us to calculate the speed of the car wheel on the base of measurement of the speed of the support roller (for diagnostic purposes). The surface of support rollers ought to be coated with special material which has high adhesion coefficient when dry and wet. The

stand makes it possible to change the tire-road coefficient of friction. Individual spraying water on the drums surface allows for any combination of changes of the adhesion under the wheels. The stand makes it possible to test cars with 2.35m x 2.85m wheel base.

3. RESULTS OF INVESTIGATION

3.1. Qualitative analysis of ABS operation

Fig. 2 shows changes of the peripheral speed of drums v_s (matching car speed) and wheels speed v_k, at time of intensive braking with ABS acting. These dependencies correspond to the car braking on the road with constant tire to road friction coefficient during straight ahead braking.

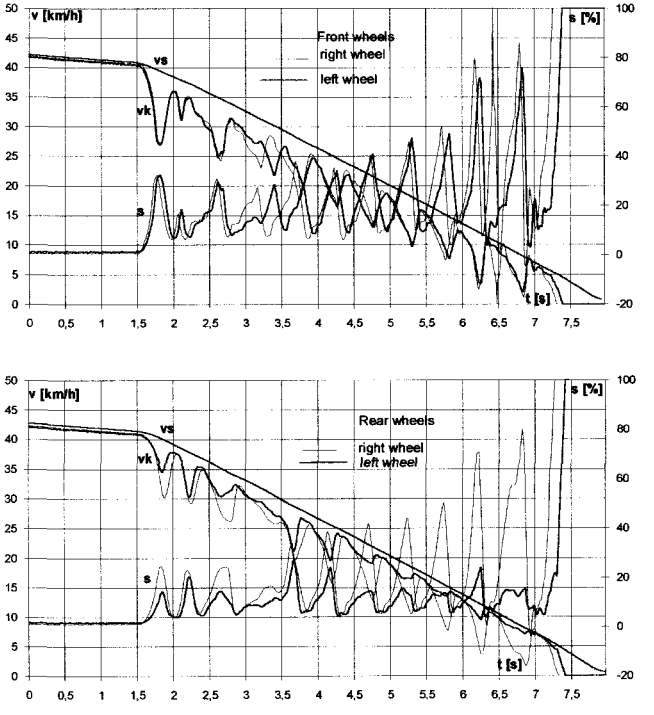

Fig. 2. Changes of the speed of drums v_s (matching vehicle speed), wheels speed v_k and slip $s=(v_s-v_k)/v_s$ during braking with working ABS on dry, homogeneous surface

The qualitative assessment of ABS operation consists of:
- Estimation of lock duration of the braked wheels and the frequency of regulation. According to (1) permissible are momentary locks, without causing loss of stability and steerability of the car. For the tested ABS the lock moments did not occur for the vehicle speed above 10 km/h.
- Estimation of the lower speed of ABS operation. Tested ABS switched off the operation when the wheel speed reached 5 - 10 km/h and the car wheels stopped with blocking. This is a correct operation of ABS.

- Estimation of symmetry of ABS operation on a homogeneous surface of the stand by covering the courses of speeds for left and right wheels, Fig. 2.
- Estimation of ABS adaptation to changing conditions of adhesion between wheel and drum surface, Fig. 3. The braking wheel "comes suddenly" from the surface with bigger tire-road coefficient to the surface with smaller coefficient of friction. This effect is obtained by sudden wetting of the dry surface of drum. Courses of the speed and slip of braking wheels allow checking if the wheel is locked in changing conditions of road adhesion. Fig. 3 shows that passage from rough to more slippery surface causes increase of the wheel slip but the wheel is not locked. This test enables us to check the response of ABS to the jumping input (step function input).

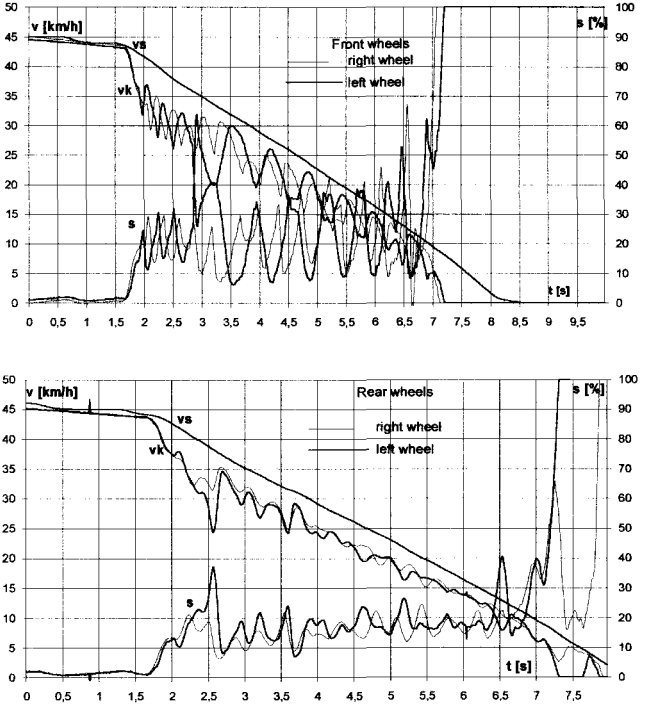

Fig. 3. Changes of the speed v_s (matching vehicle speed) and wheel speed v_k during braking with working ABS on the surface with changing tire-road coefficient of friction under left wheels

3.2. Quantitative analysis of ABS operation

The quantitative assessment of ABS operation consists of:
- Estimation of the wheel slip regulation.

Diagnostic criterion of the slip course correctness has to be unique and constant for the given category of cars. For that reason it is necessary to establish a value of optimum slip s_{opt}. For the diagnostic estimation of the ABS operation it was assumed, that s_{opt} means the slip, for which adhesion coefficient between tire and stand surface reaches maximum value. It depends

on the kind of surface, tire model, changing wheel speed (5). The results of investigation show that on the stand with dry steel surface of drums, optimum slip was 0.18....0.25. When this type of estimation is used in the practice of diagnostics of ABS, value s_{opt} should be determined in consultation with the manufacturers of these systems, because this parameter results from the ABS control strategy adopted. After establishing s_{opt} value we can determine the coefficient of the optimum slip utilisation:

$$k = 1 - \frac{\Delta L}{L_{kopt}} = 1 - \frac{\int_{t1}^{t2} |s_k - s_{opt}| v_s dt}{\int_{t1}^{t2} (1 - s_{opt}) v_s dt}$$

Parameter ΔL represents the difference between the real distance passed by braking wheel in time $t_2 \div t_1$ and the distance which the wheel would pass for the optimum brake slip in the same time $t_2 \div t_1$:

$$\Delta L = \int_{t1}^{t2} |s_k - s_{opt}| v_s dt$$

$t_1 \div t_2$ analyzed time of ABS operation,
s_k real slip of the wheel, $s_k = (v_s - v_k)/v_s$
s_{opt} optimum brake slip on the drum surface,
v_k real speed of the wheel,
v_s speed of the vehicle (drums)

The physical interpretation of the ΔL value is shown in Fig. 4. Value L_{kopt} represents the length of the road, which the wheel would cover if its slip was constant and optimum, and deceleration the same as in time of real braking:

$$L_{kopt} = \int_{t1}^{t2} v_{kopt} dt = \int_{t1}^{t2} (1 - s_{opt}) v_s dt$$

The calculation of ΔL and L_{kopt} values requires determination of s_{opt}. Coefficient k is calculated in the range at braking speed 40 - 20 km/h. The narrow interval of speed for determining coefficient k allows us to assume a constant value of s_{opt}. For our stand, on the base of the results of tests, the assumed $s_{opt} = 0.18$.
The value of coefficient k ought to tend to limit 1. From the tests done so far it follows that for efficient ABS unit, coefficient k ought to be higher than 0.9.
As the ABS tests on the stand are carried out in the same conditions, the results of investigation for different cars are comparable.

- Estimation of adhesion utilization

Detailed analysis of the estimation of adhesion utilization is presented in (4). In stand conditions, for diagnosis of the ABS, parameter e_{st} is determined from the following dependence:

$$e_{st} = \frac{\varepsilon_{ABS}}{\varepsilon_{max}} = \frac{\left[(\omega_{40} - \omega_{20}) / (t_{40} - t_{20})\right]_{ABS}}{\varepsilon_{max}}$$

It is a ratio of deceleration of stand inertial mass ε_{ABS} for braking with ABS acting, to maximum deceleration of these mass ε_{max} in time of braking without ABS. Value ε_{max} is calculated at the moment when the first of the wheels achieves the limit of blocking. Because there is no effect of loading and lightening of the car axes on the stand, coefficient e_{st}

represents coefficient of adhesion utilization. The results of stand investigation show that the value of that coefficient was in the range 0.82.....0.89.

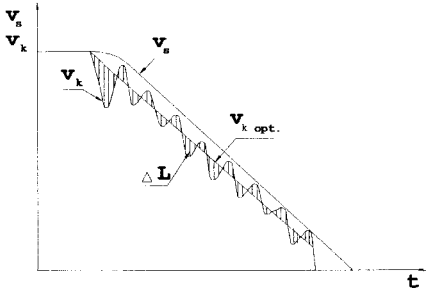

Fig. 4. Simplification of ABS operation. v_s - speed of the car, v_k - speed of the wheel, v_{kopt} - optimum speed of the wheel for constant slip s_{opt}

- Estimation of symmetry of ABS operation

Symmetry of ABS operation can be determined by amplitude-frequency characteristics of wheels deceleration or wheels slip. Wheels deceleration $a_h(t)$ is calculated on the base of measurement of wheels speed. If we set out that characteristics $a_h(t)$ are continuous and periodical functions, satisfying Dirichlette conditions, than we can write Fourier integral (in complex form):

$$a_h(t) = 1/2\pi \int_{-\infty}^{\infty} A(i\omega) \cdot e^{i\omega t} d\omega$$

and analyse amplitude-frequency spectrum of the function of wheel deceleration:

$$A(i\omega) = \int_{-\infty}^{\infty} a_h(t) \cdot e^{-i\omega t} dt,$$

The results of these analyses for front wheels (calculated with application of Fast Fourier Transform FFT (6)) is shown in Fig. 5. The investigation shows that for braking on a homogeneous surface, frequencies of maximum amplitude of harmonics $A(\omega_n)$ for left and right wheels are the same or very close.

The difference between main harmonic frequencies of Fourier series for left and right wheels can be a diagnostic parameter for determining symmetry of ABS, acting on homogeneous surface. For efficient ABS unit that difference ought to tend to the limit zero.

Similar results (more clear) can be obtained by determination of power spectral density (PSD) for function of wheels deceleration $a_h(t)$. For function $a_h(t)$ we calculate mean square value:

$$< a_h^2(t) >= \frac{1}{T} \int_{-T/2}^{T/2} a_h^2(t) dt$$

For Fourier series the mean square value is:

$$< a_h^2(t) >= a_0^2 + \frac{1}{2} \sum_{n=1}^{\infty} (a_n^2 + b_n^2) \qquad a_n,\ b_n \text{ - coefficients of Fourier series}$$

or in a complex form:

$$< a_h^2(t) >= c_0^2 + \sum_{n=1}^{\infty} 2|c_n(i\omega_n)|^2,$$

$$c_0 = a_0, \quad c_n(i\omega_n) = \frac{1}{2}(a_n - ib_n), \quad |c_n(i\omega_n)| = \frac{1}{2}\sqrt{a_n^2 - b_n^2}$$

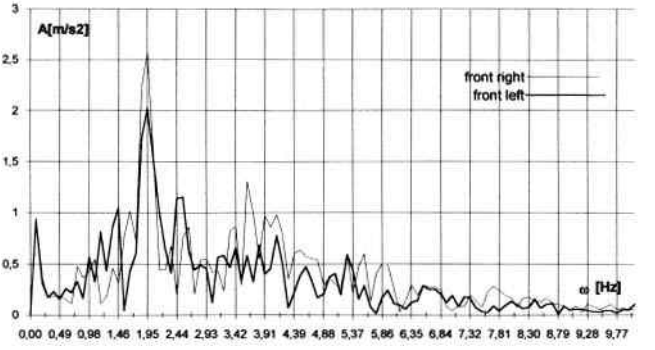

Fig. 5. Amplitude - frequency characteristics for function of front wheels deceleration $a_h(t)$ on dry homogeneous surface

Addend of that series are power fractions of $a_h(t)$ function, corresponding to n harmonic in the surroundings of frequency ω_n. If we divide power fractions per corresponding frequency intervals $\Delta\omega$, then we obtain power spectral density for $a_h(t)$ function (6):

$S(\omega_n) = \frac{|c_n(i\omega_n)|^2}{\Delta\omega}$ or $G(\omega_n) = \frac{2|c_n(i\omega_n)|^2}{\Delta\omega}$ for unilateral (one side) the spectrum.

The results of these analyses are shown in Fig. 6. In the stand conditions the main harmonic of PSD occurred for about 2 Hz frequency. Bigger frequencies for local maximum values of PSD depend on the algorithm of ABS operating (algorithm of steering of pressure modulators). The estimation of PSD course for tested ABS ought to be made by comparison with standard characteristic or only by comparison of main harmonic frequencies for left and right wheels.

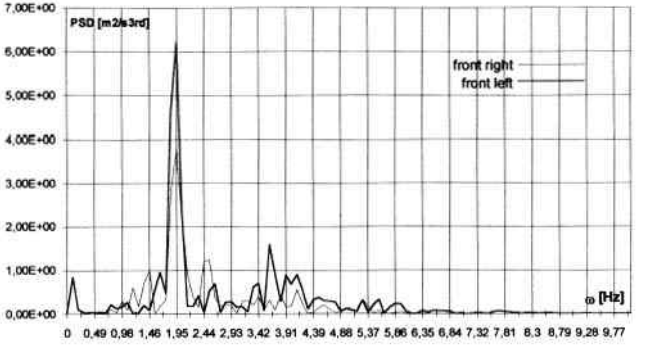

Fig. 6. Power spectral density (PSD) for function of front wheels deceleration $a_h(t)$ on dry, homogeneous surface

Similar PSD parameter, as for $a_h(t)$ function, can be determined for function of wheel slip $s(t)$, Fig. 7. It should be remembered that maximum PSD for $\omega<1$ does not result from basic

frequency of ABS operation. It is caused by the fact that amplitude of wheel slip increases when the speed of the car decreases, at time of braking. As a result, in the Fourier series there is harmonic, whose frequency is less than 0.5 Hz, where a local maximum of PSD has occurred for frequency of about 2 Hz and corresponds to frequency of ABS operation. It was the same frequency as for function $a_h(t)$.
The estimation of the symmetry of ABS operation allows us to establish the state of hydraulic elements of brakes (ABS modulator, callipers, brake cylinders).

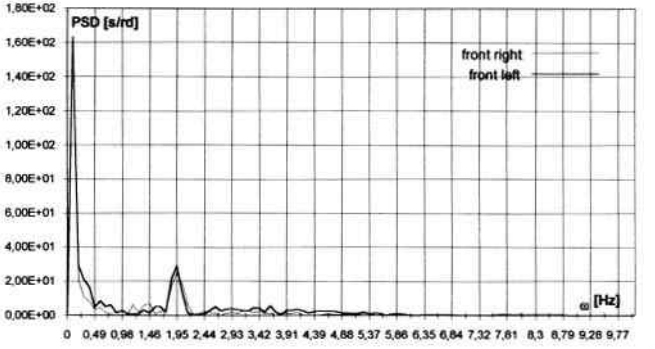

Fig. 7. Power spectral density (PSD) for function of front wheels slip $s(t)$ on dry, homogeneous surface

- Statistical analysis of ABS operation
In order to give a statistic estimation of ABS operation on the basis of a single realisation of braking process performed on a test stand, it has to be stationary and ergodic (6). Because of good repeatability of the test conditions we can make an assumption that process of braking on the homogeneous surface of the stand with ABS operating is near ergodic. The Fig. 8 shows a probability distribution $P(s_i)$ for discrete variable of wheel slip S. The wheel slip is analysed in time t, and values of the slip are calculated in constant time intervals t_i. If for each value of slip s_i duration time interval of s_i is assigned then the probability distribution of the wheel slip also represents distribution of slip duration time.
The histograms of the time duration of wheel slip, calculated on the base of braking on the stand are shown in Fig. 8. They enable us to estimate scatter of results around the average value or optimum value of the slip.
Much information about the wheel slip and also adhesion utilisation can be obtained on the base of cumulated distribution of the duration time of wheel slip P_k :

$$P_k\{s_i \le s_k\} = \frac{n_k(0 \le s \le s_k)}{n} = \sum_{i=0}^{i=k} p(s_i)\,[\%]$$

n_{si} - number of events whose value is s_i (slip values),
n - number of all events (slip values),
s_k - value of slip, for which cumulated distribution is calculated,
n_k - number of events when $s_i \le s_k$

Cumulated distribution of the slip time duration allows us to establish distribution and dissipation of the slip around average or optimum value and to establish the probability of slip lower or higher than the given value. Fig. 9 shows cumulated distribution for the front and rear

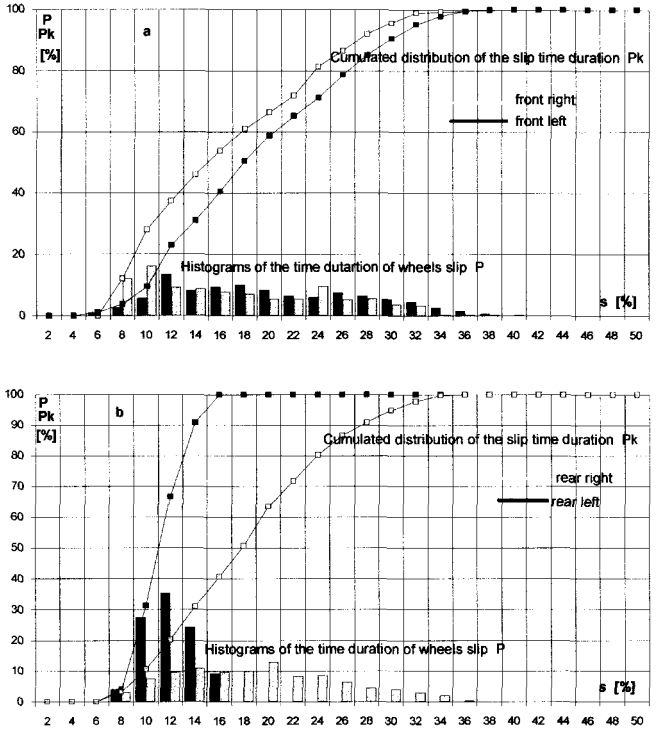

Fig. 8. Probability of the wheel slip time duration P and P_k for front and rear wheels

wheels. For the theoretical, ideal antilock unit cumulated distribution of the wheel slip is a straight perpendicular line passing through the s_{opt} value. The characteristics of slip distribution for tested ABS allow us to find what is the difference between the ideal course of the slip and real ABS operation. If the characteristic of the cumulated distribution of the slip is more steep and near s_{opt}, the ABS unit is more exact and precise. On the base of results of investigation and calculations of cumulated distribution of the slip time duration a universal criterion of correct operation of ABS was developed:

1) Wheel slip in the range: $s_{opt} - \Delta s_1 \div s_{opt} + \Delta s_2$ ought to last no less than $c\%$ of the analysed time of ABS operation. Time $c\%$ has to be situated in the range $a\%$ x $b\%$ time of ABS operation, $(a\%-b\%) \geq c\%$.

2) There should be no wheel slip smaller than s_{min} and higher than s_{max}.

This criterion has been shown graphically in the Fig. 9. In the range between lines $a\%$ - $b\%$ and Δs_1 -Δs_2 ought to be curves of the cumulated distribution of slip probability for $c\%$ time of ABS operation. The tests ought to be done on the surface with constant coefficient of friction. Fig. 9 shows that the analysed test slip of the rear left wheel was outside the optimum range. Values $a\%$, $b\%$, $c\%$, Δs parameters, establishing the range of correct ABS operation has to be determined together with the authors of ABS control algorithms and producers of these units.

Simplification of these statistical analysis is calculation of the slip mean value $\bar{s}$ and range $\bar{s} \pm \sigma t_\alpha$ for efficient ABS (σ - standard deviation of the slip, t_α - parameter of slip distribution

for significance level α). For the tested car these ought to be: $|\bar{s}_{test} - s_{opt}| \leq \Delta s_{lim}$ and $\sigma_{test} t_\alpha < D_{lim}$, $D_{lim} = \sigma t_\alpha$. Parameters Δs_{lim} and D_{lim} ought to be determined experimentally.

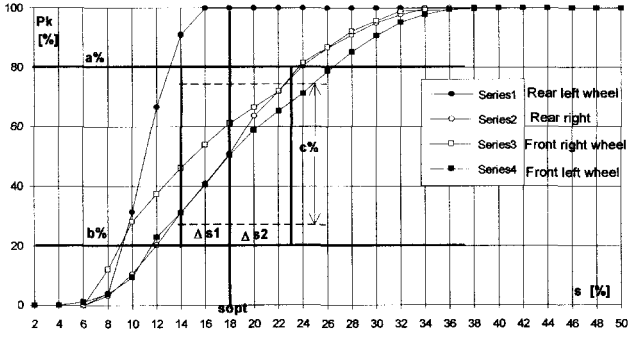

Fig. 9. Cumulated distribution of the wheel slip time duration. ***a%, b%, c%, Δs_1, Δs_2*** - parameters for criterion of ABS correct operation

4. CONCLUSION

The presented method of diagnostic testing of ABS in stand conditions allows us to examine the antilock units irregardless of the construction, electronics and program versions. The criteria of estimation are universal for all kinds of ABS systems.
The investigation shows that a braking car maintains stability on the stand; there is no danger of throw out from the drums and there is no necessity for special holding of the car during tests. Bringing up to speed of about 50 km/h lasts about 3 min., time of the test is about 10 sec. The results of test (speeds, slips) are obtained directly after braking on the stand monitor. Establishing of the boundary values of diagnostic parameters for estimation of ABS operation requires consultations with producers of antilock units. The diagnostic stand also allows us to test TCS systems preventing excessive wheel slip at time of acceleration.

REFERENCES

1. Regulations NR 13 ECE, Ann. NR 13: Requirements for investigation of brakes equipped with ABS systems
2. Wolff C., Rothmann W.: Sicherheitsgewinne erhalten durch wiederkehrende Prüfungen von automatischen Blockierverhinderern /ABV/, ATZ 5/1989
3. Gajek A.: Diagnostic control of the ABS operation, PAN, Dep. Cracow, Commission of Motorization, Vol. 5/1995
4. Gajek A.: Estimation of ABS operation in stand conditions. Brake Conference 97', Institute of Vehicles, University of Technology, Łódź 09/1997
5. Durski B.: Analytic expression of dependencies between coefficient of adhesion, wheel slip and speed of the vehicle. Brake Conference 88', Institute of Vehicles, University of Technology, Łódź 09/1988
6. Kamiński E., Pokorski J.: Dynamics of suspensions and power transmission systems in car vehicles. WKŁ, Warszawa 1983

The author gratefully acknowledges the support of this work by the Committee for Scientific Research (Poland) within grant No 378/T12/97/13

Vehicle sensitivity to brake torque differences – test and simulation results

L ROGER
Nissan European Technology Centre, Barcelona, Spain

ABSTRACT

Vehicle pulling to one side when braking is a known phenomenon in various vehicles and, in some cases is not fully understood. In the first phase of this work the sensitivity of the vehicle to brake torque differences in the front axle was determined. The study is focused on a light commercial vehicle having front (FR) and rear (RR)rigid axle suspension with leaf springs, FR disc brake and RR drum brake, but the results are fully applicable to all types of vehicles.

A test was defined to measure brake torque differences and their relation to vehicle pulling, in order to determine the sensitivity of the vehicle to torque differences when braking. Brake torque wheels and gyroscopes were used to measure the vehicle yaw rate, vehicle deceleration and brake torque.

Once vehicle sensitivity was defined by this test, measurement of suspension kinematics and compliance was carried out in a bench test. The next step was vehicle simulation by means of the CALLAS® commercial vehicle dynamic simulation software. Once an exceptionally good correlation with the test results was obtained, countermeasures related to vehicle dimensions and layout, suspension and tyre characteristics were defined to improve behaviour when braking.

Finally, several ideas to improve vehicle pulling to one side when braking are presented.

1. INTRODUCTION

Vehicle pulling when braking in a straight line is increasingly important in light commercial vehicles because of the generalised increments in running speed. As in any other vehicle, the safety level of this vehicle has increased. Additionally, its power performance has dramatically increased in recent years, basically due to the new TDI engine. In the past, it was assumed that this type of vehicle ran mainly in the city at limited speeds and braking performance was poor. However, there are now numerous urban motorways where speed limits of 80 km/h are common and there is a need for sudden braking manoeuvres due to traffic jams. Braking performance has increased considerably and decelerations greater than 0.9 g are not unusual.

In the past, the chassis configurations of the light commercial vehicle generally consisted of rigid front and rear axles, both with leaf springs, disc brakes at the front and drum brakes at the rear. Nowadays, this configuration is changing to front independent suspension, while the rear rigid axle with leaf springs is maintained. At the present, the rigid front axle with leaf springs, a configuration making the vehicle prone to brake pull, is still commonly used for trucks with a gross vehicle weight (GVW) greater than 3.5T.

The vehicle under study was instrumented to determine whether brake pull is more influenced by the brake system or the suspension and steering system. The first aim of this study was to define vehicle sensitivity to brake torque differences in the front axle. Second, through vehicle simulation with the CALLAS® commercial vehicle dynamic simulation software (SERA, France), the main parameters influencing this sensitivity were identified.

2. VEHICLE STABILITY WHEN BRAKING

Vehicle stability when braking in a straight line is related to the yaw moment of inertia, the wheelbase and weight distribution. The higher the yaw inertia, the greater the stability. At least two wheelbases are available for each model of light commercial vehicle. The shorter the wheelbase, the greater the instability when braking. Generally, a very narrow turning radius is valued in this type of vehicle, implying a short wheelbase and, therefore, a low yaw moment of inertia. Additionally, the cab over engine (COE) power train layout and fuel tank near the "x" position of the longitudinal Centre of Gravity (CDG) of the vehicle provide small contributions to the yaw moment of inertia at kerb condition. Most racing and sports cars have a low yaw moment of inertia for agile handling, but this characteristic is not desirable for light commercial vehicles because of the quick response in yaw.

Additionally, in the "driver only weight" (DOW) condition, these vehicles have a very favourable weight-to-power ratio, making them prone to be driven fast. In this weight condition, the contribution of the rear brake to the total braking force is very small because of the weight on the rear axle. Thus, the greatest influence regarding the brakes comes from the front brake system and, therefore, the front suspension.

3. TEST PROCEDURE DESCRIPTION

Before beginning the study, a test procedure was designed to measure vehicle instability when braking. A flat proving ground was selected to exclude effects related to ground camber, and wind conditions in which the test would not be considered representative were defined. For vehicle brake deceleration it was decided to carry out the test at 0.7g for both DOW and GVW weight conditions, from an initial speed of 80 km/h. All the brake applications were done with locked steering.

Since the vehicle has no ABS system and to avoid the "square tyre" effect due to repetitive brake applications, the tyres were changed several times during the test. To further minimise a potential influence of the tyres on the measurements, tyres from the same manufacturer were used in all the tests and tyre and proving ground temperatures were controlled.

The vehicle had a uni-axial accelerometer to measure deceleration in relation to the vehicle body and a gyroscope to measure the yaw rate. Later, it was fitted with four-wheel torque transducers to measure brake torque.

Previously to this study a test procedure was defined for measuring the vehicle instability when braking.

4. VEHICLE DESCRIPTION

The family of vehicles considered in this test has a power train configuration COE, rear wheel drive. The FR and RR suspension are rigid axle with leaf springs. The brake circuit is I+H with disc brake at front and drum brake at rear. The front caliper is a dual piston, one for the
front circuit and the other one for the rear circuit.

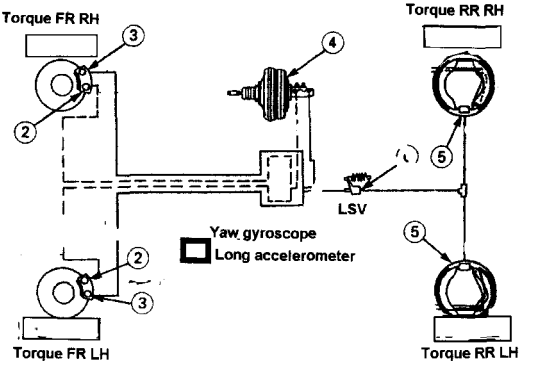

5. TEST PROCEDURE

The object of this test was to define what is known as the "sensitivity" of the vehicle to brake torque differences (1). Figure 2 shows the results for GVW before bedding and Figure 3 for DOW.

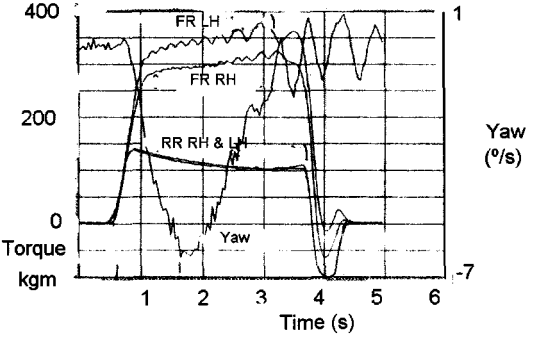

Figure 2

As can been seen, there were no torque differences in the rear axle and noticeable differences in the FR axle starting at 0.6s after the brake pedal was pushed. (Not shown in Figures 4 & 5, but no difference pressure was detected between both wheels in the same axle). Results after a number of tests with brand new pads, bedded pads, and use of various temperatures are shown in Figures 4 and 5.

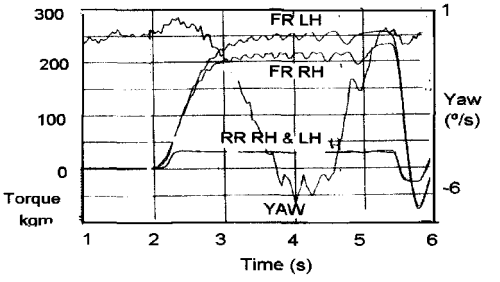

Figure 3

Since the target of this test was to achieve brake torque differences of around +/-5% in order to draw the correlation line as in Figures 4 and 5 (1), a standard pad combination was not used in some of the brake combinations tested (e.g. those in Figures 2 and 3).

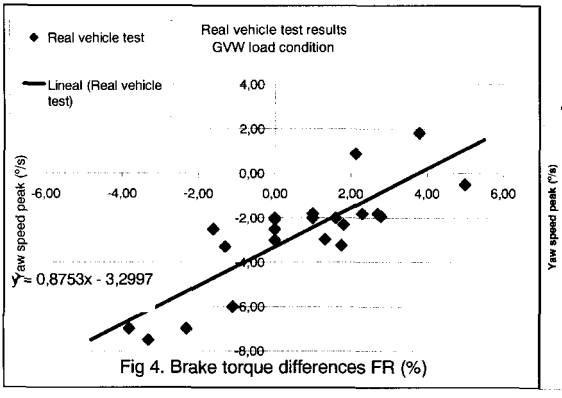

Fig 4. Brake torque differences FR (%)

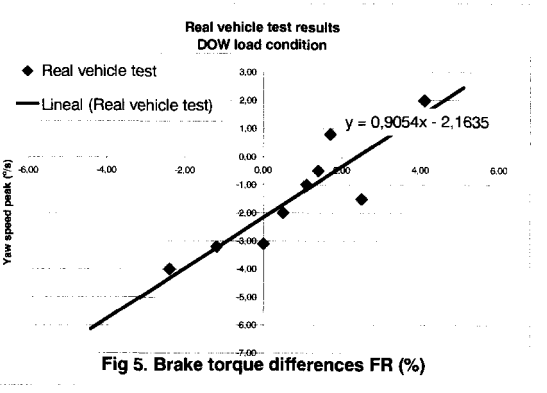

Fig 5. Brake torque differences FR (%)

6. TARGET DEFINITION

According to previous experience, a strong relation was anticipated between the brake torque difference and yaw rate in the front axle, since an earlier study showed a correlation between these two measurements (1). After analysing this tendency, two highly important figures were manifested, the slope and the vertical offset for no torque difference. With regard to target definition, the target was separated into two main items: brake torque difference and vehicle pulling. According to the experience of the NETC-E and the brake supplier, a 5% torque difference is acceptable for the front disc brake system used in this type of vehicle.

After a search into all the available brake regulations for different countries (2, 3), analysis of test feeling by the drivers and review of market survey results, it was considered that the best way to measure vehicle deviation was the yaw rate, as expressed in °/s. Several brake regulations define a lane width within which the vehicle has to remain at the end of the brake manoeuvre and others establish how much the vehicle can deviate from the original line. This leads to a maximum yaw rate of 1.5°/s. Thus, the target for this test was defined as shown in Figure 6.

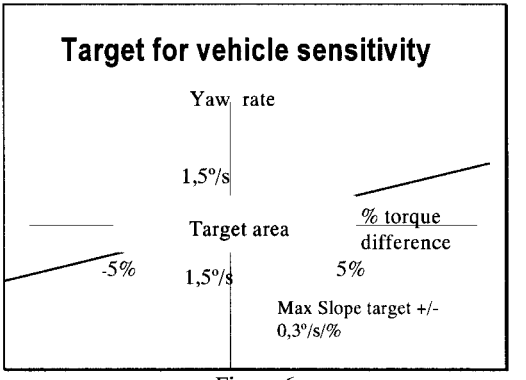

Figure 6

7. VEHICLE SIMULATION

7.1 Purpose

The purpose of vehicle simulation is to reproduce vehicle behaviour for +/- 5% brake torque difference in front axle and once a good correlation with the vehicle test results is obtained, to improve vehicle sensitivity by modifying some of its characteristics.

The CALLAS® software, presently in use by the NTC-E(S) to simulate vehicle dynamics, was employed. All the data need for the simulation were available except for the elasto-kinematic characteristics of the suspension, which were obtained after vehicle measurement in suspension elasto-kinematics bench tests.

7.2 Results

The purpose of this simulation was to determine vehicle sensitivity as defined in heading 3. Three computations were done with each vehicle for each weight condition. The first was for no torque difference in the front axle and the other two were for +/-5% of torque difference.

Once the parameters were adjusted, a good correlation was obtained for GVW see Figure 7. The same excellent correlation was obtained for DOW condition. Figure 7 shows vehicle sensitivity as measured in the vehicle and vehicle sensitivity as obtained through simulation. Taking into account that it is not possible to get the same brake torque versus time with software simulation as in a vehicle, the correlation was considered good enough to go ahead with the vehicle characteristics study. The yaw tendency with zero torque difference that can be seen in the on Figures 4, 5, 7, & 9 is due to some causes.
First is suspension and steering geometry layout, Figure 9, second is transverse position of CDG, not in the vehicle longitudinal symmetrical plane at DOW and finally tyre cornering stiffness, Figure 9.

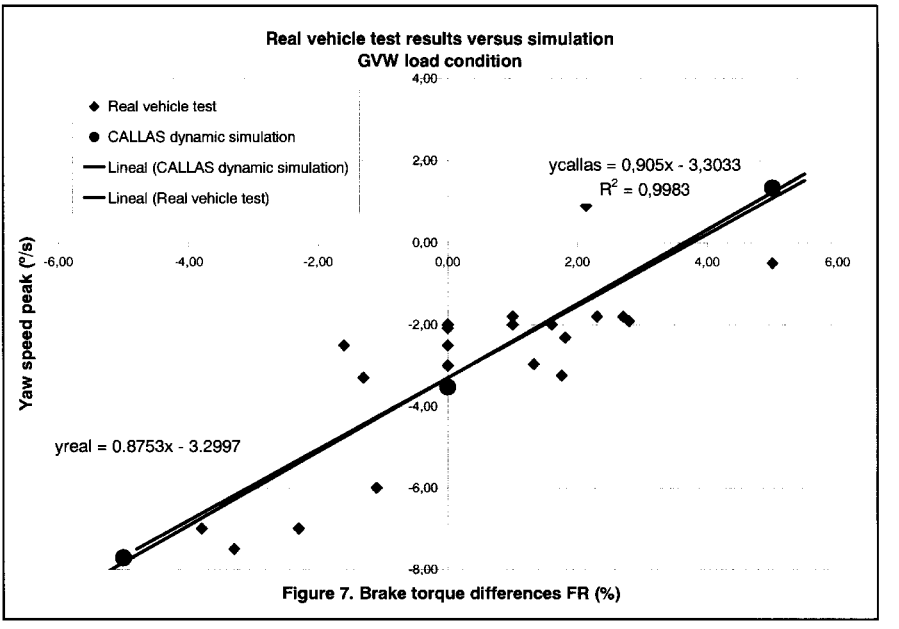

Figure 7. Brake torque differences FR (%)

7.3 Vehicle definition in simulation

CALLAS® works with a 3D-vehicle model and computes the 6 chassis degrees of freedom and the vehicle definition can be separated into different items.

1. Generalities: masses; geometry; inertia; passengers; tires pressure
2. Suspension (FR and RR): Type, kinematics and compliance characteristics as travel vs. force; camber, caster, wheelbase, ... vs.
3. Transmission: type of differential and ratios
4. Aerodynamics
5. Tire (FR and RR) Pacejka coefficients; rolling radius vs. speed and load ...
6. Engine: engine torque and power; engine brake; performances vs. Environment
7. Steering
8. Braking Brake characteristics defined as ....
9. Defects. For the different simulations done it is possible to use brake torque differences between right and left hand.

8. VEHICLE CHARACTERISTICS STUDY

Before beginning to modify the characteristics of the vehicle, the most effective options with regard to considerations of cost and timing were established.

8.1 Tyres

Since the tyres join the vehicle to the ground and the slip angle commonly has a great influence on vehicle behaviour, the tyres were the first element to be studied. Quite notable

slip angles were detected during the simulation, thus, this phase was focused on reducing the slip angles. Without changing the dimensions of the tyre, there is only one other characteristic that can be modified: tyre pressure.

8.1.1 Tyre Pressure

The simulation showed that once the vehicle started to pull to one side, the slip angles in both axles were considerable (5) and the vehicle showed very little understeering.

An attempt was made to reduce slip angle as much as possible in both axles and to increase the understeering characteristics. Since the vehicle is equipped with a commercial tyre, special attention had to be paid to cornering stiffness and its relation to tyre pressure. The following table 1 shows the original pressure and the modified pressure used for the test.

	ORIGINAL	MODIFIED
	DOW and GVW	DOW and GVW
FR	3,6 bar	4,5 bar
RR	4,5 bar	3,9 bar

Table 1

In these particular tyres, the higher the pressure, the lower the cornering stiffness for the range of load under study. Therefore, FR tyre pressure was increased and RR tyre pressure decreased. The influence of tyre pressure was found to be very important for the vehicle's pulling sensitivity (Figure 9). The slope was reduced from 0.96 to 0.61 (57%) in DOW condition and from 0.9 to 0.64 (40%) in GVW.

However (unfortunately, because tyre pressure has no cost effect), there are some important drawbacks to this option. First, RR tyre pressure cannot be reduced to below 3.9 bar, because of the load on the RR axle. The only concern regarding increased pressure in FR axle tyres is a loss of comfort to the rider. Another concern is the difficulty of controlling tyre pressures on the market. Thus, in spite of the great improvement found with this simulation, implementation to the vehicle is not easily accomplished.

8.1.2 Tyre Wear

Once the influence of tyre pressure was detected, the changes in cornering stiffness due to pattern height were investigated to see if a worn tyre had effects similar to tyre pressure modifications. According to information from the manufacturer, the tyre's cornering stiffness changes dramatically with wear; however, the change is entirely related to the vertical load. Another series of simulations was carried out to determine the cornering stiffness of tyres under different conditions of wear.

As a general result, vehicle sensitivity to brake torque difference decreased (as did the slope) as tyre wear increased. Therefore, a brand new vehicle would show the worst vehicle sensitivity. The brake torque difference might be quite significant due to a lack of bedding in the FR brake system and the tyres are in the worst condition for cornering stiffness.

8.1.3 Another Tyre Solution

Once the influence of tyre pressure and tyre wear on vehicle sensitivity was defined, other options were investigated, such as installing the same tyre on a wider rim or using a wider tyre with higher load index so that tyre pressure would be lower for the same vertical load.

8.2 Wheelbase Influence

The next phase of the simulation involved the wheelbase. The weight distribution was identical for the three wheelbase specifications studied. The moment of inertia in the z-axis (Izz) was adjusted for each wheelbase. The rest of the parameters of the vehicle, including the CDG height, were not altered. Results are presented in Figure 8.

The longer the wheelbase of the vehicle, the lower is the weight transfer to the front axle. The vertical load to the FR tyre decreases as the wheelbase increases by the wheelbase/H cdg ratio. Wheelbase increment also affects the turning radius of the vehicle, due to the difference in front and rear slip angles. For the same slip angles, greater in the front axle than in the rear axle, there will be less vehicle pulling.

For the vehicle under study it was concluded that a wheelbase of around 3200mm was the minimum acceptable to reach the target. The drawback of this configuration is that buyers might find the turning radius to be too limited for an urban vehicle.

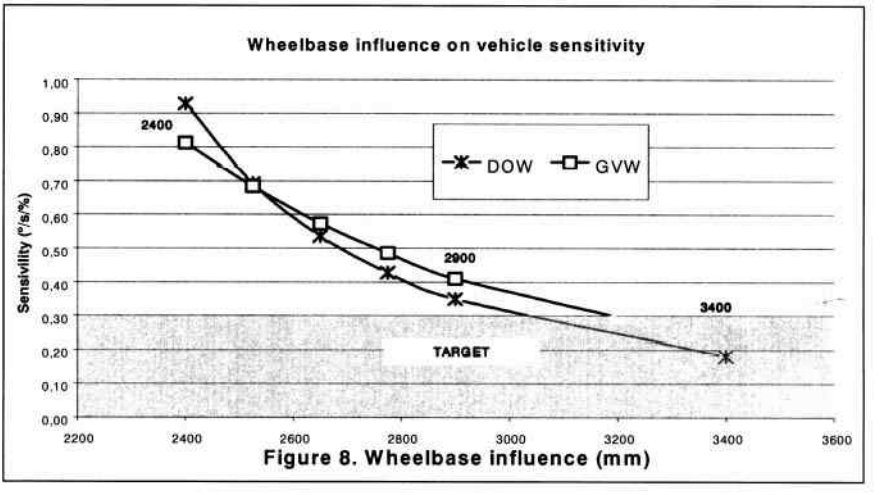

Figure 8. Wheelbase influence (mm)

8.3 Front Suspension Vertical Stiffness

Next, the simulation contemplated changes in front suspension vertical stiffness. This item is not easy to introduce in a real vehicle. When vertical stiffness is changed in a vehicle with front suspension and leaf spring, the lateral, transverse and wind-up stiffness are also affected. Although practical application is not easy, this factor was studied for additional data. The FR vehicle posture would also change, but in any case, simulation with a softer front suspension was decided.

Results are shown in Figure 9. As can be seen, there was a large influence on vertical offset for no torque difference, but the slopes of both lines are quite similar. It was concluded that changing the vertical stiffness of the front suspension does not alter vehicle sensitivity; but it does alter vertical offset for no torque difference. When the front vehicle posture is changed,

there is a displacement of the point in the bump steer graph in which the slope of toe change versus suspension travel is not constant (Figure 10).

8.4 Weight Distribution and Moment of Inertia Influence

The next step in vehicle simulation dealt with the influence of front and rear axle weight distribution, and, as a consequence, the moment of inertia in the vertical axis. There are at least two other vehicle layout configurations that can increase the moment of inertia in the vertical axis, the so-called semi cab over engine (SCOE) and cab behind engine (CBE). Both these configurations imply a dramatic change in vehicle layout. Thus, while maintaining the vehicle configuration, the influence of the fuel tank and spare wheel on Izz was calculated. The spare wheel was placed as rearwards as possible in the rear overhang for this simulation.

The influence of the fuel tank depended on the fuel level only in DOW condition. The effect of an empty fuel tank on Izz was very low (Figure 9). It was concluded that this factor had a very small influence on vehicle sensitivity.

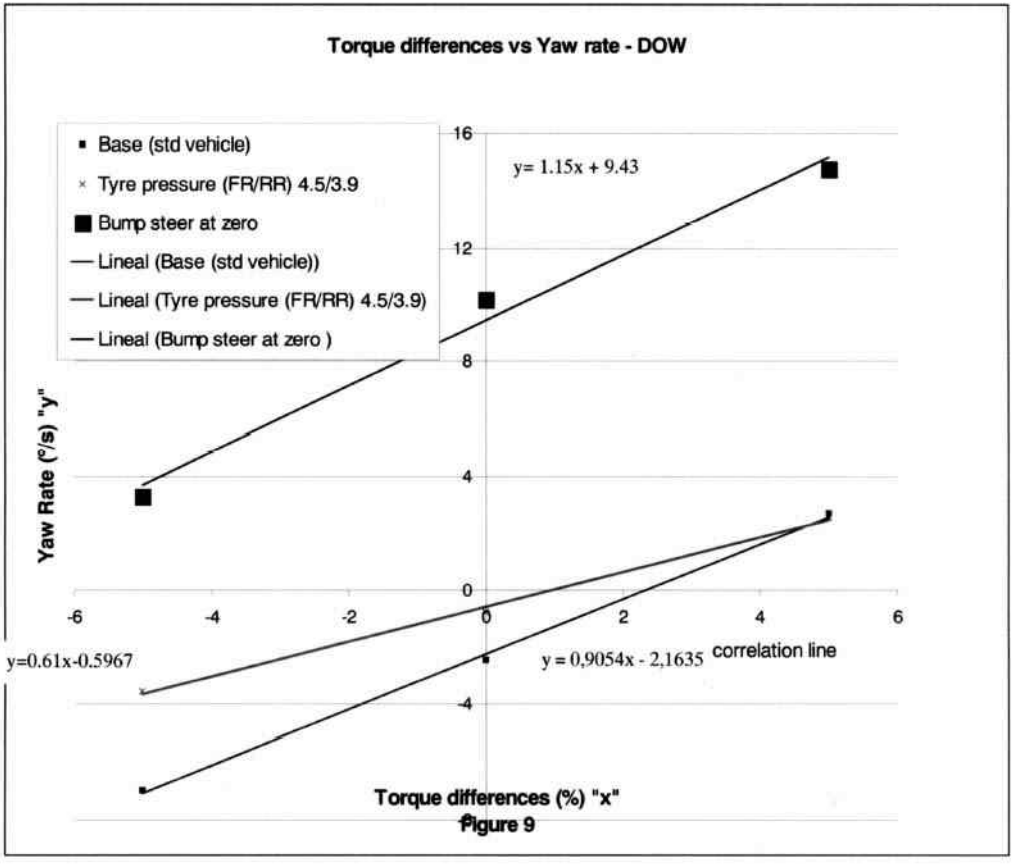

Figure 9

8.5 Bump- Steer Influence

Finally, the influence of bump-steer kinematics on vehicle pulling was studied (4, 5& 7). Using the simulation software, it is possible to carry out a simulation of vehicle sensitivity with no bump steer change for bump to bump suspension stroke, see Figure 10. Both bump steer suspension characteristics were simulated. See Figure 9

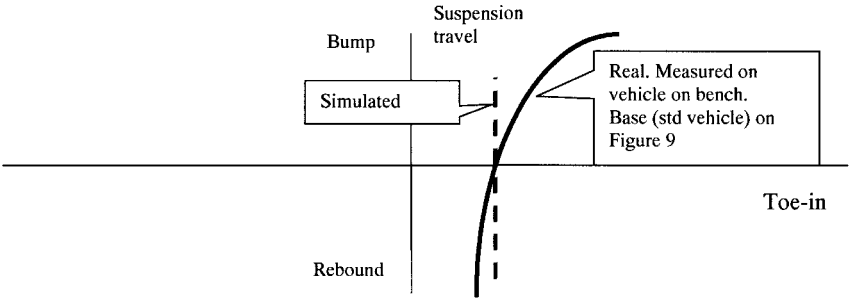

Figure 10

The no bump-steer characteristic, simulated on Figure 10, has as effect to increases the yaw deviation for no torque difference from –2.16 to 9.43 °/s and the vehicle sensitivity was increased a little bit for 0.9 to 1.15. That means, that due to the suspension vehicle characteristics some bump steer as in Figure 10, helps to reduce the yaw tendency with no torque difference and also to reduce the vehicle sensitivity to torque differences.

9. CONCLUSION

The correlation between the test results and simulation results was excellent, indicating the suitability of the software and the accuracy of the data used. This correlation resulted in fast advances in improving vehicle sensitivity to brake torque difference and considerable savings in prototypes and manpower.

Several parameters, including wheelbase and tyre pressure, were found to have a great influence on vehicle sensitivity. Since the simulation results are totally related to the available data, some changes in the characteristics of front suspension stiffness, such as longitudinal, lateral and steering stiffness are difficult to simulate. By applying the above modifications and improving front suspension stiffness the target is reached.

10. BIBLIOGRAPHY AND REFERENCES

1. Ll. Roger, EAEC 99C204, Vehicle stability when braking. Brake Torque difference in Front Axle and its relation and its relation to vehicle pulling to one side
2. FMVSS $ 571.135
3. EEC Brake regulation n°13
4. R.A. Verschoore. SAE 865124. Steering geometry errors induced by braking
5. Kambara, Nakanao, SAE 871232. An Analysis on vehicle Behaviours during braking.
6. Kato, Haraguchi, JASE Review 17(1996) 65-77. Improvement on steering pull during braking on rutted road.

7. T.D. Gillespie, SAE 760025. Front Brake Interactions with Heavy Steering and Handling During Braking

11. ACKNOWLEDGEMENTS

To all NETC-E brake and ride & handling department, for they collaboration in this paper. Special thanks to Mrs. A, Moya, A. Martorell, R. Mateu, G. Filella, J. Jordà for their work in such a difficult item and also to Mr. Cuixeres, in charge of the simulation, for their help in writing this paper. Also thanks to NIVISA and to NETC-E Mrs. Jose. Verdú, Miquel Bisbe and Francisco Garcia, for giving authorisation to publish this information.

This page intentionally left blank

Steering drift during braking

J KLAPS
Ford Motor Company, Genk, Belgium
A J DAY
University of Bradford, Bradford, UK

ABSTRACT

This paper presents a study of braking-related steering drift in motor vehicles, where the driver must apply a corrective steering torque in order to maintain course. During normal conditions of braking, steering drift was found not to be a result of side-to-side variation in braking torque, but to be influenced by the suspension compliance and steering offset. These lead to changes in wheel alignment during braking which in turn affect the toe steer characteristics of each wheel and therefore the straight-line stability during braking. It is concluded that a robust design of suspension is possible in which side-to-side variation in toe steer is not affected by changes in suspension geometry during braking.

1. INTRODUCTION

Motor vehicles have friction brakes on each wheel to meet the legal requirements of stopping in a safe, controlled and predictable fashion. Brake "pull" is often identified with unequal side-to-side braking forces interacting with steering geometry. Steering "drift" during braking usually refers to a relatively minor deviation from straight-line braking, although even minor deviation remains unacceptable by today's standards of vehicle drivability.

Most modern passenger cars and light commercial vehicles are fitted with front disc brakes and rear disc or drum brakes. Automatic adjusters (1) have become mandatory for disc/drum combinations, because adjustment of the clearance between the lining and the brake drum is important for braking stability. If the disc brakes become too hot, deterioration in brake performance may result from a number of causes such as (3) brake fade, excessive thermal distortion, and surface cracking. Trace elements, e.g. Titanium and Vanadium, have been found to significantly affect brake torque generated; two discs of different trace element content fitted to either side of the steered axle can cause asymmetric braking forces and braking pull (4).

Moves to reduce the unsprung mass of the next generation of passenger vehicles have led to interest in the replacement of traditional cast iron brake rotors with a lightweight alternative. Many vehicle manufacturers have considered the suitability of aluminium metal matrix composites (Al-MMC) for use in passenger vehicle rotors (5). However, friction stability has not been noticeably improved, and therefore braking stability may remain an area of concern even with these "new generation" rotor materials.

Four parameters associated with steering geometry which can affect steering drift are toe-steer, camber, caster, and scrub radius. The toe setting is designed to compensate for the amount the tyres turn away from straight ahead under driving conditions. Poor adjustment of the toe setting can cause unstable straight-line drivability, and a steering reaction is generated if the toe steer angles are different between left and right track. The amount of toe-in or toe-out can also depend on the suspension position relative to the steering gear. Toe-in or toe-out is usually the same in the design ride position, but can change in opposite directions during body roll, thereby causing the vehicle to pull to one side.

Wheel camber generates camber scrub, in which true rolling is achieved only in the centre of the tread. This produces camber steer: positive camber will make the wheels turn away from each other, i.e. toe-out, whereas negative camber will make the wheels turn towards each other, i.e. toe-in. The wheel track must be set to match the design of suspension to counteract the inherent tendency of the wheels to either move away from or towards each other (6).

Caster is employed to provide stability through self-aligning of the steered wheels. Decreasing caster will reduce directional stability (and decrease steering effort). In the steered wheels of a motor car, uneven road surfaces cause alternating lateral forces at the centre of the tyre contact patch which can cause moments about the steering axis, resulting in steering disturbances.

Scrub radius is the geometric distance between the centre line of the tyre contact path and the steering axis at the ground plane(7). A negative scrub radius can improve the straight-line stability of a vehicle while braking on split μ conditions or during failure of one brake circuit.

Tyre lateral force and self aligning torque arising from pneumatic trail determine the effective slip angle and total axle lateral forces (9). A different lateral stiffness between tyres of the left and right track of a vehicle leads to a permanent steering drift, independent of the driving situation. Six factors which are commonly considered to be associated with steering drift are: tyre inflation pressure, tyre temperature, conicity, ply-steer, residual self-aligning torque (RSAT), and torque steer.

Higher tyre pressure increases the cornering stiffness; for a given small slip angle, an increase in pressure will give an increase in lateral force. As tyre pressure is decreased, the contact patch becomes longer and the centre of lateral force moves rearward. increasing self-aligning torque. Changes in the under/over-steer balance of the vehicle can be achieved by varying the pressures front to rear.

Conicity is the lateral force offset at zero slip angle (10) and acts in the same direction whether the tyre is rolling forwards or backwards. An off-centre belt causes 80% or more of conicity forces, the force sensitivity being typically 30 N/mm of belt offset (11). Ply-steer

forces result from the angle of the belt plies; the outer ply exerts the dominant effect, and the direction of the ply-steer lateral force depends on the direction of rolling.

For a vehicle to move in a straight line, the sum of the lateral forces acting on the axle must equal zero. However, even though the sum of the lateral forces may be zero, the sum of the self-aligning torques acting on the two steering tyres may not be zero (11). Residual self aligning torque (RSAT) is a measure of tyre contribution to steering pull; if the total RSAT is zero there is no pull. RSAT is related to tyre conicity and ply steer and is the self aligning torque at the slip angle for which the lateral force becomes zero (10).

Torque steer can be generated when the outboard constant velocity (CV) joint of a front wheel drive car is not in line with the wheel spindle because of ride height changes caused by vehicle loading, body roll or weight transfer. As long as the system is symmetrical the effects on each side of the car will be equal and opposite. However, if the driveshafts are unequal in length, the articulation angles each side will be different and a resultant steering torque generated (12).

The kinematics of vehicle suspension systems and the way in which compliance steer is affected by the use of rubber components in suspensions is of major interest in motor vehicle design. Compliance steer results from the application of lateral or longitudinal forces at the tyre contact path, which deflect the suspension bushings and change the camber and toe angles (13). Compliance can be introduced into suspension systems by:

- Elastomeric (rubber) suspension pivots,
- Rubber mounted cross-members,
- Rubber mounted steering racks and other steering joints,
- Component deflection under load; including suspension links, steering links, and the chassis mounts for suspension and steering.

Compliance in the suspension system is necessary to achieve a good ride characteristic, but compliance steer is considered to be one of the biggest contributors to straight-line stability during braking (14). As an example, when the control arms move because of bushing deflection they also can cause a change in steering angle. If this is different side-to-side, the vehicle can steer to one side while braking.

2. INITIAL INVESTIGATION OF STEERING DRIFT DURING BRAKING

An initial experiment was carried out in order to investigate which parts of the front suspension/steering/braking system might have the greatest influence on steering drift during braking. The experiment was designed according to a statistical Design of Experiment methodology, based on a two level L16 orthogonal array (15). This enabled main effects to be identified and gave no confounding between the major two-way interactions. Two passenger cars of identical specification were driven on a 1.2 kilometre long by 8 metres wide straight test track for the experimental measurement of steering drift during braking (16).

The selected test car had a MacPherson strut design of front suspension (12), in which a lower suspension arm or wishbone provided lateral and longitudinal location. The parts of the front suspension/steering/braking system selected for investigation were as follows:

A. Tyre & brake temperature
B. Suspension geometry toe-steer curve
C. Steering gear housing/engine subframe reinforcement cover
D. Front suspension Lower wishbone rear bush stiffness
E. Wheel offset (y-direction)

Side-to-side variation of braking force (e.g. from different brake discs or friction materials) was not included as such in this initial experiment since this was a known effect. (See Section 3).
The tyre & brake temperature (factor A) was considered to be dependent upon braking under different driving styles. A change in temperature could produce different braking torques which could influence steering drift during braking.
The suspension geometry toe-steer curve (factor B), the steering gear housing/engine subframe reinforcement cover (factor C) and the front suspension lower wishbone rear bush stiffness (factor D) were selected because they imparted compliance to the front suspension assembly.
The wheel offset in the y-direction (factor E) was chosen to investigate the effect of scrub radius.

Two levels for each factor were identified as shown below:

Factor	**Level**	**Setting**
Tyre & brake temperature	A-	tyres and brakes cold
	A+	tyres and brakes hot
Suspension geometry toe-steer curve	B-	standard (without spacer) between steering gear-housing and subframe
	B+	2.5mm spacer between the steering gear-housing and subframe on the left hand side
Steering gear housing/engine subframe reinforcement cover	C-	without reinforcement
	C+	with reinforcement
Front suspension Lower wishbone rear bush stiffness	D-	"voided rear bush" (1200 N/mm in 'x'-direction and 4000 N/mm in 'y'-direction)
	D+	"non voided" bush (5000 N/mm radial stiffness)
Wheel offset (y-direction)	E-	Standard (49.5mm wheel offset)
	E+	with 6mm thick spacer between wheel spider and hub (55.5 mm wheel offset, right hand side only)

The measured response was the lateral displacement, measured by the number of carriageway lanes moved from the straight-ahead position during the braking manoeuvre (17).

The test procedure was designed to be representative of actual road usage. After checking the setting and test conditions, the vehicle was braked (with driver and observer) to rest in neutral gear from 100 km/h at a set deceleration with "free" (hands-off) steering wheel. The deviation from straight-line braking was measured, and the procedure was repeated for five runs from a virgin brake condition. The results are summarised in Table 1:

Factor		Effect
A	tyre and brake temperature	Insignificant.
B	suspension geometry toe-steer curve	Insignificant
C -	steering gear housing / engine subframe reinforced cover	Significant negative effect. Best suitable level is + (with perimeter frame reinforcement cover)
D	The front suspension lower wishbone rear bush stiffness,	Most significant effect. D+ (voided rear bush) gave smallest steering drift.
E	wheel offset	Second most significant effect
A x B	tyre and brake temperature / suspension geometry toe-steer curve interaction	Insignificant
A x C	tyre and brake temperature / steering gear housing / engine subframe reinforced cover interaction	Insignificant
A x D	tyre and brake temperature / front suspension Lower wishbone rear bush stiffness interaction	Minor interaction effect. When 'D' and 'A' were +, A x D became + as well, which meant a reduction of the steering drift.
A x E	tyre and brake temperature / wheel offset interaction	Insignificant
B x C	suspension geometry toe-steer curve / engine subframe reinforced cover interaction	Insignificant
B x D	suspension geometry toe-steer curve / front suspension Lower wishbone rear bush stiffness interaction	Insignificant
B x E	suspension geometry toe-steer curve / wheel offset interaction	Insignificant
C x D	steering gear housing / engine subframe reinforced cover / front suspension Lower wishbone rear bush stiffness interaction	Insignificant
C x E	steering gear housing engine subframe reinforced cover / wheel offset interaction	Insignificant.
D x E	front suspension Lower wishbone rear bush stiffness / wheel offset interaction	Largest significant interaction effect. When D is +, and E is +, then the interaction also becomes +. This has a negative effect on the response (greater steering drift).

Table1: Results of initial investigation of steering drift during braking

3. VEHICLE TESTS

3.1 Test equipment

Having established that the suspension compliance and steering offset had a significant effect on steering drift during braking, vehicle tests were carried out to investigate how steering drift during braking could be reduced or eliminated if it occurred in a production vehicle. An example of the same model of car was obtained which demonstrated a small but noticeable steering drift characteristic during braking. This vehicle was fitted with instrumentation which allowed the dynamic longitudinal deflections and forces in the suspension components, the brake forces, and the dynamic steering behaviour to be measured. A portable computer with A/D-converter and measuring acquisition software (DIA/DAGO®) was used to log these data (16).

To measure the longitudinal and lateral acceleration and the yaw velocity, a gyrostabilised platform was installed near the centre of gravity which provided measurements independent of the roll and pitch angle of the vehicle. The steering wheel torque and angle were measured with an instrumented steering wheel, which replaced the original steering wheel. A positive steering angle was clockwise, and vice-versa. A positive steering torque required the driver to apply a reaction torque counter-clockwise. To measure the steering tyre rod forces of the rack and pinion power steering the original tie rods were equipped with strain gauges to sense only tension (+) and compression (-) forces. A Datron Correvit sensor was mounted at the rear of the vehicle to measure the longitudinal speed of the vehicle. To measure the dynamic toe steer and camber angles the vehicle was equipped with a Zimmer Autokollimator mounted on a light weight frame. This optical device measured the deflection of a light beam which was projected on to a mirror mounted at the wheel rim.

3.2 Dynamic Straight-line Braking Test

The following open loop straight-line braking test was employed which required the driver to apply no correction to any perceived steering drift during braking:

- Drive the test car in a straight line at a speed of 100 km/h,
- Apply a braking deceleration of 7 m/s² to rest (engine braking is included; the clutch is disengaged just before the vehicle comes to rest).

Two different steering methods were employed; free control and fixed control. Free control meant that the vehicle was driven "hands-off" the steering wheel; in this case the steering wheel torque was zero. Under fixed control the steering wheel angle was held at zero. The recording of the measured parameters was started 2 seconds before braking commenced, and finished 2 seconds after the vehicle came to rest. A deceleration of 7 m/s² was chosen because this showed the most repeatable results without any influence of the anti lock braking system.

The control parameters were:

- Longitudinal velocity
- Longitudinal deceleration
- Steering wheel angle ⇒ fixed control
- Steering wheel torque ⇒ free control

The measured parameters during the tests were:
Vehicle response:

- Lateral acceleration
- Yaw velocity
- Steering wheel angle ⇒ free control
- Steering wheel torque ⇒ fixed control

Steering system:

- Toe steer angles, front axle
- Camber angles, front axle
- Steering wheel torque and angle
- Steering tie rod forces

4. RESULTS

The test vehicle showed steering drift during braking to the Left as shown in figure 1; note that data-logging started at time zero, and the braking manoeuvre commenced at approximately 2 seconds into the logging time. Under fixed control the yaw velocity initially increased and then decreased towards the end of the deceleration, but remained positive throughout indicating a continuous drift to the Left. Under free control the yaw velocity characteristic also remained positive throughout showing an initial increase, then a sharp decrease then an increase before decreasing towards the end of the deceleration. Again this represented a drift to the Left, but less continuous. This result could have been an effect arising from side-to-side variation of the braking torque; and when the brake pressures were measured they were found to be higher at the left front wheel than at the right front wheel. However, when the brake pipe connections were swapped from left to right, the steering drift to the Left remained. This indicated that the steering drift effect during braking, which might previously have been ascribed to side-to-side variation in brake torque, had another cause.

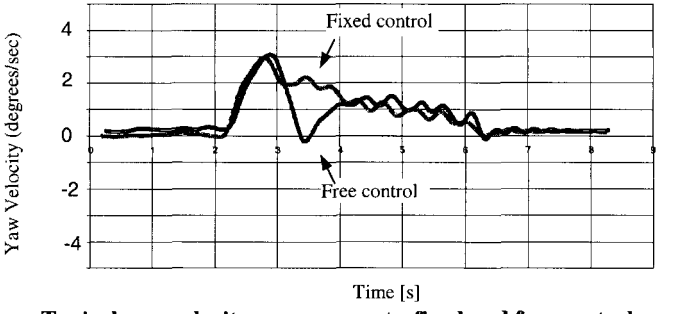

Figure 1: Typical yaw velocity measurements, fixed and free control

To identify possible other causes, further investigations were undertaken. Figure 2 shows the steering geometry of the test car, and figure 3 shows the measured steering tie rod forces during the test under fixed control. Under deceleration the steering tie rod forces were in tension (positive), and, assuming no side-to-side brake force variation, the relative change in the Left/Right steering tie rod forces indicated that the steering offset varied during the braking test, although it remained negative.

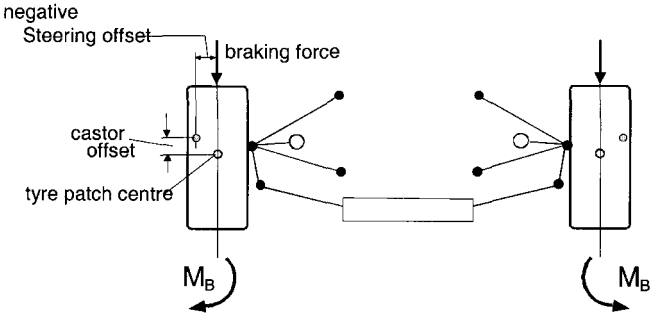

Figure 2: Steering layout

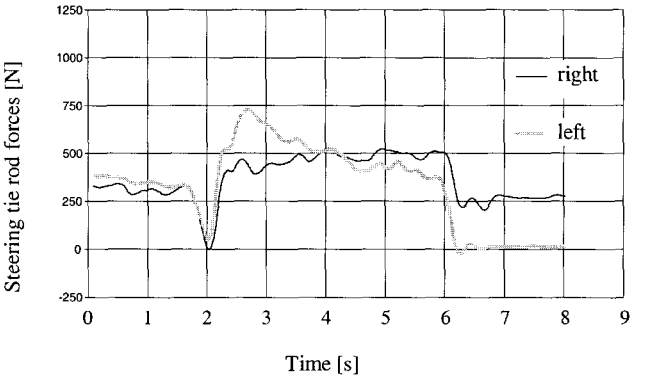

Figure 3: Steering tie rod forces during braking test, fixed control

The higher tension (positive) force in the left tie rod between the start and approximately 2 seconds into the braking manoeuvre (2 and 4 seconds into the data-logging time shown in figure 3) indicated that the left wheel toe steer (inwards) exceeded the right wheel toe steer (inwards). Therefore the vehicle would steer to the right during braking (assuming no other compliance steer influences and equal braking torque side-to-side). The corresponding measured steering wheel torque is shown in figure 4; a positive steering wheel torque over the same time period under fixed control indicates that a counter-clockwise torque was required at the steering wheel, which is consistent with restraining the toe steer mentioned above.

2 seconds after applying the brakes, the force in the left tie rod decreased to less than that in the right tie rod, indicating toe steer to the left. The corresponding measured steering wheel torque switched to negative 2 seconds into the braking (figure 4), which was consistent with restraining the left toe steer and confirmed the relationship between tie rod force and toe steer angle.

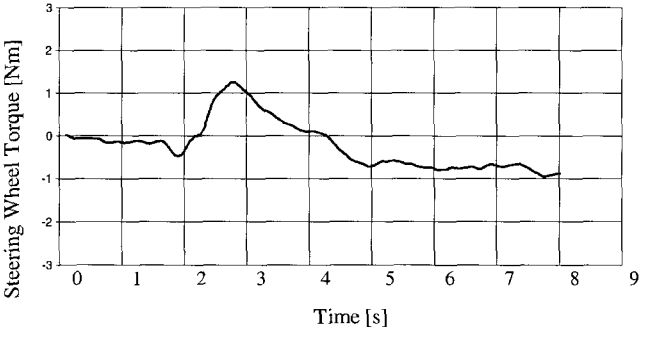

Figure 4: Steering wheel torque, fixed control

When the vehicle was driven under free control, no significant difference between left and right tie rod forces was seen (figure 5). In this case, the vehicle would drift to the direction of the toe steer during braking assuming that there were no other influences.

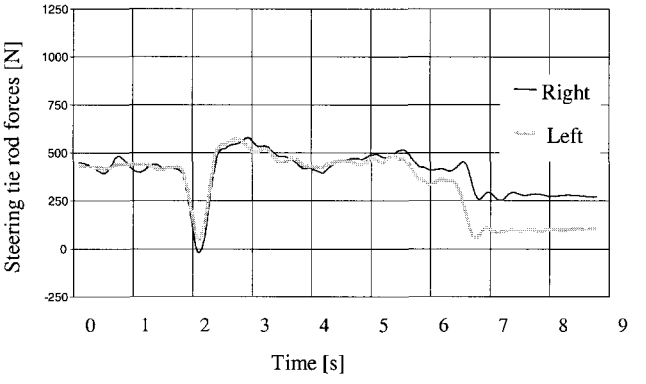

Figure 5: Steering tie rod forces, free control

These measured toe steer effects could thus explain the yaw response characteristics under free and fixed control discussed above.

The steering offset of the vehicle was changed from –6.5 to + 1.5mm by fitting a spacer between both front wheels and the hubs, thereby changing the tyre contact patch centre but not the kingpin geometry. Figure 6 shows the steering tie rod forces; during deceleration the tie rods were still in tension, though the magnitude of the tie rod forces was lower. The vehicle yaw velocity response was little changed from that shown in Figure 1.

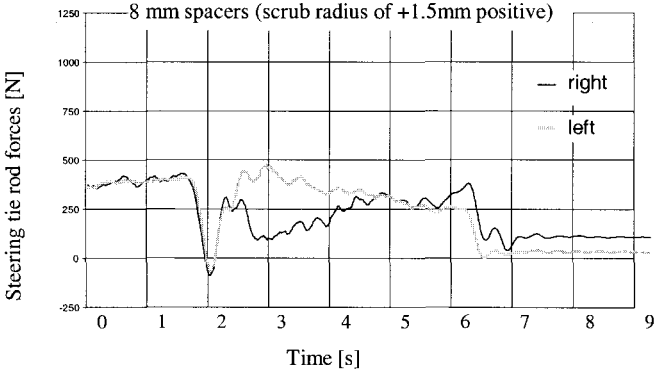

Figure 6: Steering tie rod forces with additional spacers, fixed control

A dynamic change in the caster angle is a direct result of the longitudinal stiffness of any front suspension. The deflections related to the x- and z-axis of the wheel centre point were measured during braking, together with the x-deflection of the top of the suspension strut. Knowing this and the body pitch angle allowed the absolute caster to be calculated.

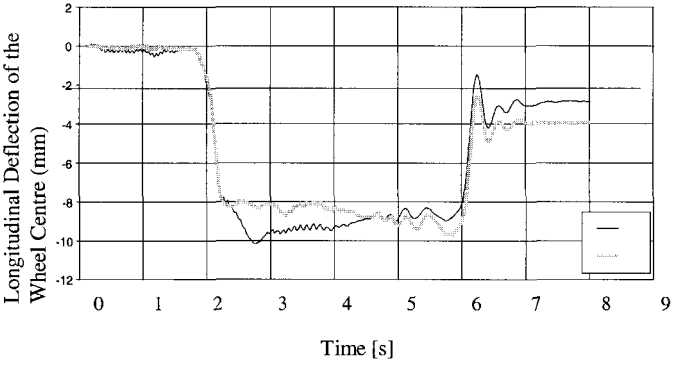

Figure 7: Longitudinal deflection of the wheel centre point

The dynamic change in the right wheel longitudinal deflection was found to be initially larger, which would cause a steering drift to the Right, as shown in figure 7. From these measurements the corresponding maximum caster angle changes were calculated, and are shown in Table 2.

Definition	Nominal Value	Static Measured Value Left track	Static Measured Value Right track	Dynamic Measured Caster Value Left track	Dynamic Measured Caster Value Right track
Caster angle [°]	3.00	1.60	1.68	-0.45	-0.8
Caster Trail at wheel centre (mm)	0	-2.96	-1.48	Not measurable	Not measurable
Caster offset [mm]	14.64	10.46	9.38	-1.5	-3.8
Scrub radius (mm)	-6.05	-6.695	-6.55	Not measurable	Not measurable

Table 2: Maximum values of the dynamic caster

Under dynamic braking the Right caster angle changed from +1.68° to -0.8°, equivalent to a dynamic change of the caster offset from 9.38 mm to -3.8 mm. The Left caster angle changed from +1.60 mm to –0.45 mm. A negative caster angle does not automatically lead to a change of steering direction, but a dynamic change from positive to negative caster angle during braking will not improve vehicle stability.

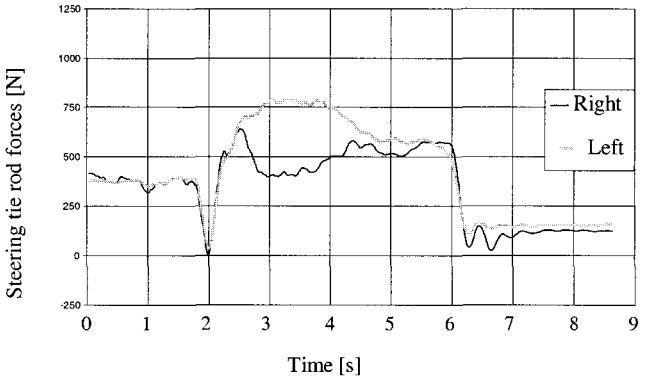

Figure 8: Steering tie rod forces, with stiffer lower wishbone rear bushes, fixed control

The effect of a stiffer bush on the deflection of the front suspension lower wishbones was previously identified as of significance in steering drift. This was investigated further by measuring the steering tie rod forces and the toe steer angles and the results are shown in figure 8. The toe steer angles with the original bushes and the stiffer bushes are compared in figures 9 and 10. At this level no discernible steering drift during braking was generated.

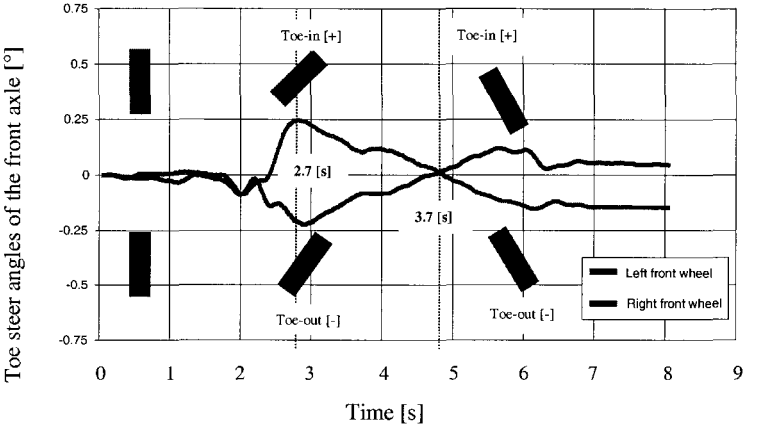

Figure 9: Toe steer angles, lower wishbone with original rear bushes

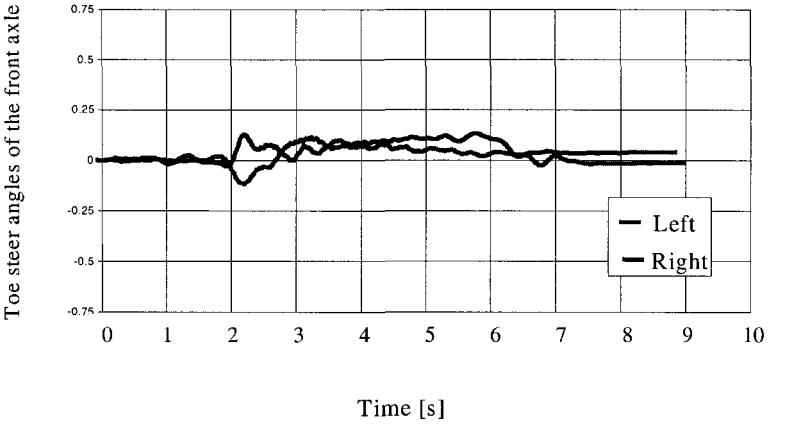

Figure: 10 Toe steer angle, lower wishbone with stiffer rear bushes

5. DISCUSSION AND CONCLUSIONS

The initial cause of steering drift during braking was thought to be side-to-side variation in the braking torque. The brake, in particular the friction material, is often blamed for steering pull during braking. However, this investigation has shown that the brakes were innocent; the major cause of steering drift during braking in this case was side to side dynamic variation in the deformation and deflection of suspension and steering components. The results have clearly indicated that for this particular design of suspension and steering geometry (6mm nominal negative offset), side-to-side variation in the braking forces at the front wheels was not a significant factor in the generation of steering drift during braking. This confirms that any attempt to enhance straight line braking stability by close control of the frictional performance of the brakes would not, in this instance, be appropriate.

The results demonstrated that the toe steer characteristic (defined as the way in which the toe-in setting of the front (steered) wheels changes as the suspension deflects in jounce or rebound), was also not significant in steering drift during braking. This was initially considered to be a possible major influence, because of the suspension movement of the steered wheels relative to the fixed steering rack, and another factor (the fitment of a steering gear housing reinforced mounting cover on the front subframe) was investigated for the same reason. It was suggested that suspension and subframe deformation during braking could possibly change the alignment of the steering rack and cause side to side variation in the toe steer characteristic. This was found to have a small significant effect, the third largest, but was not considered worth investigating further.

The most significant effect arising from dynamic variation in the deformation and deflection of suspension and steering components was the stiffness of the rear bush in the lower suspension wishbone. Not only did this deflection generate large changes in suspension geometry, mainly in the side to side camber and steering offset, but it also changed toe steer angles during braking which actually reversed side to side during the braking manoeuvre.

Changing to a stiffer rear bush in the lower wishbone minimised the deflection and controlled the wheel orientation better during braking.

Steering offset was confirmed as an important design parameter for vehicle drive safety. In this case, measurement of the static and dynamic values of wheel offset showed only a small variation during braking, and little side to side variation.

The vehicle tests confirmed the findings from the initial tests, and gave an indication of the practical significance of the identified parameters in the generation of steering drift during braking on an actual vehicle. The results of the tests showed clearly that the steered wheels did change their orientation during braking, as measured by the toe steer angle.

The most effective means of controlling any tendency towards steering drift during braking is to ensure, in the design of the steering and suspension system, that there is minimum side to side variation in suspension deflection and body deformation both statically and dynamically. In this particular case, the lower wishbone rear bush was found to play a major role in controlling the wheel deflections, and, in terms of steering drift during braking, offered a robust design for this type of MacPherson strut suspension.

ACKNOWLEDGEMENTS

This paper presents research carried out as part of an MPhil. study with the University of Bradford, U.K.. The authors are grateful to all who contributed to the research, including staff in the Ford Motor Company, IKA (Aachen), and supplier companies. Thanks also go to the Directors of the Ford Motor Company for permission to publish this paper.

REFERENCES

1. Newcomb T.P., Spurr R.T., "A Technical History of the Motor Car", ISBN 0852740743, IOP Publishing Ltd.,1989.
2. Day, A.J., Tirovic, M., Newcomb, T.P., "Thermal effects and pressure distributions in brakes", Proc. Instn. Mech. Engrs., Vol. 205, Part D, 1991, pp. 199 - 205.
3. Newcomb T.P., Spurr R.T., "Braking of Road Vehicles" Chapman and Hall Ltd., 1967.
4. Chapman, B.J., Hatch, D., Cast Iron Brake Rotor Metallurgy", paper C35/76, Braking of Road Vehicles Conference, Instn. Mech. Engrs, 1976.
5. Greave D G., Barton D C., Crolla D A., Chapman J L., Buckingham J T., "Alternative Disc Brake Materials", Advances in Automotive Braking Technology, Instn. Mech. Engrs, 1996.
6. Yoshiroh, T., Keisuke, Y., Masaru, K., "The effects of the tyre camber angle on vehicle controllability and safety", SAE 860245, 1986.
7. Goddard, S., Elwood, P., "The impact of scrub radius on sport utility vehicle handling", SAE 982834, 1998.
8. Banholzer, D., "Improving directional stability under braking", Fifth International Technical Conference on Experimental Safety Vehicles, ESV-746076, London, June 4 – 7 1974.
9. Pottinger, M.G., "Ply steer in radial carcass tyres", SAE 760731, 1976.
10. Pottinger, M, "Tire/vehicle pull: an introduction emphasizing ply steer effects", Tire Science and Technology, TSTCA, vol 18, no. 3, July-September 1990.

11. Matyja, F.E., "Tread design and belt angle effects on residual aligning torque", SAE 870423, 1987.
12. Bastow, D., Howard, G.P., "Car suspension and handling", ISBN 1560914041, SAE Pentech Press, 1993.
13. Holdman, P., Kohn, P., Moller, B, Willems, R., "Suspension kinematics and compliance – measuring and simulation", SAE 980897, 1998.
14. Momoiyama, F., Miyazaki, K., "Compliance steer and road holding of rigid rear axle for enhancing the running straightness of large sized vehicles", SAE 933009, 1993.
15. Grove, D.M., Davis, T.P., Engineering Quality and Experimental Design, ISBN 0470218487, Longman 1992.
16. Klaps, J., "Investigation of the effects of the longitudinal stiffness of the engine subframe and suspension system during straight-line braking in passenger cars", MPhil. thesis, University of Bradford, U.K., 1999.

Developments in compressed air management for CV braking systems

A H BECK and **M J HAIGH**
WABCO Vehicle Control Systems, Leeds, UK
H DIEKMEYER and **K H SCHÖNFELD**
WABCO Vehicle Control Systems, Hannover, Germany

SYNOPSIS

The control system for the typical commercial vehicle compressed air braking system has not fundamentally changed for several decades. That is in itself a tribute to the engineers who first designed and developed the compressor unloader and protection valve systems. But times move on and expectations expand. In this paper two key aspects of the compressed air management system, which are currently being improved and overhauled, are presented.

1 INTRODUCTION

The first development described is in the manipulation of the compressor's activity when it is not required to pump air, in short the parasitic loss imposed on the vehicle by an idling compressor. Traditionally the compressor was "unloaded" by a separate valve, which diverted the compressed air flow away from the reservoirs to an exhaust port. Both first and second-generation Power Reduction (PR) systems which minimise the wasted pumping power in modern compressors are considered. Also described are recent advances in the control of oil carry-over into the compressed air, and explanation is given on how "Labyrinth" compressors help to optimise system operation and simplify vehicle design.

The developments made in electronic vehicle networks - the Controller Area Network (CAN) system are briefly summarised. This has made both desirable and feasible the introduction of an electronic management system for air supply, processing and storage. The principles of operation of a first generation Electronic Air Processing Unit are further described and, specifically how the live vehicle data enables desiccant management to be much more effective, and how a compressor control algorithm further enhances the modern commercial vehicle.

2 COMPRESSOR ENHANCEMENTS

2.1 First Generation Power Reduction

Prior to the 1990s significant reductions in the off-load power consumption of compressors were achieved with the first generation of Power Reduction systems (PR). To explain the improvements connected with the Second Generation PR, the First Generation Systems are outlined below.

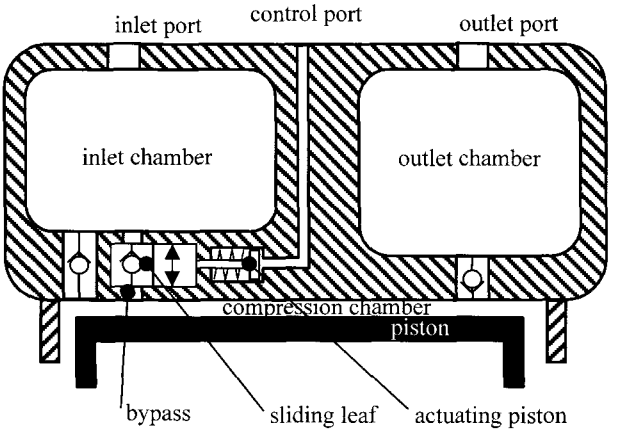

Figure 1 : Schematic section of First Generation PR - cylinder head

Figure 1 shows a section of a single cylinder air compressor. During the on-load phase, the control port is exhausted. The spring-loaded actuating piston keeps the sliding leaf in a position closing a bypass between compression chamber and induction chamber. The compressor will then feed air into the system. For a twin cylinder compressor the basic layout is comparable, with both cylinders having a common inlet chamber and a common dead chamber. This commonality is a matter of internal packaging within the cylinder head only.

In the off-load phase, the unloader pressurises the control port. The actuating piston is pushed back, thus bringing the sliding leaf into a position opening the bypass. Now, by upwards movement of the piston a part of the induced air is delivered at no pressure via the purge valve of the unloader, back into the atmosphere. The remaining part of the induced air is pushed back and forth (via the open cross-section of the sliding leaf) between the inlet and outlet chambers. The divided mass flow means reduced air flow velocities and correspondingly reduced power losses. Furthermore the large cross section of the off-load slot of the sliding leaf significantly reduces throttling, thus lowering power consumption (Figure 2) and temperature level (Figure 3).

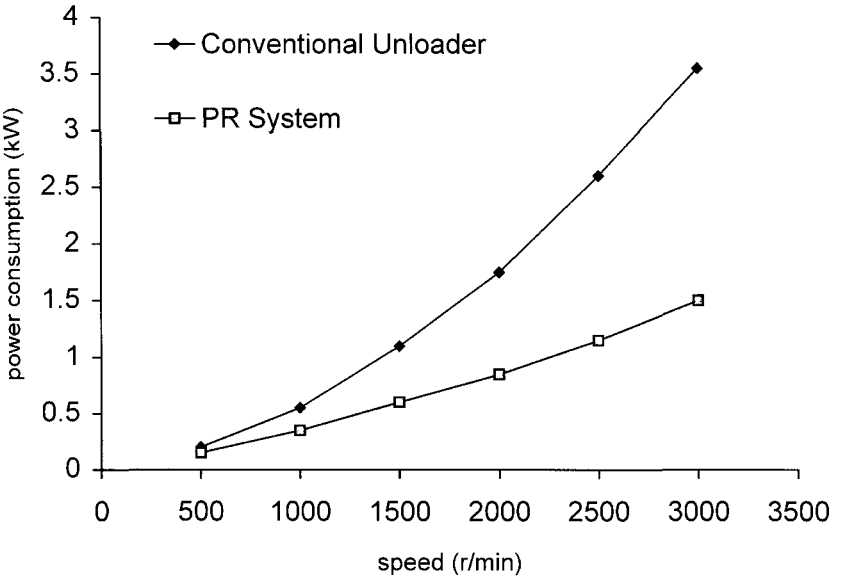

Figure 2 Power Consumption off-load

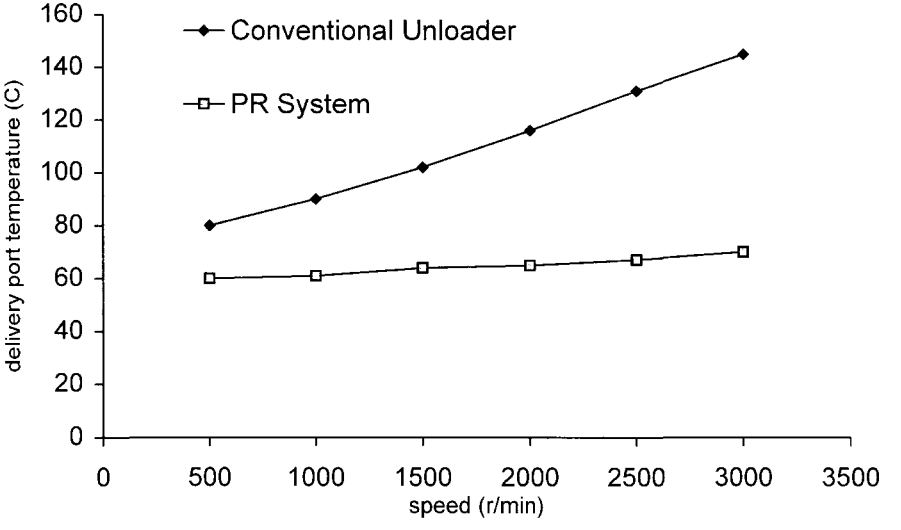

Figure 3 : Delivery port temperature off load

Apart from significant power savings, there are further benefits connected with the system:

- Add-on costs are comparatively low,
- No additional space is required for installation, as the PR-system is integrated into the casting of a "normal" cylinder head.
- Through-drive (e.g. for a power steering pump) is possible.

Continuous scavenging of the compressor with fresh air under modest pressure build-up during off-load results in:

- Significantly lower temperature level
- "Washing" off oil film from top of piston, valves and cylinder head
- Any oil carry-over is exposed to the heated interior of compressor only for a short time, contributing to less sensitivity with regard to oil carry-over and carbonisation,

PR is also a prevention against "collecting" all oil carry-over, that inevitably is generated during the off-load phase, and feeding the total (even if extremely small) amount of oil into the air system at the beginning of the on-load phase. Continuous scavenging of the delivery line with air during the off-load phase also helps prevent freezing during low load cycles of the compressor under cold climate conditions.

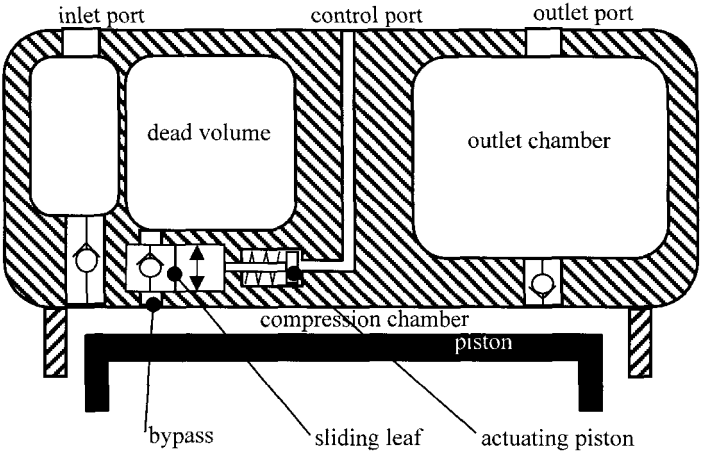

Figure 4 : Schematic section of Second Generation PR cylinder head

2.2 Second Generation Power Reduction

The development of second generation PR-systems mainly focused on further improvements concerning temperature levels, oil film washing and heat exposure. Figure 4 shows a cross-section of such a cylinder head for a single cylinder compressor.

With this new design, the slot of the sliding leaf opens to a separate "dead volume" chamber. In comparison to the First Generation PR principal, the differences and benefits are:

- dead volume chamber of dedicated size (c.f. First Generation where the inlet line connects to a virtually infinite volume) giving a pressure pulsation of up to 3 bar (close to zero in lst generation.) preventing oil creeping up from the sump of the compressor crankcase, via the gap between cylinder wall and piston into the compression chamber. The pressure pulsation also results in higher scavenging, significant improvements in temperature levels, oil film washing and heat exposure.
- compression chamber de-coupled from inlet, resulting in less sensitivity to inlet depression from the engine.

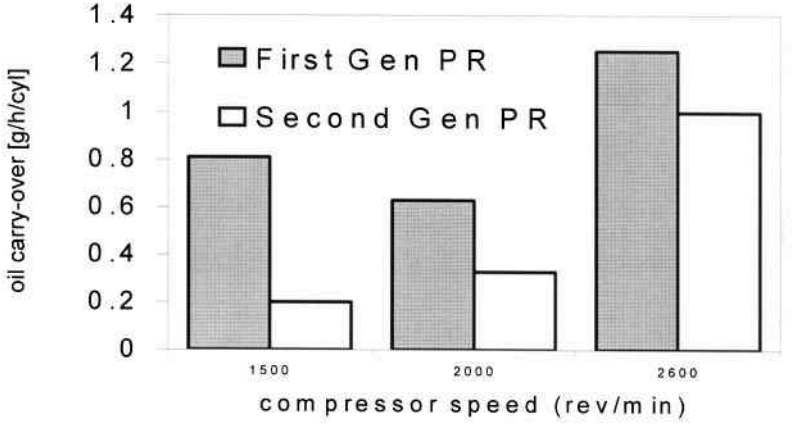

Figure 5 Oil carry-over (conventional vs. enhanced compressor)

Figure 5 indicates the improvement with regard to a reduction in oil carry-over of the order of 50% compared to first generation PR.

The quality of the pressurised air delivered by the compressor into the braking system is characterised by its (undesired) content of oil, and additionally - with regard to the oil content - its preferably low temperature level for avoiding carbon build-up. The latter either can block the delivery line (in the end totally) or can have a negative impact on the reliability and lifetime of the components of the braking system, especially delivery line, unloader valve and air dryer.

Furthermore, a low temperature of the delivered air is recommended. The lower the temperature, the higher is the efficiency of the air dryer. Moreover, for air dryers the average inlet temperature should not exceed 65°C to ensure proper function. On the other hand the inlet temperature should be high enough to avoid freezing under cold climate conditions, requiring a short delivery line. Therefore, from these two points of view good cooling efficiency of the compressor helps to improve the reliability of the braking system.

2.3 Oil Carry-over

Oil carry-over occurs when oil leaks from the compressor crankcase, via the gap between the piston and the cylinder wall, into the compression chamber. These losses must not be made

"zero" as there is a minimum of lubrication required, which varies depending on the particular compressor in question. Furthermore, inlet and delivery valves of the compressor would be subject to excessive wear if running absolutely dry.

Therefore, the challenge is to optimise this oil flow to provide stable lubrication over the operating time at an extremely low level, but not to make it too low, regardless of the wide span of influencing tolerances, whether manufacturing, maintenance, or in operation.

Moreover, the key aspects in meeting this challenge compiled from experience and design knowledge are:

- geometry of piston / cylinder bore clearance:
- roundness of cylinder bore.
- secondary movement of the piston, deformation of cylinder bore due to tightening forces on cylinder head and different thermal expansion rates
- piston ring configuration: shape and tangential forces, e.g. incorporating a backing spring to the oil control ring
- blow-by of compressed air into the compressor crankcase
- oil level within crankcase, e.g. improving the oil return from the compressor and at the same time allowing the compressor crankcase to breath.

For example, a 440cm^3 twin cylinder compressor incorporating the following design changes:

- cylinder head assembly with PR-system and better cooling properties,
- reduced clearance between piston and cylinder bore
- oil control ring spring backed

resulted in approximately 50% reduction in oil carry-over rate under test rig conditions. A further 50% reduction could be achieved by attention to the cylinder walls, giving a total reduction of down to 25% compared to the original results.

2.4 Temperature Reduction (TR)

Although almost negligible in quantity, oil in the compressed air combined with high delivery temperatures may result in carbon build-up. This is caused when average cylinder head wall temperatures are high for long periods (especially in excess of 150°C average over on/off-load). Hence reduction of heat generation and good cooling efficiency are important. A new milestone in reducing the air temperature at the delivery port is a labyrinth cylinder head as shown in Figure 6.

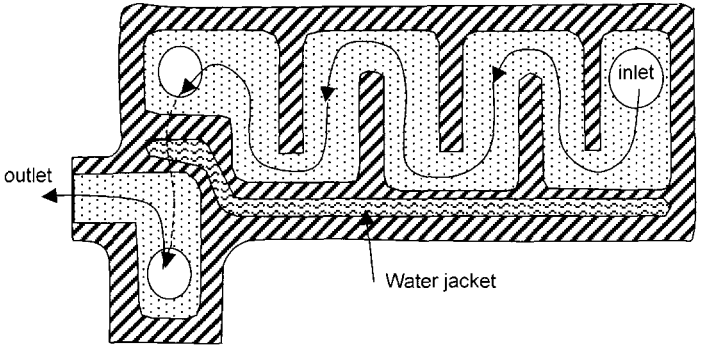

This more complex airflow path allows the hot compressed air to exploit more fully the cooling potential of the cylinder head's water cooling circuit. For a minimum of cost this system reduces the delivery port temperatures to 130C, compared with values exceeding 220°C for traditional designs.

To achieve even less heat generation, an adequate off-load control is useful. Thus the average temperature level will be reduced, with further reduction in the peak temperature under normal driving conditions. The PR-control also has a positive effect on delivery temperature in the off-load phase. Its low air velocities and permanent scavenging result in a low temperature level.

The combination of these three provisions ensures a moderately low temperature level without a large temperature spread. Thus it helps to overcome the "classical" conflict when specifying the layout of the delivery line:

- too short for long-lasting on-load operation with potential to exceed the permissible upper inlet temperature at the air dryer,
- too long for long-lasting off-load operation during cold climate conditions, with potential of the air to fall-below the freezing point as it passes through the delivery line to the air dryer.

Where a traditional layout of the delivery line was a costly cooling coil of 6m length, these aforementioned provisions enable shortening it to only 2m of low cost straight pipe.

3. CONTROL ADVANCES

3.1 Databus Architecture

Modern vehicles - and this applies only to vehicles introduced in the last 2-3 years - are equipped with many sophisticated electronic control and monitoring systems. Electronic Engine controls have proved essential to allow vehicles to comply with emissions regulations. Computer gearshift systems aid the driver's task of coping with many different ratios whilst keeping an eye on modern traffic. Smart suspension controls allow rapid matching of vehicle and loadbay height without resulting in huge air use when on the move. ABS and EBS have revolutionised the driver's control of the vehicle under braking. Since the SAE published its standard SAE J1939, these systems have increasingly been linked by high-speed ultra-reliable serial data bus connections. This is the Controller Area network (CAN) system. Any system on the CAN "bus" can collect data from the sensors fitted to all of the systems on the vehicle.

Developments in this field are rapid. Vehicle builders are specifying CAN-aware systems for tachographs, dashboards and chassis/cab management. Status and diagnostic information is required from all vehicle systems, and diagnostic information is marshalled for display to the driver and detailed analysis by garage technicians. These influences alone require that Air Management Systems enter the electronic age, but there are also many more benefits to be obtained from the wealth of information on the CAN bus.

Improvements to the management of compressor and desiccant drying have a number of aspects to them. The Air management system consists of the compessor, the Electronic Air

Processing Unit, which takes the place of conventional governor, purge valve and protection valve system, as well as the air dryer itself. This configuration is shown in Figure 7

In this paper the benefits which can be obtained by smart use of the databus have been grouped into two parts: DESICCANT MANAGEMENT and COMPRESSOR USE

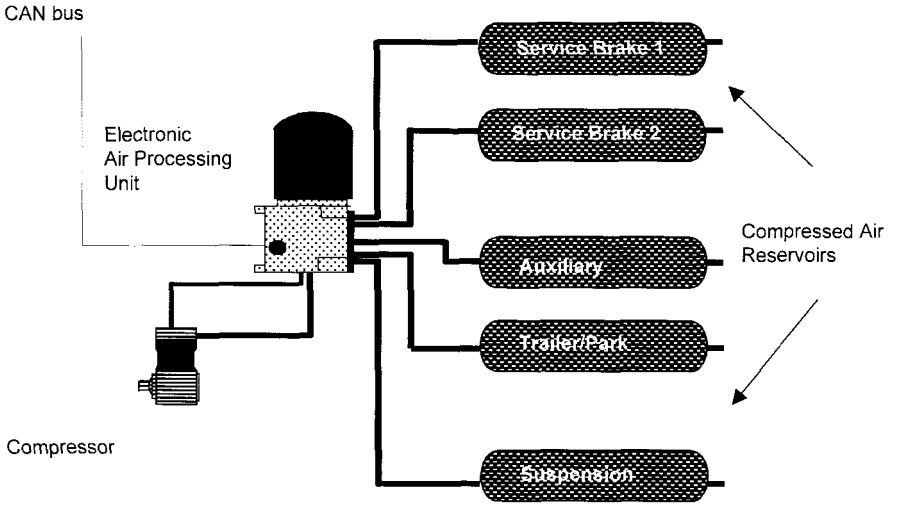

Figure 7 Electronic Air Dryer system layout

OPTIMISATION.

3.2 Desiccant Management

Current air management systems use a bed of desiccant material to provide enhanced drying. Desiccant materials require periodic reverse-flow operation in order to remove the adsorbed water and enable the desiccant to continue to perform its function. This is referred to as "regeneration". The reverse flow is also used to purge any accumulated liquid water, and contaminating oil, from the air dryer body. The layout is shown in Figure 8

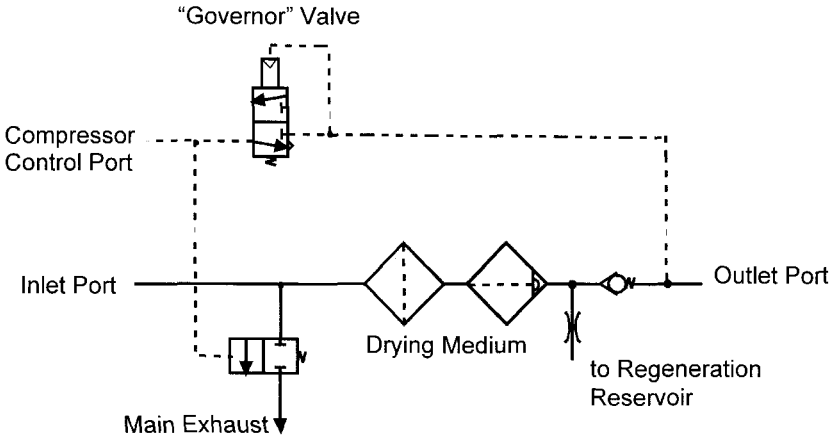

Figure 8 Schematic layout of Conventional Air Dryer

The addition of desiccant beds to the traditional compressed air supply system has greatly enhanced the quality of the compressed air supplied to the various valves and actuators in a modern CV system. The control system used to regulate the amount of back flow has, however, been quite crude. The pressure-sensitive pneumatic signal generated by the governor opens the usual main exhaust valve, which diverts the compressor output to exhaust. As explained above, the latest designs also operate power reduction (PR) valves which prevent the compressor from generating full airflow in the first place. This signal is further used to open a reservoir of air downstream of the desiccant which is allowed to back flow through the desiccant bed and regenerate it.

Such a regeneration reservoir costs money, must be sited somewhere and connected up. It is therefore seen as undesirable by a majority of vehicle manufacturers. Other systems which take air from the main reservoirs have been designed. These do remove the need for a separate reservoir, but add complexity and are easily confused by varying operating regimes. Regeneration devices rely on a design-time calculation based on the vehicle's reservoir capacity, the compressor output and the hysteresis band of the governor. This means that variations in capacity - either between vehicle variants or simply through coupling a trailer, or operation outside the hysteresis band (due to high use from (eg) ABS or on pump-up after an overnight stop), can result in inefficient drying. In extreme cases of heavy use this can result in significant quantities of water entering the air system.

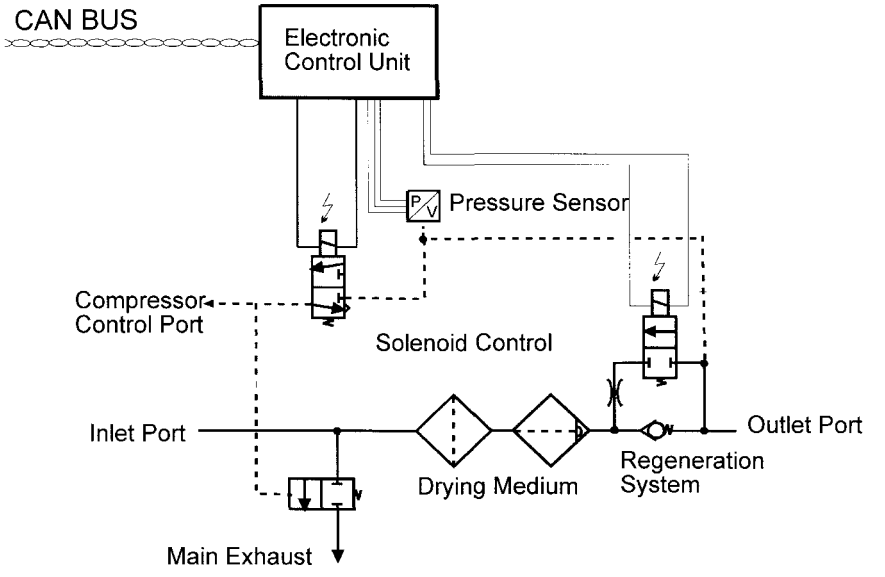

Figure 9 Schematic layout of Electronic Air Dryer

With a system such as that shown in Figure 9, the use of CAN data and of course a computer control unit, allows these calculations to be performed live in the ECU according to the prevailing conditions. Furthermore, by the addition of a few simple parameters (such as compressor size, drive ratio, reservoir configuration) the systems are able to make detailed estimations of the amount of compressed air forwarded by the system. Ideally, the airflow would be monitored for moisture content, but at the moment reliable moisture sensors which operate predictably at pressure are not readily available. Fortunately it is not an unreasonable assumption that the air, having been pressurised, is saturated with water. This is true at all but the most extreme of dry conditions. Regeneration is then made based on the integrated volume of air forwarded by the compressor. When sufficient air has been compressed to require that the desiccant be regenerated, the ECU operates the regeneration cycle, using air from the system reservoirs. The system cross checks the calculated pressure drop with the necessary regeneration time, and is able to determine if the regeneration was successful.

This optimisation results in some extra regeneration events - for example after heavy use or when pumping up an empty system - but removes the need for "worst case" calculations. In many cases the compressor is able to cut-out without needing a regeneration, thus saving a substantial amount of air. The result of this optimisation is better and more reliably dried air, irrespective of duty cycle or compressor size. Indeed the amount of desiccant can be parameterised, allowing different desiccant cartridges to be used in order to suit various applications. The improved air use leads to far less over-purging and a consequent small saving in energy from the unnecessary re-inflation of the regeneration source.

3.3 Compressor use optimisation

The advent of CAN bus data interchange, together with the development of electronically controlled Air Management Systems has made it possible for the use of the compressor to be

coupled to the use - or duty - of the vehicle which drives it. Good and bad times to run the compressor have been identified as:

Good Times	**Bad Times**
Overrun driving	During engine cranking
(use kinetic energy that will be wasted)	*(to minimise cranking load)*
During Braking	When hill-climbing
(use kinetic energy that is being wasted, reduce load on brake system)	*(to maximise available power)*
Downhill driving	Engine Idling
(use gravitational energy, augment retarder)	*(to minimise fuel used at idle)*

The CAN information stream is used to establish the state of the vehicle - including a number of intermediate states not mentioned here for the sake of clarity. This is compared to the urgency of the requirement for compressed air. Clearly if a vehicle has air brake reservoir pressures which fall below that required to meet its needs for safe braking, then the above considerations are ignored, and the compressor is run. However, between the normal compressor control hysteresis limits - often referred to as cut-out and cut-in - there is scope for choosing to operate the compressor according to energy saving and indeed comfort factors.

Initially it was thought that such considerations could not result in any useful savings when air could not be stored "at will". Clearly if the air reservoirs are full, then no further amount of downhill running can be utilised. A simple test was therefore conceived in which a vehicle with a normal air control system was characterised according to the compressor run-time in each of several phases. This was then compared with the same vehicle running the electronic control algorithm. The results were highly significant and are shown in Figure 10.

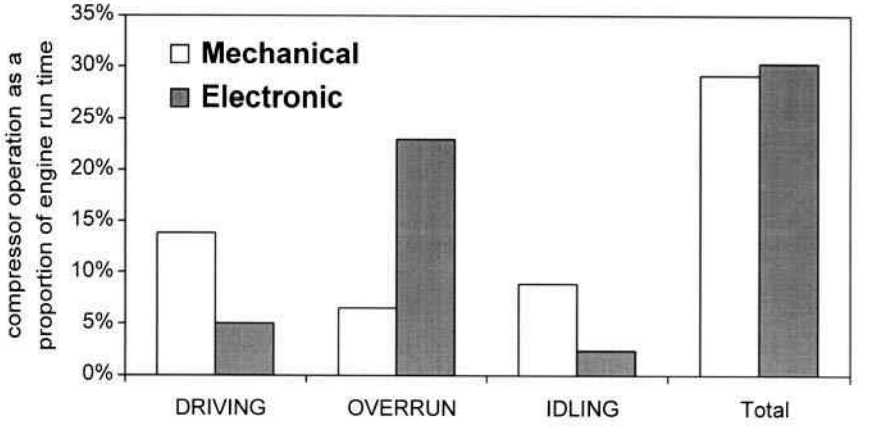

Fig 10 Compressor Activity Histogram

The results show that:

- Compressor run whilst idling was almost eliminated.
- The overrun utilisation was tripled,
- The use while driving correspondingly reduced.

The information from these tests was used to estimate the potential fuel saving that a vehicle might make from this technique and concluded that fuel savings approaching £200 per year would have been obtained using the given test vehicle as a model, and assuming about 2000 hours running time per year. Typical results are shown in Figure 11.

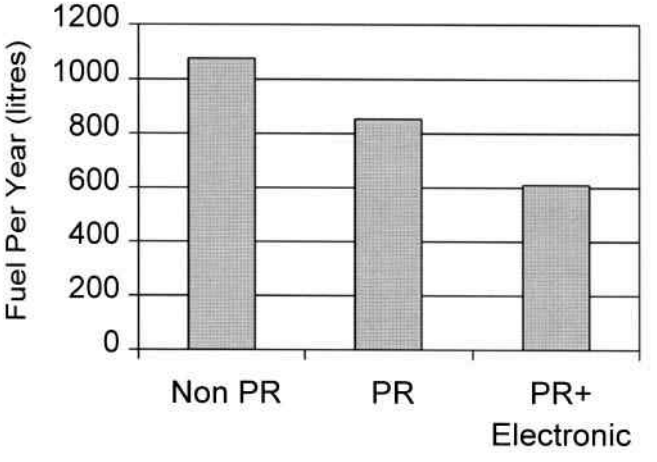

Figure 11 Example of Potential Fuel Saving

These estimates are very dependent on operating environment (traffic, blend of motorway & urban running), compressor size (bigger is better) and vehicle details (air usage rates, reservoir configurations, cut-in/cut-out thresholds). The test vehicle was chosen to be deliberately worst-case in as many respects as possible (small compressor with low control hysteresis).

4. CONCLUSIONS

The new generation of PR compressors further pushes out the boundaries of fuel economy and reliability. The current state-of-the-art Air Processing Unit now embraces all the requirements of the new electronic architectures, paving the way for electronic dashboard information, and allowing air management to take its place in "smart vehicle" architectures. The improved control offers even further fuel saving over and above that attainable with PR and a conventional control system. Together, these technologies represent a major advance in the development of vehicular compressed-air management technology.

There are many more synergies in this area: For example the short pipe / long pipe compromise referred to in section 2.4 can be improved at both extremes by electronic control. The elimination of excessively long pumping phases (which is a corollary of the desiccant

management algorithm) shortens the average on-load time, and so reduces peak and average temperatures. Simple body temperature monitoring allows the unit to switch to the old line-unload system until enough energy is "wasted" to avoid freezing the pipe and the dryer inlet galleries. Test work is under-way to develop the necessary algorithms, and explore the limits of this technology. Further synergies mean EBS system algorithms can be better optimised when reservoir pressures are known on the CAN bus, and electronic air suspension response can be enhanced.

The potential for development and enhancement of the basic prime mover in an air system - the compressor - must not be underestimated either. The adoption of simple but well thought-out and designed modifications coupled with the introduction of CAN-connected Air Management systems will greatly enhance the practical acceptability and technical lifespan of compressed air as a very robust power transmission medium.

5. REFERENCES

1. Conklin & Hodgins, Electronic Compressor & Air Dryer Control, Nov 1999
   SAE 199901-3771A
2. Recommended Practice for Serial Control & Communications Network
   SAE J1939

This page intentionally left blank

Authors' Index

S

T

V

W